

Kraftspektroskopie an einzelnen Membranproteinen

Dissertation an der Fakultät für Physik
der Ludwig-Maximilians-Universität
München



vorgelegt von

Max Keßler
aus München

München, 28. November 2005

Erster Gutachter: Prof. Dr. Hermann Gaub
Zweiter Gutachter: Prof. Dr. Erwin Frey
Tag der mündlichen Prüfung: 3. April 2006

Inhaltsverzeichnis

1	Zusammenfassung	4
2	Einleitung	6
3	Synthese und Struktur von Proteinen	9
3.1	Aufbau von Proteinen	9
3.2	Mechanismen und Kräfte bei der Faltung von Proteinen	9
3.3	Faltung von Membranproteinen	11
4	Funktionsweise eines Rasterkraftmikroskopes	14
4.1	Aufbau und Funktion	14
4.2	Abbildung von Membranproteinen mit submolekularer Auflösung	15
4.3	Limitierungen der Kraftauflösung	17
5	Bestimmung der Barrierepositionen	20
5.1	Elastizität von Polymeren	20
5.2	Das Modell der frei verbundenen Kette	20
5.3	Das Modell der wurmartigen Kette	21
5.4	Enthalpische Beiträge zur Elastizität von Polymeren	23
5.5	Bestimmung der Entfaltungszwischenzustände	24
6	Charakterisierung der Energielandschaft	29
6.1	Übergangsraten zwischen Faltungszuständen	29
6.2	Bestimmung der Potentialparameter mit Hilfe von Monte-Carlo-Simulationen	30
6.3	Analytische Berechnung der Verteilungsfunktion der Abrißkräfte	31
7	Literaturverzeichnis	34
8	Anhang	37

1 Zusammenfassung

Membranproteine sind in fast jeden Prozeß involviert, bei dem Zellen mit ihrer Umgebung interagieren, sei es die Übertragung von Informationen oder der Austausch von Molekülen. Sie sind deshalb in der Biologie von grundlegender Bedeutung. Als eines der wenigen Membranproteine, deren räumliche Struktur mit atomarer Auflösung bekannt ist, hat sich Bakteriorhodopsin als Modellsystem für die Untersuchung der Faltung einer bedeutenden Klasse von strukturell ähnlich aufgebauten Proteinen etabliert. Im Rahmen dieser Arbeit wurden einzelne Bakteriorhodopsin-Moleküle mit einem Rasterkraftmikroskop mechanisch entfaltet. Dabei wurde der Einfluß von Änderungen des pH-Wertes des umgebenden Mediums sowie der Temperatur und der Geschwindigkeit, mit der das Protein entfaltet wurde, auf die durch zahlreiche charakteristische Spitzen gekennzeichneten Entfaltungsspektren untersucht. Eine weitere Fragestellung war, inwieweit es mit der verwendeten Methode möglich ist, Faltungsprozesse an einzelnen Proteinen zu beobachten. Die erzielten Ergebnisse lassen sich wie folgt zusammenfassen:

- Durch die Analyse der scharfen Anstiege in den Entfaltungsspektren gelang es, die Entfaltungsbarrieren, d.h. die Position bis zu der ein Protein jeweils entfaltet ist, mit einer Genauigkeit von etwa drei Aminosäureresten zu bestimmen. Diese Positionen korrelieren in ca. 90 % der Fälle mit den Enden von Helices, mit durch Proline verursachten Knicken in bestimmten Helices oder mit intramolekularen Wasserstoffbrücken.
- Es zeigte sich, daß das Auftreten der meisten Entfaltungsbarrieren davon abhängt, von welchem Ende her das Protein entfaltet wird. Das deutet darauf hin, daß die betreffenden Barrieren -wahrscheinlich durch intramolekulare Wechselwirkungen zu benachbarten Helices- durch den jeweils noch gefalteten Teil der lokalen Umgebung stabilisiert werden.
- Drei Entfaltungsbarrieren, die unabhängig davon auftreten, von welchem Ende aus das Protein entfaltet wird, korrelieren mit Aminosäuren, die jeweils in beide Richtungen der Sequenz durch Wasserstoffbrücken stabilisiert sind.
- Während der pH-Wert des Mediums im Bereich von pH 4.2 bis pH 10.0 keine Auswirkung auf die Häufigkeit verschiedener Entfaltungspfade durch die Energielandschaft zeigt, begünstigt eine Erhöhung der Temperatur im Bereich von 8 ° C bis 52 ° C das paarweise Entfalten von α -Helices.
- Durch geschwindigkeitsabhängige Messungen konnten die Reichweiten der Entfaltungspotentiale und die Entfaltungsraten einzelner Strukturelemente bestimmt werden. Dadurch konnte gezeigt werden, daß das paarweise Entfalten von Helices auf anderen Pfaden durch die Energielandschaft stattfindet als die Entfaltung zweier Helices über Zwischenzustände.
- In der vorliegenden Arbeit gelang es erstmalig, die gesteuerte Rückfaltung von einzelnen, partiell entfalteten Bakteriorhodopsin-Molekülen experimentell zu untersuchen. Dabei konnte sowohl die Rückfaltung einzelner Helices als auch die von Helixpaaren nachgewiesen werden. Außerdem ergaben sich Hinweise auf einen sehr schnell

faltenden Zwischenzustand, bei dem jeweils etwa die Hälfte der ersten Helix eines Helixpaares gefaltet ist.

- Es wurden Hinweise auf einen Zwischenzustand gefunden, in dem ein Paar von Helices in die Membran zurück gefaltet ist, aber noch nicht die finale Lage innerhalb der nativen Struktur des Proteins angenommen hat. Dies resultiert bei erneuter Entfaltung in einer niedrigeren Abrißkraft. Ein solcher Zwischenzustand steht in Einklang mit den etablierten Modellen zur Faltung von Membranproteinen.
- Während des Faltungsvorganges überwindet das Molekül zum Teil externe Kräfte von bis zu 50 pN. Aus der mechanischen Arbeit, die dabei geleistet wird, läßt sich eine Obergrenze der freien Faltungsenthalpie berechnen.

2 Einleitung

Ein Protein besteht aus einer Kette von Aminosäuren, die durch Peptidbindungen miteinander verknüpft sind und deren Reihenfolge genetisch vorgegeben ist. Proteine sind maßgeblich in fast alle chemischen Vorgänge involviert, die in lebenden Zellen ablaufen, so katalysieren sie beispielsweise chemische Reaktionen oder bilden das Zytoskelett der Zellen. Neben intrazellulären Transportvorgängen und dem Transport durch die Zellmembran sind sie unter anderem auch maßgeblich an der Signalverarbeitung beteiligt. Zur Erfüllung seiner spezifischen Aufgabe ist die räumliche Struktur, in die sich ein Polypeptid selbstständig oder - in manchen Fällen - mit der Unterstützung von weiteren Proteinen, wie z.B. Chaperonen, faltet von entscheidender Bedeutung. Die Faltung eines Polypeptids ist durch die spezifischen Wechselwirkungskräfte zwischen den verschiedenen Aminosäureresten getrieben, wodurch seine native räumliche Struktur letztendlich durch das Genom des jeweiligen Organismus festgelegt ist. Aufgrund der hohen Komplexität des Zusammenhangs zwischen der dreidimensionalen Struktur eines Proteins und seiner (linearen) Aminosäuresequenz stellt die - theoretisch mögliche - Vorhersage der Struktur gegenwärtig eines der herausragenden Probleme der Biowissenschaften dar. Der Raum der möglichen Konformationen, die ein Polypeptid einnehmen kann, läßt sich durch eine hochdimensionale Energielandschaft beschreiben, die eine große Zahl von lokalen Minima aufweist. Der native Faltungszustand eines Polypeptids entspricht in diesem Bild dem globalen Minimum der Energielandschaft.

Typischerweise 30% aller Gene eines jeden Organismus kodieren Membranproteine, zu denen diverse Ionenpumpen, Zelladhäsionsproteine und Rezeptoren zählen. Unter den Membranproteinen nehmen wiederum die sogenannten G-Protein-gekoppelten Rezeptoren (*G-Protein coupled receptors GPCR*)¹ eine besondere Stellung ein. Sie spielen bei den verschiedensten Signalübertragungsprozessen eine Schlüsselrolle und sind deshalb auch medizinisch von höchster Bedeutung. So wirken etwa 40% aller verschreibungspflichtigen Arzneimittel direkt auf GPCR. Die herausragende biologische Bedeutung von GPCR steht allerdings in eklatantem Gegensatz zu unserer weitgehenden Unkenntnis ihrer exakten Struktur. Der Grund hierfür liegt darin, daß sich GPCR generell sehr schlecht kristallisieren lassen und deshalb die klassischen Methoden der Strukturanalyse, die Röntgenstrukturanalyse und die Elektronenbeugung hier nicht angewandt werden können².

¹Bei G-Protein-gekoppelten Rezeptoren handelt es sich um Membranproteine die aus sieben Transmembran- α -Helices aufgebaut sind und mit einem sogenannten GTP-bindenden oder kurz G-Protein in Wechselwirkung stehen. G-Proteine bestehen aus den drei Untereinheiten α , β und γ , wobei die α -Untereinheit im inaktiven Zustand ein GDP trägt. Die Bindung eines Liganden an den Rezeptor (GPCR) verursacht in diesem eine Konformationsänderung, die wiederum bewirkt, daß das frei in der Membran diffundierende G-Protein ebenfalls an den Rezeptor bindet. Dadurch erfährt das G-Protein eine Konformationsumwandlung, was den Austausch des gebundenen GDP gegen GTP zur Folge hat. Dies führt zum Zerfall des G-Proteins in ein $\beta\gamma$ -Dimer und die α -Untereinheit. Letztere wird dadurch aktiviert und überträgt das Signal, nachdem sich beide Untereinheiten wieder von dem GPCR gelöst haben, an einen *second messenger* (Stryer, 1995)

²Ein vielversprechender Ansatz diesbezüglich könnte der von Katragadda et al. sein, die mit Hilfe der NMR-Spektroskopie die Strukturen einer Serie von 13 kurzen, synthetischen Peptiden bestimmten, welche die gesamte Sequenz von Bakteriorhodopsin umspannen. Das durch die Überlagerung der überlappenden Teile dieser 13 Strukturen erzeugte, dreidimensionale Modell stimmt gut mit der bekannten Röntgenstruktur von Bakteriorhodopsin überein (Katragadda et al., 2001).

Der einzige GPCR, von dem bis dato eine Röntgenstruktur vorliegt, ist der Lichtrezeptor Rhodopsin, der für die visuelle Wahrnehmung von Bedeutung ist.

Wie in der Vergangenheit an verschiedenen Beispielen demonstriert wurde, läßt sich zumindest der nicht in die Membran eingebettete Teil der Oberfläche von Membranproteinen unter geeigneten Bedingungen mit Hilfe der Rasterkraftmikroskopie mit submolekularer Auflösung abbilden. Mit dieser Methode wurden bereits verschiedene bakterielle Außenmembranproteine, der Wasserkanal Aquaporin, Rhodopsin, der Natrium-Kanal NhaA sowie die Protonenpumpe Bakteriorhodopsin untersucht. Bei diesen Experimenten zeigte sich, daß der Terminus eines Membranproteins gelegentlich an die Spitze der Abtastnadel des Rasterkraftmikroskopes adhärert, wenn diese lange genug mit der Probe in Kontakt gebracht wird. Das Molekül kann dann durch Zurückfahren der Spitze mechanisch entfaltet werden. Für solche durch eine externe Kraft erzwungene Entfaltungsmessungen von Polymeren hat sich der Begriff *Kraftspektroskopie* eingebürgert. Bei Membranproteinen erfolgt die Entfaltung, anders als bei wasserlöslichen Proteinen, in zahlreichen Zwischenschritten, deren Reihenfolge aufgrund der Verankerung in der Zellmembran der Reihenfolge der Aminosäuren entspricht.

Die vorliegende Arbeit befaßt sich primär mit der kraftspektroskopischen Untersuchung von Bakteriorhodopsin, einem bei manchen Archaeen auftretenden Membranprotein, das unter Lichteinfluß Protonen aus dem Inneren der Zelle nach außen pumpt und hierdurch einen Protonengradienten über die Zellmembran aufbaut. Aufgrund seiner topologischen Gemeinsamkeiten mit GPCR kann Bakteriorhodopsin, das ebenfalls aus sieben α -Helices besteht und dessen Struktur mit einer Auflösung von 1.55 Å bekannt ist, als Modellsystem für letztere dienen. Es zeigte sich, daß die Entfaltung bei Bakteriorhodopsin und einer wachsenden Zahl von weiteren mittlerweile untersuchten Membranproteinen über eine Reihe von quasistabilen Zwischenzuständen erfolgt, bei denen das Polypeptid jeweils bis zu einer bestimmten Position entfaltet ist, die einem lokalen Minimum seiner Energielandschaft entspricht. Die Positionen innerhalb der dreidimensionalen Struktur, bis zu denen ein Protein jeweils entfaltet ist, werden im folgenden auch als Entfaltungsbarrieren bezeichnet.

Während dem weiteren Zurückfahren der Abtastspitze steigt die Kraft, mit der die Entfaltungsbarriere belastet wird, kontinuierlich an, bis das Protein schlagartig weiter in den nächsten Zwischenzustand entfaltet. Das verursacht in der gemessenen Kraft-Abstands-Kurve einen scharfen Anstieg, aus dem sich die Länge des bereits entfalteten Teils des Polymers und damit die Anzahl der entfalteten Aminosäuren berechnen läßt. Aufgrund der Kenntnis der dreidimensionalen Struktur von Bakteriorhodopsin ist es somit relativ einfach möglich zu bestimmen, bis zu welcher Position das Protein jeweils entfaltet ist.

Prinzipbedingte Vorteile von kraftspektroskopischen Messungen an einzelnen Molekülen sind zum einen die Möglichkeit unter physiologischen Bedingungen arbeiten zu können und zum andern, daß die Entfaltungskurven für jedes einzelne Molekül einzeln ausgewertet werden können. Dadurch läßt sich analysieren, welche Spitzen allen Entfaltungskurven gemeinsam sind - und somit Entfaltungszwischenzuständen entsprechen, die bei allen Kraftkurven auftreten - und welche Spitzen nur bei einem Teil der Daten auftreten. Bei letzteren läßt sich untersuchen, wie die Auftrittswahrscheinlichkeit von äußeren Parametern, wie der Temperatur oder der Geschwindigkeit abhängt, mit der das Protein entfaltet wird. Durch die Messung der Abrißkräfte einzelner Spitzen in Abhängigkeit von der

Zuggeschwindigkeit lassen sich auch Aussagen über die lokale Beschaffenheit der Energielandschaft treffen. Ein weiterer interessanter Aspekt ist die Frage, ob das Auftreten einer bestimmten Entfaltungsbarriere davon abhängt, von welchem Terminus her das Protein entfaltet wird. Hieraus können Hinweise darauf gewonnen werden, ob eine Entfaltungsbarriere nur zu einer Entfaltungsrichtung hin stabilisiert ist - etwa durch eine interhelikale Wasserstoffbrücke -, oder ob sie durch die intrinsische Stabilität von Sekundärstrukturelementen verursacht wird.

Schließlich soll in dieser Arbeit noch die kontrollierte Rückfaltung von partiell entfaltenen Bakteriorhodopsinmonomeren untersucht werden. Dazu wird die Abtastspitze vor der endgültigen Extraktion des Proteins aus der Membran wieder ein Stück weit an die Membranoberfläche angenähert. Aus den Meßdaten, die während der darauffolgenden erneuten Separation der Spitze von der Membranoberfläche aufgenommen werden, läßt sich ermitteln inwieweit das Protein in die Membran zurückgefaltet wurde. Diese Untersuchungen demonstrieren sehr anschaulich die weitreichenden Möglichkeiten der Manipulation von einzelnen Molekülen, die sich mit Hilfe der modernen Rasterkraftmikroskopie erzielen lassen.

3 Synthese und Struktur von Proteinen

3.1 Aufbau von Proteinen

Zur Synthese von Proteinen bedient sich die Natur aus einem Repertoire von 22³ so genannten proteinogenen Aminosäuren, die sich lediglich durch eine Seitenkette, den Aminosäurerest (in Abbildung 1 durch R_1 und R_2 bezeichnet) unterscheiden. Die als Primärstruktur bezeichnete Sequenz, nach der die einzelnen Aminosäuren in den Ribosomen der Zellen aneinandergesetzt werden, ist durch die m-RNA (*messenger RNA*) und damit letztendlich durch das Genom des betreffenden Organismus vorgegeben. Bei der Proteinsynthese werden die einzelnen Aminosäuren, wie in Abbildung 1 dargestellt, durch Peptidbindungen verknüpft. Aufgrund der gegenseitigen Wechselwirkungen der Aminosäurereste faltet sich das auf diese Weise entstehende Polypeptid unter physiologischen Bedingungen in eine definierte räumliche Struktur, die so genannte Tertiärstruktur⁴. Die Wechselwirkungen der Aminosäurereste sind maßgeblich durch deren unterschiedliche chemische Eigenschaften, wie die Hydrophobizität, die Fähigkeit Wasserstoffbrücken auszubilden und ihre Ladung, bedingt. Damit ist die für die biologische Funktion eines Proteins verantwortliche räumliche Struktur über die Sequenz kodiert.

Unter der Sekundärstruktur eines Proteins versteht man kleinere, meist sehr schnell faltende strukturelle Motive, die von sequenziell nahe benachbarten Aminosäuren gebildet werden, und als eine Art von Bausteinen in praktisch allen Proteinen auftreten. Beispiele hierfür sind α -Helices und β -Faltblätter. Unter einer α -Helix versteht man eine rechtsgängige Helix, bei der auf jede Umdrehung 3.6 Aminosäuren entfallen. Sie wird durch achsenparallel angeordnete Wasserstoffbrücken stabilisiert. Die die Membran durchspannenden Teile von Membranproteinen bilden häufig α -Helices; wie aus Abbildung 2 ersichtlich, besteht z.B. Bakteriorhodopsin nahezu ausschließlich aus α -Helices. Bei einem β -Faltblatt bilden sich Wasserstoffbrücken zwischen benachbarten Ketten des Polypeptids, die entweder parallel (paralleles β -Faltblatt) oder, wie bei dem BC-loop von Bakteriorhodopsin⁵, antiparallel (antiparalleles β -Faltblatt) angeordnet sind (vgl. Abbildung 2). Die herausragende Eigenschaft von Proteinen ist der eindeutige Zusammenhang zwischen der durch die Erbinformation vorgegebenen Primärsequenz und der räumlichen Struktur.

3.2 Mechanismen und Kräfte bei der Faltung von Proteinen

Zu den wichtigsten Interaktionen zwischen den einzelnen Peptideinheiten zählen elektrostatische Wechselwirkungen zwischen geladenen Seitenketten, sowie Van der Waalsche Wechselwirkungen und Wasserstoffbrückenbindungen. In erster Näherung ergibt sich das Potential somit als Summe über die zwischen zwei beliebigen Aminosäuren i und j wir-

³Dieser Wert beinhaltet die beiden Aminosäuren Selenocystein und Pyrrolysin, deren Codierung in den letzten Jahren nachgewiesen werden konnte (Hao et al., 2002, Thanbichler und Bock, 2002).

⁴In vivo erfolgt die Faltung teilweise mit der Unterstützung von weiteren Proteinen: den Chaperonen oder Chaperoninen. Die Insertion von Membranproteinen erfolgt zum Teil unter der Mithilfe von so genannten translocons.

⁵Die sieben α -Helices in Bakteriorhodopsin werden normalerweise durch die Buchstaben A bis G bezeichnet.

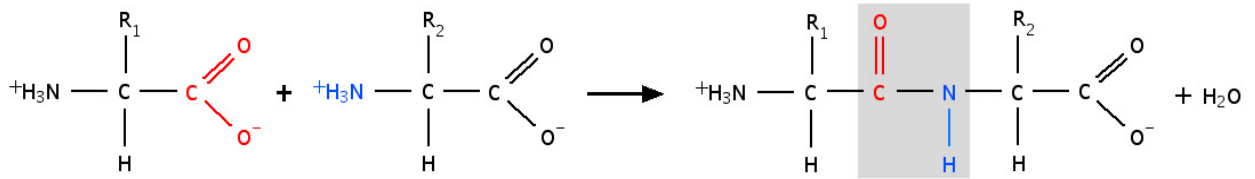


Abbildung 1: Verknüpfung zweier Aminosäuren durch eine Peptidbindung: Die (rot dargestellte) Carboxylgruppe der einen Aminosäure reagiert unter Wasserabspaltung kovalent mit der (blau dargestellten) Aminogruppe der zweiten Aminosäure. Die entstehende (grau hinterlegte) so genannte Peptideinheit ist aufgrund des partiellen Doppelbindungscharakters der Kohlenstoff-Stickstoffbindung planar. Im Gegensatz zu den anderen Bindungen im Polymerrückgrat kann das Polymer um diese Bindung nicht rotieren. (Abbildung nach (Stryer, 1995))

kenden Kräfte:

$$V = \frac{1}{4\pi\epsilon_0} \sum_{\substack{i,j \\ i \neq j}}^N \frac{Q_i \cdot Q_j}{r_{ij}} + \sum_{\substack{i,j \\ i < j}}^N \left(-\frac{A_{ij}}{r_{ij}^6} + \frac{B_{ij}}{r_{ij}^{12}} \right) + \sum V_{H-Brücken}^{ij} + \text{weitere Beiträge.}$$

Hierbei sind die Beiträge der elektrostatischen Kräfte durch den ersten, die der Van-der-Waals-Kräfte durch den zweiten und die der Wasserstoffbrücken durch den dritten Summanden gegeben. Der Abstand der Seitengruppen i und j mit den Ladungen Q_i und Q_j beträgt r_{ij} , ϵ_0 bezeichnet die elektrische Feldkonstante. Die durch induzierte Dipol-Dipol-Wechselwirkungen verursachte attraktive Komponente des Potentials sowie der extrem kurzreichweitige, durch den Überlapp der Elektronenhüllen verursachte, repulsive Anteil werden im zweiten Summanden durch ein Lennard-Jones-Potential beschrieben. Dabei charakterisieren die empirischen Parameter A_{ij} bzw. B_{ij} die attraktive bzw. repulsive Komponente der Wechselwirkung. Des weiteren beeinflussen auch entropische Beiträge, intramolekulare Disulfidbrücken und hydrophobe Wechselwirkungen zwischen den einzelnen Aminosäureresten, sowie zwischen umgebendem Medium und dem Polypeptid die Energiebilanz bei der Proteinfaltung.

C. Levinthal zeigte bereits 1968, daß ein noch nicht gefaltetes Protein seine native Konformation unmöglich innerhalb biologisch relevanter Zeitskalen durch einen ungerichteten „random-walk“ durch sämtliche möglichen Konformationen findet (Jackson, 1993). Geht man etwa von drei Einstellungsmöglichkeiten der Bindung jeder Aminosäure im Rückgrat des Polymers aus, so ergeben sich $\sim 5 \cdot 10^{47}$ (3^{100}) mögliche Konformationen. Unter der Annahme einer Zeitdauer von 10^{-13} s für die Reorganisation von einem Zustand in einen anderen ergäbe sich für das Durchlaufen aller möglichen Konformationen eine Zeitdauer von $\sim 1.6 \cdot 10^{27}$ Jahren, ein Wert, der biologisch relevante Dimensionen um Größenordnungen übersteigt.

Die Ursache dafür, daß Polypeptide ihre native Konformation selbstständig in Zeiträumen von einigen Sekunden oder weniger annehmen, liegt vielmehr darin, daß energetisch günstigere Konformationen aufgrund der zwischen den einzelnen Aminosäureresten und dem Polypeptidrückgrat wirkenden Kräfte favorisiert werden. Die $(3N - 6)$ -dimensionale Energielandschaft, mit der sich die Konformationsenergie eines aus N Ato-

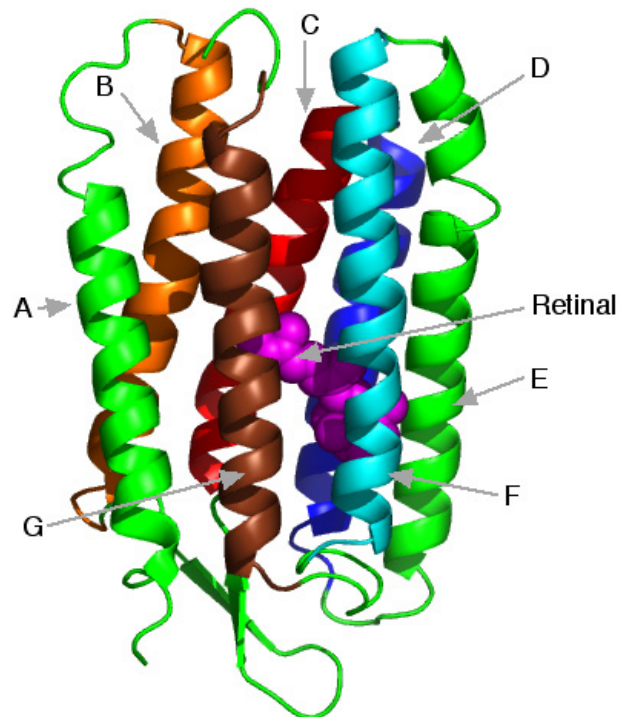


Abbildung 2: Ribbon-Darstellung der räumlichen Struktur eines Bakteriorhodopsin-Monomers, laterale Ansicht. Das Molekül besteht aus sieben die Membran durchspannenden α -Helices. Das photoaktive Retinal ist über die Schiff'sche Base kovalent an Helix G gebunden. In der Zellmembran von *Halobacterium salinarium* lagert sich Bakteriorhodopsin zu Trimeren zusammen, die wiederum ein hexagonales Gitter bilden. (Darstellung nach Essen et al. (Essen et al., 1998), pdb-Code 1BRR).

men bestehenden Proteins beschreiben läßt, hat somit ein trichterförmiges Erscheinungsbild. Der Gewinn an freier Enthalpie in Richtung der nativen Konformation übersteigt die Rauigkeit der Potentiallandschaft (Nymeyer et al., 1998). Dieser in Abbildung 3 schematisch dargestellte „faltungsfreudige“ Verlauf ist kein Merkmal beliebiger Sequenzen von Aminosäuren, sondern war und ist ein wichtiges Selektionskriterium bei der Entwicklung der Sequenz heutiger Proteine (Onuchic und Wolynes, 2004, Pande et al., 1997). Nach dem derzeitigen Stand der Erkenntnis erfolgt zu Beginn des Faltungsprozesses ein hydrophober Kollaps (*hydrophobic collapse*), der dadurch bedingt ist, daß ein völlig entfaltetes Polypeptid in Wasser aufgrund der zahlreichen exponierten unpolaren Seitengruppen instabil ist. Hierauf erfolgt nach der Faltung der Sekundärstruktur die Ausbildung der Tertiärstruktur. Der Zustand, bei dem die Interaktionen zwischen den einzelnen Helices noch nicht richtig ausgebildet sind, wird als *molten globule state* bezeichnet.

3.3 Faltung von Membranproteinen

Eine Besonderheit von Membranproteinen ist, daß die Anzahl ihrer möglichen Konformationen durch den Einfluß der umgebenden Lipid-Doppelschicht stark eingeschränkt ist. Aufgrund der Kontakte, die hydrophobe Seitenketten von Helices zu dem hydrophoben Bereich der Lipidschicht ausbilden, werden die Helices in ihrer Transmembran-Konformation stabilisiert (Popot und Engelman, 2000). Transmembran- α -Helices sind

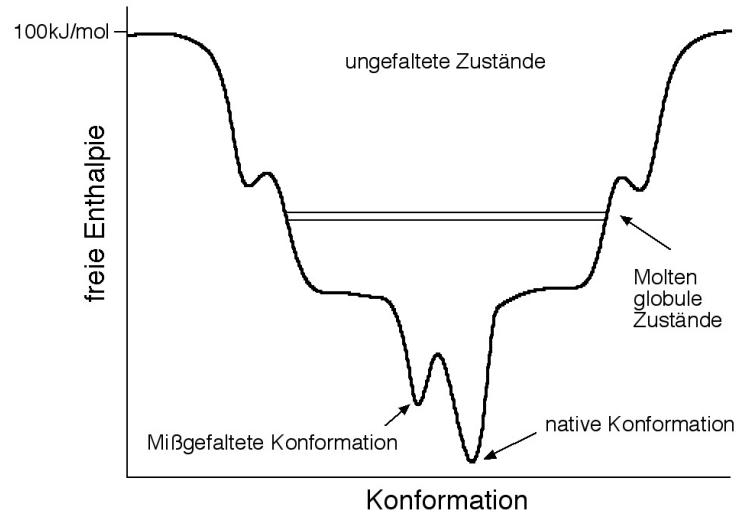


Abbildung 3: Schematische Repräsentation der Energielandschaft eines Proteins. Die vertikale Achse bezeichnet den Unterschied der freien Enthalpie zwischen gebundenem und ungebundenem Zustand. Die horizontale Achse stellt eine eindimensionale Repräsentation des hochdimensionalen Konformationsraumes des Polypeptids dar. Der Energieunterschied zwischen gefaltetem und ungefaltetem Zustand von Proteinen liegt in der Größenordnung von 25 kcal/mol (Onuchic et al., 1997). (Zeichnung abgewandelt nach (Nölting, 1999)).

damit in Lipidschichten wesentlich stabiler als Sekundärstrukturelemente gleicher Länge in Wasser (Popot und Engelman, 1990). Die freie Enthalpie, die zum Aufbrechen einer Wasserstoffbrückenbindung innerhalb der Membran aufgebracht werden muß, beträgt, bezogen auf eine Aminosäure, 4-5 kcal/mol. Für eine aus 20 Aminosäuren bestehende Transmembran-Helix ergäbe sich somit ein Wert zwischen 80 und 100 kcal/mol (White und Wimley, 1999).

Popot und Engelman schlugen zur Erklärung der Faltung von Membranproteinen ein zweistufiges Modell vor, bei dem die einzelnen α -Helices als unabhängige Faltungseinheiten agieren. Der erste Schritt besteht nach diesem Modell in der Einfügung der α -Helices in die Membran, während der zweite Schritt die Anordnung der α -Helices in ihre, oft durch interhelikale Wasserstoffbrücken stabilisierte, Tertiärstruktur beschreibt (Popot und Engelman, 1990). Dieser Ansatz wird auch durch die Beobachtung gestützt, daß isolierte Fragmente von Bakteriorhodopsin unter geeigneten Bedingungen selbstständig in eine Lipid-Doppelschicht falten und sich dort zu einem funktionierenden Protein arrangieren (Kahn und Engelman, 1992, Liao et al., 1984, Popot et al., 1986). Jacobs und White unterteilten den Faltungsprozeß aufgrund von thermodynamischen Messungen der Faltung kleiner hydrophober Peptide in drei Schritte: Die Anlagerung des Polypeptids an die Membran-Wasser-Schnittstelle, die Faltung an der Membran-Wasser-Schnittstelle und das Eindringen des Peptides in die Membran (Jacobs und White, 1989, White und Wimley, 1999).

Beide Modelle lassen sich zu einem aus vier Schritten bestehenden thermodynamischen Kreisprozeß kombinieren, bei dem die einzelnen Schritte, die Anlagerung des Polypeptids, die Faltung der Sekundärstruktur, das Eindringen in die Membran und die Assoziation der Sekundärstrukturelemente in die Tertiärstruktur entweder in Wasser, an der Membran-

Wasser-Schnittstelle oder einer Kombination von beidem stattfinden (White und Wimley, 1999). Im Verlauf der vorliegenden Arbeit konnte die Faltung von individuellen α -Helices, sowie Paaren von α -Helices beobachtet werden. Die Faltung erfolgte dabei gegen externe, über ein Rasterkraftmikroskop angelegte Kräfte von bis zu 50 pN (Kessler et al., 2006)⁶.

⁶Die entsprechende Veröffentlichung ist im Anhang abgedruckt.

4 Funktionsweise eines Rasterkraftmikroskopes

4.1 Aufbau und Funktion

Nachdem im vorhergehenden Abschnitt knapp auf den Aufbau von Proteinen eingegangen worden ist, sollen im vorliegenden Kapitel Funktionsweise und Limitationen des von Binnig et al. (Binnig et al., 1986) entwickelten Rasterkraftmikroskopes diskutiert werden. Bei einem Rasterkraftmikroskop (*atomic force microscope - AFM*) wird die auf einem festen und flachen Substrat immobilisierte Probe mit einer sehr feinen Spitze, welche sich am Ende einer Blattfeder (*cantilever*) befindet, abgerastert. Die Bildentstehung erfolgt aufgrund der kurzreichweitigen mechanischen Wechselwirkungen zwischen der Abtastspitze und der Probe. Somit ist es möglich, Proben auch in Flüssigkeit zu untersuchen. Für die Untersuchung biologischer Proben, etwa lebender Zellen, unter nativen Bedingungen ist dies oft eine zwingende Voraussetzung. Abbildung 4 zeigt eine rasterelektronenmikroskopische Aufnahme eines Cantilever-Chips und eine schematische Darstellung der Funktionsweise eines Rasterkraftmikroskopes. Die Federkonstanten von kommerziell erhältlichen Si_3Ni_4 -Cantilevern, wie sie zur Untersuchung biologischer Proben verwendet werden, liegen typischerweise im Bereich von ca. 10 - 200 pN/nm, die Krümmungsradien der Spitzen zwischen 20 und 50 nm. Im einfachsten Fall, dem Modus konstanter Höhe,

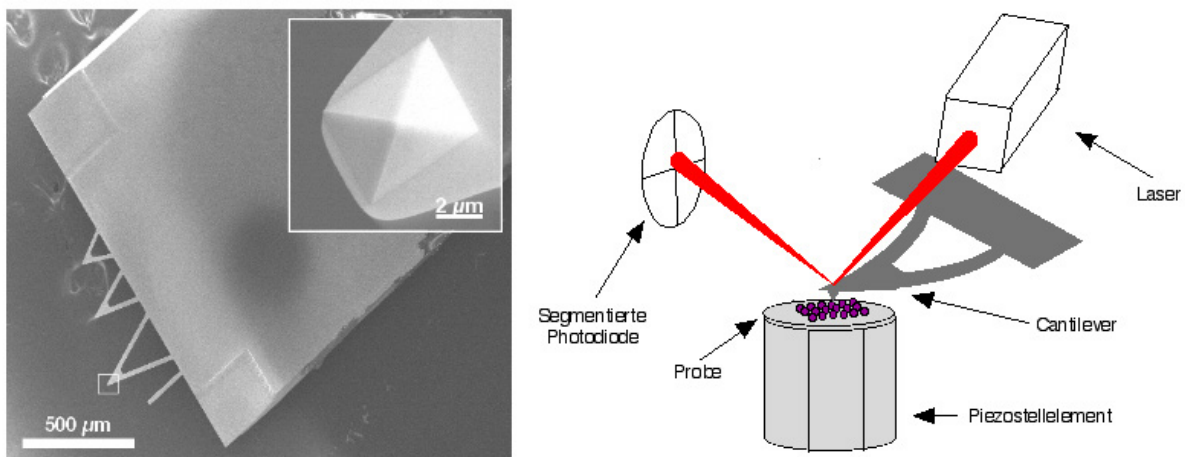


Abbildung 4: Linke Seite: Rasterelektronenmikroskopische Aufnahme eines Cantilever-Chips mit 4 Cantilevern. Der Ausschnitt zeigt eine Detailaufnahme der Spitze des größten dreieckigen Cantilevers. Beide Aufnahmen wurden freundlicherweise von Ferdinand Kühner zur Verfügung gestellt. Rechte Seite: Schematische Darstellung eines Rasterkraftmikroskopes. Mittels einer an die x-Komponente des Piezostellelementes angelegten Dreiecksspannung und einer weiteren in y-Richtung wirkenden Dreiecksspannung niedrigerer Frequenz wird die Probe relativ zur Abtastspitze verschoben und somit zeilenweise abgerastert. Währenddessen wird die Auslenkung des Cantilevers über den Auftreffpunkt des reflektierten Laserstrahles auf der segmentierten Photodiode detektiert.

wird die vertikale Auslenkung des Piezostellelementes während des Abbildungsvorganges konstant gehalten. Die ausgeübte Kraft hängt damit von der lokalen Höhe der Probe ab. Dies ist bei harten, eher flachen und unempfindlichen Proben unproblematisch und ermöglicht relativ hohe Abtastgeschwindigkeiten. Bei empfindlichen Proben, wie den in der vorliegenden Arbeit untersuchten Membranproteinen, ist jedoch eine möglichst nied-

rige und konstante Auflagekraft notwendig. Dies läßt sich dadurch erreichen, daß die Auslenkung des Cantilevers durch elektronische Nachregelung der vertikalen Auslenkung des Piezostellelementes permanent auf einem konstanten, niedrigen Wert gehalten wird. Die gesamte Information über die Probenotopographie liegt bei dem so genannten Modus konstanter Auslenkung somit in der vertikalen Auslenkung des Piezostellelementes.

4.2 Abbildung von Membranproteinen mit submolekularer Auflösung

Der nominelle Krümmungsradius von kommerziellen Cantileverspitzen liegt etwa eine Größenordnung über den lateralen Abmessungen von typischen Membranproteinen⁷. Die Ursache dafür, daß mit manchen Spitzen dennoch submolekulare Auflösung erreicht werden kann, liegt in der Mikrostruktur der Spitze. Aufgrund von Ungenauigkeiten im Herstellungsprozeß weisen die Spitzen oft kleine Erhebungen im Å-Bereich auf, mit deren Hilfe sich aufgrund von sehr kurzreichweitigen Kräften auf flachen Proben sehr hohe Auflösungen erreichen lassen. Die Wechselwirkungen zwischen der unter physiologischen Bedingungen negativ geladenen Membranoberfläche und der ebenfalls negativ geladenen Spitze beruhen im wesentlichen auf Van der Waalsschen und elektrostatischen Kräften. Während erstere im allgemeinen anziehend wirken, können die elektrostatischen Kräfte auch abstoßend wirken und sind außerdem stark von Elektrolytkonzentration und pH-Wert des Puffermediums abhängig. Das Zusammenspiel zwischen elektrostatischen und Van der Waalsschen Kräften läßt sich durch die DLVO-Theorie beschreiben. Die langreichweitigen elektrostatischen Doppelschicht-Kräfte, die keinen Beitrag zur submolekularen Abtastung der Probe liefern (Muller et al., 1999), lassen sich durch Einstellung des pH-Wertes und der Elektrolytkonzentration so justieren, daß sie auf einen relativ großen Bereich der Probenoberfläche wirken. Dadurch lassen sich die vertikalen und lateralen Kräfte, die lokal zwischen Spitze und Probe wirken, weitgehend reduzieren, wodurch die Deformation der Probe minimiert wird.

Zur Modellierung der Abhängigkeit des Abstandes zwischen Spitze und Probenoberfläche von der angelegten Kraft und der Salzkonzentration näherten Müller et al. (Muller, et al., 1999) den der Probe am nächsten stehenden Teil der Spitze durch eine Kugel mit dem Radius R_{glo} an, auf welcher sich eine halbkugelförmige lokale Erhebung vom Radius R_{lok} befindet. Diese lokale Erhebung steht jeweils mit einem einzelnen Protein in Wechselwirkung, das durch eine Kugel mit einem zu R_{lok} vergleichbaren Radius angenähert wird. Die wirkende Kraft $F_{DLVO}^{lok}(z)$ setzt sich hierbei additiv aus der elektrostatischen Komponente $F_{el}(z)$ und der Van der Waalsschen Komponente $F_{vDW}(z)$ zusammen, wobei z den Abstand beider Oberflächen beschreibt. Für die Kraft zwischen zwei Kugeln gilt:

$$F_{DLVO}^{lok}(z) = F_{el}(z) + F_{vDW}(z) = \frac{2\pi\sigma_s\sigma_t R_{lok}\lambda_D}{\epsilon_0\epsilon_c} e^{-z/\lambda_D} - \frac{H_a R_{lok}}{12z^2} \quad (1)$$

(Israelachvili, 1991). Dabei bezeichnen σ_s und σ_t die Oberflächenladungsdichte der Probe und der Spitze, ϵ_0 die elektrische Feldkonstante, ϵ_c die dielektrische Konstante des

⁷Der Durchmesser eines Bakteriorhodopsin-Trimers beträgt ca. 4 nm.

Mediums und H_a die Hamaker Konstante. Die Debye-Hückel-Länge λ_D ergibt sich zu

$$\lambda_D = \sqrt{\frac{\epsilon_0 \epsilon_c k_B T}{e^2 N \sum_i c_i q_i^2}}. \quad (2)$$

Hierbei bezeichnet k_B die Boltzmannkonstante, e die Elementarladung, N die Avogadrokonstante, c_i die Konzentration eines bestimmten Ions und q_i die entsprechende Ladungszahl. Die Debye-Hückel-Länge entspricht derjenigen Entfernung von einer Oberfläche, in der das Potential der elektrischen Doppelschicht auf den e -ten Teil abfällt. Für die Kraft zwischen einer Kugel und einer Ebene gilt nach (Israelachvili, 1991):

$$F_{DLVO}^{glo}(z) = \frac{4\pi\sigma_s\sigma_t R_{glo}\lambda_D}{\epsilon_0\epsilon_c} e^{-z/\lambda_D} - \frac{H_a R_{glo}}{6z^2}. \quad (3)$$

Durch diese Formel läßt sich die langreichweitige Kraft F_{DLVO}^{glo} zwischen dem durch den Krümmungsradius R_{glo} approximierten Teil der Spitze und der Membranoberfläche berechnen. Zusammengenommen ergibt sich für die Summe der kurzreichweitigen Wechselwirkung zwischen der lokalen Erhebung und dem einzelnen Protein nach Gl. 1 und der langreichweitigen Wechselwirkung nach Gl. 3:

$$\begin{aligned} F_{DLVO}(z) &\approx F_{DLVO}^{glo}(z) + 1/2 F_{DLVO}^{lok}(z) \\ &= \frac{4\pi\sigma_s\sigma_t R_{glo}\lambda_D}{\epsilon_0\epsilon_c} e^{-(z+R_{lok})/\lambda_D} - \frac{H_a R_{glo}}{6(z+R_{lok})^2} + \frac{\pi\sigma_s\sigma_t R_{lok}\lambda_D}{\epsilon_0\epsilon_c} e^{-z/\lambda_D} - \frac{H_a R_{lok}}{24z^2} \end{aligned}$$

(Muller, et al., 1999). Hierbei ist zu beachten, daß der durch R_{glo} angenäherte Teil der Spitze um den Betrag R_{lok} weiter von der Probe entfernt ist als der höchste Punkt der lokalen Erhebung.

Aufgrund der Milieu-Abhängigkeit der elektrostatischen Kraft lassen sich die abstandsabhängigen DLVO-Kräfte zwischen Spitze und Membranoberfläche durch Änderung der Elektrolytkonzentration oder des pH-Wertes so einstellen, daß die globale Spitzenoberfläche primär über langreichweitige elektrostatische Wechselwirkungen mit einem größeren Bereich der Membran interagiert. Die näher an der Membranoberfläche befindliche mikroskopische Erhebung wechselwirkt hingegen vor allem über die kurzreichweitigen Van-der-Waals-Kräfte und die Pauli-Abstoßung. Ausgehend von den Werten $R_{glo} = 100$ nm und $R_{lok} = 2$ nm berechneten Müller et al. den Abstand, der sich bei einer Kraft von 200 pN in einer 10 mM Lösung eines monovalenten Salzes (z.B. KCl) zwischen der Probe und der lokalen Erhebung auf der Spitze einstellt, zu 9 nm. In diesem Bereich ist der Gradient der DLVO-Kraft relativ gering und damit sind Änderungen des Abstandes z im Angström-Bereich nicht detektierbar. Bei einer Salzkonzentration von 100 mM KCl reicht hingegen schon eine Kraft von 100 pN dazu aus, z auf 1 nm zu reduzieren.

In der Praxis läßt sich die Abstandsabhängigkeit der Kraft anhand von Kraft-Abstands-Kurven bestimmen. Hierbei wird der Cantilever durch Verschieben des Piezostellelementes in z -Richtung mit dem Substrat in Kontakt gebracht und wieder von diesem getrennt, während die Auslenkung des Cantilevers und die des Piezostellelementes aufgezeichnet werden. Zur Berechnung des Abstandes zwischen Spitze und Oberfläche wird für jeden Datenpunkt die Auslenkung des Cantilevers von der des Piezostellelementes subtrahiert. Die Kraft ergibt sich aus der Multiplikation der Cantileverauslenkung mit

der Federkonstanten. Anhand des Kurvenverlaufes einer Kraft-Abstands-Kurve unmittelbar vor dem Kontakt mit der Membranoberfläche läßt sich gut erkennen, ob eine Spitze prinzipiell für hochauflösende Abbildung geeignet ist. Häufig befinden sich auf einer Cantilever Spitze auch mehrere lokale Erhebungen (Doppelspitze). Aufgrund der sehr geringen Höhenunterschiede auf der Oberfläche von Membranproteinkristallen hilft es hier oft, den Cantilever leicht zu verkippen, um zu erreichen, daß die Oberfläche lediglich von einer solchen Erhebung abgerastert wird. Aufgrund der sehr flachen Oberfläche von Membranproteinkristallen ist zu deren Charakterisierung mittels Rasterkraftmikroskopie auch ein atomar flaches Substrat notwendig; sehr geeignet ist hierzu frisch gespaltener Glimmer.

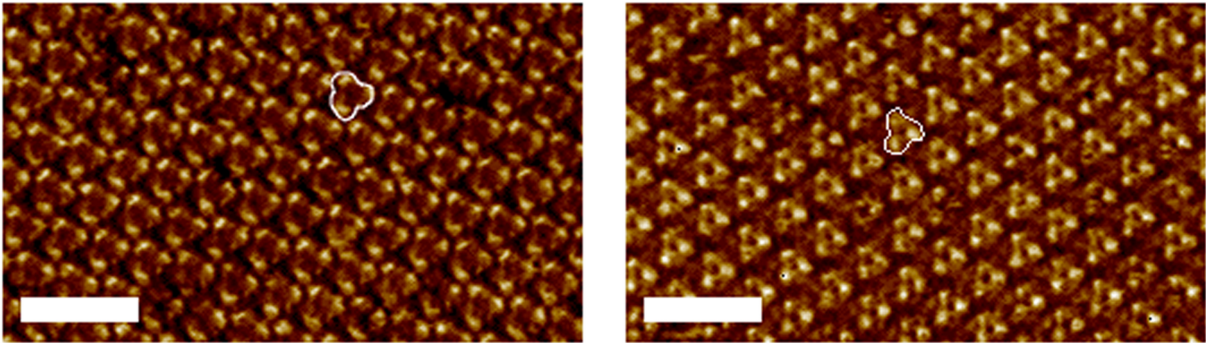


Abbildung 5: Hochaufgelöste Abbildung der zytoplasmatischen (links) und der extrazellulären Oberfläche (rechts) zweier auf Glimmer adsorbierter Bakteriorhodopsin-Kristalle. Beide Aufnahmen erfolgten in Pufferlösung (300 mM KCl, 10 mM Tris, pH 7.8) bei Raumtemperatur bei einer Auflagekraft von etwa 150 pN. Zur Illustration ist jeweils ein Trimer durch eine weiße Umrandung gekennzeichnet. Der Farbbereich von schwarz nach weiß entspricht einer vertikalen Distanz von 1.2 nm (links) bzw. 1.0 nm (rechts), die Breite des weißen Balkens beträgt bei beiden Abbildungen 15 nm.

4.3 Limitierungen der Kraftauflösung

Die Empfindlichkeit und die Dynamik eines Cantilevers werden vorwiegend durch seine Federkonstante k_c und seine Resonanzfrequenz bestimmt. Um eine möglichst hohe Kraftauflösung zu erreichen, muß die vertikale Auslenkung Δz des Cantilevers schon bei kleinen Kräften ausreichend groß sein, um überhaupt detektiert werden zu können. Das erfordert einen weichen Cantilever. Andererseits sollten die durch das thermische Rauschen bedingten Kraftfluktuationen des Cantilevers möglichst gering sein. Im thermischen Gleichgewicht entfällt auf jeden Freiheitsgrad eines Systems nach dem Äquipartitionsprinzip die Energie $k_B T/2$. Für die Grundschiwingung eines Cantilevers gilt somit:

$$\frac{1}{2}k_c \langle z^2 \rangle = \frac{1}{2}k_B T \implies \langle z^2 \rangle = \frac{k_B T}{k_c}, \quad (4)$$

wobei $\langle z^2 \rangle$ die mittlere quadratische Auslenkung bezeichnet. Die mittlere quadratische Fluktuation der Kraft ergibt sich hieraus zu:

$$\langle F^2 \rangle = \langle k_c^2 z^2 \rangle = k_B T k_c$$

und beträgt damit für einen weichen Cantilever ($k_c = 10 \text{ pN/nm}$) etwa 6.5 pN . Aus der Fouriertransformierten $\tilde{z}(\omega)$ der über eine bestimmte Zeitdauer T aufgenommenen Auslenkung $z(t)$ des freien Cantilevers läßt sich über $\tilde{z}(\omega) \cdot \tilde{z}^*(\omega)/T$ das so genannte Intensitätsspektrum des Cantilevers berechnen, wie es exemplarisch in Abbildung 6 dargestellt ist. Aus dem Intensitätsspektrum läßt sich die Federhärte und Resonanzfrequenz eines Cantilevers sehr genau bestimmen, indem man das erste Maximum, das von der thermischen Bewegung dominiert wird (Sarid, 1994), durch eine Lorentzkurve (in der Abbildung rot dargestellt) approximiert und über diese integriert (Butt und Jaschke, 1995, Florin et al., 1995). Unter Ausnutzung des Parsevalschen Theorems, nach dem die Integrale über die Betragsquadrate von $z(t)$ bzw. $\tilde{z}(\omega)$ im Orts- bzw. Frequenzraum identisch sind, gilt für die mittlere thermische Auslenkung des Cantilevers:

$$\langle z^2(t) \rangle = \lim_{T \rightarrow \infty} \frac{1}{T} \int_0^T z(t)z^*(t)dt = \lim_{T \rightarrow \infty} \frac{1}{T} \int_0^T \tilde{z}(\omega)\tilde{z}^*(\omega)d\omega.$$

Aus $\langle z^2(t) \rangle$ ergibt sich damit die Federkonstante nach Gl. 4 zu:

$$k_c = \frac{k_B T}{\langle z^2 \rangle}.$$

Der Vorteil dieser Methode liegt darin, daß durch die Approximation des Intensitätsspek-

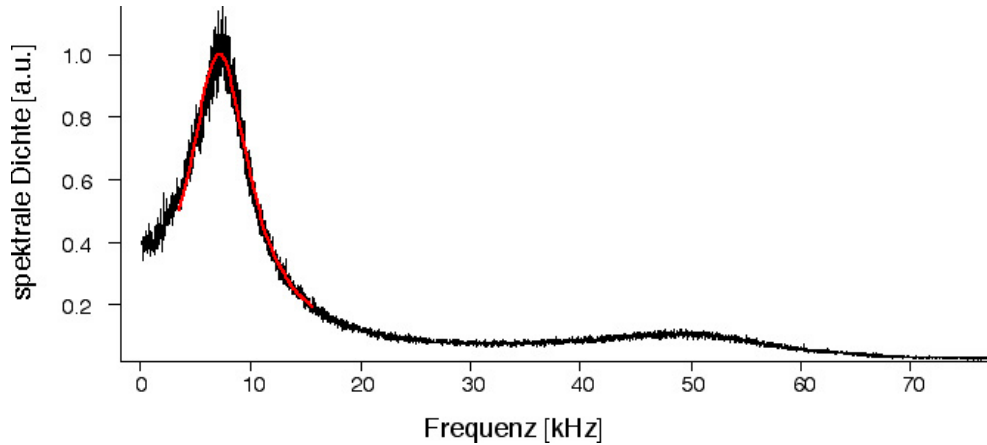


Abbildung 6: Intensitätsspektrum eines OMCL TR400PS-Cantilevers (Olympus, Tokyo, Japan) in Pufferlösung. Es handelt sich um den kürzeren Cantilever dieses Typs, der eine Federkonstante von etwa 90 pN/nm aufweist und für die meisten Messungen, die in dieser Arbeit diskutiert werden, verwendet wurde.

trums durch die Lorentzkurve die nicht-thermischen Beiträge zum Gesamttrauschen weitgehend ausgefiltert werden. Wie aus Abbildung 6 ersichtlich, erstreckt sich das Rauschspektrum eines Cantilevers über den gesamten Frequenzbereich, wobei es im Bereich der Resonanzfrequenz die höchsten Werte annimmt. Das Signal-Rausch-Verhältnis läßt sich damit durch Verwendung eines Tiefpaßfilters, der unterhalb der Resonanzfrequenz einsetzt, verbessern. Eine weitere Verbesserung bietet die Verwendung von Cantilevern mit höherer Resonanzfrequenz, da bei diesen auch der Großteil des thermischen Rauschens

zu höheren Frequenzen verschoben ist. Aufgrund des Niquist-Theorems ist die minimale noch detektierbare Kraft F_{min} bei einer thermisch limitierten Messung durch:

$$F_{min} = \sqrt{4k_B T \gamma B}$$

gegeben (Sarid, 1994, Viani et al., 1999) und hängt damit neben der Temperatur, die sich bei Messungen an biologischen Proben nur bedingt erniedrigen läßt, und der Bandbreite B auch von der viskosen Dämpfung γ ab. Die Dämpfung läßt sich durch die Verringerung der Abmessungen eines Cantilevers reduzieren. Viani et al. (Viani, et al., 1999) erreichten mit solchen kleinen Cantilevern bei gleicher Filterfrequenz wesentlich höhere Kraftauflösung als mit kommerziellen Cantilevern gleicher Federhärte. Der kommerziellen Verwendung solcher kleinen Cantilever stehen derzeit noch die speziellen Anforderungen entgegen, die diese an den optischen Detektionspfad des verwendeten Rasterkraftmikroskopes stellen.

5 Bestimmung der Barrierepositionen

5.1 Elastizität von Polymeren

In diesem Abschnitt soll eine kurze Einführung in die theoretischen Beschreibungsmöglichkeiten des Dehnungsverhaltens von Polymeren unter dem Einfluß einer externen Zugkraft gegeben werden. Bei einem rasterkraftmikroskopischen Entfaltungsexperiment wird die Kraft als Funktion des erzwungenen End-zu-End-Abstandes eines Polymers gemessen. Der Zusammenhang zwischen beiden Meßgrößen ist dabei über eine Reihe von intrinsischen Parametern des Polymers sowie über seine Gesamtlänge, die so genannte Konturlänge, gegeben. Aus der Untersuchung dieser Zusammenhänge anhand von Polymermodellen lassen sich geeignete Fit-Funktionen ableiten, die es ermöglichen die Konturlänge eines Polymers zu bestimmen⁸.

In Abwesenheit einer äußeren Kraft bildet ein Polymer ein permanent unter dem Einfluß von thermischen Anregungen fluktuierendes Knäuel, dessen End-zu-End-Abstand im zeitlichen Mittel sehr viel kleiner ist als seine Konturlänge. Wird nun ein Polymer zwischen dem Cantilever eines Rasterkraftmikroskopes und dem Substrat eingespannt und gestreckt, wird hierdurch zunächst die Anzahl seiner Konfigurationsmöglichkeiten immer weiter eingeschränkt. Das entspricht einer Erniedrigung der Entropie S und resultiert in einer kontraktilen Kraft F , die über die Auslenkung des Cantilevers detektiert werden kann; man spricht von entropischer Elastizität. Die enthalpischen Beiträge, die durch Dehnung von Bindungswinkeln und Bindungen verursacht werden, kommen, wie die Experimente zeigen, erst bei relativ hohen Kräften zu tragen, d.h. wenn sich der erzwungene End-zu-End-Abstand $\langle z \rangle$ der Konturlänge nähert. Auf eine einfache Möglichkeit zur Berücksichtigung der enthalpischen Beiträge in den Näherungsformeln wird weiter unten eingegangen. Der Zusammenhang zwischen einem bestimmten End-zu-End-Abstand und der zu seiner Erzwingung notwendigen Kraft ist durch die Anzahl der Realisierungsmöglichkeiten dieses Abstandes, d.h. der Zustandssumme Z , gegeben:

$$F = -k_B T \left(\frac{\partial \ln Z}{\partial r} \right)_{T,V}, \quad (5)$$

(Tinoco Jr. und Bustamante, 2002). Hierbei bezeichnet k_B die Boltzmannkonstante, T die absolute Temperatur und V das Volumen. Die Zustandssumme beinhaltet die spezifischen Annahmen, die bei der Modellbildung über die Beweglichkeit der einzelnen Monomere gemacht werden und bestimmt damit über Gl. 5 den Verlauf der Kraft als Funktion des erzwungenen End-zu-End-Abstandes.

5.2 Das Modell der frei verbundenen Kette

Als einfachstes Modell sei hier das Modell der frei verbundenen Kette (*freely jointed chain* - *FJC*) erwähnt, bei dem das Polymer durch eine Kette von N gleichartigen Segmenten

⁸Wie experimentell gezeigt, entfalten Membranproteine unter dem Einfluß einer äußeren Kraft schrittweise über eine Reihe von Zwischenzuständen, deren Reihenfolge aufgrund der Verankerung in der Zellmembran der Reihenfolge der Aminosäuresequenz entspricht. Deshalb läßt sich bei bekannter dreidimensionaler Struktur aus den Konturlängen der einzelnen Entfaltungsschritte detailliert berechnen, bis zu welcher Position das Protein jeweils entfaltet wurde. Hieraus lassen sich detaillierte Einsichten in den Zusammenhang zwischen Stabilität und Struktur von Membranproteinen gewinnen.

der Länge l repräsentiert wird, deren Bindungswinkel mit gleicher Wahrscheinlichkeit beliebige Werte annehmen können (vgl. Abbildung 7). Hierbei entspricht das Produkt

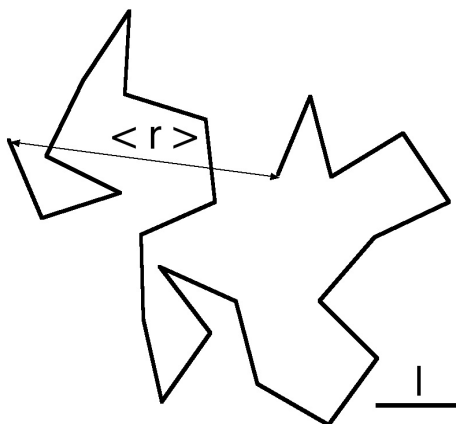


Abbildung 7: Schematische Darstellung einer aus N Teilstücken der Länge l bestehenden, frei verbundenen Kette. Die Winkel zwischen benachbarten Teilstücken können bei diesem Modell beliebige Werte annehmen

$N \cdot l$ der Konturlänge des realen Polymers. Der End-zu-End-Abstand als Funktion der Kraft ist bei diesem Modell durch:

$$\langle r \rangle = N \cdot l \cdot \left(\coth \left(\frac{Fl}{k_B T} \right) - \frac{k_B T}{Fl} \right) = N \cdot l \cdot L \cdot \left(\frac{Fl}{k_B T} \right) \quad (6)$$

gegeben (Hugel und Seitz, 2001). Als Fit-Parameter fungiert die Anzahl N sowie die Länge l der Segmente⁹. Die rechte Seite der Gleichung wurde durch die Einführung der Langevinfunktion: $L = \coth(x) - 1/x$ vereinfacht. Die Segmentlänge stellt ein Maß für die Flexibilität des Polymers dar. Da das Rückgrat eines realen Polymers die vorausgesetzten Bedingungen in der Regel nicht erfüllt, entspricht l nicht einfach der realen Bindungslänge der Kohlenstoff-Atome, sondern muß so angepaßt werden, daß die gemessenen Daten optimal repräsentiert werden. Das FJC-Modell eignet sich gut zur Beschreibung von sehr flexiblen Polymeren, wie z.B. einzelsträngiger DNS oder PEG (Polyethylenglycol). Zu dem Modell der frei verbundenen Kette existieren eine Reihe von Weiterentwicklungen, die hier lediglich am Rande erwähnt werden sollen. Dazu gehört das Modell der frei rotierenden Kette (*freely rotating chain* - *FRC*), bei dem Segmente gleicher Länge um fest vorgegebene Bindungswinkel rotieren, und das Modell der elastisch verbundenen Kette (*elastically jointed chain* - *EJC*), bei dem gleich lange Segmente durch Bindungen mit definierter Steifigkeit verbunden sind (Livadaru et al., 2003).

5.3 Das Modell der wurmartigen Kette

Im Gegensatz zu dem Modell der frei verbundenen Kette und dessen Erweiterungen beschreibt das 1949 von Kratky und Porod (Kratky und Porod, 1949) vorgestellte Modell der

⁹Der typische Verlauf einer FJC-Kurve ist in Abbildung 9 im folgenden Abschnitt dargestellt.

wurmartigen Kette (*wormlike chain - WLC*), das sich gut zur Beschreibung des Dehnungsverhaltens von Polypeptiden (Rief et al., 1997) und doppelsträngiger DNA (Livadaru, et al., 2003) eignet, ein Polymer als kontinuierliche Raumkurve mit endlicher Biegesteifigkeit (siehe Abbildung 8). Der differentielle Beitrag eines durch den Tangentenvektor \mathbf{t}

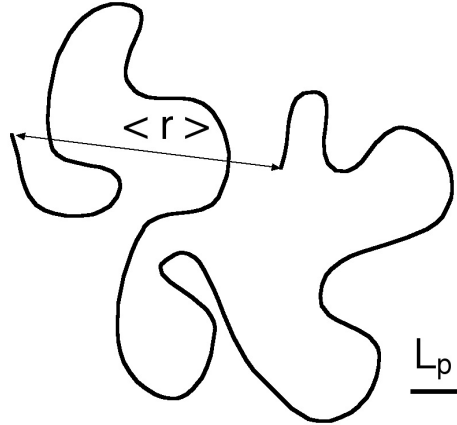


Abbildung 8: Schematische Darstellung einer wurmartigen Kette. Bei diesem Modell, das sich zur Beschreibung des Dehnungsverhaltens von Polypeptiden bewährt hat, wird das Polymer durch eine kontinuierliche Raumkurve beschrieben, deren entropische Elastizität durch die Persistenzlänge L_p und die Konturlänge vollständig bestimmt ist.

charakterisierten, infinitesimalen Teilstückes zu der gesamten Energie einer bestimmten Konfiguration des Polymers ist umgekehrt proportional zum Quadrat des Krümmungsradius und läßt sich durch den Term:

$$e_b(s) = \frac{A}{2} \left| \frac{d\mathbf{t}(s)}{ds} \right|^2 = \frac{A}{2R^2} \quad (7)$$

beschreiben (Bouchiat et al., 1999, Marko und Siggia, 1995). Hierbei bezeichnet s die Bogenlänge, R den Krümmungsradius und A die Biegesteifigkeit. A hängt über die Gleichung $A = L_p k_B T$ mit der Persistenzlänge L_p und der Temperatur zusammen. Die Persistenzlänge ist ein Maß für die durchschnittliche Wegstrecke, über die die Korrelation der Tangenten zweier Punkte verschwindet. Sie ist als intrinsischer Parameter von der Konturlänge unabhängig. Bei einem realen Polypeptid ist die Persistenzlänge durch Interaktionen der Seitenketten und daraus resultierenden Einschränkungen der Rotationsmöglichkeiten um einzelne Bindungen bedingt (Flory, 1988). Die Gesamtenergie einer bestimmten Konformation ergibt sich nun aus dem Wegintegral über Gl. 7 abzüglich der in Zugrichtung wirkenden Komponente einer externen Kraft F zu:

$$E_{WLC} = \int_0^{L_0} \left(\frac{A}{2} \left| \frac{d\mathbf{t}(s)}{ds} \right|^2 - F \cos \Theta(s) \right) ds.$$

Hierbei bezeichnet $\cos \Theta(s)$ den Winkel zwischen dem Teilstück $\mathbf{t}(s)$ und der Zugrichtung, die in Richtung der z -Achse angenommen wurde. Da eine analytische Lösung des WLC-Modells nicht möglich ist, bedient man sich zur Bestimmung der Konturlänge L_0 aus

Kraft-Abstands-Kurven in der Praxis oft der Näherungsformel von Bustamante et al.:

$$F(r) = \frac{k_B T}{L_p} \left(\frac{1}{4(1 - r/L_0)^2} - \frac{1}{4} + \frac{r}{L_0} \right) \quad (8)$$

(Bustamante et al., 1994), welche die numerische Lösung an den Grenzwerten $r \rightarrow 0$ und $r \rightarrow L_0$ exakt widerspiegelt. Für die Beschreibung der Elastizität von Polypeptiden hat sich für die Persistenzlänge L_p ein Wert von 0.4 nm bewährt (Rief et al., 1997). Da alle sonstigen Parameter auf der rechten Seite der Gleichung bekannt sind, bleibt die Konturlänge als eigentlicher Fit-Parameter. Die Abweichungen der Näherung nach Gl. 8 von der exakten Lösung wirken sich bei Auslenkungen in der Größenordnung der halben Konturlänge am stärksten aus und lassen sich durch ein von Bouchiat et al. entwickeltes Korrekturpolynom mit den Koeffizienten α_i ¹⁰ weitestgehend kompensieren:

$$F(r) = \frac{k_B T}{L_p} \left(\frac{1}{4(1 - r/L_0)^2} - \frac{1}{4} + \frac{r}{L_0} + \sum_{i=2}^{i \leq 7} \alpha_i \left(\frac{z}{L_0} \right)^i \right) \quad (9)$$

(Bouchiat, et al., 1999). Da diese Abweichungen, wie auch aus Abbildung 9 ersichtlich, überwiegend einen relativ niedrigen Kraftbereich betreffen und zudem relativ gering sind, spielen sie für die Analyse von AFM-Experimenten in der Praxis keine große Rolle. Für die Auswertung der in dieser Arbeit präsentierten Daten wurde daher ausschließlich Gl. 8 verwendet.

5.4 Enthalpische Beiträge zur Elastizität von Polymeren

Durch elastische Verformungen des Polymerrückgrates verursachte enthalpische Beiträge zu der Rückstellkraft des Polymers werden beim FJC-Modell nicht berücksichtigt. Bei dem WLC-Modell erfolgt dies nur insoweit, als daß der Konformationsraum durch die dem Konzept der Persistenzlänge zugrunde liegende Biegesteifigkeit eingeschränkt wird (Rief, 1997). Eine Überstreckung des Rückgrates, wie sie bei realen Polymeren möglich ist, wird von keinem der beiden Modelle berücksichtigt. Da die Dehnung von Bindungswinkeln und Bindungsabständen erst bei Auslenkungen nahe der Konturlänge erfolgt, lassen sich die Kraftkurven, wie auch im Experiment gezeigt, in Bereiche mit überwiegend entropischer und überwiegend enthalpischer Elastizität aufteilen. In den Kraft-Abstands Relationen Gl. 6 und Gl. 8 kann die Überstreckung des Rückgrates in guter Näherung durch die additive Erweiterung der relativen Auslenkung um einen Beitrag Hookscher Elastizität beschrieben werden, wobei k die Federkonstante bezeichnet. Damit wird aus Gl. 6:

$$\langle r \rangle = N \cdot l \cdot L \cdot \left(\frac{Fl}{k_B T} \right) + \frac{N}{k} \cdot F$$

(Rief, 1997). Für das WLC-Modell erhält man nach (Hugel und Seitz, 2001) nach der Einführung der normalisierten Federkonstante K_0 ¹¹ aus Gl. 8:

$$F(r) = \frac{k_B T}{L_p} \left(\frac{1}{4(1 - r/L_0 + F/K_0)^2} - \frac{1}{4} + \frac{r}{L_0} - \frac{F}{K_0} \right).$$

¹⁰Die Koeffizienten lauten: $\alpha_2 = -0.5164228$, $\alpha_3 = -2.737418$, $\alpha_4 = 16.07497$, $\alpha_5 = -38.87607$, $\alpha_6 = 39.49944$ und $\alpha_7 = -14.17718$.

¹¹Wobei gilt: $K_0 = k \cdot L$

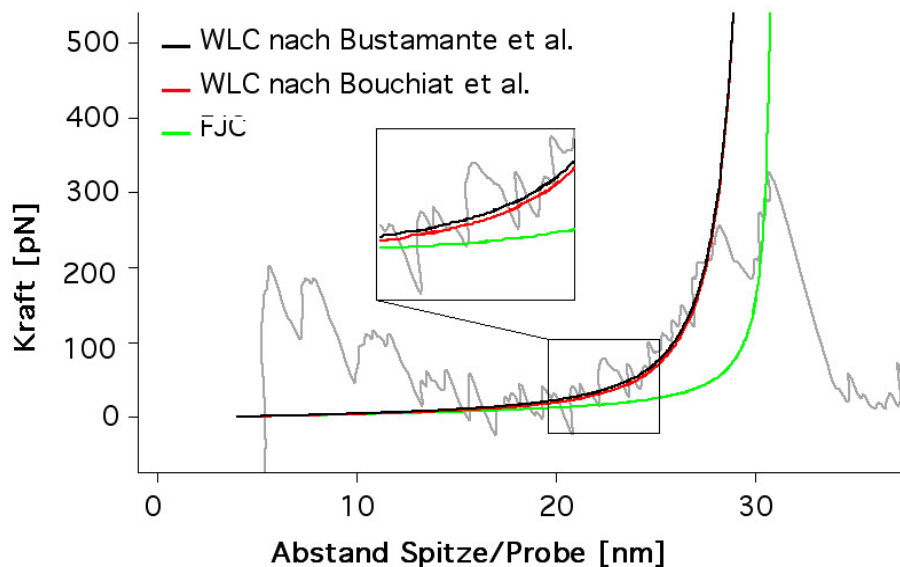


Abbildung 9: Vergleich des FJC-Modells nach Gl.6 mit dem WLC-Modell nach Bustamante et al. (Bustamante et al., 1994) (Gl. 8) und dem korrigierten WLC-Modell nach Gl. 9. Der Anfangsbereich der Kraft-Abstands-Kurve eines einzelnen, vom C-Terminus her entfalteten Bakteriorhodopsin-Monomers ist grau dargestellt. Die dargestellten Modell-Kurven weisen eine Konturlänge von 31 nm auf; dies entspricht der Länge von 86 Aminosäuren. Es ist zu erkennen, daß die Rückstellkraft bei der FJC-Kurve verglichen mit den WLC-Kurven erst bei höheren Auslenkungen signifikant ansteigt und diese den Verlauf der Meßdaten wesentlich besser widerspiegeln.

5.5 Bestimmung der Entfaltungszwischenzustände

Membranproteine entfalten unter dem Einfluß einer an einen der Termini angelegten äußeren Kraft schrittweise über eine Reihe von Zwischenzuständen (Abbildung 11). Da die angelegte Kraft aufgrund der Verankerung der α -Helices bzw. der β -Faltblätter in der Membran jeweils am letzten Strukturelement angreift, das noch nicht entfaltet ist, entspricht die Reihenfolge der Entfaltungsereignisse der Aminosäuresequenz. Die Position innerhalb der dreidimensionalen Struktur, bis zu der ein Membranprotein jeweils entfaltet ist, läßt sich deshalb prinzipiell über die gefittete Konturlänge des entsprechenden Entfaltungspeaks bestimmen.

Hierbei ist allerdings der Einfluß zu berücksichtigen, den der Abstand zwischen der Oberfläche der Membran und dem Punkt, bis zu dem das Polypeptid jeweils entfaltet ist, auf den Verlauf der resultierenden Kraft-Abstands-Kurve ausübt. Da anzunehmen ist, daß der Konformationsraum des bereits entfalteten Teils eines Polypeptids innerhalb der Membran stark eingeschränkt ist, wurde dieser Teil, wie in Abbildung 10a dargestellt, als gestreckt angenommen und nicht in die Berechnung der entropischen Elastizität einbezogen. In diesem Fall gilt für die gemessene Konturlänge $L_m = L_0 - d_{aa}$. Dabei bezeichnet L_0 die Zahl der entfalteten Aminosäuren und d_{aa} die Anzahl der Aminosäuren, die die Distanz d überbrücken. Die Distanz d bezeichnet hierbei die Strecke zwischen dem Punkt, bis zu dem das Molekül entfaltet ist, und der Membranoberfläche. Da eine einzelne Aminosäure im Rückgrat des Polypeptids eine Länge von 0.36 nm einnimmt, gilt: $d_{aa} = d/0.36$ nm. Zu Kontrollzwecken und zur Abschätzung der Fehler dieser Vorgehensweise wurde

eine Anzahl von Kraft-Abstands-Kurven zusätzlich unter der Annahme analysiert, daß die Beweglichkeit des Polypeptids innerhalb der Membran nicht eingeschränkt ist (siehe Abbildung 10b). In diesem Fall entspricht die gemessene Konturlänge der Anzahl der entfalteten Aminosäuren $L_m = L_0$, allerdings weist die zugehörige WLC-Kurve in horizontaler Richtung einen Offset von d auf.

Die aus beiden Ansätzen resultierenden WLC-Kurven sind in Abbildung 10c im Vergleich dargestellt. Dabei wurde ein Polypeptid mit einer Gesamtlänge von 28.3 Aminosäurelängen angenommen, das 3 nm unter der Membranoberfläche verankert ist. Es ist zum einen zu erkennen, daß die Kraft im Falle des innerhalb der Membran als unflexibel angenommenen Polypeptids (rote Kurve) später ansteigt, was daran liegt, daß die zur Überbrückung von d dienenden Aminosäuren hier als bereits gestreckt angenommen werden. Zum anderen sind die Unterschiede der beiden Modelle (die bei wachsender Länge des freien Polypeptidstranges weiter abnehmen) relativ gering.

In der Praxis ist der Punkt, bis zu dem das Polypeptid jeweils entfaltet, nicht von vornherein bekannt, sondern soll aus den gemessenen Kraft-Abstands-Kurven bestimmt werden. Dazu wurde zunächst der Abstand d jeder einzelnen Aminosäure von derjenigen Membranoberfläche, von der aus das Protein entfaltet wurde, anhand des Strukturmodells von Essen et al. (Essen et al., 1998) berechnet. Bei der Analyse der Meßwerte nach der in Abbildung 10a dargestellten Methode wurde aus allen möglichen Verankerungspunkten derjenige bestimmt, für den die Abweichung zwischen dem nach $L_m = L_0 - d_{aa}$ berechneten Wert der Konturlänge und dem gefitteten Wert am geringsten ist. Zum Vergleich wurden die Meßdaten zusätzlich unter der in Abbildung 10b skizzierten Annahme ausgewertet. Hierbei entspricht die Konturlänge der theoretischen WLC-Kurve der Anzahl der bereits entfalteten Aminosäuren, weist jedoch einen horizontalen Offset von $-d$ auf. Als Verankerungspunkt wurde jeweils diejenige Aminosäure angenommen, für die die beste Übereinstimmung zwischen den berechneten Kurven und den Meßwerten erzielt wurde.

Der Vergleich beider Verfahren anhand der Güte der Fits an die vorhandenen Meßdaten¹² zeigt zweierlei auf: Zum einen erfordert die experimentelle Bestimmung des Fluktuationsverhaltens innerhalb der Membran eine deutliche Verbesserung des Signal-Rausch-Verhältnisses des Versuchsaufbaus. Zum anderen kommen hier die Limitationen des WLC-Modells in bezug auf die realistische Beschreibung des Dehnungsverhaltens von realen Polypeptiden zu tragen. Die Abweichungen der nach beiden Verfahren berechneten Verankerungspunkte liegen in jedem Fall innerhalb der geschätzten Fehlergrenzen von etwa 3 Aminosäuren. Da die Annahme, daß das Polypeptid durch die umgebende Membran nicht beeinflußt wird, wenig realistisch anmutet, wurde die in Abbildung 10a dargestellte Methode favorisiert¹³. Wesentliche Erkenntnisse über das Fluktuationsverhalten innerhalb der Membran sind von derzeit durchgeführten Molekulardynamiksimulationen des kraftinduzierten Entfaltens von Bakteriorhodopsin zu erwarten. Im Zusammenhang mit

¹²Dieser Vergleich erfolgte anhand des Datensatzes, der der im Anhang abgedruckten Veröffentlichung „Unfolding barriers in Bakteriorhodopsin probed from the cytoplasmic and the extracellular side by AFM“, (Kessler und Gaub, 2006) zugrunde liegt.

¹³Es ist hier anzumerken, daß die Angaben zu den Positionen von Verankerungspunkten, die in den drei ersten im Anhang abgedruckten Veröffentlichungen gemacht wurden, auf einer vereinfachten und weniger exakten Version des in Abbildung 10a dargestellten Verfahrens beruhen. Zur Bestimmung der Position von Verankerungspunkten, die auf der extrazellulären Seite der Membran vermutet wurden, wurden hier lediglich 11 Aminosäuren zu der gemessenen Konturlänge addiert, um die Dicke der Membran (~ 4 nm) zu kompensieren.

verbesserten theoretischen Ansätzen zur Beschreibung des Dehnungsverhaltens von Polymeren ließen sich die Ungenauigkeiten bei der Bestimmung der Verankerungspunkte weiter reduzieren. In Abbildung 11 ist das typische Entfaltungsspektrum von Bakteriorhodopsin exemplarisch anhand einer zytoplasmatischen sowie einer extrazellulären Kraft-Abstands-Kurve dargestellt. In beiden Fällen treten bestimmte Peaks bei allen gemessenen Kurven auf (bei zytoplasmatischen Kurven sind dies 86, 147 und 216 aa, bei extrazellulären 83, 133 und 225 aa). Diese Peaks werden fortan als Hauptpeaks bezeichnet, während solche Peaks, die nicht immer auftreten, als Nebenpeaks bezeichnet werden. Die beiden abgebildeten Kurven zeigen lediglich einen Teil der möglichen Nebenpeaks. Eine vollständige Beschreibung dieser Peaks findet sich in der im Anhang befindlichen Veröffentlichung (Kessler und Gaub, 2006). Hierbei ist anzumerken, daß im Falle einer zytoplasmatischen Kurve die Anzahl der jeweils entfalteten Aminosäuren von der Gesamtzahl der

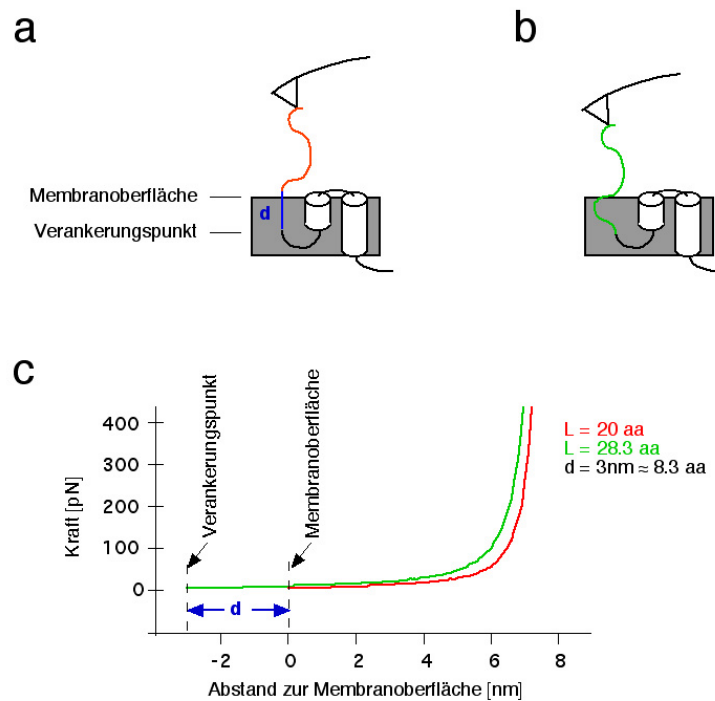


Abbildung 10: Vergleich der beiden Ansätze zur Berücksichtigung des Abstandes des Verankerungspunktes von der Membranoberfläche. a: Schematische Darstellung der Situation unter der Annahme, daß der (blau dargestellte) bereits entfaltete Teil des Polypeptids aufgrund der Einschränkung seiner Konformationsmöglichkeiten innerhalb der (grau dargestellten) Membran nicht fluktuieren kann und somit nicht zur entropischen Elastizität beiträgt. b: Schematische Darstellung eines Polypeptids, dessen entfalteter Teil (grün) auch in der Membran frei fluktuieren kann. c: Vergleich beider Ansätze anhand von berechneten WLC-Kurven. Für den Abstand d des Verankerungspunktes von der Membranoberfläche wurde ein Wert von 3 nm, für die Persistenzlänge 0.4 nm und für die Konturlänge 28.3 aa angenommen. Hierbei bezeichnet aa die Länge einer Aminosäure (0.36 nm). In dem in a skizzierten Fall (rote Kurve) befinden sich etwa 8.3 aa ($3 \text{ nm}/0.36 \text{ nm}$) des Polypeptids innerhalb der Membran, dadurch reduziert sich der Wert für die Konturlänge, der in die WLC-Kurve eingeht, zu 20 aa. In dem in b skizzierten Fall (grüne Kurve) hat die Position des Verankerungspunktes keinen Einfluß auf die Konturlänge. Die WLC-Kurve weist jedoch aufgrund der Verschiebung des Verankerungspunktes in horizontaler Richtung einen Offset von ~ 3 nm auf.

vorliegenden Aminosäuren (248) subtrahiert werden muß, um die Position der jeweils als Verankerungspunkt fungierenden Aminosäure innerhalb der Sequenz zu bestimmen. Die Zwischenzustände, in denen das Molekül bei den Hauptpeaks vorliegt, korrelieren damit mit Minima in der Energielandschaft, die von jedem auftretenden Entfaltungspfad durchlaufen werden. Interessanterweise repräsentieren die Hauptpeaks von C-terminalen Kraft-Abstands-Kurven diejenigen Fälle, in denen Bakteriorhodopsin jeweils bis zum C-terminalen Ende einer Helix entfaltet ist, bei der dieses Ende auf der zytoplasmatischen Seite liegt (siehe Abbildung 11a). Der Weg von einem Hauptpeak zum nächsten repräsentiert somit die Entfaltung eines Helixpaares (*helical hairpin*), während die Nebenpeaks fakultative Zwischenzustände repräsentieren, die bei der Entfaltung dieses Helixpaares auftreten können (Muller et al., 2002).

Dieses Bild gilt entsprechend für N-terminale Kraft-Abstands-Kurven. Hier korrelieren die Hauptpeaks mit Ausnahme des letzten Peaks, mit Zuständen, in denen das Molekül bis zum N-terminalen Ende einer Helix entfaltet ist, bei der dieses Ende auf der extrazellulären Seite liegt. Auffälligerweise entfaltet jedoch Helix G zusammen mit Helix F so, daß das extrazelluläre Ende von Helix G keinen Peak im Entfaltungsspektrum verursacht. Der letzte Hauptpeak bei einer Abrißlänge von 223 Aminosäuren spiegelt die Extraktion des aus 23 Aminosäuren bestehenden C-Terminus aus der Membran wider.

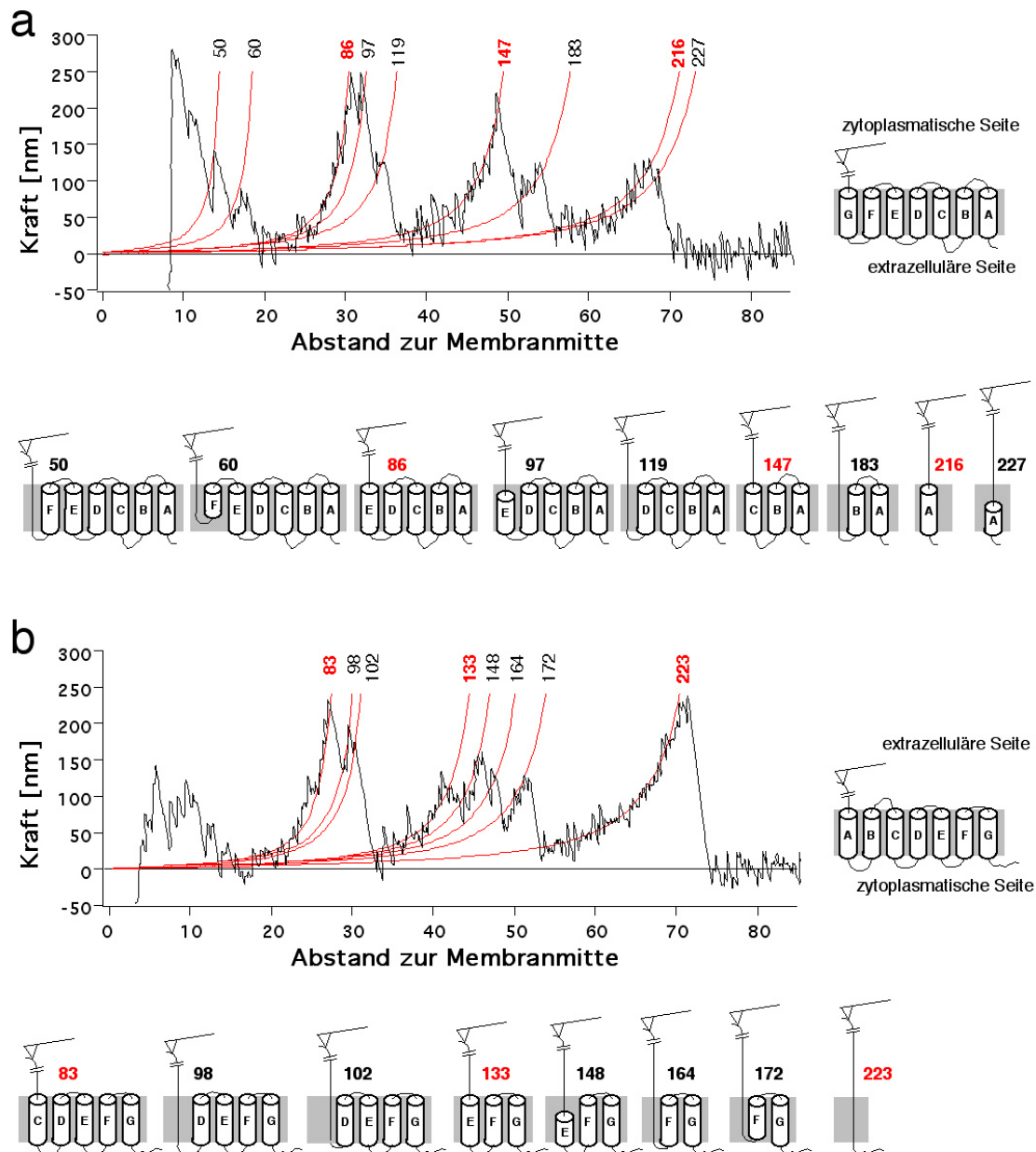


Abbildung 11: Kraft-Abstands-Kurve eines einzelnen, vom C-Terminus (a) bzw. vom N-Terminus (b) her entfalteten Bakteriorhodopsin-Monomers. Die Ausgangssituation ist jeweils rechts neben den Kraft-Abstands-Kurven schematisch dargestellt. Die Ziffern über den WLC-Kurven entsprechen der Anzahl der jeweils entfalteten Aminosäuren, die, wie im Text erläutert, unter der Annahme berechnet wurde, daß das Polypeptid innerhalb der (grau dargestellten) Membran nicht fluktuieren kann. Die Zwischenzustände, bis zu denen das Protein jeweils entfaltet ist, sind unter der jeweiligen Kraft-Abstands-Kurve schematisch dargestellt. Diejenigen Peaks, die bei allen Meßkurven auftreten, und die Zwischenzustände sind durch rote Beschriftung gekennzeichnet. Beide Kraft-Abstands-Kurven wurden mit einer Zuggeschwindigkeit von $1.4 \mu\text{m/s}$ in 20 mM Tris, 300 mM KCl bei pH 7.8 aufgenommen.

6 Charakterisierung der Energielandschaft

6.1 Übergangsraten zwischen Faltungszuständen

Im vorhergehenden Kapitel wurde dargestellt, wie mit Hilfe des WLC-Modells aus dem kraftabhängigen Dehnungsverhalten eines Polypeptidstranges dessen Länge bestimmt werden kann, und wie sich im Falle eines Membranproteins hieraus die Position ermitteln läßt, bis zu der es jeweils entfaltet ist. Im vorliegenden Kapitel soll nun gezeigt werden, wie aus der Abhängigkeit der Verteilungsfunktion der Abrißkraft eines bestimmten Peaks von experimentell beeinflussbaren Parametern grundlegende Eigenschaften der Potentiallandschaft erschlossen werden können. Das zu diesem Zweck hier vorgestellte Zwei-Zustands-Modell eignet sich neben der Beschreibung der Entfaltungskinetik von Proteinen auch zur Beschreibung von kraftinduzierten Konformationsübergängen im Rückgrat von Polymeren, wie sie z.B. bei Dextran beobachtet wurden, und zur Beschreibung der Entfaltungskinetik von Rezeptor-Ligand-Paaren. Die Ableitung dieses Zwei-Zustand-Modells wurde in wesentlichen Zügen aus (Rief et al., 1998) und (Rief, 1997) adaptiert.

Generell beruhen die Bindungen zwischen und innerhalb von Biomolekülen zumeist auf schwachen nicht-kovalenten Wechselwirkungen und brechen, verursacht durch thermische Fluktuationen, schon unter dem Einfluß geringer Zugkräfte auf, sofern diese nur lange genug wirken (Evans und Ritchie, 1997). Übertragen auf die Proteinfaltung bedeutet dies, daß die freie Enthalpie des gefalteten Zustandes nur geringfügig unter der des ungefalteten Zustandes liegt. Beide Zustände nehmen lokale Minima in der Energielandschaft ein. Die hochkomplexe Energielandschaft eines realen Proteins wird in der folgenden Betrachtung durch ein einfaches schematisches Modell repräsentiert, indem, wie in Abbildung 12 dargestellt, die freie Enthalpie entlang einer eindimensionalen Reaktionskoordinate betrachtet wird, die der Richtung der Zugkraft entspricht. Der Übergang zwischen den beiden durch eine Energiebarriere getrennten Zuständen ist durch die Entfaltungsrates k_u^0 und die Faltungsrates k_f^0 bestimmt, die sich aus der Arrhenius-Gleichung zu:

$$k_f^0 = \omega \cdot e^{-\frac{\Delta G_f^*}{k_B T}} \quad \text{und} \quad k_u^0 = \omega \cdot e^{-\frac{\Delta G_u^*}{k_B T}} \quad (10)$$

ergeben. Dabei bezeichnet ω die so genannte Probiefrequenz. Die beiden Parameter ΔG_f^* und ΔG_u^* bezeichnen die Differenz der freien Enthalpie zwischen dem gefalteten beziehungsweise dem ungefalteten Zustand und dem Übergangszustand. Die Probiefrequenz ω entspricht nach der Kramers-Theorie dem Kehrwert der mittleren Diffusionszeit τ_D , die das Protein benötigt, um von den beiden lokalen Energieminima aus den Übergangszustand zu erreichen (Evans und Ritchie, 1997, Rief et al., 1998).

Der Einfluß einer externen Zugkraft F wirkt sich nach der linearen Approximation nach Bell (Bell, 1978) in einer Reduktion von ΔG_u^* um den Faktor $F \cdot x_u$ aus, wobei x_u die Breite der Aktivierungsbarriere bezeichnet¹⁴. Dies entspricht einem Verkippen der Energielandschaft. Für die Entfaltungsrates ergibt sich somit:

$$k_u(F) = \omega \cdot e^{-\frac{(\Delta G_u^* - F \cdot \Delta x_u)}{k_B T}} = k_u^0 \cdot e^{\frac{F \cdot \Delta x_u}{k_B T}}. \quad (11)$$

¹⁴Hierbei wird vernachlässigt, daß sowohl Δx_u als auch Δx_f von F abhängen. Dies ist gerechtfertigt, so lange die Zustände eine verglichen mit der Konturlänge geringe Dehnung erfahren (vgl. (Schwaiger, 2005)).

Analog dazu erhöht sich der Wert für ΔG_f^* , was in einer Verringerung der Faltungsrates um den Faktor $F \cdot x_f$ resultiert:

$$k_f(F) = \omega \cdot e^{-\frac{(\Delta G_f^* + F \cdot \Delta x_f)}{k_B T}} = k_f^0 \cdot e^{-\frac{F \cdot \Delta x_f}{k_B T}}. \quad (12)$$

Sobald also die angelegte Kraft einen bestimmten Wert überschreitet, findet praktisch keinerlei Faltung mehr statt. Bei Potentials, deren Δx_f deutlich größer ist als Δx_u , ist dies schon bei kleinen Kräften der Fall.

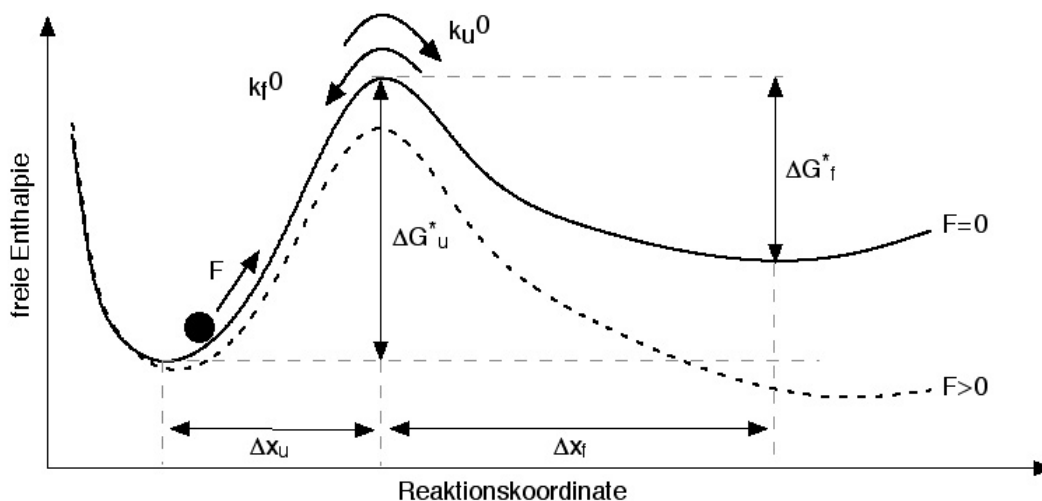


Abbildung 12: Verlauf der freien Enthalpie entlang des End-zu-End-Abstandes als Reaktionskoordinate. Der Übergang zwischen den beiden auf verschiedenen Niveaus der freien Enthalpie liegenden Faltungszuständen eines Moleküls (durchgezogene Kurve) läßt sich durch das Zwei-Zustands-Modell beschreiben. Die natürliche Entfaltungsrate k_u^0 und die Faltungsrate k_f^0 entsprechen der pro Sekunde auftretenden Anzahl der Faltungs- und Entfaltungsvorgänge in Abwesenheit einer äußeren Kraft. Der Einfluß einer auf das Protein wirkenden Zugkraft läßt sich in erster Näherung durch ein Verkippen der Energielandschaft beschreiben (gestrichelte Kurve). Jede mögliche Konformation eines Moleküls ist in dieser Betrachtungsweise durch einen Punkt gegeben.

6.2 Bestimmung der Potentialparameter mit Hilfe von Monte-Carlo-Simulationen

Wird die an eine bestimmte gefaltete Struktur angelegte Kraft kontinuierlich erhöht, gilt für die Wahrscheinlichkeit, daß die Entfaltung in einem bestimmten Kraftintervall dF auftritt:

$$dP_u = k_u(F) \cdot dF. \quad (13)$$

Wobei lediglich vorausgesetzt wird, daß die Entfaltung nicht bereits aufgetreten ist. Mit Hilfe der Zusammenhänge Gl. 10 - Gl. 13 läßt sich die Verteilungsfunktion der Abrißkräfte, wie sie auch in Entfaltungsexperimenten gemessen wird, über Monte-Carlo-Simulationen

ermitteln (Rief et al., 1998). Hierzu geht man von einer geringen Anfangsauslenkung x aus, die in den Zeitschritten Δt schrittweise um den Betrag

$$\Delta x = v \cdot \Delta t$$

erhöht wird, wobei v die Geschwindigkeit des Piezostellelementes bezeichnet. Nach jedem Schritt wird die anliegende Kraft nach dem WLC-Modell berechnet und hieraus nach Gl. 11 und Gl. 13 die Entfaltungsrates bestimmt. Anschließend wird aufgrund einer Zufallszahl entschieden, ob der Abriß (bei der gerade angelegten Kraft) auftritt oder nicht. Die Kraft, bei der die Barriere, durch die thermischen Fluktuationen bedingt, überschritten wird, wird als Entfaltungskraft gespeichert. Es ist hierbei notwendig, den Wert für Δt niedrig genug zu wählen, so daß dP_u stets deutlich kleiner als eins ist und somit eine ausreichende Zahl von Simulationsschritten durchlaufen wird. Die Parameter Δx_u und k_u^0 lassen sich durch die Anpassung von simulierten Abrißkraftverteilungen an gemessene Kraftverteilungen bestimmen. Für Bakteriorhodopsin wurde dies für die unterschiedlichen Entfaltungspfade der drei Hauptpeaks bei 86 aa, 147 aa und 216 aa durchgeführt (Janovjak et al., 2004)¹⁵. Zur Illustration ist in Abbildung 13 eine nach der beschriebenen Methode simulierte Kraftverteilung im Vergleich zu einer analytisch bestimmten Kraftverteilung dargestellt, deren Ableitung im nächsten Abschnitt erfolgt.

6.3 Analytische Berechnung der Verteilungsfunktion der Abrißkräfte

Die Wahrscheinlichkeitsverteilung der Abrißkräfte läßt sich alternativ auch analytisch berechnen. Dazu wird im folgenden die Wahrscheinlichkeit, daß die Entfaltung bis zu einem bestimmten Zeitpunkt t stattfindet, als P_u bezeichnet. Die Wahrscheinlichkeit, daß das Protein bis zu diesem Zeitpunkt noch nicht entfaltet ist beträgt somit $1 - P_u$, woraus sich die Wahrscheinlichkeit, daß die Entfaltung im Zeitintervall dt auftritt zu

$$dP_u = (1 - P_u) \cdot k_u(t) \cdot dt$$

ergibt. Durch Integration unter der Randbedingung $P_u(0) = 0$, d.h. ausgehend von dem gefalteten Zustand zum Zeitpunkt $t=0$, ergibt sich nach Division durch den Faktor $(1 - P_u)$ zunächst:

$$\ln(1 - P_u)|_0^{P_u(t)} = - \int_0^t k_u(t') \cdot dt'$$

und nach Einsetzen beider Seiten der Gleichung in die Exponentialfunktion schließlich:

$$P_u(t) = 1 - \exp\left(- \int_0^t k_u(t') \cdot dt'\right).$$

Aus dieser zeitabhängigen Beschreibung der Abrißkraftverteilung läßt sich durch die Einführung einer zu t proportionalen Zugkraft $F(t) = v_p k_c t$ die kraftabhängige Gleichung

$$P_u(F) = 1 - \exp\left(- \frac{1}{v_p k_c} \int_0^F k_u(F') \cdot dF'\right)$$

¹⁵Die entsprechende Veröffentlichung ist im Anhang abgedruckt.

herleiten. Hieraus ergibt sich die Wahrscheinlichkeitsdichte zu:

$$\frac{P_u(F)}{dF} = \frac{1}{v_p k_c} \cdot k_u(F) \cdot \exp\left(-\frac{1}{v_p k_c} \int_0^F k_u(F') \cdot dF'\right).$$

bzw. nach Einsetzen von Gl. 11 und anschließender Integration zu:

$$\frac{P_u(F)}{dF} = \frac{k_u^0}{v_p k_c} \cdot \exp\left(\frac{F \cdot \Delta x_u}{k_B T} - \frac{1}{v_p k_c} \frac{k_B T \cdot k_u^0}{\Delta x_u} \left(e^{\frac{F \cdot \Delta x_u}{k_B T}} - 1\right)\right). \quad (14)$$

Der Verlauf der Wahrscheinlichkeitsdichte nach Gl. 14 ist in Abbildung 13 schematisch

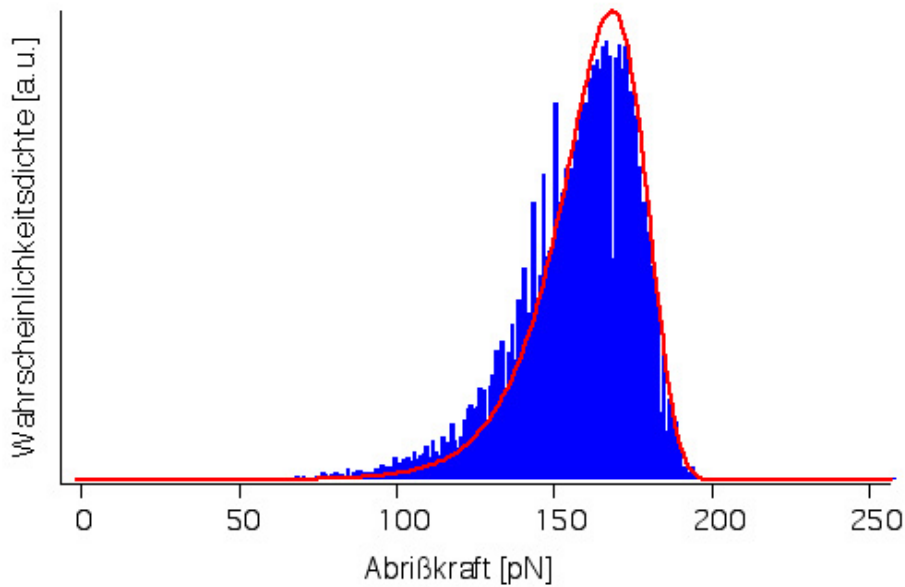


Abbildung 13: Vergleich der nach Gl. 14 berechneten Wahrscheinlichkeitsdichte der Abrißkräfte (rot) mit einer Monte-Carlo-Simulation (blau) anhand der Potentialparameter, die für die paarweise Entfaltung von Helix D und E ermittelt wurden ($L_0 = 86$ aa, $\Delta x_u = 0.32$ nm, $k_u^0 = 1 \cdot 10^{-2} \text{s}^{-1}$, vgl. (Janovjak et al., 2003), siehe Anhang S. A32ff). Für die Zuggeschwindigkeit v_p und die Federkonstante k_c wurden die Werte 654 nm/s bzw. 90 pN/nm angenommen. Für die Monte-Carlo-Simulation wurden $250\,000$ einzelne Entfaltungsschritte simuliert. Auf die Abweichungen von der berechneten Wahrscheinlichkeitsdichte wird im Text eingegangen.

dargestellt. Die Abweichungen von der Simulation resultieren daraus, daß die vorgestellte analytische Herleitung den als Abstandshalter (*spacer*) wirkenden, bereits entfalten Teil des Polypeptids nicht berücksichtigt. Der relativ langsame Anstieg der Kraft zu Beginn der WLC-Kurve (Abbildung 9) bewirkt, daß die zu entfaltende Struktur im Vergleich zu der Annahme in der Gleichung $F(t) = v_p k_c t$ statistisch gesehen länger mit einer relativ niedrigen Kraft belastet wird. Dadurch erhöht sich wiederum die Wahrscheinlichkeit einer Entfaltung bei niedrigerer Kraft. Bei nicht zu großen spacer-Längen wird der Wahrscheinlichkeitsverlauf der Abrißkräfte jedoch von Gl. 14 gut wiedergegeben. Auch lassen sich aus dieser Gleichung einige grundlegende Eigenschaften des Zwei-Zustands-Modells herleiten.

Das Maximum der Wahrscheinlichkeitsverteilung F_A und damit die wahrscheinlichste Abrißkraft ergibt sich aus Gl. 14 zu:

$$F_A = \frac{k_B T}{\Delta x_u} \ln \left(\frac{v_p k_c}{k_B T} \cdot \frac{\Delta x_u}{k_u^0} \right). \quad (15)$$

Der hieraus ersichtliche logarithmische Zusammenhang zwischen der Zuggeschwindigkeit v_p und der wahrscheinlichsten Abrißkraft F_A wurde experimentell bestätigt (Janovjak et al., 2004)¹⁶ und ist ein Anzeichen dafür, daß bei Bakteriorhodopsin den einzelnen Entfaltungsschritten tatsächlich jeweils eine einzelne, scharfe Barriere, wie in Abbildung 12 dargestellt, zugrunde liegt. Zur Untersuchung der Steigung der Abrißkraft als Funktion der Temperatur läßt sich unter der Annahme, daß ΔG_u^* nicht von der Temperatur abhängt und damit $d\Delta G_u^*/dT$ verschwindet durch Einsetzen von k_u^0 (Gl. 10) in Gl. 15 folgender Zusammenhang ableiten:

$$\frac{dF_A}{dT} = \frac{k_B}{\Delta x_u} \left(\ln \left(\frac{v_p k_c \Delta x_u}{k_B T} \right) - \ln(\omega) - 1 \right).$$

Nach Ersetzen der Probiefrequenz durch die mittlere Diffusionszeit $\tau_D = 1/\omega$ und Einführung der Kraft-Ladungs-Rate $r_f = v_p k_c$ (Evans, 1998) ergibt sich hieraus für die Steigung der Abrißkraft als Funktion der Temperatur:

$$\frac{dF_A}{dT} = -\frac{k_B}{\Delta x_u} \ln \left(\left(\frac{k_B T}{\Delta x_u \tau_D r_f} \right) + 1 \right).$$

Wie in der im Anhang abgedruckten Veröffentlichung (Janovjak et al., 2003)¹⁷ detailliert diskutiert, läßt sich mit dieser Formel die thermisch induzierte Abschwächung der Bindungskräfte von Bakteriorhodopsin in dem Temperaturbereich von 8 °C bis 52 °C recht gut beschreiben. Für die Kraft-Ladungs-Rate, die Potentialbreite und die mittlere Diffusionszeit wurden die Werte $r_f = 1$ nN/s, $\Delta x_u = 0.3$ nm und $\tau_D = 10^{-10}$ s angenommen.

¹⁶Die entsprechende Veröffentlichung ist im Anhang abgedruckt.

¹⁷Die entsprechende Veröffentlichung ist im Anhang abgedruckt.

7 Literaturverzeichnis

- Bell, G.I. (1978) *Models for the specific adhesion of cells to cells*. Science 200, 618-627.
- Binnig, G., Quate, C.F., and Gerber, C. (1986) *Atomic force microscope*. Physical Review Letters 56, 930-933.
- Bouchiat, C., Wang, M.D., Allemand, J.-F., Strick, T., Block, S.M., and Croquette, V. (1999) *Estimating the Persistence Length of a Worm-Like Chain Molecule from Force-Extension Measurements*. Biophysical Journal 76, 409-412.
- Bustamante, C., Marko, J.F., Siggia, E.D., and Smith, S. (1994) *Entropic elasticity of lambda-phage DNA*. Science 265, 1599-1600.
- Butt, H.-J., and Jaschke, M. (1995) *Calculation of thermal noise in atomic force microscopy*. Nanotechnology 6, 1-7.
- Essen, L., Siegert, R., Lehmann, W.D., and Oesterhelt, D. (1998) *Lipid patches in membrane protein oligomers: crystal structure of the bacteriorhodopsin-lipid complex*. Proc Natl Acad Sci U S A 95, 11673-11678.
- Evans, E., and Ritchie, K. (1997) *Dynamic strength of molecular adhesion bonds*. Biophys J 72, 1541-1555.
- Evans, E. (1998) *Energy landscapes of biomolecular adhesion and receptor anchoring at interfaces explored with dynamic force spectroscopy*. Faraday Discuss, 1-16.
- Florin, E.L., Rief, M., Lehmann, H., Ludwig, M., Dornmair, C., Moy, V.T., and Gaub, H.E. (1995) *Sensing specific molecular interactions with the atomic force microscope*. Biosensors Bioelectr. 10, 895 - 901.
- Flory, P.J. (1988) *Statistical Mechanics of Chain Molecules* (New York: Oxford University Press)
- Hao, B., Gong, W., Ferguson, T.K., James, C.M., Krzycki, J.A., and Chan, M.K. (2002) *A new UAG-encoded residue in the structure of a methanogen methyltransferase*. Science 296, 1462-1466.
- Hugel, T., and Seitz, M. (2001) *The Study of Molecular Interactions by AFM Force Spectroscopy*. Macromol. Rapid Commun. 22, 989-1016.
- Israelachvili, J. (1991) *Intermolecular and Surface Forces*, Second Edition (London: Academic Press Limited)
- Jackson, M.B. (1993) *On the time scale and time course of protein conformational changes*. J. Chem. Phys. 99, 7253-7259.
- Jacobs, R.E., and White, S.H. (1989) *The nature of the hydrophobic binding of small peptides at the bilayer interface: implications for the insertion of transbilayer helices*. Biochemistry 28, 3421-3437.
- Janovjak, H., Kessler, M., Oesterhelt, D., Gaub, H., and Muller, D.J. (2003) *Unfolding pathways of native bacteriorhodopsin depend on temperature*. Embo J 22, 5220-5229.
- Janovjak, H., Struckmeier, J., Hubain, M., Kedrov, A., Kessler, M., and Muller, D.J. (2004) *Probing the energy landscape of the membrane protein bacteriorhodopsin*. Structure (Camb) 12, 871-879.
- Kahn, T.W., and Engelman, D.M. (1992) *Bacteriorhodopsin can be refolded from two independently stable transmembrane helices and the complementary five-helix fragment*. Biochemistry 31, 6144-6151.

- Katragadda, M., Alderfer, J.L., and Yeagle, P.L. (2001) *Assembly of a polytopic membrane protein structure from the solution structures of overlapping peptide fragments of bacteriorhodopsin*. *Biophys J* 81, 1029-1036.
- Kessler, M., and Gaub, H.E. (2006) *Unfolding barriers in Bacteriorhodopsin probed from the cytoplasmic and the extracellular side by AFM*. *Structure (Camb)* 14, 521-527.
- Kessler, M., Gottschalk, K.E., Janovjak, H., Muller, D.J., and Gaub, H.E. (2006) *Bacteriorhodopsin folds into the membrane against an external force*. *J. Mol. Biol.* 357, 644-654.
- Kratky, O., and Porod, G. (1949) *Röntgenuntersuchung geloster Fadenmoleküle*. *Recueil Des Travaux Chimiques Des Pays-Bas* 68, 1106-1123.
- Liao, M.J., Huang, K.S., and Khorana, H.G. (1984) *Regeneration of native bacteriorhodopsin structure from fragments*. *J Biol Chem* 259, 4200-4204.
- Livadaru, L., Netz, R.R., and Kreuzer, H.J. (2003) *Stretching Response of Discrete Semiflexible Polymers*. *Macromolecules* 36, 3732-3744.
- Marko, J., F, and Siggia, E.D. (1995) *Stretching DNA*. *Macromolecules* 28, 8759-8770.
- Muller, D.J., Fotiadis, D., Scheuring, S., Muller, S.A., and Engel, A. (1999) *Electrostatically balanced subnanometer imaging of biological specimens by atomic force microscope*. *Biophys J* 76, 1101-1111.
- Muller, D.J., Kessler, M., Oesterhelt, F., Moller, C., Oesterhelt, D., and Gaub, H. (2002) *Stability of bacteriorhodopsin alpha-helices and loops analyzed by single-molecule force spectroscopy*. *Biophys J* 83, 3578-3588.
- Nymeyer, H., Garcia, A.E., and Onuchic, J.N. (1998) *Folding funnels and frustration in off-lattice minimalist protein landscapes*. *Proc Natl Acad Sci U S A* 95, 5921-5928.
- Nölting, B. (1999) *Protein Folding Kinetics* (Berlin Heidelberg New York: Springer-Verlag Berlin Heidelberg)
- Oesterhelt, F., Oesterhelt, D., Pfeiffer, M., Engel, A., Gaub, H.E., and Muller, D.J. (2000) *Unfolding pathways of individual bacteriorhodopsins*. *Science* 288, 143-146.
- Onuchic, J.N., Luthey-Schulten, Z., and Wolynes, P.G. (1997) *Theory of protein folding: the energy landscape perspective*. *Annu Rev Phys Chem* 48, 545-600.
- Onuchic, J.N., and Wolynes, P.G. (2004) *Theory of protein folding*. *Curr Opin Struct Biol* 14, 70-75.
- Pande, V.S., Grosberg, A.Y., and Tanaka, T. (1997) *Statistical mechanics of simple models of protein folding and design*. *Biophys J* 73, 3192-3210.
- Popot, J.L., Trehwella, J., and Engelman, D.M. (1986) *Reformation of crystalline purple membrane from purified bacteriorhodopsin fragments*. *Embo J* 5, 3039-3044.
- Popot, J.L., and Engelman, D.M. (1990) *Membrane protein folding and oligomerization: the two-stage model*. *Biochemistry* 29, 4031-4037.
- Popot, J.L., and Engelman, D.M. (2000) *Helical membrane protein folding, stability, and evolution*. *Annu Rev Biochem* 69, 881-922.
- Rief, M. (1997) *Kraftspektroskopie an einzelnen Molekülen*. Doktorarbeit, Ludwig-Maximilians Universität, München.
- Rief, M., Gautel, M., Oesterhelt, F., Fernandez, J.M., and Gaub, H.E. (1997) *Reversible unfolding of individual titin immunoglobulin domains by AFM*. *Science* 276, 1109-1112.

- Rief, M., Fernandez, J.M., and Gaub, H.E. (1998) *Elastically coupled two-level-systems as a model for biopolymer extensibility*. Phys. Rev. Lett. 81, 4764-4767.
- Sarid, D. (1994) *Scanning force microscopy*, (Oxford Press)
- Schwaiger, I. (2005) *Kraftspektroskopische Untersuchung einzelner Zytoskelett-Proteine*. Doktorarbeit, Ludwig-Maximilians-Universität, München.
- Stryer, L. (1995) *Biochemistry*, 4 Edition (W.H. Freeman and Company, New York)
- Thanbichler, M., and Bock, A. (2002) *The function of SECIS RNA in translational control of gene expression in Escherichia coli*. Embo J 21, 6925-6934.
- Tinoco Jr., I., and Bustamante, C. (2002) *The effect of force on thermodynamics and kinetics of single molecule reactions*. Biophysical Chemistry 101-102, 513-533.
- Viani, M.B., Schaffer, T.E., Chand, A., Rief, M., and Gaub, H.E. (1999) *Small Cantilevers for Force Spectroscopy of Single Molecules*. Applied Physics 86, 2258-2262.
- White, S.H., and Wimley, W.C. (1999) *Membrane protein folding and stability: physical principles*. Annu Rev Biophys Biomol Struct 28, 319-365.

8 Anhang

- Muller, D.J., Kessler, M., Oesterhelt, F., Moller, C., Oesterhelt, D., and Gaub, H. (2002). **A1**
Stability of bacteriorhodopsin alpha-helices and loops analyzed by single-molecule force spectroscopy. Biophys J 83, 3578-3588.
- Moller, C., Fotiadis, D., Suda, K., Engel, A., Kessler, M., and Muller, D.J. (2003). **A12**
Determining molecular forces that stabilize human aquaporin-1. J Struct Biol 142, 369-378.
- Janovjak, H., Kessler, M., Oesterhelt, D., Gaub, H., and Muller, D.J. (2003). **A22**
Unfolding pathways of native bacteriorhodopsin depend on temperature. Embo J 22, 5220-5229.
- Janovjak, H., Struckmeier, J., Hubain, M., Kedrov, A., Kessler, M., and Muller, D.J. **A32**
(2004). *Probing the energy landscape of the membrane protein bacteriorhodopsin .* Structure (Camb) 12, 871-879.
- Kessler, M., and Gaub, H.E. (2006). **A41**
Unfolding barriers in Bacteriorhodopsin probed from the cytoplasmic and the extracellular side by AFM. Structure (Camb) 14, 521-527.
- Kessler, M., Gottschalk, K.E., Janovjak, H., Muller, D.J., and Gaub, H.E. (2006). **A48**
Bacteriorhodopsin folds into the membrane against an external force. J. Mol. Biol. 357, 644-654.

Stability of Bacteriorhodopsin α -Helices and Loops Analyzed by Single-Molecule Force Spectroscopy

Daniel J. Müller,^{*†} Max Kessler,[‡] Filipp Oesterhelt,[‡] Clemens Möller,^{*} Dieter Oesterhelt,[§] and Hermann Gaub[‡]

^{*}Max-Planck-Institute of Molecular Cell Biology and Genetics, 01307 Dresden; [†]BIOTEC, Technical University Dresden, 01602 Dresden;

[‡]Center for Nano Science, Physics Section, Ludwig Maximilians University Munich, 80799 Munich; and [§]Max-Planck-Institute of Biochemistry, 82152 Martinsried, Germany

ABSTRACT The combination of high-resolution atomic force microscopy imaging and single-molecule force spectroscopy allows the identification, selection, and mechanical investigation of individual proteins. In a recent paper we had used this technique to unfold and extract single bacteriorhodopsins (BRs) from native purple membrane patches. We show that subsets of the unfolding spectra can be classified and grouped to reveal detailed insight into the individualism of the unfolding pathways. We have further developed this technique and analysis to report here on the influence of pH effects and local mutations on the stability of individual structural elements of BR against mechanical unfolding. We found that, although the seven transmembrane α -helices predominantly unfold in pairs, each of the helices may also unfold individually and in some cases even only partially. Additionally, intermittent states in the unfolding process were found, which are associated with the stretching of the extracellular loops connecting the α -helices. This suggests that polypeptide loops potentially act as a barrier to unfolding and contribute significantly to the structural stability of BR. Chemical removal of the Schiff base, the covalent linkage of the photoactive retinal to the helix G, resulted in a predominantly two-step unfolding of this helix. It is concluded that the covalent linkage of the retinal to helix G stabilizes the structure of BR. Trapping mutant D96N in the M state of the proton pumping photocycle did not affect the unfolding barriers of BR.

INTRODUCTION

Structure as well as dynamics, and thus the function, of biomolecules are determined by multiple inter- and intramolecular forces (Brooks et al., 1998; Haltia and Freire, 1995; Nakamura, 1996; White and Wimley, 1999). Such molecular interactions are typically inferred indirectly from equilibrium binding and kinetic measurements or are calculated with molecular models. With the development of single-molecule force spectroscopy such inter- and intramolecular interactions of biological macromolecules have become directly accessible. Consequently, this technique has been applied to measure interactions in proteins such as forces that mediate molecular recognition (Fritz et al., 1998; Lee et al., 1994; Moy et al., 1994), stabilize molecular structures (Fisher et al., 1999; Rief et al., 2000), and drive intermolecular interactions (Dammer et al., 1996), molecular bonds (Grandbois et al., 1999; Merkel 2001), and molecular elasticities (Bustamante et al., 2000; Clausen-Schaumann et al., 2000; Kellermayer et al., 1997; Rief et al., 1999, 1998a). Modular proteins were unfolded and revealed for the first time a direct correlation between folding pattern and mechanical function. Models were developed that allow a theoretical description of the molecular compliances based on the combination of established polymer models in com-

bination with discrete unfolding events (Rief et al., 1998a; Zhang et al., 1999). Forced unfolding experiments performed on fibronectin (Rief et al., 2000), tenascin (Oberhauser et al., 1998), and titin (Oberhauser et al., 1999; Rief et al., 2000), showed these modular proteins to unfold domain after domain but only in an all-or-none event with no intermediate states. Only in rare cases have intermittent steps been reported recently (Marszalek et al., 1999).

Because all these mechanical unfolding experiments had been performed on either modular proteins or tandem constructs of multiple domains, the assignment of a certain unfolding event to a certain domain was not possible: the weakest domain unfolds first, not the first in the chain. We could overcome this limitation by unfolding membrane proteins. The highest resolution was obtained with bacteriorhodopsin (BR). Here individual structural elements of the protein were found to unfold sequentially, which made the assignment of certain features of the measured force spectra to the corresponding amino acid (aa) sequence possible. Such spectra then provided detailed information on structural properties of individual BR molecules within the native purple membrane from the halophilic archaeon *Halobacterium salinarum* (Forbes and Lorimer, 2000; Oesterhelt et al., 2000).

The light-driven proton pump BR was chosen as model system for this study because it represents one of the most extensively studied membrane proteins (Haupts et al., 1999; Oesterhelt, 1998). BR converts the energy of light ($\lambda = 500\text{--}650$ nm) into an electrochemical proton gradient, which in turn is used for ATP production by the cellular ATP synthase. Its structural analysis has revealed the photoactive retinal embedded in seven closely packed trans-

Submitted January 16, 2002, and accepted for publication July 29, 2002.

Address reprint requests to Dr. Hermann E. Gaub, Center for Nano Science, Sektion Physik, Ludwig Maximilians-Universität München, Amalienstrasse 54, 80799 München, Germany. Tel.: 49-89-2180-3173; Fax: 49-89-2180-2050; E-mail: gaub@physik.uni-muenchen.de. or to Dr. Daniel Müller, BIOTEC, 01307 Dresden, Germany. Tel.: 49-351-210-2586; Fax: 49-351-210-2020; E-mail: mueller@mpl1-6BG.DE.

© 2002 by the Biophysical Society

0006-3495/02/12/3578/11 \$2.00

membrane α -helices (Belrhali et al., 1999; Essen et al., 1998; Grigorieff et al., 1996; Luecke et al., 1999; Mitsuoka et al., 1999), which builds a common structural motif among a large class of related G-protein-coupled receptors (Baldwin, 1993; Helmreich and Hofmann, 1996; Kolbe et al., 2000; Palczewski et al., 2000; Royant et al., 2001). The BR helices are lettered A, B, C, D, E, F, and G, to which the C-terminal end is connected. With increasing knowledge of its structural and functional properties, BR has become a paradigm for α -helical membrane proteins in general and for ion transporters in particular (Lanyi, 1999). Together with adjacent lipids BR molecules assemble into trimers, which are packed into a two-dimensional hexagonal lattice of the purple membrane as a chemically distinct domain of the cell membrane.

In this study we measure the unfolding spectra of BR by high-resolution atomic force microscopy (AFM) imaging and single-molecule force spectroscopy. In extension of our previous work we improved and expanded the experimental and data analysis procedures. To test whether drastic changes of the physiological conditions influence the stability, wild-type BR was unfolded within a pH range from 4.2 to 10. Subsequent analysis of the unfolding spectra in combination with the classification of individual force peaks provided a detailed insight into the stability and the unfolding steps of BR's secondary structural elements. To elucidate the influence of retinal and its different configurations on the folding potential we additionally unfolded photobleached BR and the D96N BR mutant trapped in the M state of the photocycle.

MATERIALS AND METHODS

Purple membrane preparation

Wild-type purple membrane was extracted from *H. salinarum* as described (Oesterhelt and Stoerkenius, 1974) and adsorbed onto freshly cleaved mica (Müller et al., 1997). The cysteine mutant (G241C) has been created by recombinant techniques replacing the glycine at position 241 with a cysteine as described (Pfeiffer et al., 1999). The BR D96N mutant showing a significantly retarded photocycle has been created by replacing the aspartic acid at position 96 with asparagine and characterized by spectroscopic methods as described (Butt et al., 1989; Holz et al., 1989). During the unfolding of the D96N mutant it was illuminated with sufficient yellow light intensity ($\lambda = 475$ nm; filtered from a 75-W halogen lamp, with heat filter focused on a spot of 5 cm) to trap the BR molecules in the M state of the catalytic cycle. Controlled photobleaching of purple membranes (10 μ g/ml) was performed in the presence of 200 mM hydroxylamine (pH 7.2, 20 mM Tris-HCl) as described (Möller et al., 2000; Oesterhelt et al., 1974).

Attachment of BR to the AFM tip

In previous studies, two different strategies have been developed to attach the protein to the tip. In a recent paper we showed that the cysteine of the G241C mutant binds with a 90% likelihood to a gold-coated cantilever (Oesterhelt et al., 2000) when the tip is brought into contact with the cytoplasmic purple membrane surface even at forces below 200 pN. This procedure allows for a highly efficient and well localized attachment.

However, it requires the AFM tip to be replaced after a few experiments because it is covered with reacted protein. The alternative method, the nonspecific attachment in combination with a subsequent imaging and force trace classification, was shown to provide equivalent results; however, it allows a much higher throughput. Because this study here is a systematic investigation, we chose the nonspecific attachment in combination with AFM imaging as described below.

Single-molecule force spectroscopy and imaging

The contact mode AFM (Nanoscope E, Digital Instruments, Santa Barbara, CA) used was equipped with a 100- μ m piezo scanner. The spring constants k of the 100- μ m-long Si_3N_4 AFM cantilevers (OMCL TR400PS, Olympus, Tokyo, Japan) were calibrated in solution after the experiments using the equipartition theorem (Butt and Jaschke, 1995; Florin et al., 1995). Within the uncertainty of this method ($\sim 10\%$) all cantilevers used exhibited the same $k = 0.1$ N/m. All experiments were done in buffer solution (300 mM KCl, 10 mM Tris-HCl, and unless noted otherwise, pH 7.8) at room temperature. To perform force spectroscopy experiments on BR we recorded topographs of the cytoplasmic purple membrane surface (Müller et al., 1999b) at sub-nanometer resolution as described (Müller et al., 1999a). After this, we selected an area of BR trimers and zoomed in, positioning the AFM tip. To allow the C-terminal end of BR to adsorb onto the tip, both were kept in contact for ~ 1 s while applying a force of 0.5–1 nN. The AFM stylus and protein surface were then separated at a velocity of 40 nm/s while recording the force spectrum. In $\sim 15\%$ of all retraction curves we detected an adhesive peak, which was correlated to a removal of a single BR molecule, and $\sim 30\%$ of these adhesion curves showed a force extension curve exhibiting a length between 60 and 70 nm (see data analysis). After detecting one discontinuous force curve the protein surface of the same area was re-imaged. Defects of missing BR monomers allowed us to unambiguously correlate the force spectra to a single protein. Fig. 1 shows the image of a purple membrane before (Fig. 1 b) and after (Fig. 1 c) extraction of a single BR (note the persistent defect in both images).

Data analysis

To analyze the force curves, a clear criterion is required that distinguishes curves of BR molecules attached to the AFM tip with different regions of their polypeptide backbone. One suitable criterion is the overall length of the force curve, which reflects the tip-sample distance at which the last force peak occurs. It is evident that a molecule attached to the cantilever by one of its loops results in a force curve with smaller overall length than a molecule attached by one of its termini. If the AFM tip binds to the EF loop, the force adhesion curve could exhibit a maximum length of ~ 152 aa. The maximal length of the stretched polypeptide chain (152 aa) was calculated assuming attachment to the EF loop (aa 157–164 as derived from the atomic model of BR) and that the extracellular N-terminal end forms the last potential barrier against extraction of BR from purple membrane. Stretching 152 aa, at an approximate force of 200 pN, corresponds to a maximum rupture length of ~ 48 nm, calculated using the worm-like chain (WLC) model. Taking this approach, the maximum rupture length of the unfolded BR molecule would be 92 aa (~ 29 nm) if the tip binds to the CD loop and 158 aa (~ 50 nm) if the tip binds to the AB loop (here the last potential barrier would be built by the G-helix). Some of the adhesion peaks of these curves would then represent simultaneous pulling on two secondary structural elements, each of them connected to one end of the polypeptide loop. Thus, in most cases the classification and analysis of such concurrent multiple unfolding events cannot be made unambiguously. The classification of force curves exhibiting a length of ~ 50 nm was further complicated by the partial unfolding of BR molecules that attached via their C-terminal end to the tip. Such analytical problems do not occur when the protein is fully unfolded, beginning from the C-terminal end. Force-extension curves corresponding to an extension of significantly

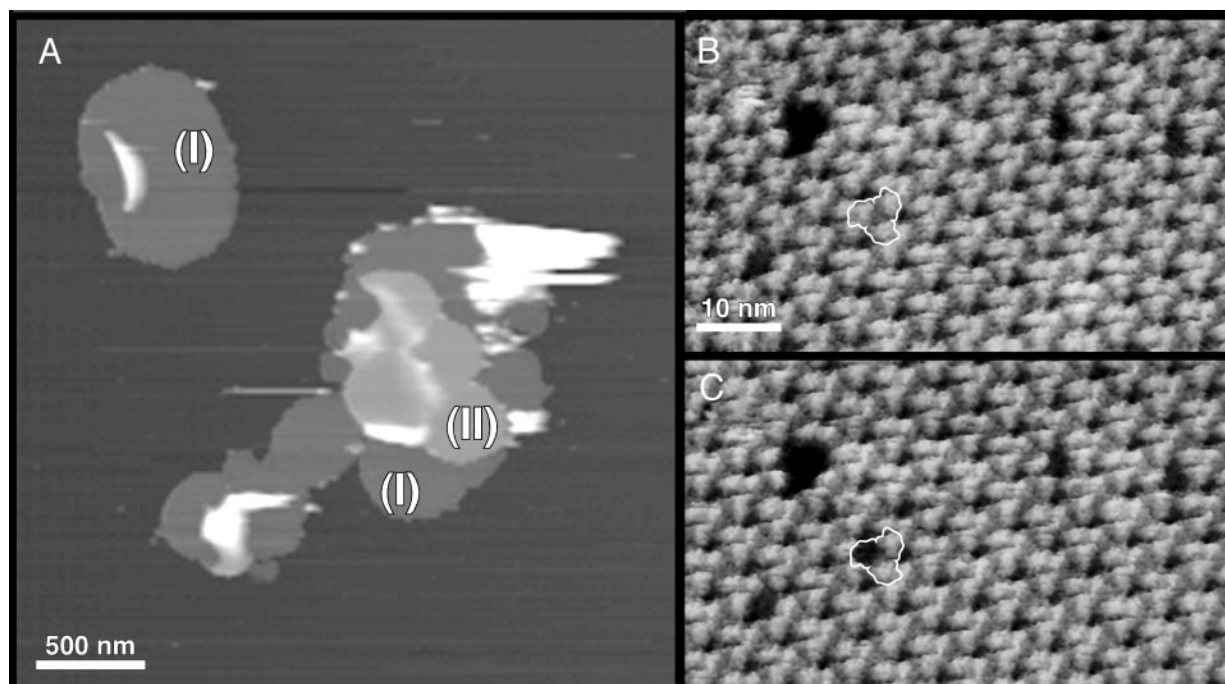


FIGURE 1 Purple membrane imaging and manipulation. (a) Purple membrane patches (I) adsorbed onto freshly cleaved mica and imaged in buffer solution (pH 7.8, 20 mM Tris-HCl, 300 mM KCl). In some areas, purple membrane patches overlap with other membranes, forming double layers (II). (b) High-resolution image of the cytoplasmic purple membrane surface showing BR trimers (outline) arranged into a hexagonal lattice. The topograph was recorded at minimum force allowing the longest cytoplasmic loops of the individual BR molecules (loop EF) to protrude fully from the membrane surface (Müller et al., 1999b). Individual defects show single or multiple BR monomers missing. After imaging, the AFM tip was brought into contact to the membrane surface (circle). This allowed the polypeptides of individual BR molecules to adsorb to the tip. During separation of tip and sample, this molecular bridge was used to pull on the protein, and the force spectrum was recorded (see Fig. 2). (c) Same purple membrane area imaged after the manipulation shows one individual BR monomer missing (circle). Vertical full gray levels of topographs correspond to 50 nm (a) and 1.2 nm (b and c).

more than 158 aa (~ 50 nm) can result only from attaching the C-terminal end to the tip. Therefore, only those force-extension curves exhibiting a length above 60 nm were selected and analyzed. This stringent criterion ensured that all the analyzed curves belonged to the same subset, thus allowing a detailed analysis to be made.

By selection of the force-extension curves exhibiting an overall length between 60 and 70 nm we were sure to analyze only spectra from BR molecules that were attached by their C-terminus to the AFM tip and that were completely elongated during extraction (Oesterhelt et al., 2000). All force curves exhibiting these overall lengths were selected and aligned at the second main peak at a tip-to-purple membrane separation of ~ 27 nm (Fig. 2). The force curves were aligned at the second main peak because the curves showed offsets in the distance between stylus and purple membrane (Fig. 2; region around 0 nm). The main reason for this offset is that principally every amino acid of the C-terminal can bind to the AFM tip and that the point of contact is not necessarily located at the tip apex but can also occur at the side of the tip. Avoiding statistical difficulties we analyzed only relative positions of the peaks. We used identical procedures and criteria to align each data set.

To analyze the side peaks, however, we superimposed every main peak separately (see Figs. 3–6 and 8). Every single peak of these superimpositions was fitted by the WLC model with a persistence length of 4 Å (Rief et al., 1997a) and a monomer length of 3.6 Å. We calculated the number of unfolded aa at each peak using the contour length as obtained from the WLC model. When pulling the polypeptide from the cytoplasmic surface, the anchor of the peptide sometimes had to be assumed to exist at the opposite, extracellular surface. In this case, the membrane thickness (~ 4 nm) had to be considered, and 11 aa ($11 \times 3.6 \text{ Å} \approx 4 \text{ nm}$) were added to the number of aa determined by the WLC model. This allowed calculating

the entire rupture length of the unfolded polypeptide. To compare the polypeptide length derived from the WLC fits with the BR structure we have chosen the atomic model of Mitsuoka et al. (1999).

RESULTS AND DISCUSSION

Protein extensibility

With state-of-the-art AFM or, if higher force resolution is required, with force spectroscopy equipment (Oesterhelt et al., 1999; Rief et al., 1997b), the extensibility of molecules can be measured by stretching the molecule that is attached to the AFM tip and recording the cantilever deflection while increasing the cantilever sample distance. The deflection is converted into a force by multiplication with the spring constant, which is determined for each cantilever by the thermal fluctuation method (Butt and Jaschke, 1995; Florin et al., 1995). By subtracting the cantilever's deflection from the tip-sample distance for each point of the measurement, the so-called force-extension traces are calculated.

Fig. 2 shows a multitude of force-extension traces, each one recorded on one single BR (such as shown in Fig. 1), exhibiting a richness of detailed information on the mechanics of this molecule. In these figures ~ 25 traces are superposed and plotted. This kind of graphic representation high-

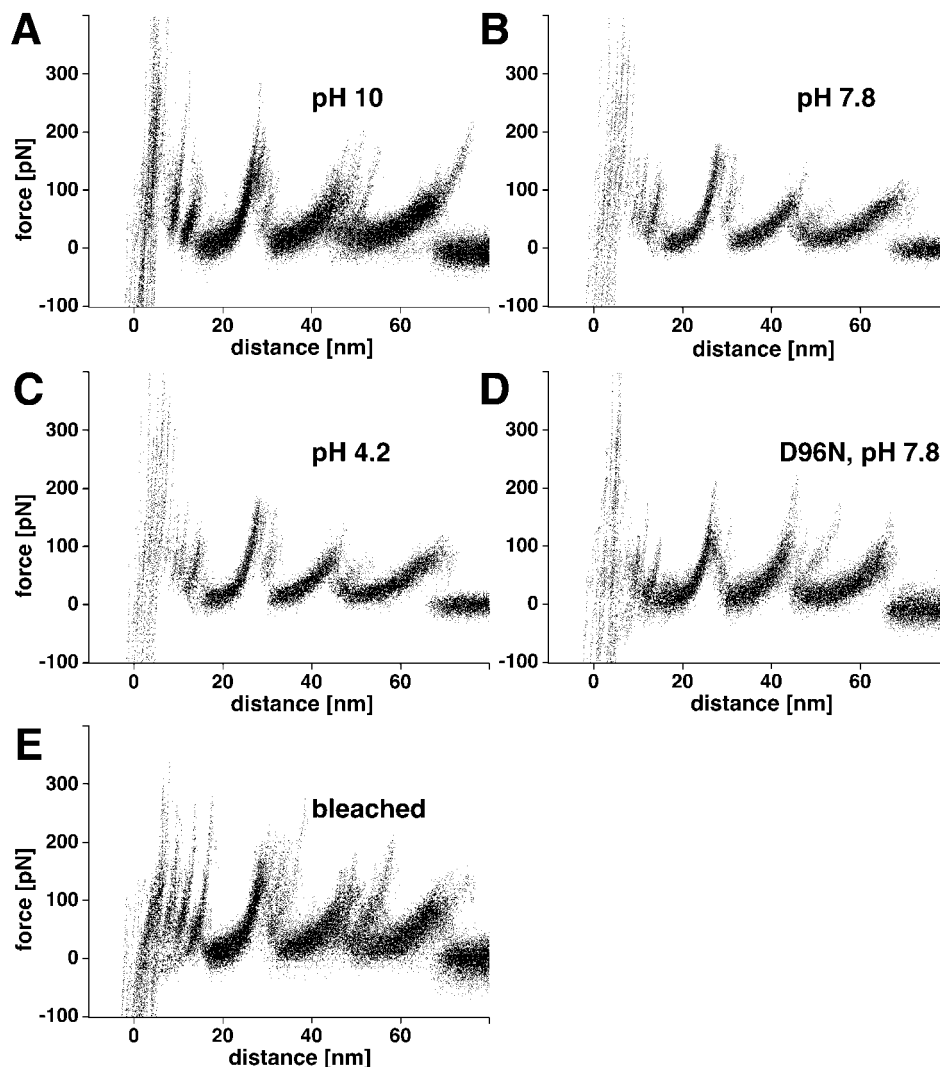


FIGURE 2 Unfolding BR at various conditions. To show common unfolding patterns among single-molecule events, the force spectra were superposed. (A–C) BR unfolded at pH 10 ($n = 31$), pH 7.8 ($n = 32$), and pH 4.2 ($n = 20$), respectively. (D) BR mutant D96N ($n = 18$) unfolded at pH 7.8. During recording the force spectra the mutant was illuminated with yellow light ($\lambda = 475$ nm), thereby trapping the M state of the photocycle. (E) BO unfolded at pH 7.8 ($n = 29$). BO was formed after cleaving the covalent retinal bond (Schiff base) using hydroxylamine. Temperature (21°C) and electrolyte concentration (300 mM KCl) were kept constant in all experiments. All molecules were unfolded by grabbing the C-terminus at the cytoplasmic surface (Oesterhelt et al., 2000). The force curves recorded on native purple membrane (A–D) exhibited a SD of 9.6 pN ($n = 20$) whereas those recorded on the apo-membrane (E) exhibited a SD of 12.9 pN ($n = 20$).

lights common features through the accumulation of the measured points and at the same time represents the individualism of traces. The individualism of the traces is dealt with in Figs. 3–8. The common feature of all the traces is that upon stretching the force builds up in a gradual but nonlinear fashion until at a certain force the trace drops abruptly to lower forces before it rises again upon further extension. Beyond an extension of 70 nm no interaction force is measured. To exclude that the membrane bending contributed to the force spectra we compared force extension curves recorded on purple membranes of different sizes and on different areas of the membrane (e.g., center or outer

rim) itself. Apparently, the force curves showed no differences, indicating such effects to be negligible.

In previous studies we learned that unfolded proteins behave in a first approximation like random coils whose elasticity is well described by the WLC model with an apparent persistence length of 4 Å (Rief et al., 1997a). It should be noted here that this apparent persistence length includes also enthalpic contributions to the molecular elasticity, which become apparent at higher forces (Bouchiat et al., 1999; Oesterhelt et al., 1999; Rief et al., 1998b). The gradual, nonlinear force increase in the extension traces can be well fitted with the WLC model with only one free

parameter: the contour length of the stretched portion of the molecule. As seen in Figs. 3–6 and 8 this fit describes the increasing slopes of the traces at low forces with good agreement. At higher forces the deviations are sometimes marked, indicating that additional processes occur.

From these fits we conclude that in the region of increasing force we stretch an unfolded protein backbone until at a certain force the tension drops suddenly. Because the force builds up again upon further stretching (except for the last peak) we interpret this drop as the extraction of another segment of the protein from the membrane. Upon extraction this segment unfolds, and because the unfolded configuration is less compact, the additional contour length of the freely fluctuating protein backbone results in a drop of the entropically dominated restoring force of the protein.

The WLC fit of the rising slope of the peaks thus provides the contour length of the unfolded protein and by means of this the position of the corresponding barrier against unfolding. With the known attachment point of the protein to the AFM tip, the position of this barrier with respect to the aa sequence of the backbone can thus be counted backwards from the C-terminus. Based on the well established structure of BR, we then can, at least in principle, assign for each peak the corresponding aa in the folded protein, which marks the transition point to the unfolded portion of the protein. The force, which under the given experimental conditions is required to overcome this barrier, is given by the height of the peak.

In previous studies we and others have shown that unfolding forces are rate dependent and that additional information on the geometry of the potential barriers may be extracted from the unfolding traces by varying the pulling speed (Heymann and Grubmüller, 2000; Merkel et al., 1999; Rief et al., 1998a). We have not yet exploited this potential in this study. Because all the conclusions drawn here are based on length arguments rather than forces, our conclusions are independent of the pulling speed.

In summary, each adhesion peak of the discontinuous force spectrum marks a potential barrier of the BR molecule whose position is determined by a WLC fit.

Unfolding traces of BR

Fig. 2 shows five panels of BR unfolding traces recorded under different conditions. In all traces the gross features are alike, with systematically differing details (Figs. 3–8). In a previous study (Oesterhelt et al., 2000), we already had assigned the main peaks to different processes: the peaks below 20 nm include unfolding of helices G and F. At 27, 45, and 65 nm, helices E and D, B and C, and A unfold, respectively. Whereas these main peaks remain more or less unaltered for all the different conditions, the side peaks vary significantly. These side peaks therefore merit detailed analysis.

It is the major benefit of single molecule experiments that each experiment with each molecule may be analyzed individually. This unique option allows the discrimination between the molecules as individuals (be it temporarily or persistently in a different state) as well as between different pathways, which the individual experiments follow. Based on the analysis of each unfolding trace the traces may be sorted and grouped according to certain criteria. Because the effort is enormous, we performed this task for only one pH value per block. All blocks were analyzed for pH 4.2 except for the data in Figs. 3 and 8, which were recorded at pH 7.8 to be comparable with the M state data in Fig. 2 *D*. The result is depicted in Figs. 3–6 and 8.

Mutant D96N was investigated to elucidate the influence of the intermediate (M) state conformation of BR on the unfolding pattern. As can be seen by the direct comparison between Fig. 2 *D* with the other traces, no significantly marked changes occur whether BR was trapped in the M state of the photocycle or not.

Unfolding helices G and F

The low extension part, below 30 nm, of all traces superimposed in Fig. 2 *B* was analyzed individually. Three different main groups became apparent that were superimposed in Fig. 3, *a–c*. The first group of traces exhibited only the 36-aa peak (Fig. 3 *a*). In a second group an additional peak at 48 aa occurred with slightly higher probability (Fig. 3 *b*). Only a very minor fraction exhibited a peak at ~26 aa (Fig. 3 *c*), which will be discussed below in connection with the apoprotein. The peaks below 5 nm could not be ordered in any systematic way. We interpret them as the stretching of the C-terminus. Their variation in position reflects the different attachment sites of the molecule at the tip and thus the length variation of the freely fluctuating segment of the chain. The schematic in Fig. 3 depicts the model that corresponds to the measured positions of the barriers. According to this model the sequence of the extraction/unfolding process is as follows. First the free C-terminal chain is stretched and then helix G unfolds. Then the force acts on the GF loop (peak at 36 aa), and in ~65% of the traces this loop is stretched and pulled through the membrane resulting in the peak at 48 aa (Fig. 3 *b*). Alternatively, the loop may be extracted together with helix F so that this peak is skipped (Fig. 3 *a*), and the force starts rising only when it acts directly on helix E. The forces that are required to overcome both barriers are both ~100 pN, the first one slightly higher than the second.

Unfolding helices E and D

The trace segments of Fig. 2 *C*, showing interactions separated between 15 and 40 nm from the membrane surface,

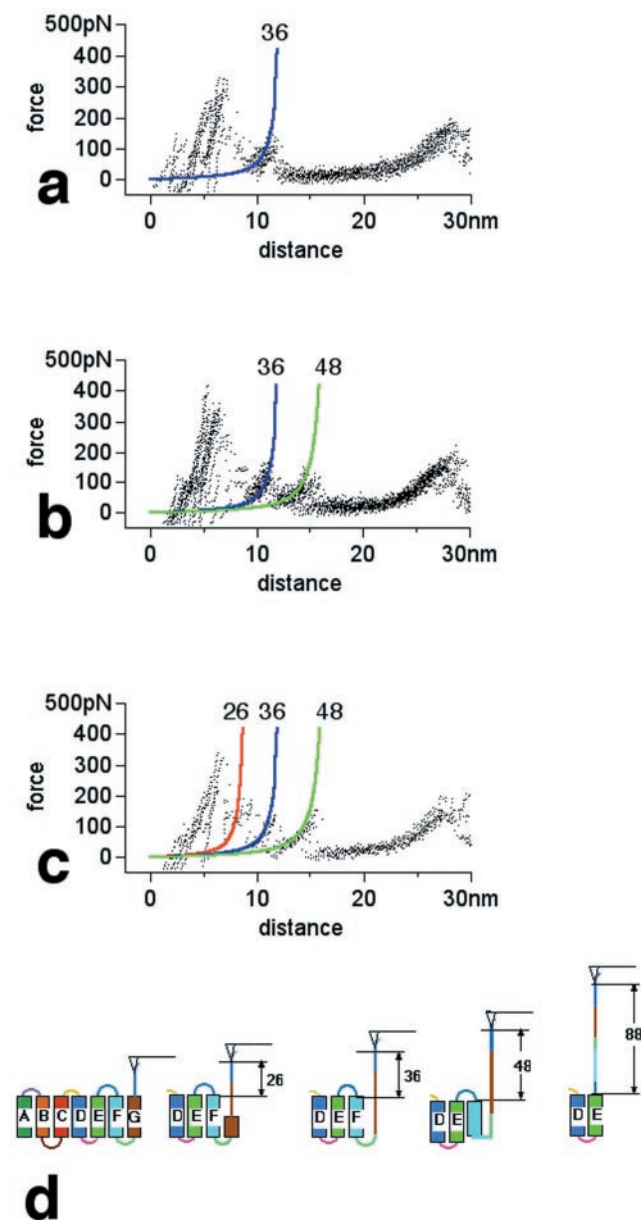


FIGURE 3 Unfolding pathways of transmembrane α -helices G and F. (a) Unfolding helices G and F in two steps. After unfolding helix G the polypeptide chain, bridging the AFM tip and purple membrane, exhibits a length of 36 aa (blue fit). The loop connecting helices G and F remains at the opposite, extracellular surface, and helix F remains embedded in the membrane. The latter two structures and the loop connecting helices E and F are unfolded within a single step, exceeding a force of 111 ± 34 pN ($n = 10$). (b) Unfolding of helices G and F and their connecting loop in a three-step process. First, helix G is unfolded, increasing the length of the stretched polypeptide to 36 aa (blue fit). Then, the hydrophilic GF loop is pulled into the hydrophobic membrane (at 124 ± 28 pN), and the stretched polypeptide then exhibits a length of 48 aa (green fit). After this, helix F and the cytoplasmic loop connecting helices F and E are unfolded in a single step at forces $\geq 110 \pm 32$ pN ($n = 17$). (c) Helices G and F and loop GF unfold in a four-step process. The first part of helix G is unfolded to the approximate retinal location, which forms an internal potential barrier (red fit). The polypeptide is stretched again, and what remains of helix G is unfolded at 148 ± 36 pN, increasing the stretched polypeptide length to 36 aa (blue fit). After this, the FG loop is pulled into the membrane (at

were analyzed accordingly. Here we found four distinctly different groups of traces that are depicted in Fig. 4.

In the simplest case, which accounts for $\sim 22\%$ of all traces, one peak at 88 aa is seen (Fig. 4 a). Our only explanation for this finding is that helices E and D both unfold in an all-or-none event together. In $\sim 12\%$ of the cases we find an intermittent peak at 94 aa, which reflects a barrier around aa 154 of BR (derived from 248–94 aa; Fig. 4 b). In 45% of the traces we find a peak at 105 aa (Fig. 4 c), which, based on the model (Fig. 4 e), corresponds to a state where helix E is completely unfolded, but helix D is still intact. Approximately 20% of the traces show all three peaks (Fig. 4 d), which means that the BR molecules measured here went through both intermittent states upon unfolding. The peak heights were ~ 160 pN for the first two barriers and significantly lower for the third (90 pN). The most striking feature of this set is the potential barrier in the proximity of aa 154 of BR.

Unfolding helices C and B

In the length window between 35 and 55 nm we found again four different groups of traces (Fig. 5). The majority of the traces exhibited no extra peak between 148 and 220 aa, indicating a simultaneous unfolding of helices B and C. A minor fraction of the traces (9%) showed an additional peak at 158 aa (Fig. 5 b) and 35% a second peak at 175 aa (Fig. 5 c). The first case would fit to the extracellular BC loop still untouched, whereas in the second case this loop is completely stretched. In both cases helix B is intact. In 10% of the traces we find all three peaks (Fig. 5 d), indicating that both intermittent states are visited on the unfolding pathway. All peaks are ~ 100 pN in height.

Unfolding helix A

In 65% of the traces the last peak (Fig. 6) occurs at 65 nm, corresponding to a stretched unfolded polypeptide of 220 aa in length (Fig. 6 a). In these traces the last helix is pulled out of the membrane in a single step at forces of ~ 100 pN. In the other cases, a second peak follows (Fig. 6 b). This second peak is smeared out considerably, and the rupture point varies. Drawn in blue is the WLC fit for the fully stretched length of 232 aa from BR. Because this last peak also occurs on multilamellar membrane stacks (see discussion below) it must reflect the destabilization of the N-

102 ± 44 pN), increasing the length to 48 aa (green fit). Finally, helix F and the loop connecting helices F and E are unfolded in a single step at 102 ± 31 pN ($n = 5$). (d) Schematic drawing of the unfolding pathways of helices G and F and of loop FG. All unfolding events were fitted using the WLC model as described in Materials and Methods. The total number of force curves shown corresponds to 32.

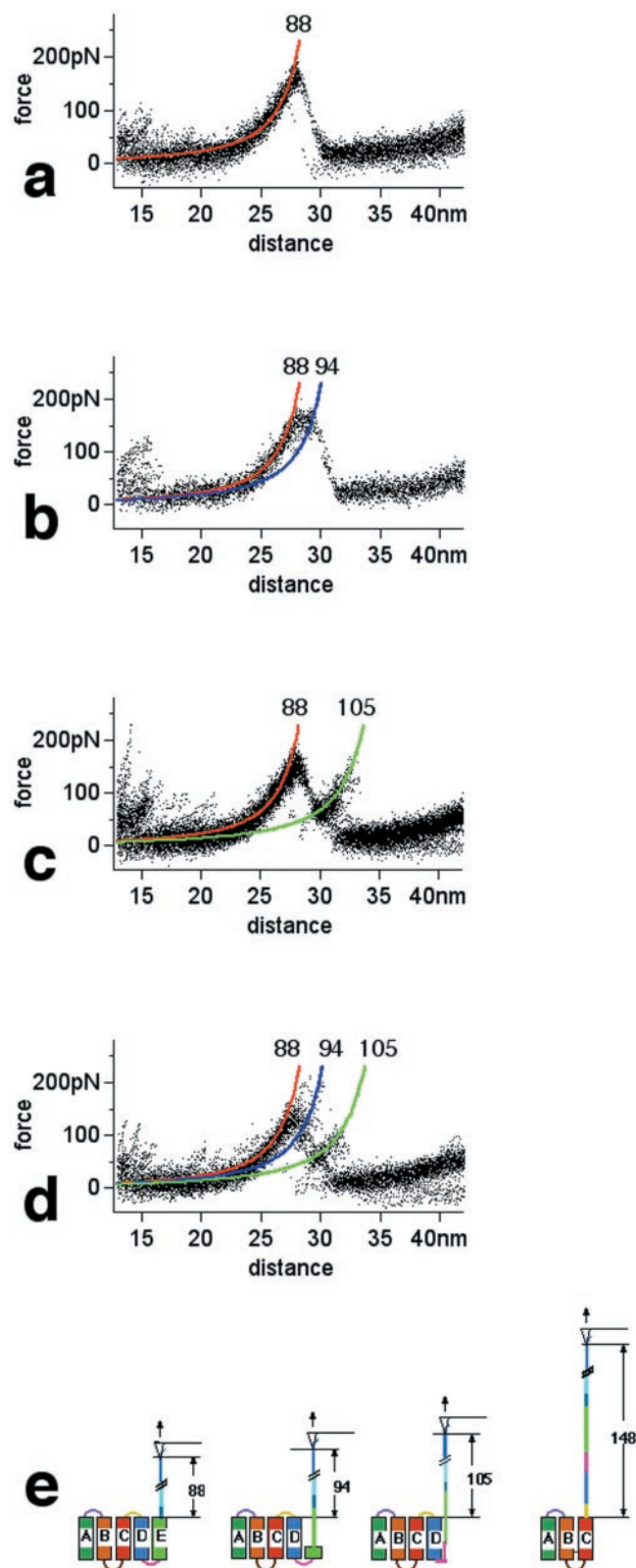


FIGURE 4 Unfolding pathways of transmembrane α -helices E and D. After unfolding helices F and G, the polypeptide chain, bridging the AFM tip and purple membrane, exhibits a length of 88 aa (red fit). All other helices remain embedded in the purple membrane. (a) The structural motif of helices E and D, loop ED, and loop DC unfold in a single step upon

terminus, its possible interaction with the neighboring proteins, and the pulling through the hydrophobic membrane.

Stability of the loops

One remarkable finding of this study is the measured potential barrier associated with the N-terminus and the extracellular loops connecting the transmembrane α -helices. To exclude adhesion of the loops to the mica surface as a potential explanation we performed the same experiments on the upper membrane of double-layered purple membrane patches (compare Fig. 7) like the ones shown in Fig. 1 and of purple membrane adsorbed onto hydrophobic graphite (data not shown). In both cases, we did not observe a change in the adhesion peak positions and distributions. Because it would be highly unlikely that a hypothetical adhesive interaction of the loops with mica is the same as with another purple membrane or with graphite, we conclude from these experiments that the loops are stable structural elements. Thus, a potential barrier comparable with the one that is associated with the unfolding of the α -helices needs to be overcome to stretch the loops and to pull them through the membrane. Interestingly, these forces required to overcome the barriers do not depend in an obvious way on the length of the loop (i.e., 102 pN for loop GF, 4 aa; 135 pN for loop ED, 3 aa; and 109 pN for loop CB, 17 aa). This indicates that the process is dominated by an activation barrier. Because these forces are on the order of 100 pN, the width of these barriers must be far less than the thickness of the membrane to be compatible with measured unfolding free energy changes. This again speaks for a breakup of a structure. On the other hand, x-ray and electron diffraction studies on crystallized BR shows these loops to exhibit a well defined structural conformation. The B-factors and temperature factors of the BR structures are similar for all

exceeding an average pulling force of 167 ± 20 pN ($n = 20$). (b) Helices E and D unfold in a two-step process. First, helix E unfolds partly (at 169 ± 22 pN), thereby lengthening the stretched polypeptide to 94 aa (blue fit). After this, the force pulls the remaining part of helix E and, on the hydrophilic loop, connecting helices E and D located on the opposite, extracellular surface. Upon exceeding an average pulling force of 169 ± 21 pN, the remaining part of helix E, the loop ED, helix D, and the cytoplasmic loop CD are unfolded simultaneously ($n = 10$). (c) Helices E and D unfold in an alternate two-step process. First, part of helix E and the loop ED connecting both helices unfold at 161 ± 14 pN, thereby lengthening the stretched polypeptide to 105 aa (green fit). Upon exceeding an average pulling force of 86 ± 23 pN, helix D and loop CD are unfolded ($n = 39$). (d) Helices E and D and loop ED unfold in a three-step process. First, part of helix E unfolds at 152 ± 22 pN, thereby lengthening the stretched polypeptide to 94 aa (blue fit). Second, what remains from helix E and loop ED is pulled into the membrane at 135 ± 30 pN, lengthening the polypeptide strand to 105 aa (green fit). Third, helix D and loop CD unfold at a pulling force above 83 ± 23 pN ($n = 19$). (e) Schematic drawing of the unfolding pathways found. The total number of force curves shown corresponds to 88.

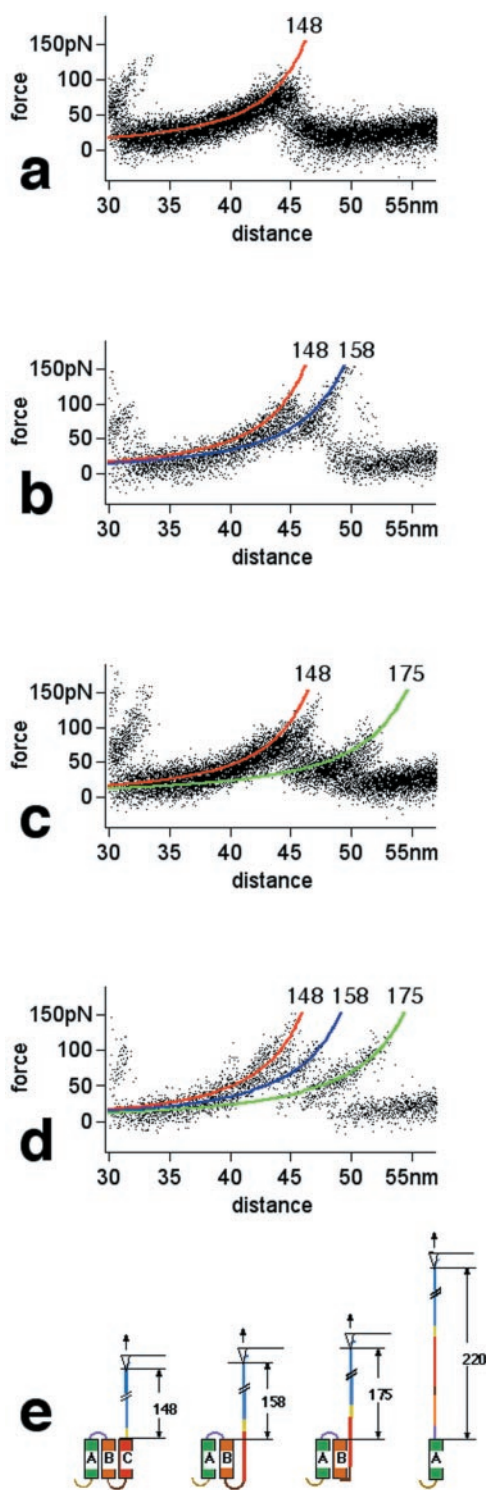


FIGURE 5 Unfolding pathways of transmembrane α -helices C and B. After unfolding helices E and D, the polypeptide chain, bridging the AFM tip and purple membrane, exhibits a length of 148 aa (red fit). Helices C, B, and A remain embedded in the purple membrane. (a) Helices C and B unfold in a single step upon exceeding an average pulling force of 99 ± 16 pN ($n = 40$). (b) Helices C and B unfold in a two-step process. First, helix C unfolds at 109 ± 18 pN, thereby lengthening the stretched polypeptide to 158 aa (blue fit). After this, the force pulls on the hydrophilic loop connecting helices C and B located on the opposite, extracellular surface.

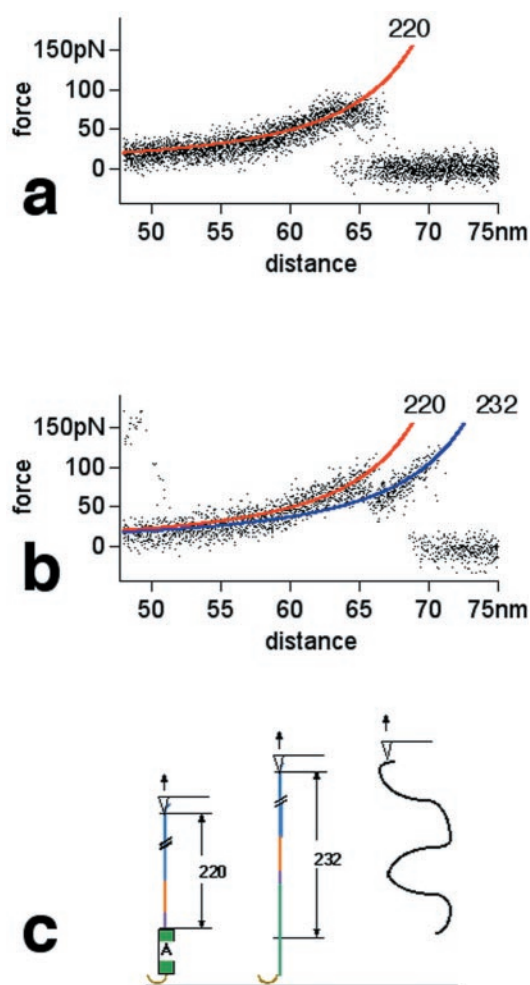


FIGURE 6 Unfolding pathways of the transmembrane α -helix A. After unfolding helices C and B, the polypeptide chain, bridging the AFM tip and purple membrane, exhibits a length of 220 aa (red fit). Only helix A remains embedded in the membrane. (a) Helix A and the N-terminal end are pulled through the membrane within a single step at average pulling force of 87 ± 9 pN ($n = 12$). (b) Helix A unfolds at 99 ± 11 pN, and the N-terminal end anchors the polypeptide ($n = 6$). The length of the stretched polypeptide corresponds to 232 aa (blue fit). After this, the force pulls on the hydrophilic N-terminus located on the opposite, extracellular surface. By exceeding a pulling force of 105 ± 11 pN, the polypeptide end is pulled through the membrane. (c) Schematic drawing of the unfolding pathways found. The total number of force curves shown corresponds to 18.

Upon exceeding an average pulling force of 105 ± 15 pN, the extracellular loop BC, helix B, and the cytoplasmic loop AB are unfolded simultaneously ($n = 8$). (c) Helices C and B unfold in an alternate two-step process. First, helix C and the loop connecting these helices unfold at 95 ± 20 pN, thereby lengthening the stretched polypeptide to 175 aa (green fit). Upon exceeding an average pulling force of 80 ± 17 pN, helix B and loop AB are unfolded ($n = 31$). (d) Helices C and B unfold in a three-step process. First, helix C unfolds at 108 ± 26 pN, thereby lengthening the stretched polypeptide to 158 aa (blue fit). Second, loop BC is pulled into the membrane at 116 ± 33 pN (green fit). Third, helix B unfolds at pulling forces above 87 ± 31 pN ($n = 9$). (e) Schematic drawing of the unfolding pathways found. The total number of force curves shown corresponds to 88.

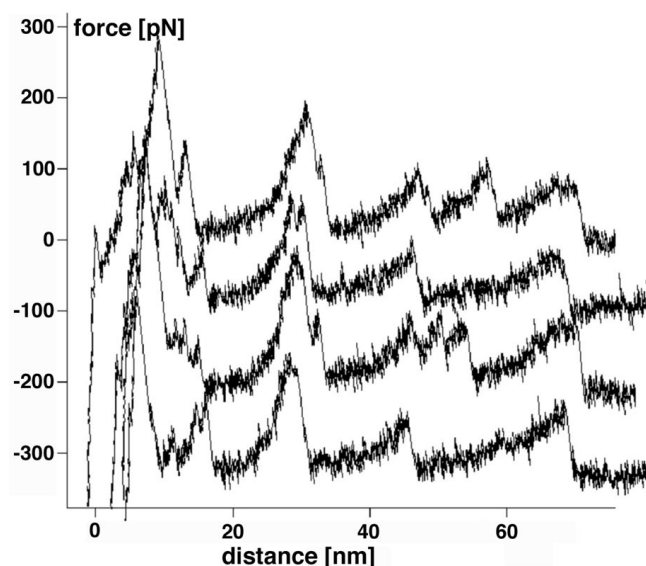


FIGURE 7 Unfolding BR on double-layered purple membrane. To show that the common unfolding patterns of BR do not depend on interactions with the supporting mica surface, single BRs of double-layered purple membranes were unfolded at pH 7.8, 300 mM KCl. Although only a few force curves were shown, their traces show almost all the unfolding pathways described in Figs. 3–6.

extracellular loops and the transmembrane α -helices, indicating that they exhibit equally high conformational stability (Belrhali et al., 1999; Essen et al., 1998; Luecke et al., 1999; Mitsuoka et al., 1999). This finding was also confirmed by experiments determining the solution structure of truncated BR loops, which showed conformations close to those observed on intact BR (Katragadda et al., 2000).

Adsorbed to an atomically flat surface, lipid membranes can be assumed to be separated by an ~ 1 -nm-thick water layer (Sackmann, 1996). A water layer of similar thickness can be assumed to separate purple membrane adsorbed to the mica surface or even to exist between stacked purple membranes. Such thin water layers, however, exhibit different properties compared with water of the bulk solution and behave more as a gel-like material. This effect may also influence the surface structures of BR as detected by the enhanced stability in our experiments.

Apo-membrane

Bulky side groups like tyrosine are possible candidates establishing helix-breaking regions. Thus, it can be assumed that such side groups may also divide the unfolding barriers of transmembrane α -helices. Which role does the retinal moiety play with respect to this aspect? Illuminating BR in the presence of hydroxylamine is known to cleave off the retinal, which is covalently attached through the Schiff base to Lys216 (Oesterhelt et al., 1974). The photobleaching

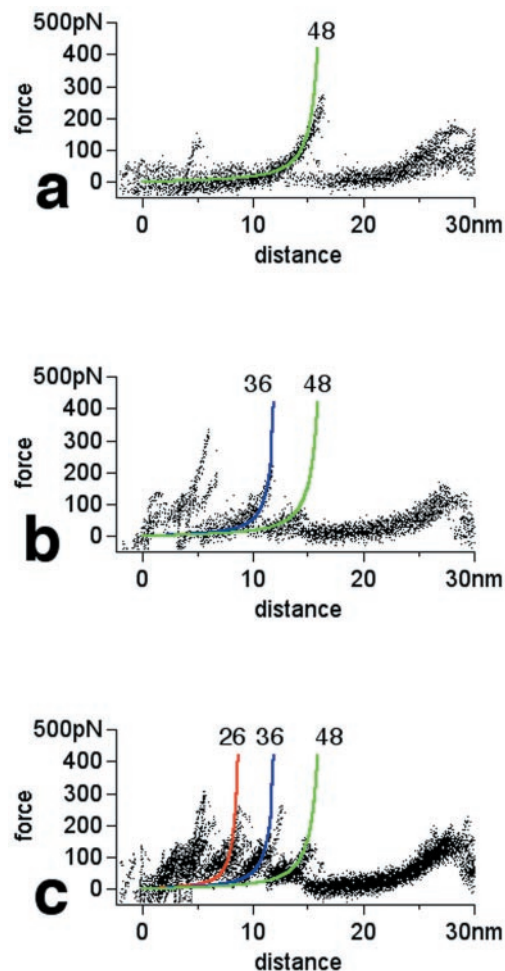


FIGURE 8 Transmembrane α -helices F and G of BO prefer different unfolding pathways compared with native BR. (*a–c*) Events are described by similar pathways as those shown in Fig. 3, *a–c*, respectively. In contrast to BR, however, BO prefers the four-step unfolding pathway shown in *c*. Adhesion forces and frequencies were 189 ± 56 pN ($n = 6$) in *a*; 113 ± 64 pN (blue fit) and 61 ± 13 pN (green fit) at $n = 6$ in *b*; and 122 ± 41 pN (red fit), 130 ± 61 pN (blue fit), and 124 ± 58 pN (green fit) at $n = 17$ in *c*. The total number of force curves shown corresponds to 29.

reaction of BR yields the apoprotein bacterio-opsin (BO) and retinaloxime.

A comparison of Fig. 2 *B* (BR) with Fig. 2 *E* (BO) reveals that only minor changes in the force traces have occurred after cleavage of the retinal. The only significant change occurred in the area of the GF peaks. A direct comparison between these areas in Fig. 3 (BR) and Fig. 8 (BO) shows that the peak at 26 aa, which was negligible in BR, is now prominent in BO (Fig. 8 *c*). Although small, the average forces of the detected peaks were three times larger compared with the standard deviation of the noise (~ 13 pN). The probability distribution of the unfolding pathways of helices G and F is shown in Fig. 9. The probability of potential barriers occurring simultaneously at 26 and 48 aa decreased from 53% (BR) to 21% (BO), whereas the prob-

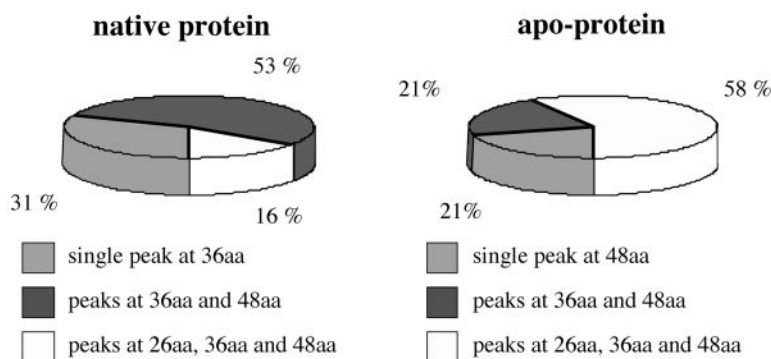


FIGURE 9 Probability distribution of pathways detected upon unfolding helices G and F. Probability of the unfolding pathways are shown for native BR (Fig. 3) and for the apoprotein (Fig. 8). Although 58% of the unfolding events of apoprotein showed an additional unfolding barrier at 26 aa, this barrier was observed in only 16% of the unfolding traces of wild-type BR.

ability of potential barriers occurring simultaneously at 26, 36, and 48 aa increased from 16% (BR) to 58% (BO). Correlation with the secondary structural model of BR shows that the additional peak fitted at 36 aa can be assigned to the position of the Schiff base of helix G to which the retinal is bond. It is counterintuitive, but the removal of this rather bulky retinal from the aa backbone results in the formation of an additional barrier in the unfolding pathway. However, the results indicate that the breakage of the Schiff base, which covalently links the retinal to helix G, destabilizes this α -helix.

Concluding remarks

It is the combination of high-resolution imaging with single-molecule force spectroscopy that has enabled us to record and unambiguously identify force traces from individual protein unfolding events. The one-by-one analysis of these unfolding traces allowed us to unravel correlations between the individual events and to discover distinct unfolding patterns, which led to a classification of the different unfolding pathways. There exists, however, a common unfolding principle of the BR structure in which a structural element is described by two transmembrane α -helices connected by their polypeptide loop. In most experiments, these three structural elements unfold within a single step. Some unfolding traces show these structural elements to choose separate unfolding pathways. As a result, every helix and the connecting loop are unfolded in a single step. In most cases, the second helix of this structural motif unfolds at smaller forces compared with the first helix. Most probable, this effect results from the destabilization of the structural motif by the unfolding process. The individualism of the unfolding pathways emerged as a very prominent feature throughout the study. Whether or not this individualism of the pathways reflects the individualism of the proteins remains to be decided in future studies. Although we have quite precisely measured the positions of the different un-

folding barriers, we have not yet identified their underlying mechanisms. Particularly, our finding that the extracellular loops resist unfolding with a force that is comparable to the force required to unfold a transmembrane α -helix will require additional future investigations.

We thank Harald Janovjak and Matthias Rief for stimulating discussions. This work was supported by the Volkswagenstiftung and the German Science Foundation.

REFERENCES

- Baldwin, J. M. 1993. The probable arrangement of the helices in G protein-coupled receptors. *EMBO J.* 12:1693–1703.
- Belrhali, H., P. Nollert, A. Royant, C. Menzel, J. P. Rosenbusch, E. M. Landau, and E. Pebay-Peyroula. 1999. Protein, lipid and water organization in bacteriorhodopsin crystals: a molecular view of the purple membrane at 1.9 Å resolution. *Struct. Fold. Des.* 7:909–917.
- Bouchiat, C., M. D. Wang, J-F. Allemand, T. Strick, S. M. Block, and V. Croquette. 1999. Estimating the persistence length of a worm-like chain molecule from force-extension measurements. *Biophys. J.* 76:409–412.
- Brooks, C. L., M. Grueberle, J. N. Onuchic, and P. G. Wolynes. 1998. Chemical physics of protein folding. *Proc. Natl. Acad. Sci. U.S.A.* 95:11037–11038.
- Bustamante, C., S. B. Smith, J. Liphardt, and D. Smith. 2000. Single-molecule studies of DNA mechanics. *Curr. Opin. Struct. Biol.* 10: 279–285.
- Butt, H. J., K. Fendler, E. Bamberg, J. Tittor, and D. Oesterhelt. 1989. Aspartic acids 96 and 85 play a central role in the function of bacteriorhodopsin as a proton pump. *EMBO J.* 8:1657–1663.
- Butt, H.-J., and M. Jaschke. 1995. Calculation of thermal noise in atomic force microscopy. *Nanotechnology.* 6:1–7.
- Clausen-Schaumann, H., M. Seitz, R. Krautbauer, and H. Gaub. 2000. Force spectroscopy with single bio-molecules. *Curr. Opin. Chem. Biol.* 4:524–530.
- Dammer, U., M. Hegner, D. Anselmetti, P. Wagner, M. Dreier, W. Huber, and H. J. Güntherodt. 1996. Specific antigen/antibody interactions measured by force microscopy. *Biophys. J.* 70:2437–2441.
- Essen, L.-O., R. Siebert, W. D. Lehmann, and D. Oesterhelt. 1998. Lipid patches in membrane protein oligomers: Crystal structure of the bacteriorhodopsin-lipid complex. *Proc. Natl. Acad. Sci. U.S.A.* 95: 11673–11678.

- Fisher, T. E., A. F. Oberhauser, M. Carrion-Vazquez, P. E. Marszalek, and J. M. Fernandez. 1999. The study of protein mechanics with the atomic force microscope. *Trends Biochem. Sci.* 24:379–384.
- Florin, E. L., M. Rief, H. Lehmann, M. Ludwig, C. Dornmair, V. T. Moy, and H. Gaub. 1995. Sensing specific molecular interactions with the atomic force microscope. *Biosens. Bioelectron.* 10:895–901.
- Forbes, J. G., and G. H. Lorimer. 2000. Unravelling a membrane protein. *Science*. 288:63–64.
- Fritz, J., A. G. Katopodis, F. Kolbinger, and D. Anselmetti. 1998. Force-mediated kinetics of single P-selectin/ligand complexes observed by atomic force microscopy. *Proc. Natl. Acad. Sci. U.S.A.* 95:12283–12288.
- Grandbois, M., M. Beyer, M. Rief, H. Clausen-Schaumann, and H. E. Gaub. 1999. How strong is a covalent bond? *Science*. 283:1727–1730.
- Grigorieff, N., T. A. Ceska, K. H. Downing, J. M. Baldwin, and R. Henderson. 1996. Electron-crystallographic refinement of the structure of bacteriorhodopsin. *J. Mol. Biol.* 259:393–421.
- Haltia, T., and E. Freire. 1995. Forces and factors that contribute to the structural stability of membrane proteins. *BBA Bioenerg.* 1228:1–27.
- Haupts, U., J. Tittor, and D. Oesterhelt. 1999. Closing in on bacteriorhodopsin: progress in understanding the molecule. *Annu. Rev. Biophys. Biomol. Struct.* 28:367–399.
- Helmreich, E. J. M., and K-P. Hofmann. 1996. Structure and function of proteins in G-protein coupled signal transfer. *Biochem. Biophys. Acta.* 1286:285–322.
- Heymann, B., and H. Grubmüller. 2000. Dynamic force spectroscopy of molecular adhesion bonds. *Phys. Rev. Lett.* 84:6126–6129.
- Holz, M., Drachev, L. A., Mogi, T., Otto, H., Kaulen, A. D., Heyn, M. P., Skulachev, V. P., Khorana, H. G. 1989. Replacement of aspartic acid-96 by asparagine in bacteriorhodopsin slows both the decay of the M intermediate and the associated proton movement. *Proc. Natl. Acad. Sci. U.S.A.* 86:2167–2171.
- Katragadda, M., J. L. Alderfer, and P. L. Yeagle. 2000. Solution structure of the loops of bacteriorhodopsin closely resembles the crystal structure. *Biochim. Biophys. Acta.* 1466:1–6.
- Kellermayer, M. S., S. B. Smith, H. L. Granzier, and C. Bustamante. 1997. Folding-unfolding transitions in single titin molecules characterized with laser tweezers. *Science*. 276:1112–1116.
- Kolbe, M., H. Besir, L. O. Essen, and D. Oesterhelt. 2000. Structure of the light-driven chloride pump halorhodopsin at 1.8 Å resolution. *Science*. 288:1390–1396.
- Lanyi, J. K. 1999. Progress toward an explicit mechanistic model for the light-driven pump, bacteriorhodopsin. *FEBS Lett.* 464:103–107.
- Lee, G. U., D. A. Kidwell, and R. J. Colton. 1994. Sensing discrete streptavidin-biotin interactions with atomic force microscopy. *Langmuir*. 10:354–357.
- Luecke, H., B. Schobert, H. T. Richter, J. P. Cartailier, and J. K. Lanyi. 1999. Structure of bacteriorhodopsin at 1.55 Å resolution. *J. Mol. Biol.* 291:899–911.
- Marszalek, P. E., H. Lu, H. Li, M. Carrion-Vazquez, A. F. Oberhauser, K. Schulten, and J. M. Fernandez. 1999. Mechanical unfolding intermediates in titin modules. *Nature*. 402:100–103.
- Merkel, R. 2001. Force spectroscopy on single passive biomolecules and single biomolecular bonds. *Phys. Rep.* 346:343–385.
- Merkel, R., P. Nassoy, A. Leung, K. Ritchie, and E. Evans. 1999. Energy landscapes of receptor-ligand bonds explored with dynamic force microscopy. *Nature*. 397:50–53.
- Mitsuoka, K., T. Hirai, K. Murata, A. Miyazawa, A. Kidera, Y. Kimura, and Y. Fujiyoshi. 1999. The structure of bacteriorhodopsin at 3.0 Å resolution based on electron crystallography: implication of the charge distribution. *J. Mol. Biol.* 286:861–882.
- Möller, C., G. Büldt, N. Dencher, A. Engel, and D. J. Müller. 2000. Reversible loss of crystallinity on photobleaching purple membrane in presence of hydroxylamine. *J. Mol. Biol.* 301:869–879.
- Moy, V. T., E-L. Florin, and H. E. Gaub. 1994. Intermolecular forces and energies between ligands and receptors. *Science*. 266:257–259.
- Müller, D. J., M. Amrein, and A. Engel. 1997. Adsorption of biological molecules to a solid support for scanning probe microscopy. *J. Struct. Biol.* 119:172–188.
- Müller, D. J., D. Fotiadis, S. Scheuring, S. A. Müller, and A. Engel. 1999a. Electrostatically balanced subnanometer imaging of biological specimens by atomic force microscopy. *Biophys. J.* 76:1101–1111.
- Müller, D. J., H-J. Sass, S. Müller, G. Büldt, and A. Engel. 1999b. Surface structures of native bacteriorhodopsin depend on the molecular packing arrangement in the membrane. *J. Mol. Biol.* 285:1903–1909.
- Nakamura, H. 1996. Roles of electrostatic interaction in proteins. *Q. Rev. Biophys.* 29:1–90.
- Oberhauser, A. F., P. E. Marszalek, M. Carrion-Vazquez, and J. M. Fernandez. 1999. Single protein misfolding events captured by atomic force microscopy. *Nat. Struct. Biol.* 6:1025–1028.
- Oberhauser, A. F., P. E. Marszalek, H. P. Erickson, and J. M. Fernandez. 1998. The molecular elasticity of the extracellular matrix protein tenascin. *Nature*. 393:181–185.
- Oesterhelt, D. 1998. The structure and mechanism of the family of retinal proteins from halophilic archaea. *Curr. Opin. Struct. Biol.* 8:489–500.
- Oesterhelt, F., D. Oesterhelt, M. Pfeiffer, A. Engel, H. E. Gaub, and D. J. Müller. 2000. Unfolding pathways of individual bacteriorhodopsins. *Science*. 288:143–146.
- Oesterhelt, F., M. Rief, and H. E. Gaub. 1999. Single molecule force spectroscopy by AFM indicates helical structure of poly(ethylene-glycol) in water. *N. J. Phys.* 1:6.1–6.11.
- Oesterhelt, D., L. Schuhmann, and H. Gruber. 1974. Light-dependent reaction of bacteriorhodopsin with hydroxylamine in cell suspensions of *Halobacterium halobium*: demonstration of an apo-membrane. *FEBS Lett.* 44:257–261.
- Oesterhelt, D., and W. Stoeckenius. 1974. Isolation of the cell membrane of *Halobacterium halobium* and its fraction into red and purple membrane. *Methods Enzymol.* 31:667–678.
- Palczewski, K., T. Kumasaka, T. Hori, C. A. Behnke, H. Motoshima, B. A. Fox, I. Le Trong, D. C. Teller, T. Okada, R. E. Stenkamp, M. Yamamoto, and M. Miyano. 2000. Crystal structure of rhodopsin: a G protein-coupled receptor. *Science* 289:739–45.
- Pfeiffer, M., T. Rink, K. Gerwert, D. Oesterhelt, and H-J. Steinhoff. 1999. Site-directed spin-labelling reveals the orientation of the amino acid side-chains in the E-F loop of bacteriorhodopsin. *J. Mol. Biol.* 287:163–171.
- Rief, M., H. Clausen-Schaumann, and H. Gaub. 1999. Sequence-dependent mechanics of single DNA molecules. *Nat. Struct. Biol.* 6:346–349.
- Rief, M., J. M. Fernandez, and H. E. Gaub. 1998a. Elastically coupled two-level systems as a model for biopolymer extensibility. *Phys. Rev. Lett.* 81:4764–4767.
- Rief, M., M. Gautel, and H. E. Gaub. 2000. Unfolding forces of titin and fibronectin domains directly measured by AFM. *Adv. Exp. Med. Biol.* 481:129–136.
- Rief, M., M. Gautel, F. Oesterhelt, J. M. Fernandez, and H. E. Gaub. 1997a. Reversible unfolding of individual titin immunoglobulin domains by AFM. *Science*. 276:1109–1112.
- Rief, M., M. Gautel, A. Schemmel, and H. E. Gaub. 1998b. The mechanical stability of immunoglobulin and fibronectin III domains in the muscle protein titin measured by AFM. *Biophys. J.* 75:3008–3014.
- Rief, M., F. Oesterhelt, B. Heymann, and H. E. Gaub. 1997b. Single molecule force spectroscopy on polysaccharides by AFM. *Science*. 275:1295–1298.
- Royant, A., P. Nollert, K. Edman, R. Neutze, E. M. Landau, E. Pebay-Peyroula, and J. Navarro. 2001. X-ray structure of sensory rhodopsin II at 2.1-Å resolution. *Proc. Natl. Acad. Sci. U.S.A.* 98:10131–10136.
- Sackmann, E. 1996. Supported membranes: scientific and practical applications. *Science*. 271:43–48.
- White, S. H., and W. C. Wimley. 1999. Membrane protein folding and stability: physical principles. *Annu. Rev. Biophys. Biomol. Struct.* 28:319–365.
- Zhang, B., G. Xu, and J. Evans. 1999. A kinetic molecular model of the reversible unfolding and refolding of titin under force extension. *Biophys. J.* 77:1306–1315.

Determining molecular forces that stabilize human aquaporin-1

Clemens Möller,^a Dimitrios Fotiadis,^b Kitaru Suda,^b Andreas Engel,^b
Max Kessler,^c and Daniel J. Müller^{a,d,*}

^a Max Planck Institute of Molecular Cell Biology and Genetics, Pfotenhauerstrasse 108, 01307 Dresden, Germany

^b M.E. Müller Institute for Structural Biology, Biozentrum, University of Basel, 4056 Basel, Switzerland

^c Center for Nanoscience (CenSC), Sektion Physik, Ludwig Maximilians-Universität München, 80799 Munich, Germany

^d BIOTEC, Technical University Dresden, 01062 Dresden, Germany

Received 10 December 2002, and in revised form 28 February 2003

Abstract

Atomic force microscopy (AFM) was used to measure the forces stabilizing human aquaporin-1 (hAQP1), a tetrameric transmembrane protein that forms highly specific water channels. To this end, the AFM tip was attached to the C-terminus of hAQP1 and secondary structure elements were extracted from the membrane while the single-molecule force-extension curve was being recorded. Force peaks, reflecting the unfolding of secondary structure elements, could be interpreted in depth using the atomic model of hAQP1. Different classes of force-extension curves indicated the existence of alternative unfolding pathways for individual proteins. In addition, transmembrane helices at the periphery of the hAQP1 tetramer exhibited smaller extraction forces than helices at the interface between hAQP1 monomers. These results represent the first direct assessment of intermolecular forces defining the oligomeric state of a membrane protein.

© 2003 Elsevier Science (USA). All rights reserved.

Keywords: Aquaporin; Atomic force microscopy; Force spectroscopy; Molecular interactions; Membrane protein assembly; Secondary structure; Worm-like chain model

1. Introduction

Water is the universal solvent in all living organisms. The amount of water that passes across membranes in plants and animals is immense and sums up to hundreds of liters per day in humans. This enables living cells to change their size and shape and to maintain their osmotic balance. Simple diffusion of water molecules through a pure lipid bilayer occurs with an Arrhenius activation energy of >10 kcal/mol (Fettiplace and Haydon, 1980) and cannot account for the observed massive osmotically driven water flow through biological membranes. In the plasma membrane of red blood cells an activation energy of <5 kcal/mol was measured, leading to the hypothesis that water pores must exist (Sidel and Solomon, 1957). Furthermore, water permeation through red blood cells was shown to

be inhibited by HgCl₂ and certain organomercurials, indicating the presence of a proteinaceous water pore with a critical sulfhydryl group (Macey and Farmer, 1970).

The first molecular water channel discovered and cloned was aquaporin-1 from red blood cells and renal tubules (Denker et al., 1988; Preston and Agre, 1991). Its water transport capacity was demonstrated by expression in *Xenopus* oocytes (Preston et al., 1992). Since then, a large number of similar channel-forming integral membrane proteins have been found in diverse forms of life, constituting the aquaporin superfamily (Heymann and Engel, 1999; Park and Saier, 1996; Zardoya and Villalba, 2001).

Sequence analysis of the 269-amino-acid(aa)-long human AQP1 (hAQP1)¹ protein suggests that it consists of six membrane-spanning α -helices (H1–H6), five

* Corresponding author. Fax: +49-351-210-2020.

E-mail address: mueller@mpi-cbg.de (D.J. Müller).

¹ Abbreviations used: AFM, atomic force microscopy; hAQP1, human aquaporin-1; WLC, worm-like chain.

connecting loops (LA–LE), and the termini located on the cytoplasmic side (Preston and Agre, 1991). The sequence exhibits a pronounced homology between the N- and the C-terminal halves of the protein (Heymann and Engel, 1999; Park and Saier, 1996), each half containing the highly conserved Asn-Pro-Ala (NPA) motif, which is part of the aquaporin superfamily signature (Pao et al., 1991). The NPA motifs are located on loops B and E, which form short α -helices (Mitsuoka et al., 1999) and extend into the membrane core to create a constitutively open, narrow aqueous channel as proposed in the “hourglass model” (Jung et al., 1994).

Human AQP1, which exists as noncovalently associated homotetramers in the native membrane, comprises three nonglycosylated subunits and one bearing a large polylactosaminoglycan (Smith and Agre, 1991). The first atomic model of hAQP1 revealed the dual function of the NPA motif (Murata et al., 2000). First, the two prolines are stacked in the center of the molecule forming the platform from which the two short α -helices emanate toward the extracellular and cytoplasmic surface of hAQP1. Second, the asparagines protrude into the water pore, providing a critical hydrogen bonding site for water molecules tumbling through the channel at a rate of 3×10^9 H₂O/s (de Groot and Grubmüller, 2001). This particular architecture of hAQP1 has also been found in the 2.2-Å structure of the bacterial glycerol facilitator GlpF (Fu et al., 2000) and has been confirmed by the 2.2-Å structure of bovine AQP1 (Sui et al., 2001).

Prediction of the stability and three-dimensional (3D) structure of a membrane protein from its sequence is yet a difficult undertaking. For this purpose, the energetics of the interactions of the peptide chains with each other and with the various components of their environment, i.e., the lipid bilayer, need to be fully understood. In some cases, theoretical models (Grubmüller et al., 1996; Lazaridis and Karplus, 1999; Lu and Schulten, 1999) allow these interactions to be estimated, while experimental data are typically obtained from integrative measurements revealed from high protein densities immersed in solutions, i.e., by assessing their stability against chemical or thermal denaturation (Booth et al., 2001). Such high protein densities are required to generate a sufficient signal from the biochemical processes under study, with the disadvantage that nonspecific protein–protein contacts may change significantly the signal measured. Moreover, conditions used to unfold proteins are unlikely to present or mimic their physiological environment. Recent perceptions of protein (un)folding, such as are described by multidimensional landscapes or folding funnels, can be seen as a result of the complexity of inter- and intramolecular interactions (Radford, 2000). Unfolding pathways may be populated differently depending on small variations of the experimental environment. This calls for novel approaches,

other than bulk measurements, to observe coexisting minor and major (un)folding pathways.

Atomic force microscopy (AFM; Binnig et al., 1986) combined with force spectroscopy (Oberhauser et al., 2001; Rief et al., 1997a) offers the unique possibility of performing direct measurements on single proteins. Because of the high signal-to-noise ratio provided by the AFM, single proteins can be imaged in their native environment at a lateral resolution of 0.4–1.0 nm and a vertical resolution of 0.1–0.2 nm (Engel and Müller, 2000; Müller et al., 2002a) before and after measuring inter- and intramolecular forces by force spectroscopy (Müller et al., 1999a; Oesterhelt et al., 2000).

Here, we combine AFM imaging to identify membrane patches containing hAQP1 proteins with force spectroscopy to study the unfolding pathways of hAQP1. To this end, we allow the C-terminus of hAQP1 to attach to the AFM tip by contact adhesion and separate both surfaces. Upon separation, the deflection of the AFM cantilever is monitored until the entire protein is unfolded. Combined with the refined 3D structure of hAQP1 (de Groot et al., 2001), the resulting force spectra provide substantial information about inter- and intramolecular forces stabilizing the AQP1 water channel.

2. Materials and methods

2.1. Purification, crystallization, and deglycosylation of human AQP1

AQP1 from human erythrocytes was purified and crystallized in two dimensions by dialysis as described previously (Walz et al., 1994a). The 2D crystals were subsequently deglycosylated: Human AQP1 crystals were washed three times with 25 mM Na acetate–HCl (pH 6), 5 mM EDTA, 2 mM DTT, 1 mM benzamidine, 0.05% NaN₃ (DG buffer) by centrifugation. Peptide: *N*-glycosidase F (New England Biolabs, Beverly, MA, USA) was then added to a final concentration of 22 μ g/ml at an hAQP1 concentration of 1 mg/ml. The mixture was incubated for 18 h at room temperature, after which the reaction was stopped by washing the crystals by centrifugation with DG buffer.

2.2. AFM imaging and single-molecule force spectroscopy

A commercial atomic force microscope (Nanoscope E; Digital Instruments, Santa Barbara, CA, USA) equipped with a 120- μ m piezo scanner was operated in buffer solution using the standard fluid cell without an O-ring. In all experiments, the reconstituted 2D hAQP1 crystals were adsorbed to freshly cleaved mica and imaged in 10 mM Tris–HCl (pH 7.2), 150 mM KCl at room temperature (21 °C). Imaging was performed in the

contact mode as described previously (Müller et al., 1999b). The oxide-sharpened Si_3N_4 cantilevers (OMCL TR400PS) employed were purchased from Olympus Ltd. (Tokyo, Japan) and had a nominal force constant of 0.1 N/m. The exact force constants of the cantilevers were determined in solution from their thermal noise spectra using the equipartition theorem (Butt and Jaschke, 1995; Schäffer et al., 1996) deviating by about 10% from the nominal force constant.

After a crystal patch was identified, the AFM tip was brought into contact with the membrane by applying a force of ≈ 1 nN for ≈ 1 s. This allowed hAQP1 polypeptides to adhere nonspecifically to the tip. However, the nature of the bridge established between the AFM tip and the amino acid was nonspecific. Tip and protein were then separated with a velocity of 50 nm/s while the cantilever deflection was recorded. This deflection vs piezo-displacement curve was converted to a force vs tip-sample distance curve as described previously (Rief et al., 1997b).

2.3. Force curve selection

Prior to analysis, the collected force-extension curves were classified because proteins attached nonspecifically at different sites of their polypeptide chain to the AFM tip. One suitable selection criterion is the overall length of the force curve, reflected by the tip-sample distance at which the last force peak occurs: a protein attached to the cantilever by one of its loops results in a force curve with smaller overall length than that of a protein attached at one of the termini.

The classification of the curves is further facilitated by the different length of the C- (38 aa) and the N-terminal tails (9 aa; de Groot et al., 2001). The last adhesion peak of the force-extension curve of a completely unfolded hAQP1 protein arises upon extraction of the last transmembrane α -helix from the membrane. If the AFM tip is attached to the N-terminal end of hAQP1, this will be helix H6. In this case, the maximal separation between the tip and the membrane surface will correspond to a fully stretched polypeptide chain between the N-terminus and the extracellular end of H6 at Phe 206. The corresponding force curve will thus exhibit a length between 206 and 197 aa ($= 206 \text{ aa} - 9 \text{ aa}$), depending on which amino acid of the 9-aa-long N-terminal stretch the tip is attached to. In contrast, if the protein is unfolded by pulling at the 38-aa-long C-terminal end, the last adhesion peak arises upon extraction of helix H1 from the membrane. Depending on the amino acid to which the tip adheres at the C-terminus, the length of the fully extended polypeptide chain will vary between 194 and 232 aa in length. Accordingly, force-extension curves corresponding to an extension of more than 206 aa must result from adhesion of the C-terminal end to the tip. Therefore, only those force-extension curves exhibiting a

length between 207 and 232 aa were selected and analyzed. This stringent criterion ensured that all the analyzed curves belonged to the same subset, thus allowing a detailed analysis to be made.

2.4. Alignment of force curves

The selected curves were shifted so that their last force peaks were aligned and merged. The resulting force peaks were analyzed using the worm-like-chain (WLC) model with a persistence length of 4 Å (Rief et al., 1997a). This yielded the length of the peptide chain of the corresponding force peak, which in turn allowed the calculation of the number of amino acids, assuming the length of one amino acid residue to be 3.6 Å. Since only hAQP1 molecules extracted by their C-terminus were analyzed, the number of unfolded amino acids was counted from this end of the polypeptide chain. To facilitate comparison of these values with the protein sequence, the corresponding amino acid numbers counted from the N-terminus are also given (Fig. 3).

2.5. Contour length and membrane offset

The unfolding process was interpreted by comparing contour lengths of the individual unfolding events, such as those obtained from the WLC model, with the structure of hAQP1 as determined by de Groot et al. (2001). When the polypeptide was pulled from the cytoplasmic surface, the anchor of the peptide sometimes had to be assumed to exist at the opposite, extracellular, surface. In this case, the lipid bilayer thickness (≈ 4 nm) had to be considered and 11 aa ($11 \times 3.6 \text{ Å} \approx 4 \text{ nm}$) were added to the number of amino acids determined using the WLC model (Müller et al., 2002b; Fig. 5). This allowed the entire rupture length of the polypeptide to be calculated.

3. Results

3.1. Recording, selection, and alignment of force-extension curves

Crystalline hAQP1 patches were adsorbed to freshly cleaved mica and imaged in buffer solution with the AFM (Fig. 1). Under these conditions the hAQP1 2D crystals exhibited a height of 5.8 ± 0.3 nm ($n = 66$). Imaging of the surface at higher magnification revealed the p42₁2 symmetry of the hAQP1 crystal (Fig. 1, inset) (Fotiadis et al., 2002; Walz et al., 1994b). The alternating up-and-down orientation of the tetramers implies that both the cytoplasmic (lower tetramer, broken circle) and the extracellular surfaces (higher tetramer, continuous circle) of hAQP1 can be visualized.

After imaging, the AFM tip was placed over a hAQP1 patch, forced into contact with the membrane,

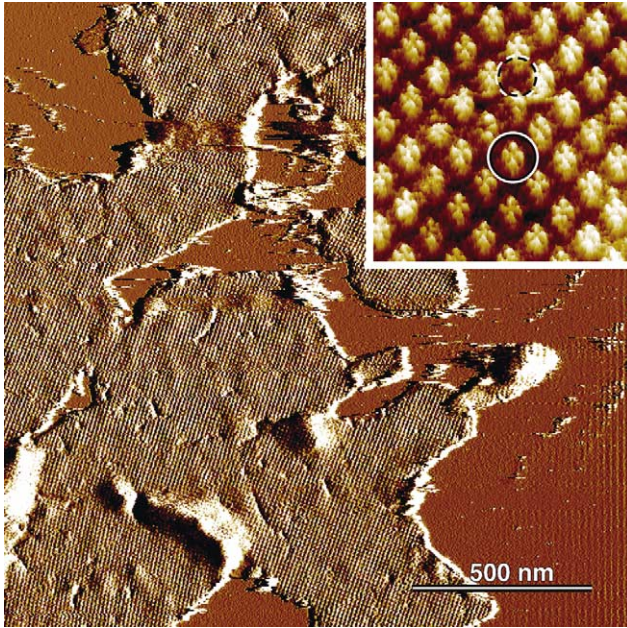


Fig. 1. Overview image of a hAQP1 2D crystal adsorbed on mica. Before force-spectroscopy experiments were performed, the aquaporin crystals were localized using AFM operated in the contact mode. The image was recorded by monitoring the cantilever deflection (deflection height: 1 nm). The inset represents a high-resolution topograph recorded with a constant force of ≈ 100 pN and exhibits a vertical height scale of 2 nm at a frame size of 75 nm. The extracellular surface of the hAQP1 tetramer is outlined by a circle, while the cytoplasmic surface of the neighboring tetramer is outlined by a dashed circle (Fotiadis et al., 2002). Imaging was performed at room temperature in 10 mM Tris-HCl (pH 7.2), 150 mM KCl.

and then retracted. The force-extension curve was recorded during retraction. About 98% of the curves showed no adhesive interactions between tip and sample. However, adhesion peaks that resulted from pulling on a molecular bridge that had been established between the hAQP1 protein and the AFM tip were occasionally observed (Fig. 2, top). Only force curves exhibiting an overall length of >75 nm were selected for further analysis because they arose from the complete unfolding of single hAQP1 molecules by being pulled at their C-terminal end (see Section 2).

As shown recently for bacteriorhodopsin (Müller et al., 2002b; Oesterhelt et al., 2000), the discontinuous shape of the force-extension curves from a membrane protein comprising several transmembrane α -helices can be explained as follows: While one end of the protein is attached to the tip, the rest of the protein remains embedded in the membrane. Upon retraction of the tip, the polypeptide forming the bridge is stretched, thereby exerting a force onto the cantilever. This force increases gradually upon further separation of tip and membrane, which puts more and more tension on the peptide stretch. Above a certain tension, parts of the protein unfold and the force suddenly drops. As the tip-membrane distance is increased further, the next unfolding

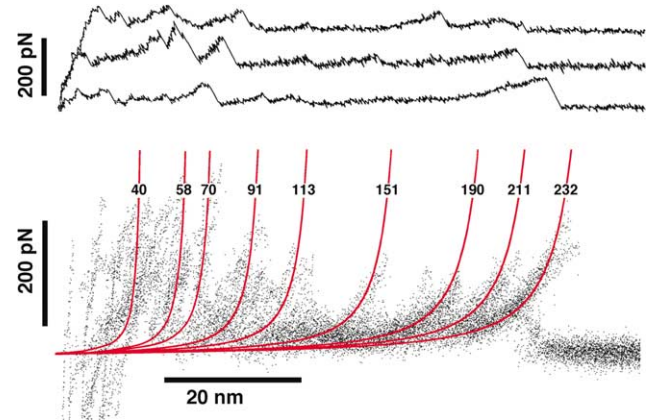


Fig. 2. Unfolding single hAQP1 molecules using the AFM. Top: A selection of single-molecule force-extension curves showing the complete unfolding of hAQP1. The individual hAQP1 molecules were unfolded by pulling at their C-termini (see Section 2). Bottom: 26 force-extension curves were aligned at the last force peak (232 aa) and fitted using the WLC model (continuous curves). The numbers on the curves indicate the contour lengths used to obtain the fit, in amino acids.

barrier causes tension to build up again. Therefore, every drop in force can be tentatively assigned to the unfolding of a certain structural region of the protein from the membrane. There is evidence that certain secondary structure elements of bacteriorhodopsin unfold before they are extracted from the membrane (Müller et al., 2002b). Unfolding and extraction result in a less compact and thereby longer polypeptide chain between tip and membrane. Before tension is again built up between protein and cantilever this longer polypeptide chain has to be fully extended.

To assess the reproducible features of the hAQP1 unfolding process, the force-extension curves recorded upon unfolding from the C-terminus were selected (see Section 2). These curves were superimposed and aligned at their last adhesion peak (Fig. 2, bottom). The resulting overlay plot contains a wealth of detailed information. However, while the common features of all force-extension curves are emphasized in this overlay plot, individual characteristics of some curves are hidden in the noise.

3.2. Fitting the force-extension curves

The WLC model (Bustamante et al., 1994; Marko and Siggia, 1995) was developed to describe the elasticity of a stretched polypeptide (Rief et al., 1997a). It describes the theoretical dependence of the force F upon the extension of the molecular chain by the distance x as

$$F(x) = \frac{k_B T}{l_p} \left(\frac{1}{4} \left(1 - \frac{x}{L} \right)^{-2} + \frac{x}{L} - \frac{1}{4} \right),$$

where l_p represents the persistence length and L the contour length of the polypeptide stretch. A persistence

length of 4 Å has been shown to hold for a variety of proteins (Rief et al., 1997a). Taking this value, the contour lengths of stretched portions of the hAQP1 molecule were determined by fitting $F(x)$ to the maxima of the force-extension curves. The continuous, nonlinear increase in force that is observed for each force maximum within the force-extension curves recorded on hAQP1 is well described by the WLC model (Fig. 2, bottom). The first force peak occurred close to the membrane surface (≈ 14 nm) within a noisy region. Fitting this peak yielded a contour length corresponding to about 40 ± 8 aa. All 26 curves superimposed exhibited peaks in this region, resulting in an average force of 206 ± 64 pN. The next force peak was detected after the tip had been retracted by ≈ 20 nm and corresponds to a contour length of 58 ± 6 aa. Twenty-four of 26 curves exhibited this peak with an average force of 157 ± 49 pN. Seventeen of all curves exhibited a peak at about 70 ± 8 aa and an average force of 125 ± 63 pN. At a tip to membrane separation of ≈ 25 nm the peaks showed a broad distribution around an average contour length of 91 ± 7 aa ($n = 22$) and exhibited an average force of 156 ± 44 pN. The next obvious peak occurred at a tip retraction of ≈ 31 nm in 13 of all curves and is described by a contour length of 113 ± 7 aa. At a separation of ≈ 42 nm a force peak was present in 20 curves and had a contour length of 151 ± 5 aa, while the following peak exhibited a contour length of 190 ± 10 aa (at ≈ 53 nm, $n = 17$). The next force peak of 77 ± 42 pN ($n = 16$) was observed at a contour length of 211 ± 6 aa (at ≈ 61 nm). The last force peak of 152 ± 62 pN was present in all force-extension curves, since it was used as selection criterion. It is described by a contour length of 232 ± 5 aa at a distance of ≈ 64 nm. Only 6 curves showed all force peaks fitted, all other curves showed most of the peaks fitted but lacked individual ones.

Table 1 summarizes the contour lengths derived from the WLC fits of the obtained force peaks, their average maximum force, and the distances from the C-terminus to individual secondary structural elements of the protein. It suggests that the positions of the helices and of their ends are rather well correlated to the contour lengths measured in the unfolding process.

4. Discussion

4.1. Unfolding events of secondary structure elements

4.1.1. Stretching of the C-terminus and unfolding of α -helix H6

Force-curve analysis was performed on curves where the C-terminus of hAQP1 had adhered to the AFM tip (see Section 2). A first adhesion peak was observed within a noisy region in the overlay plot at an AFM tip–membrane separation of ≈ 14 nm (Fig. 2). Within this close distance between tip and membrane surface, non-specific interactions occur frequently (Butt et al., 1995; Israelachvili, 1991), thereby introducing a scattering of the adhesion peaks. In addition, the C-terminus was found to be an element with complex structural properties (Fotiadis et al., 2002; Sui et al., 2001) and its stretching might further contribute to the observed noise in the overlay-plot. Nevertheless, the WLC fit of the force peak revealed a contour length of 40 ± 8 aa. This value was expected since the cytoplasmic end of helix H6 is at Leu 231, which yields a theoretical contour length of 38 aa ($= 269$ aa $- 231$ aa; see Figs. 3 and 5). This result suggests that helix H6 establishes the first potential barrier against mechanical unfolding. The structural stability of this helix is reflected by the average unfolding force of 206 ± 64 pN ($n = 26$), the highest of all peaks observed.

Table 1
Contour lengths, forces, and positions of potential barriers in hAQP1

Contour length from WLC fits (aa)	Curves exhibiting the force peak ($n_{\text{total}} = 26$)	Average force (pN)	Proposed potential barrier (Fig. 3)	aa from the C-terminus to the potential barrier (Fig. 3)	Contour length considering membrane offset (Fig. 5)
40 ± 8	26 (100%)	206 ± 64	Cytopl. end of helix H6	38	No offset
58 ± 6	24 (92%)	157 ± 49	Extra. end of helix HE	65	54 aa
70 ± 8	17 (65%)	125 ± 63	Extra. end of helix H5	85	74 aa
91 ± 7	22 (85%)	156 ± 44	Helix H5	85–102	74–102 aa
113 ± 7	13 (50%)	98 ± 54	Cytopl. end of helix H4	112	No offset
151 ± 5	20 (77%)	82 ± 53	Helix H3	155–171	144–171 aa
190 ± 10	17 (65%)	98 ± 33	Cytopl. end of helix HB	183	No offset
211 ± 6	16 (62%)	77 ± 42	Helix H2	199–220	199–209 aa
232 ± 5	26 (100%)	152 ± 62	Helix H1	232–260	222–260 aa

The membrane offset was 11 aa if the potential barrier of a secondary structure was located at the opposite extracellular surface and 0 aa if located on the cytoplasmic surface from which the tip was pulling the polypeptide end. cytopl., cytoplasmic; extra., extracellular.

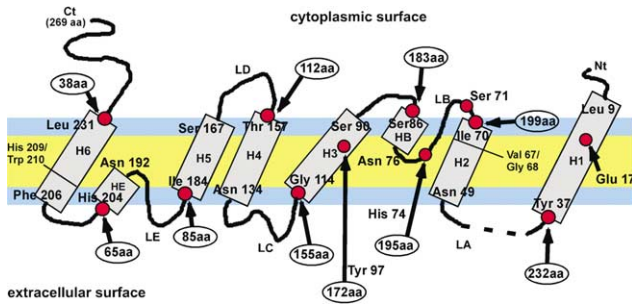


Fig. 3. Model of hAQP1. Shown are the secondary structure elements in the lipid bilayer and the amino acids where the helices start and end, as described by de Groot et al. (2001). Numbers in ovals represent the numbers of amino acids counted from the C-terminal end.

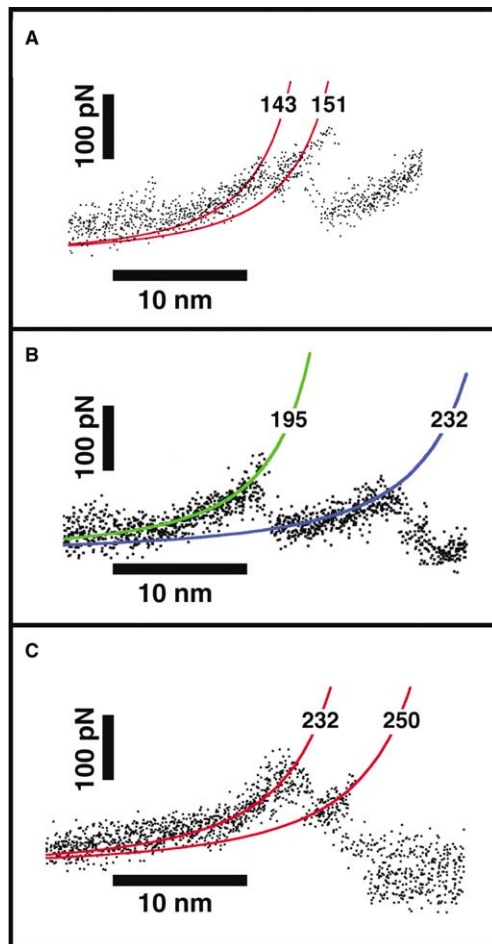
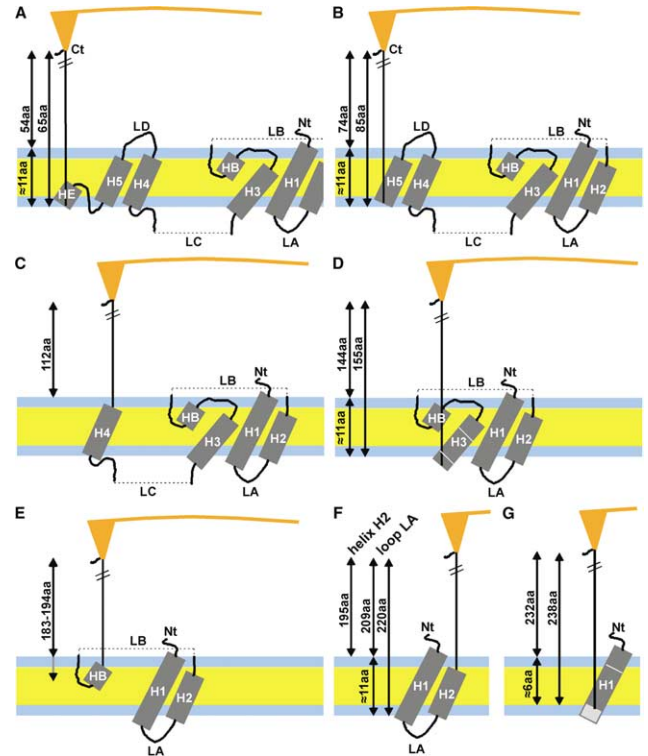


Fig. 4. Classification of side peaks reveals unfolding pathways of secondary structure elements. (A) Stepwise unfolding of helix H3. (A) Selected force-extension curves exhibiting a side peak at 143 aa contour length are superposed. The second force peak is fitted with a contour length of 151 aa as indicated. (B) Force-extension curves classified according to the peak at a contour length of 195 aa. (C) Unfolding pathways of transmembrane α -helix H1. Selected force-extension curves exhibiting a side peak upon unfolding of helix H1 have been superposed. While the unfolding of helix H1 takes place at a contour length of 232 aa, fitting of the side peak yielded a contour length of 250 aa.



4.1.2. Unfolding of α -helix HE

Similar to the first force peak, the next major force peak appeared within the noisy region but at a tip–membrane separation of about 20 nm (Fig. 2). The WLC fit showed an average contour length of 58 ± 6 aa, while the rupture event exhibited an average force of 147 ± 49 pN ($n = 23$). According to the model shown in Fig. 3, the extracellular end of helix HE is separated from the C-terminal end by 65 aa. Taking a membrane offset of ≈ 11 aa into account, the polypeptide stretch exposed from the cytoplasmic surface to the tip comprises ≈ 54 aa (Fig. 5A). This value compares favorably with the average contour length found by the WLC fit. Thus, we assume this adhesion peak to reflect the unfolding of helix HE.

4.1.3. Unfolding of α -helix H5

The third major peak was observed at a contour length of 70 ± 8 aa and a force of 125 ± 63 pN. The theoretical contour length for the unfolding starting point of helix H5 at Ile 184 is 85 aa ($= 269$ aa $- 184$ aa; Figs. 3 and 5B). Subtracting the membrane bilayer thickness (≈ 11 aa) reduces this number to ≈ 74 aa. This value agrees with the contour length found and suggests that the observed force peak reflects the potential barrier built by the extracellular end of helix H5.

The peak at 70 aa was followed by force peaks exhibiting a relatively large variation of contour lengths. While their average contour length was determined to 91 aa and to an average force of 156 ± 44 pN (Fig. 2 and Table 1), most of the peaks of this broad peak distri-

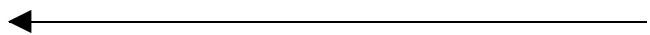


Fig. 5. Schematic model of the mechanical unfolding of hAQP1 according to the refined structure (de Groot et al., 2001). The structural elements of the protein are sequentially extracted from the membrane as the tip is withdrawn. (A) Schematic representation of the hAQP1 structure with the C-terminus attached to the tip. Helix H6 was already extracted from the membrane. At this point, the potential barrier for further unfolding is located on the extracellular side of helix HE. This would correspond to a stretched polypeptide chain exhibiting a contour length of 65 aa from which 11 aa have to be extracted to compensate for the membrane bilayer thickness. As a result, the stretched polypeptide protruding, separating membrane surface and AFM tip, corresponds to ≈ 54 aa. (B) If the externally applied force supersedes this potential barrier, helix HE unfolds. The longer polypeptide is now stretched by the retracting AFM tip. At its cytoplasmic end (Ile 184), helix H5 establishes the next potential barrier. This corresponds to a contour length of 85 aa, which results in ≈ 74 aa separating the extracellular membrane surface and the AFM tip. At a certain force, this potential barrier of helix H5 is superseded and the helical structure unfolds. Again, the AFM tip is further separated by the extended length of the polypeptide. (C) The next potential barrier is formed by the cytoplasmic end of helix H4 (Thr 157) yielding a theoretical contour length of 112 aa. (D) After helix H4 unfolds, loop C (LC) is pulled into the membrane until the extracellular end of helix H3 (Gly 114) establishes a potential barrier against mechanical unfolding. This leads to a contour length of 155 aa. To estimate the polypeptide chain extending into the cytoplasmic space, the bilayer thickness has to be taken into account, which leads to a length of ≈ 144 aa. (E) After helix H3 unfolds, helix HB establishes a potential barrier. At its cytoplasmic surface the stretched polypeptide would have a length of 183 aa, while at its extracellular end facing the membrane center the polypeptide length would correspond to ≈ 194 aa. At a certain force the complete helix HB and the loop LB unfold. (F) Helix H2 forms a potential barrier at its cytoplasmic side and 195 aa are stretched. After helix H2 unfolds, loop LA establishes a potential barrier and the polypeptide protruding from the cytoplasmic surface corresponds to ≈ 209 aa. (G) At a certain force, loop LA and ≈ 6 aa of the N-terminal helix unfold until the cytoplasmic portion of the stretched polypeptide elongates to ≈ 232 aa. The white line at the upper half of helix H1 indicates an additional potential barrier at Leu 19 and Gly 20, which are involved in intermolecular contact with helix H1 of the neighboring hAQP1 molecule. At this point, the length of the stretched polypeptide corresponds to ≈ 250 aa. If this potential is superseded by the externally applied force of the cantilever, the entire hAQP1 molecule is unfolded and extracted from its tetrameric assembly in the membrane.

bution occurred within a standard deviation of 7 aa. Helix H5 is not only tightly packed against helix H2 by van der Waals contacts involving the conserved Gly 173 and Gly 57 residues, but it also contributes to the intermolecular contact within the hAQP1 tetramer (Murata et al., 2000). These conserved, tightly packed structures are located at the center of the hydrophobic membrane and are separated by 96 aa from the C-terminal end. Thus, the average contour length of 91 aa is likely to reflect the potential barrier resulting from tight packing of helices H2 and H5, if one subtracts half of the membrane thickness (≈ 6 aa) from the 96-aa-long polypeptide. However, the contour length distribution observed by the scattered force peaks suggests multiple steps during unfolding of helix H5. The specific interaction of helices H5 and H2 may further explain why a higher force is required to unfold this central region of

helix H5 compared to its extracellular end and the following structural elements of hAQP1 (Table 1).

4.1.4. Unfolding of α -helix H4 and loop LC

The subsequent adhesion peak occurred at a contour length of 113 ± 7 aa (Fig. 2) with an average force of 98 ± 54 pN. The cytoplasmic end of helix H4 in hAQP1 is located at a distance of 112 aa from the C-terminus (Thr 157 from the N-terminus; Figs. 3 and 5C). We therefore suggest this adhesion peak to represent the force required to overcome the potential barrier established by helix H4. Once this potential barrier is demolished helix H4 and the cytoplasmic loop LC unfold in a single step (Fig. 5C).

4.1.5. α -helix H3 unfolds in several steps

The next adhesion peak has a rupture force of 82 ± 53 pN, is located in a less noisy region than all previous peaks, and exhibits a contour length of 151 ± 5 aa (Fig. 2). Fig. 4A displays a selected subset of six curves (23%) that exhibited an additional side peak at 143 aa. The extracellular end of helix H3 is located around Gly 114, which is separated by 155 aa from the C-terminus (Fig. 3). Taking the membrane bilayer into account (≈ 11 aa), the theoretical contour length lies at about 144 aa (Fig. 5D). Thus, the peak located at 143 aa is associated with the potential barrier built by the extracellular end of helix H3. It is assumed that a hydrogen bonding network in this region establishes a stable association of helix H3 with the remaining helices HB, H1, and H2. To investigate, however, whether the largest extracellular loop LC adheres to the underlying mica surface and whether this interaction may contribute to the force peak measured, we performed the same experiments on double-layered hAQP1 membranes. In these experiments, we did not find any changes of the force spectra. In most cases (77%), however, a force peak was observed at a contour length of 151 aa. This indicates that helix H3 as an entity establishes a more significant potential barrier against mechanical unfolding than the anchor at its extracellular end. This barrier is located approximately at the center of the membrane.

4.1.6. Unfolding of helix HB

The force peaks found at a contour length of 190 ± 10 aa (Fig. 2) exhibit an average rupture force of 98 ± 33 pN. This distance from the C-terminus corresponds to helix HB (Fig. 5E), which dips into the membrane from the cytoplasmic side and is only 11 aa long (Figs. 3 and 5E). Thus, this adhesion peak is likely to reflect the unfolding of HB.

4.1.7. Unfolding of α -helix H2 and loop LA

The smallest force peak (77 ± 42 pN) was observed at a contour length of 211 ± 6 aa (Fig. 2). Because the

extracellular end of helix H2 is located at Asn 49 (de Groot et al., 2001), the theoretical contour length including the membrane offset (≈ 11 aa) lies around 209 aa (Fig. 5F). Thus, the force peak at 211 aa is likely to correspond to the unfolding of loop LA and the force required to pull this hydrophilic loop into the hydrophobic membrane core. Therefore, it must be concluded that helix H2 unfolded within the previous unfolding step together with helix HB. However, the superposition of some selected curves (Fig. 4B; $n = 8$) shows an adhesion peak occurring at a contour length of 195 ± 4 aa (132 ± 15 pN), which is located at the cytoplasmic end of helix H2 (Figs. 3 and 5F). These peaks were not followed by the peak of loop LA (211 aa). The adhesion peaks of 211 and 195 aa show in a unique way that helix H2 and loop LA unfold in alternative pathways. Either helix H2 unfolds together with helix HB or it unfolds together with loop LA (Fig. 5D).

4.1.8. α -helix H1 unfolds in two steps

The last peak in the spectra was observed at a contour length of 232 ± 5 aa exhibiting an average force of 152 ± 62 pN (Fig. 2). This peak illustrates a significant interaction of helix H1 with the adjacent AQP1 molecule and the bilayer core. Taking the membrane offset into account, the potential barrier is located around Ala 32 of hAQP1, which lies 5 aa from the extracellular end of the N-terminal helix. This indicates that the potential barrier against mechanical unfolding of this helix is located 5 aa from the extracellular surface within the hydrophobic core of the membrane (Fig. 5G). Certain force-extension curves (35%) exhibited a side peak around 250 aa (100 ± 14 pN; $n = 9$; Fig. 4C), which might correspond to the conserved Leu 19 and Gly 20 that are involved in intermolecular contacts. Together, the data suggest that helix H1 of hAQP1 establishes two potential barriers against mechanical unfolding. In the case of the residues Leu 19 and Gly 20, the peak at 250 aa may represent the disruption of their interaction with H4 of the adjacent monomer.

5. Rate dependence of the unfolding process

The force required to overcome a potential barrier in the unfolding process has previously been shown to be rate dependent (Evans, 2001; Rief et al., 1997a). Instead of exploring the rate dependence, we pulled on the protein at the same constant speed in all of the experiments. This allowed acquisition of detailed information on the position of the observed potential barriers in the force curves, which correlate to secondary structure elements of the hAQP1 protein. However, the rate dependence to obtain information on the shape of the potential barriers (Evans, 2001) needs to be studied in future experiments.

6. hAQP1 exhibits an unique unfolding behavior

6.1. Transmembrane α -helices of hAQP1 unfold individually

Most of the force peaks observed in the unfolding process can unambiguously be correlated to potential barriers built up against mechanical unfolding of secondary structure elements of hAQP1. Individual peaks of the force spectra could be assigned to unfolding events of individual α -helices. Even within a region very close to the membrane surface (< 20 nm), in which the force-spectroscopy data were noisy, the unfolding of helices H6 and HE could be identified. The observation that transmembrane α -helices of hAQP1 unfold within a single step agrees with the unfolding behavior of bacteriorhodopsin from *Halobacterium salinarum* (Müller et al., 2002b; Oesterhelt et al., 2000).

These observations support the two-stage model that has been suggested to simplify the (un)foldings of membrane proteins (Popot and Engelman, 1990, 2000). In this model, transmembrane α -helices form independent stable entities within the hydrophobic bilayer. In a second step, these helices pack together and form the final protein fold, with a helical packing that is often dictated by the sequence motif GxxGxxG (Russ and Engelman, 2000). To date such insight has been mostly acquired on bacteriorhodopsin (BR), the only transmembrane α -helical protein for which the folding from a completely denatured membrane protein has been achieved (Booth et al., 2001). Our observations indicate that, similar to BR, the transmembrane α -helices of hAQP1 form stable entities within the lipid membrane and that their specific interactions give rise to higher potential barriers against unfolding than others.

Compared to bacteriorhodopsin the transmembrane α -helices of hAQP1 show a less pronounced tendency to unfold pairwise. There are two major reasons for this difference: Unlike bacteriorhodopsin, hAQP1 has several long loops (C, B, and E) connecting the transmembrane α -helices which may support the observed tendency of individual α -helices to unfold individually. In contrast, α -helices connected by short loops predominantly unfold pairwise although they were also observed to unfold as single helices (Müller et al., 2002b; Oesterhelt et al., 2000). Further, AQP1 is a right-handed bundle of highly tilted transmembrane helices. This yields the strong intermolecular interactions in the left-handed coiled coils formed by helices H1 and H2 with helices H4 and H5 of the adjacent monomer (Murata et al., 2000). Such an intermolecular helical packing arrangement appears to dictate the unfolding behavior of hAQP1. Weaker intermolecular interactions have been observed within the monomers of the bacteriorhodopsin trimer, a left-handed bundle of only slightly tilted α -helices. Thus, we propose that

the pairwise interactions between transmembrane helices of bacteriorhodopsin may be an intrinsic feature of the protein structure and interaction.

6.2. Unfolding forces of individual α -helices

The forces required to unfold the individual transmembrane α -helices showed a maximum in the beginning of the unfolding process (Table 1). Accordingly, α -helices removed at the beginning presented a higher potential barrier against mechanical unfolding compared to α -helices removed afterward. The observed decrease in force as unfolding proceeds indicates the destabilization of structural elements by the extraction of the surrounding structures. Interestingly, also the last helix required a relatively high force to be pulled out. This is likely to reflect the intermolecular forces within the coiled-coil formed by helix H1 with helix H4 of the adjacent monomer.

7. Conclusion

Individual hAQP1 molecules were unfolded in buffer solution using single-molecule force spectroscopy. All major features of the force-extension curves could be directly correlated to individual secondary structure elements, such as α -helices and loops. The positions and interactions of conserved residues stabilizing the fold of the functional protein are reflected in the force-extension curves, and the forces resulting from these interactions are directly measured. Furthermore, the positions and interactions of conserved residues forming monomer–monomer contacts and thus stabilizing the tetramer can be identified. The data provide a detailed insight into molecular interactions of the secondary structure elements of hAQP1, as well as into the interactions forming and stabilizing the tetrameric assembly of the monomers.

Acknowledgments

The authors thank Harald Janovjak and Dr. Shirley Müller for valuable discussions and for critically reading of the manuscript. This work was supported by the Deutsche Volkswagenstiftung (grant to D.J.M.). A.E. acknowledges the support by the Swiss National Research Foundation, the M.E. Müller Foundation, the Swiss National Center of Competence in Research (NCCR) “Structural Biology,” and the NCCR “Nanoscience.”

References

Binnig, G., Quate, C.F., Gerber, C., 1986. Atomic force microscope. *Phys. Rev. Lett.* 56, 930–933.

- Booth, P.J., Templer, R.H., Meijberg, W., Allen, S.J., Curran, A.R., Lorch, M., 2001. In vitro studies of membrane protein folding. *Crit. Rev. Biochem. Mol. Biol.* 36, 501–603.
- Bustamante, C., Marko, J.F., Siggia, E.D., Smith, S., 1994. Entropic elasticity of lambda-phage DNA. *Science* 265, 1599–1600.
- Butt, H.-J., Jaschke, M., 1995. Calculation of thermal noise in atomic force microscopy. *Nanotechnology* 6, 1–7.
- Butt, H.-J., Jaschke, M., Ducker, W., 1995. Measuring surface forces in aqueous solution with the atomic force microscope. *Bioelectr. Bioenerg.* 38, 191–201.
- de Groot, B.L., Engel, A., Grubmüller, H., 2001. A refined structure of human aquaporin-1. *FEBS Lett.* 504, 206–211.
- de Groot, B.L., Grubmüller, H., 2001. Water permeation across biological membranes: mechanism and dynamics of aquaporin-1 and GlpF. *Science* 294, 2353–2357.
- Denker, B., Smith, B., Kuhajda, F., Agre, P., 1988. Identification, purification, and partial characterization of a novel Mr 28,000 integral membrane protein from erythrocytes and renal tubules. *J. Biol. Chem.* 263, 15634–15642.
- Engel, A., Müller, D.J., 2000. Observing single biomolecules at work with the atomic force microscope. *Nat. Struct. Biol.* 7, 715–718.
- Evans, E., 2001. Probing the relation between force-lifetime and chemistry in single molecular bonds. *Annu. Rev. Biophys. Biomol. Struct.* 30, 105–128.
- Fettiplace, R., Haydon, D.A., 1980. Water permeability of lipid membranes. *Physiol. Rev.* 60, 510–550.
- Fotiadis, D., Suda, K., Tittmann, P., Jenö, P., Philippsen, A., Müller, D.J., Gross, H., Engel, A., 2002. Identification of a putative Ca²⁺ binding domain at the C-terminus of AQP1. *J. Mol. Biol.* 318, 1381–1394.
- Fu, D., Libson, A., Miercke, L.J., Weitzman, C., Nollert, P., Krucinski, J., Stroud, R.M., 2000. Structure of a glycerol-conducting channel and the basis for its selectivity. *Science* 290, 481–486.
- Grubmüller, H., Heymann, B., Tavan, P., 1996. Ligand binding: molecular mechanics calculation of the streptavidin–biotin rupture force. *Science* 271, 997–999.
- Heymann, J.B., Engel, A., 1999. Aquaporins: phylogeny, structure, and physiology of water channels. *News Physiol. Sci.* 14, 187–193.
- Israelachvili, J., 1991. *Intermolecular and Surface Forces*, second ed. Academic Press, London.
- Jung, J.S., Preston, G.M., Smith, B.L., Guggino, W.B., Agre, P., 1994. Molecular structure of the water channel through aquaporin CHIP. The hourglass model. *J. Biol. Chem.* 269, 14648–14654.
- Lazaridis, T., Karplus, M., 1999. Effective energy function for proteins in solution. *Proteins* 35, 133–152.
- Lu, H., Schulten, K., 1999. Steered molecular dynamics simulations of force-induced protein domain unfolding. *Proteins* 35, 453–463.
- Macey, R.I., Farmer, R.E., 1970. Inhibition of water and solute permeability in human red cells. *Biochim. Biophys. Acta* 211, 104–106.
- Marko, J.F., Siggia, E.D., 1995. Stretching DNA. *Macromolecules* 28, 8759–8770.
- Mitsuoka, K., Murata, K., Walz, T., Hirai, T., Agre, P., Heymann, J.B., Engel, A., Fujiyoshi, Y., 1999. The structure of aquaporin-1 at 4.5-Å resolution reveals short α -helices in the center of the monomer. *J. Struct. Biol.* 128, 34–43.
- Müller, D.J., Baumeister, W., Engel, A., 1999a. Controlled unzipping of a bacterial surface layer with atomic force microscopy. *Proc. Natl. Acad. Sci. USA* 96, 13170–13174.
- Müller, D.J., Fotiadis, D., Scheuring, S., Müller, S.A., Engel, A., 1999b. Electrostatically balanced subnanometer imaging of biological specimens by atomic force microscopy. *Biophys. J.* 76, 1101–1111.
- Müller, D.J., Janovjak, H., Lehto, T., Kuerschner, L., Anderson, K., 2002a. Observing structure, function and assembly of single proteins by AFM. *Prog. Biophys. Mol. Biol.* 79, 1–43.

- Müller, D.J., Kessler, M., Oesterhelt, F., Möller, C., Pfeiffer, M., Oesterhelt, D., Gaub, H., 2002b. Assignment of bacteriorhodopsin secondary structure elements by single molecule force spectroscopy. *Biophys. J.* 82, 3578–3588.
- Murata, K., Mitsuoka, K., Hirai, T., Walz, T., Agre, P., Heymann, J.B., Engel, A., Fujiyoshi, Y., 2000. Structural determinants of water permeation through aquaporin-1. *Nature* 407, 599–605.
- Oberhauser, A.F., Hansma, P.K., Carrion-Vazquez, M., Fernandez, J.M., 2001. Stepwise unfolding of titin under force-clamp atomic force microscopy. *Proc. Natl. Acad. Sci. USA* 98, 468–472.
- Oesterhelt, F., Oesterhelt, D., Pfeiffer, M., Engel, A., Gaub, H., Müller, D.J., 2000. Unfolding pathways of individual bacteriorhodopsins. *Science* 288, 143–146.
- Pao, G.M., Wu, L.F., Johnson, K.D., Hofte, H., Chrispeels, M.J., Sweet, G., Sandal, N.N., Saier Jr., M.H., 1991. Evolution of the MIP family of integral membrane transport proteins. *Mol. Microbiol.* 5, 33–37.
- Park, J.H., Saier Jr., M.H., 1996. Phylogenetic characterization of the MIP family of transmembrane channel proteins. *J. Membr. Biol.* 153, 171–180.
- Popot, J.L., Engelman, D.M., 1990. Membrane protein folding and oligomerization: the two stage model. *Biochemistry* 29, 4031–4037.
- Popot, J.L., Engelman, D.M., 2000. Helical membrane protein folding, stability, and evolution. *Annu. Rev. Biochem.* 69, 881–922.
- Preston, G.M., Agre, P., 1991. Isolation of the cDNA for erythrocyte integral membrane protein of 28 kilodaltons: member of an ancient channel family. *Proc. Natl. Acad. Sci. USA* 88, 11110–11114.
- Preston, G.M., Carroll, T.P., Guggino, W.B., Agre, P., 1992. Appearance of water channels in *Xenopus* oocytes expressing red cell CHIP28 protein. *Science* 256, 385–387.
- Radford, S.E., 2000. Protein folding: progress made and promises ahead. *Trends Biochem. Sci.* 25, 611–618.
- Rief, M., Gautel, M., Oesterhelt, F., Fernandez, J.M., Gaub, H.E., 1997a. Reversible unfolding of individual titin immunoglobulin domains by AFM. *Science* 276, 1109–1112.
- Rief, M., Oesterhelt, F., Heymann, B., Gaub, H.E., 1997b. Single molecule force spectroscopy on polysaccharides by atomic force microscopy. *Science* 275, 1295–1297.
- Russ, W.P., Engelman, D.M., 2000. The GxxxG motif: a framework for transmembrane helix–helix association. *J. Mol. Biol.* 296, 911–919.
- Schäffer, T.E., Cleveland, J.P., Ohnesorge, F., Walters, D.A., Hansma, P.K., 1996. Studies of vibrating atomic force microscope cantilevers in liquid. *J. Appl. Phys.* 80, 3622–3627.
- Sidel, V.W., Solomon, A.K., 1957. Entrance of water into human red blood cells under an osmotic pressure gradient. *J. Gen. Physiol.* 41, 243–257.
- Smith, B.L., Agre, P., 1991. Erythrocyte Mr 28,000 transmembrane protein exists as a multisubunit oligomer similar to channel proteins. *J. Biol. Chem.* 266, 6407–6415.
- Sui, H., Han, B.G., Lee, J.K., Walian, P., Jap, B.K., 2001. Structural basis of water-specific transport through the AQP1 water channel. *Nature* 414, 872–878.
- Walz, T., Smith, B.L., Agre, P., Engel, A., 1994a. The three-dimensional structure of human erythrocyte aquaporin chip. *EMBO J.* 13, 2985–2993.
- Walz, T., Smith, B.L., Zeidel, M.L., Engel, A., Agre, P., 1994b. Biologically active two-dimensional crystals of aquaporin CHIP. *J. Biol. Chem.* 269, 1583–1586.
- Zardoya, R., Villalba, S., 2001. A phylogenetic framework for the aquaporin family in eukaryotes. *J. Mol. Evol.* 52, 391–404.

Unfolding pathways of native bacteriorhodopsin depend on temperature

Harald Janovjak, Max Kessler¹,
Dieter Oesterhelt², Hermann Gaub¹ and
Daniel J. Müller³

Max-Planck-Institute of Molecular Cell Biology and Genetics and BioTec, University of Technology, 01307 Dresden, ¹Center for Nano Science, Sektion Physik, Ludwig Maximilians-Universität München, 80799 München and ²Max-Planck-Institute of Biochemistry, 82152 Martinsried, Germany

³Corresponding author
e-mail: mueller@mpi-cbg.de

The combination of high-resolution atomic force microscopy (AFM) imaging and single-molecule force-spectroscopy was employed to unfold single bacteriorhodopsins (BR) from native purple membrane patches at various physiologically relevant temperatures. The unfolding spectra reveal detailed insight into the stability of individual structural elements of BR against mechanical unfolding. Intermittent states in the unfolding process are associated with the step-wise unfolding of α -helices, whereas other states are associated with the unfolding of polypeptide loops connecting the α -helices. It was found that the unfolding forces of the secondary structures considerably decreased upon increasing the temperature from 8 to 52°C. Associated with this effect, the probability of individual unfolding pathways of BR was significantly influenced by the temperature. At lower temperatures, transmembrane α -helices and extracellular polypeptide loops exhibited sufficient stability to individually establish potential barriers against unfolding, whereas they predominantly unfolded collectively at elevated temperatures. This suggests that increasing the temperature decreases the mechanical stability of secondary structural elements and changes molecular interactions between secondary structures, thereby forcing them to act as grouped structures.

Keywords: atomic force microscopy/molecular interactions/purple membrane/secondary structure/structural stability

Introduction

Molecular forces interacting between and within biological macromolecules determine biomolecular structures, their dynamics and their functions (Haltia and Freire, 1995; White and Wimley, 1999; Popot and Engelman, 2000). But how do these forces stabilize secondary structure elements, how do they mediate interactions between these structures, and how do these forces depend on environmental conditions within physiological relevant ranges? Currently, molecular interactions are typically inferred indirectly from equilibrium binding and kinetic measure-

ments or are calculated using molecular models. Recent perceptions of protein (un)folding, such as described by multidimensional landscapes or folding funnels, can be seen as a result of the complexity of inter- and intramolecular interactions (Radford, 2000). Different (un)folding pathways may be populated in dependence of small alterations of the physiological environment, which challenges novel approaches, to observe co-existing minor and major pathways on single molecules.

With the recent developments of single-molecule force-spectroscopy, such inter- and intramolecular interactions of biological macromolecules became directly accessible (Fisher *et al.*, 1999; Rief *et al.*, 2000). In single-molecule force-spectroscopy, the two ends of a molecule are tethered to the tip of a cantilever and to a solid support, respectively, while the cantilever deflection is monitored with high accuracy of ≈ 0.1 nm upon elongation. A characteristic force distance curve for this molecule is obtained by recording the cantilever deflection against the tip-support separation. Single-molecule force-spectroscopy has been applied to measure biological interactions such as forces that mediate molecular recognition (Lee *et al.*, 1994; Moy *et al.*, 1994; Fritz *et al.*, 1998), stabilize molecular structures (Fisher *et al.*, 1999; Rief *et al.*, 2000), drive intermolecular interactions (Dammer *et al.*, 1996), form molecular bonds (Grandbois *et al.*, 1999; Merkel *et al.*, 1999) and molecular elasticities (Kellermayer *et al.*, 1997; Rief *et al.*, 1998a; Bustamante *et al.*, 2000; Clausen-Schaumann *et al.*, 2000). Constructs of modular proteins were unfolded mechanically and revealed for the first time a direct correlation between folding pattern and mechanical function (Oberhauser *et al.*, 1999; Rief *et al.*, 2000). Models were developed that allow a theoretical description of the molecular compliances based on the combination of established polymer models in combination with discrete unfolding events (Rief *et al.*, 1998a; Zhang *et al.*, 1999). Forced unfolding experiments performed on fibronectin (Rief *et al.*, 1998b), tenascin (Oberhauser *et al.*, 1998), and titin (Oberhauser *et al.*, 1999; Rief *et al.*, 2000), showed that these modular proteins unfold domain after domain preferentially in an only all or none event with no intermediate states. Only in rare cases, intermittent steps have been reported (Marszalek *et al.*, 1999). Interestingly, single-molecule spectroscopy experiments recently demonstrated titin and fibronectin domains of tenascin to unfold at different forces, although their thermal stability was shown to be identical using differential scanning calorimetry (Rief *et al.*, 1998b). This latter example indicates that force-spectroscopy can be used to reveal interactions that contribute to the structural stability of proteins, which are not accessible by thermal denaturation.

An additional principal difference between mechanical single molecule experiments and conventional unfolding

experiments by thermal or chemical denaturation should be pointed out: conventional experiments deal with high densities of proteins immersed in solutions. Consequently, possible influences between the densely packed molecules are to be suppressed and the challenge is to dilute the solution as far as possible to ensure that the unfolded proteins do not interact with each other. However, sample dilution is limited by the finite sensitivity of the detection method (Booth *et al.*, 2001). In single-molecule force-spectroscopy, however, a single protein is surrounded by quasi infinite solution.

In contrast to most unfolding experiments on globular proteins, the combination of single-molecule imaging and force-spectroscopy on the membrane protein bacteriorhodopsin (BR) yielded surprisingly detailed insights into inter- and intramolecular interactions. It has been shown that structural elements of BR unfold sequentially, making the assignment of certain features of the measured force spectra to the corresponding amino acid (aa) sequence possible. The consequent analysis provided comprehensive information on structural properties of individual BR molecules within the native purple membrane from the halophilic archaeon *Halobacterium salinarum* (Oesterhelt *et al.*, 2000). Interactions that stabilize individual structural elements of BR, such as transmembrane α -helices and polypeptide loops were detected (Müller *et al.*, 2002). In this study, we characterize the influence of temperature on the mechanical stability of BR by combining high-resolution atomic force microscopy (AFM) imaging and single-molecule force-spectroscopy. BR was unfolded at temperatures from 8 to 52°C, the latter being comparable to the physiologically relevant temperature of the halophilic bacteria. The data show that the unfolding forces decrease significantly with increasing temperature while the probability of pairwise unfolding of transmembrane α -helices increases significantly.

The light-driven proton pump BR was chosen as a model system for this study because it represents one of the most extensively studied membrane proteins (Oesterhelt, 1998; Haupts *et al.*, 1999). Together with adjacent lipids, BR molecules assemble into trimers, which are packed into the two-dimensional hexagonal lattice of purple membrane as a chemically distinct domain of the cell membrane. BR converts the energy of light ($\lambda = 500\text{--}650$ nm) into an electrochemical proton gradient, which in turn is used for ATP production by ATP-synthases. Structural analysis of BR has revealed that the photoactive retinal is embedded in seven closely packed transmembrane α -helices (Lanyi, 1999; Subramaniam, 1999), which builds a common structural motif among a large class of related G protein-coupled receptors (Helmreich and Hofmann, 1996). The BR helices are designated as helices A, B, C, D, E, F, and G, to which the C-terminal end is connected. With increasing knowledge of its structural and functional properties, BR has become a paradigm for α -helical membrane proteins in general and for ion transporters in particular (Lanyi, 1999; Subramaniam, 1999).

Results

Figure 1A shows a selection of force-extension traces recorded on single BR molecules. An interpretation of a

typical trace exhibiting common features observed among all curves is given at the top of Figure 2. After separating AFM tip and purple membrane, the C-terminal polypeptide of BR is extended. Further separating tip and membrane stretches the C-terminal end and the force builds up in a gradual but non-linear fashion. At a certain force, the first transmembrane helices G and F unfold. This increases the length of the molecular bridge between tip and membrane, the cantilever relaxes and the force drops abruptly. By further separation of the AFM tip and membrane surface, the polypeptide chain of the unfolded structural elements extends. As soon as the polypeptide is stretched again, the force rises (as detected by the cantilever deflection). At a certain force, the next (in terms of the polypeptide chain) secondary element of BR unfolds. The gradual, non-linear force increase of the extension traces can be well fitted with the wormlike chain (WLC) model with only one free parameter: the contour length of the stretched portion of the molecule. This fit describes the increasing slopes of the traces at low forces, with each peak of the discontinuous force spectrum marking the position of a potential barrier of the BR molecule. As shown previously, the fitted contour length of the force-extension curve and the secondary structure model of BR suggest that helices G and F, D and E, and B and C unfold pairwise (Oesterhelt *et al.*, 2000). The remaining seventh helix, A, is then pulled from the membrane in a single step. Beyond an extension of 70 nm no interaction is measured.

In those cases where the main force peak drops without further (often smaller) force peaks being detected (Figure 2B,C and D, black arrows), the grouped structural elements unfold within a single step. Occasionally, a main force peak drops to zero with further (smaller) force peaks. In a previous study, these side peaks were identified as unfolding events of single secondary structure elements such as transmembrane α -helices and polypeptide loops (Müller *et al.*, 2002). The assignment of the observed force peaks to the unfolding events of individual structural elements is given in Figure 2A–D.

To see to what extent these unfolding events of secondary structural elements depend on the temperature, force extension curves were recorded at 8°C (Figure 1B), room temperature (25°C; Figure 1C), 32°C (Figure 1D), 42°C (Figure 1E), and 52°C (Figure 1F). Each graph shows a multitude of force extension traces, each one recorded on one single BR (such as shown in Figure 1A). In these figures, ~25 traces are superimposed. This kind of graphic representation highlights common features through the accumulation of the measured points and at the same time still represents the individualism of traces. Independent of the temperature adjustment, each curve exhibited a richness of detailed information on the mechanics of this molecule. It becomes clear that the main peaks at 27, 45 and 65 nm remain at their position (Figure 1), but that the rupture forces of these unfolding events decrease with increasing temperature (Figure 3). The steepest decrease of the rupture forces was observed between 8 and 32°C. Above 32°C, the rupture force decreased only slightly, showing a fluctuation of a similar range as the standard deviation of the mean value.

Similarly to the main peaks, the side peaks did not change their position (contour length) upon variation of

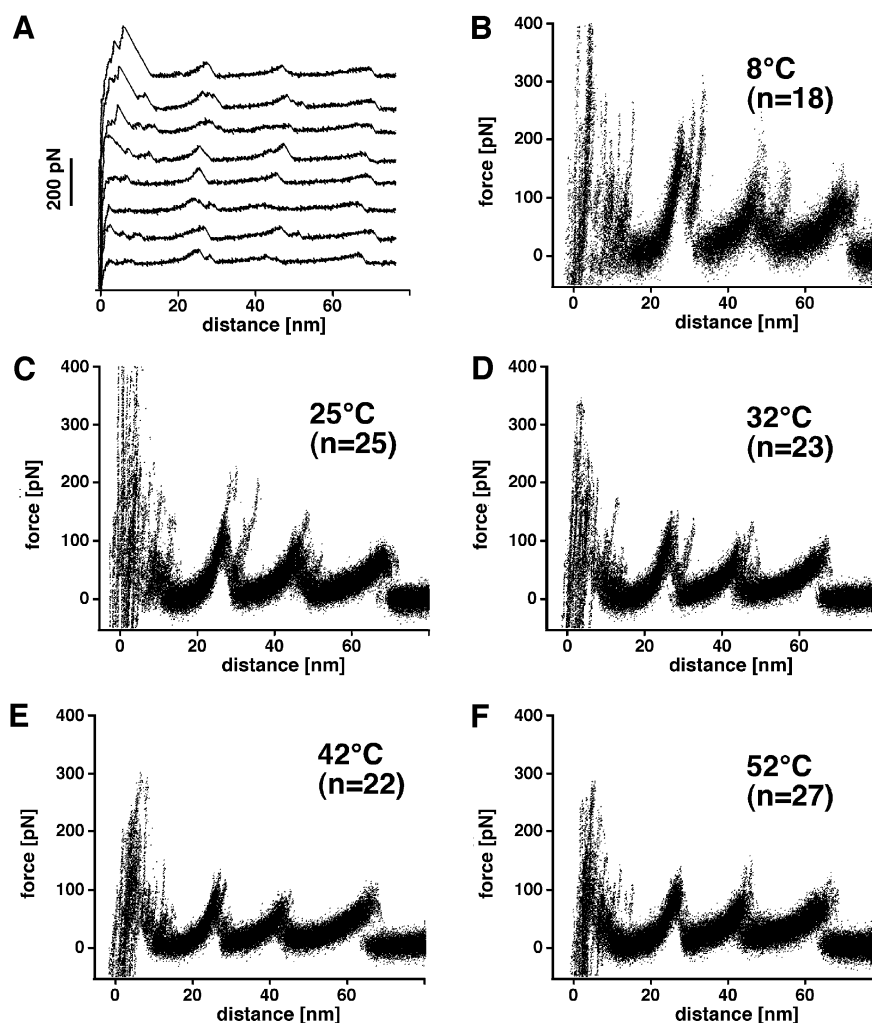


Fig. 1. Unfolding BR from native purple membrane at various temperatures. (A) Force curves of individual BR molecules recorded at 25°C. To show common unfolding patterns among single-molecule events, the force spectra recorded at different temperatures were superimposed. (B–F) BR unfolded at 8°C (B), 25°C (C), 32°C (D), 42°C (E) and 52°C (F) in 300 mM KCl, 20 mM Tris–HCl with a pH of 7.8 being adjusted for each temperature.

the temperature. To see whether the rupture force (Figure 3) or the probability (Figure 4) of the side peaks change with temperature, they were analyzed from each single force-extension curve. Interestingly, the average rupture force of all side peaks decreased with increasing temperature (Figure 3). However, the frequency of the side peaks decreased with increasing temperature (Figure 4). Accordingly, the frequency of the main peaks increased with the temperature (Figure 4). This indicates that the pairwise unfolding of transmembrane α -helices is favored with increasing temperature, while with decreasing temperature, the unfolding probability of single secondary structure elements, such as helices and loops, is enhanced.

Discussion

Stabilization and unfolding of transmembrane α -helices

In our measurements, the forces required to unfold single α -helices of BR from native purple membrane are measured directly. Our observations support the concept of independently stable transmembrane helices to be a key feature of their assembly into a higher-ordered structure (Popot and Engelman, 2000). In this so-called two-stage

model, the sequential folding of BR is explained. First, individual helices are inserted as separate stable fragments into the membrane. After this, the helices assemble into the functional protein. It is suggested that the BR fragments act like domains of soluble proteins. Together with their connecting loops the transmembrane helices assume a free energy minimum, found by the characteristic tertiary structure. As our single-molecule force-spectroscopy measurements have shown, each of these individual structural elements exhibits an energy minimum, establishing an internal potential barrier against mechanical unfolding. Although the BR helices exhibit sufficient stability to unfold in a single step, at the same time they exhibit a distinct probability to unfold pairwise. This observation proposes that a pairwise association drives transmembrane helices into a conformation of comparable mechanical stability as that observed for single helices.

Spontaneous unfolding of α -helices

The data suggest hydrophobic structural elements of BR (transmembrane α -helices) to be extracted from, or hydrophilic structures (extracellular polypeptides) to be

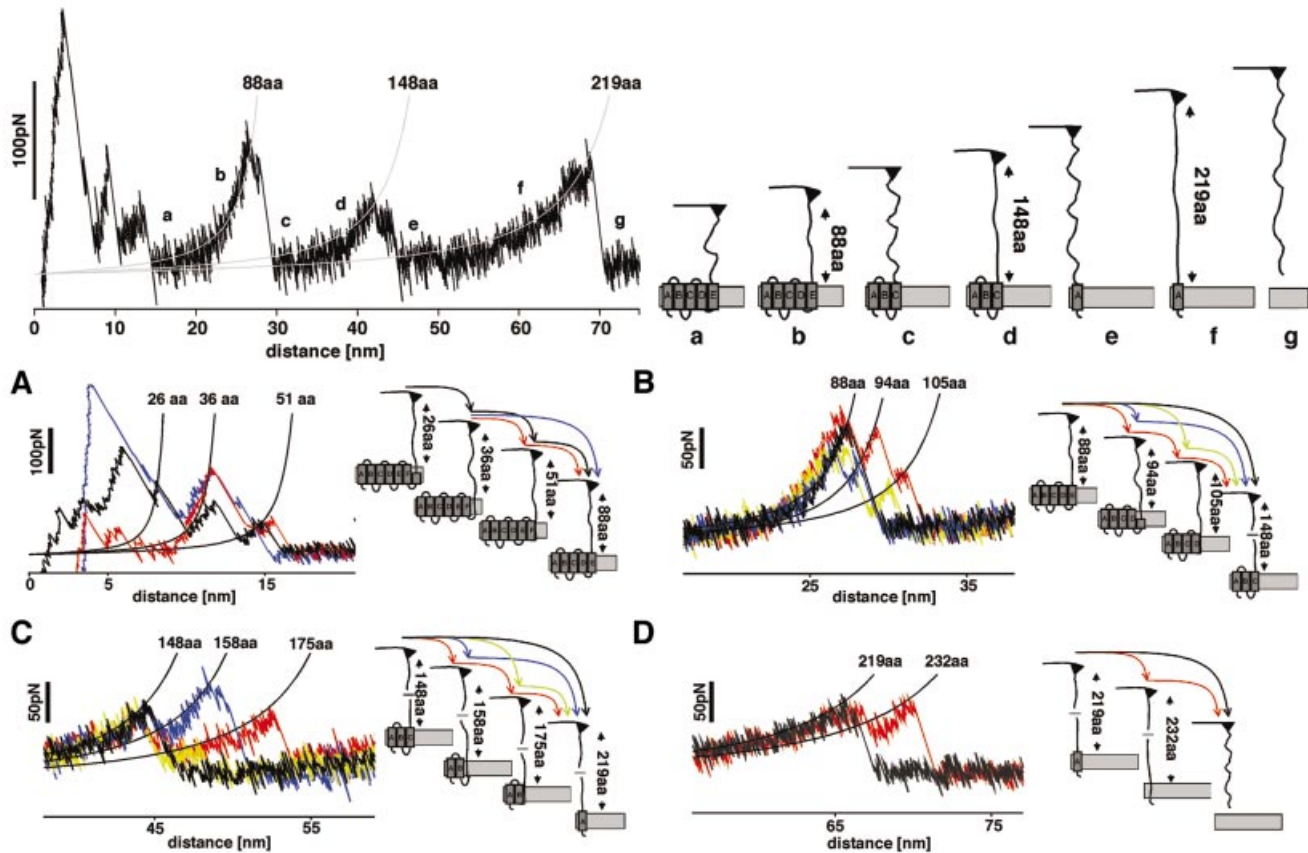


Fig. 2. Unfolding pathways of BR. Top, pairwise unfolding pathways of transmembrane α -helices. The left curve shows a representative unfolding spectrum of a single BR, while the schematic drawing of the unfolding pathways is shown on the right. The first force peaks detected within a separation of 0–15 nm to the purple membrane surface indicate the unfolding of transmembrane α -helices F and G, and of loops FG and EF. The first peaks within this region are superimposed by non-specific surface interactions between purple membrane and AFM tip. After the unfolding event (a), the amount of aa stretched is increased to 88 and the cantilever relaxes. Further separating tip and sample stretches the polypeptide (b) thereby pulling on helix E. At a certain pulling force, the mechanical stability of helices E and D is insufficient and they unfold together with loops DE and CD (c). The available 148 aa are now stretched (d), the polypeptide being pulling on helix C. Helices B and C and loops BC and AB unfold within a single step, thereby relaxing the cantilever (e). By further separating tip and purple membrane, the cantilever pulls on helix A (f) until the polypeptide is completely extracted from the membrane (g). The force-spectroscopy curve was recorded in 300 mM KCl, 20 mM Tris-HCl pH 7.8 at room temperature. (A–D) Unfolding events of individual secondary structures. (A) Occasionally the first major unfolding peak shows side peaks at about 26, 36 and 51 aa. The peak at 26 aa indicates the unfolding of the cytoplasmic half of α -helix G up to the covalently bound retinal, which is embedded in the hydrophobic membrane core. The peak at 36 aa indicates the G helix to be unfolded completely. At 51 aa, helix G and the loop connecting helices G and F are unfolded and the force pulls directly on helix F until this helix unfolds together with loop EF. (B) The side peaks of the second major peak indicate the stepwise unfolding of helices E and D and loop DE. The peak at 88 aa indicates the unfolding of helix E, that at 94 aa of the loop DE, and the peak at 105 aa indicates unfolding of helix D. (C) The side peaks of the third major peak indicate the stepwise unfolding of helices C and B and loop BC. The peak at 148 aa indicates the unfolding of helix C, that at 158 aa of the loop BC, and the peak at 175 aa indicates unfolding of helix B. (D) The side peak of the last major peak indicates the unfolding of helix A (219 aa) and of the pulling of the N-terminal end through the purple membrane (232 aa).

pulled through, the hydrophobic membrane at reduced forces if the temperature is increased. The main peaks of the force spectra, however, cannot distinguish whether the secondary structures of BR are initially extracted from the membrane followed by an unfolding process outside the hydrophobic membrane core, or whether the helices unfold spontaneously as soon as the externally applied force supersedes their mechanical stability. Occasionally, the main unfolding peaks exhibit side peaks, indicating that single helices and loops unfold individually (Figure 2). Interestingly, the unfolding spectra of helices E (Figure 2B, red and blue pathways), C (Figure 2C, red and blue pathways) and A (Figure 2D, red pathway) suggest that they remain stably embedded in the membrane until they are spontaneously unfolded in a single event. Otherwise, the directly connected extracellular polypeptide loops

could not remain folded and located at their position. Premature unfolding of such a loop would not allow detection of its discrete unfolding peak in a subsequent event and would extend the total length of the stretched polypeptide of the helix unfolded directly before. As a result, the force peaks of helices D and B would be shifted by the length of their stretched extracellular loop. Similarly, in the case of unfolding helix A, the force peak detected at 232 aa (Figure 2D) would not have been detected.

Unfolding structural motifs

As detected directly by the unfolding spectra and as suggested by Popot and Engelman (Popot *et al.*, 1987; Popot and Engelman, 2000), a structural motif of BR is built by two transmembrane helices and their connecting

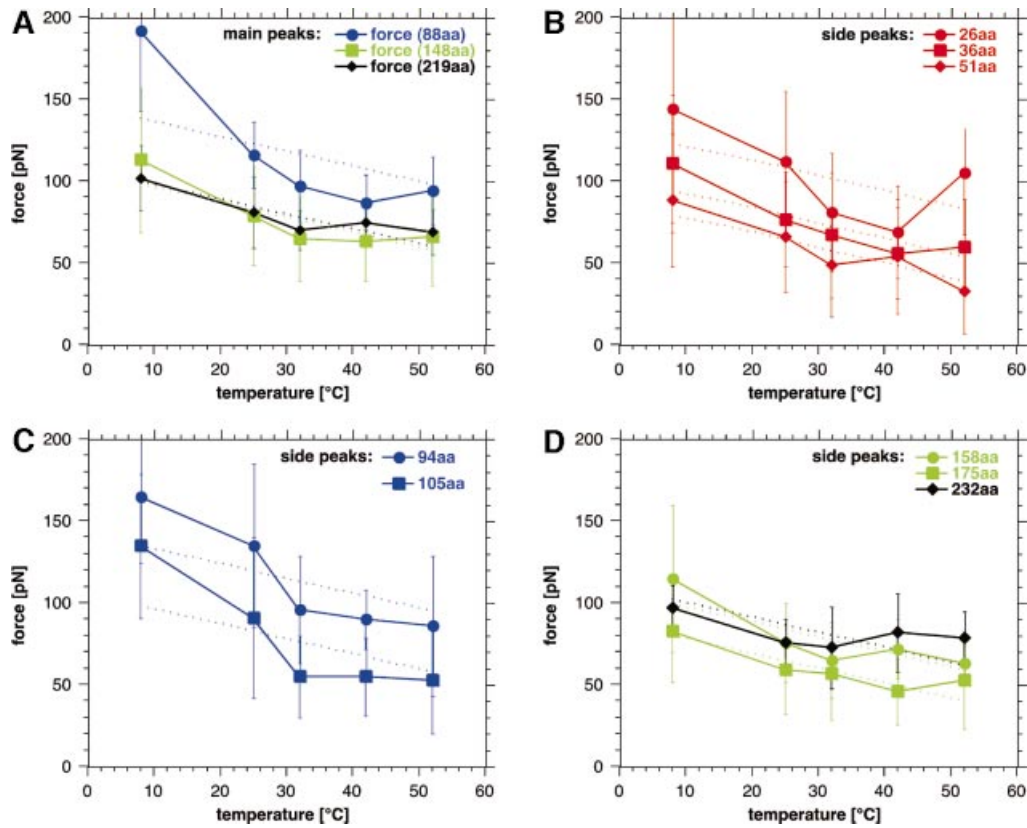


Fig. 3. Unfolding forces of secondary structural elements depend on temperature. (A) Rupture forces of main peaks, which exhibited no side peaks. The forces represent the pairwise unfolding of transmembrane α -helices E and D (88 aa), C and B (148 aa) and the unfolding of helix A (219 aa). The main peak representing the pairwise unfolding of helices G and F are not shown because of unspecific surface interactions between the AFM tip and the purple membrane scatter the position and appearance of the force peaks significantly. (B–D) Rupture forces of side peaks represent unfolding of single α -helices and of their connecting loops (see text). The thermally induced weakening of the unfolding forces was fitted (dotted lines) using equation (2).

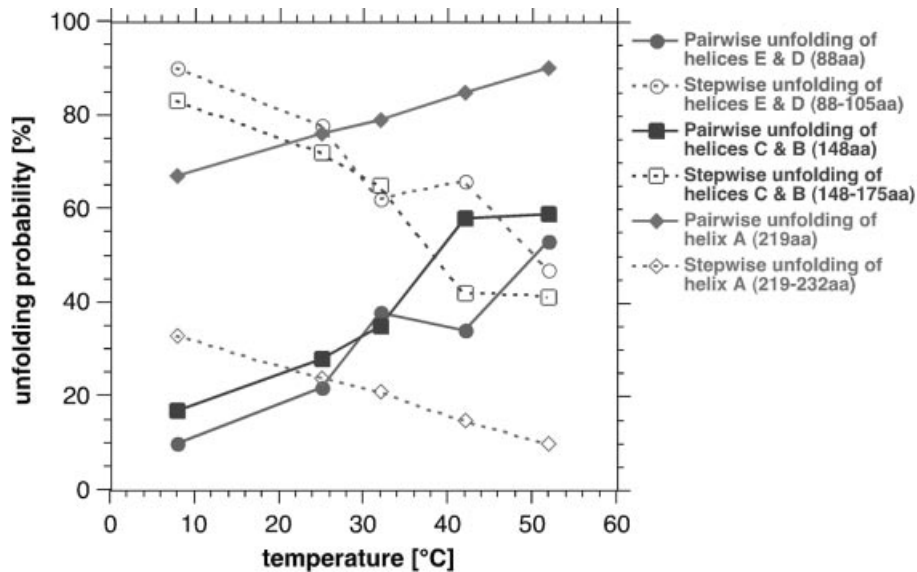


Fig. 4. Probability of unfolding pathways depends on temperature. The occurrence of main force peaks exhibiting no side peaks (solid lines) increased with increasing temperature. As a consequence, the probability of the main peaks exhibiting side peaks (dashed lines) decreased significantly. Solid lines represent probabilities for the pairwise unfolding of transmembrane α -helices E and D (88 aa, red), C and B (148 aa, blue) and of helix A (219 aa, green). The probability of their stepwise unfolding is presented by the dotted lines. This indicates α -helices of BR unfold preferentially pairwise at elevated temperatures. The probability of single structural elements, such as helices or loops, to unfold in a separate event decreases with increasing temperature.

polypeptide loop. If pulled from the C-terminal end, the second helix of this structural motif unfolds at smaller forces compared with the first helix. Most probably, this

effect results from the destabilization of the structural motif by the unfolding process. The individualism of their unfolding pathways emerged as a very prominent feature

throughout the study. Whether or not this individualism of the pathways reflects the individualism of the protein, rather than fluctuations at bifurcation points in the unfolding trajectories, remains to be elucidated in further studies. Although we have measured the positions of the different unfolding barriers quite precisely, we have not yet identified their underlying mechanisms. Particularly, our finding that the extracellular loops resist unfolding at an external force comparable with the force required to unfold a transmembrane α -helix, calls for additional future investigations.

BR structure remains mainly unchanged within the temperature range investigated

Using Fourier-transform infrared spectroscopy (Cladera *et al.*, 1992; Taneva *et al.*, 1995), X-ray diffraction (Shen *et al.*, 1993; Koltover *et al.*, 1999; Müller *et al.*, 2000) and circular dichroism (Brouillette *et al.*, 1987; Shnyrov and Mateo, 1993), it was shown that the intramembranous parts of BR do not undergo significant structural changes within the temperature range studied here. This is further supported by the proton pumping activity of BR, which is maintained (Racker and Hinkle, 1974), and the observation that no intramembranous elements become exposed to papain digestion (Brouillette *et al.*, 1987) at these temperatures. These findings suggest that BR fully maintains its native function, and that internal structural changes would be minimal within the temperature range studied here.

Temperature-dependent destabilization of transmembrane α -helices

The subset of force curves recorded at temperatures ranging from 8 to 52°C show the individual unfolding pathways of BR, such as previously detected at room temperature (22°C; Müller *et al.*, 2002). A common feature of all measurements is that the average force detected for each unfolding event decreases upon increasing the temperature. Apparently, this observation contrasts with the suggestion that the thermal influences on the BR structure are negligible within the temperature range studied here. However, force-spectroscopy detects the stability of a protein and not necessarily its structural changes. Thus, it appears interesting that, although the BR structure remains unchanged, the interactions stabilizing the structure were strongly affected by temperature variations within a physiologically relevant range.

The potential barriers detected in the force spectra can be assigned to secondary structural elements (Müller *et al.*, 2002), which are stabilized by inter- and intramolecular interactions (Haltia and Freire, 1995; White and Wimley, 1999; Popot and Engelman, 2000). The intermolecular forces involve interactions of the protein with surrounding lipids and neighboring proteins. An important contribution to the intermolecular forces is formed by hydrophobic interactions, which anchor and stabilize a membrane protein within the lipid bilayer. In model experiments, this hydrophobic interaction is frequently manipulated to adjust the solubility of membrane proteins or to favor the reconstitution of membrane proteins into a lipid bilayer (Kühlbrandt, 1992; Hasler *et al.*, 1998). From experiments measuring the solubility of hydrophobic molecules in aqueous solution, it can be concluded that the hydro-

phobic interaction increases with increasing temperature (Tanford, 1980). Other important contributions to the forces stabilizing proteins result from intramolecular interactions such as hydrogen bonding and electrostatic and van der Waals interactions.

Structural transitions of lipids may influence membrane protein stability

In this study, the most drastic decreases of unfolding force were detected with an increase in temperature from 8 to 32°C. Within this range, experimental results obtained by differential scanning calorimetry suggested purple membrane undergoes thermal transitions (Chignell and Chignell, 1975), which are potentially associated with lipid rearrangements (Wilkinson and Nagle, 1982; Blume, 1983; Tristram-Nagle *et al.*, 1986). There has been confusion about the discrepancy with other results that report no transition of purple membrane within this temperature range (Jackson and Sturtevant, 1978). Apparently, the observation of this thermal transition depends on purple membrane concentration, which must be sufficient to detect specific heats of the lipids by calorimetry (Tristram-Nagle *et al.*, 1986). Such structural rearrangements of lipids, however, change the interactions between lipids as well as interactions with the membrane protein (Tristram-Nagle *et al.*, 1986; Nishiyama *et al.*, 1987; Haltia and Freire, 1995). Thus, it may be concluded that the significant reduction of unfolding forces measured here is a result of lipid transitions occurring within the temperature range of 8–32°C.

Another aspect of the steep rupture force decrease observed between 8 and 32°C is the fact that for helices D and E the unfolding forces decrease by about 80 pN while for all other peaks a change of 30 pN is not exceeded. The space occupied by two helices equals the volume of about nine lipid molecules, corresponding to a membrane area of four and a half lipid molecules. This compares with five lipid molecules per BR in one purple membrane leaflet (Luecke *et al.*, 1998). Thus, removal of the first four helices, G, F, E and D, creates a considerable hole, which exposes the lipids to a different environment compared with those lipids that are structurally constrained within the intact protein crystal. Creation of more space and environmental changes might facilitate large structural transitions of the surrounding lipids (Israelachvili, 1991). After such structural rearrangements, the lipids surrounding the hole may not behave as those observed in native purple membrane. This may explain why we do not observe a similarly steep temperature-dependent decrease of the unfolding force for helices that have been extracted after a considerable hole has been created. Therefore, it may be assumed that the temperature-dependent decrease of rupture force revealed for those helices that have been unfolded after the first ones, might reflect their intrinsic interactions rather than those associated with lipid transitions within the membrane (see also *Theoretical considerations*).

From 32 to 52°C, the unfolding forces of transmembrane α -helices show a weak dependence on the temperature. While the force to unfold α -helices pairwise remains mainly unaffected by the temperature increase, the unfolding force of single helices decreases slightly [Figure 3, helix F (51 aa), helix D (105 aa), helix B

(175 aa) and helix A (219 aa)]. This reduction of the potential barriers of the secondary structures is in apparent contrast with the hydrophobic interaction, which increases with the temperature and anchors transmembrane helices in the membrane (Tanford, 1980; Haltia and Freire, 1995; White and Wimley, 1999; Popot and Engelman, 2000). Thus, it may be suggested that the temperature induces a thermal destabilization of secondary structural elements, which becomes, at this stage, more dominant than possible hydrophobic contributions.

Unfolding polypeptide loops

The force peaks assigned to potential barriers against the mechanical pulling of the polypeptide loops, decreased with increasing temperature. Since hydrophilic loops connecting the transmembrane α -helices are located outside of the purple membrane, it may be concluded that a temperature increase may significantly destabilize the loop structure. However, unfolding of an extracellular loop structure by mechanical pulling of the polypeptide from the cytoplasmic side is directly followed by or associated with a physical transport of the hydrophilic aa residues through the hydrophobic membrane interior. This hydrophobic interaction, which prevents hydrophilic molecules from penetrating through a membrane bilayer, increases with the temperature (Tanford, 1980). Naturally, conformational changes of the loop structure and its transport through the membrane bilayer require contributions of external energy or force, such as applied mechanically in the experiments. From the current understanding of the hydrophobic interaction, one would expect that the force required to transport a hydrophilic peptide through a hydrophobic core increases with the temperature. Thus, our measurements suggest that an individual force peak of a polypeptide loop reflects its structural stability rather than the force required to transport their hydrophilic aa through the membrane. The observed specific ordering of these loops, which was observed in high-resolution structures of BR (Belrhali *et al.*, 1999; Luecke *et al.*, 1999), may further support this hypothesis. Detailed insights into which contributions of the adhesion force measured result from the unfolding of an extracellular polypeptide loop and which result from the physical transport of the loop through the membrane, may be gained with force microscopes that allow higher force and temporal resolution.

Temperature-dependent unfolding pathways of BR

At increased temperatures, the unfolding force of every structural element of BR decreased, indicating that their potential barriers, built up against mechanical unfolding, were lowered. The temperature variation did not influence the appearance of the unfolding pathways. This means, every individual pathway was observed at each of the temperatures adjusted. However, the probability of a BR molecule choosing a certain unfolding pathway was found to depend on the temperature. Whereas the probability of pairwise unfolding of transmembrane α -helices increased significantly with the temperature, the unfolding probabilities of single helices and of helical segments decreased. Similarly, the probability of the hydrophilic polypeptide loops to unfold individually decreased with increasing temperature (Figure 4). Obviously, at elevated tempera-

tures, the potential barrier for unfolding two helices versus that of unfolding a single one decreases and groups of secondary structure elements predominantly unfold in a single step. This observation opens new questions about the molecular mechanisms that may change the unfolding pathways. Currently, one may take two possibilities into account: potential barriers of individual structural elements may simply change their height and position thereby shifting their probability for certain unfolding pathways; alternatively, one may assume the potential barrier of a side peak to reduce its height in a way that the barrier is not detected by the cantilever used in this work (Heymann and Grubmüller, 2000). To gain insight into this question, we are currently unfolding BR using cantilevers of different force constants and resonance frequencies.

Theoretical considerations: effects contributing to secondary structure stability

The secondary structure elements of BR establish various potential barriers against mechanical unfolding. From a kinetic point of view, the forced transition from one unfolding barrier to the next can be described as a thermally activated, first-order process. In a pioneering work in 1978, Bell found that an externally applied force reduces the potential barrier such that it can be superseded by thermal fluctuations within the timescale of the experiment (Bell, 1978). A more complete picture of the kinetics of bond dissociation can be revealed from Kramers' model of thermally assisted barrier crossing in liquids (Kramers, 1940; Hanggi *et al.*, 1990). Here, we apply a modified version of this model, which allows estimation of the extent of temperature-induced kinetic contributions on the most probable unbinding force f^* (Evans, 1998):

$$f^* = \frac{\Delta G^*}{x_u} - \frac{k_B T}{x_u} \ln \left(\frac{k_B T}{x_u \tau_D r_f} \right) \quad (1)$$

where ΔG^* is the height of the energy barrier of activation, x_u the distance from the folded state to the transition state representing the potential barrier width, k_B the Boltzmann constant, T the temperature, τ_D the characteristic diffusion time of motion in the system, and r_f the loading rate (Evans, 1998). Based on the assumption that the free energy of activation is not temperature dependent, only the second term depends on the temperature. Thus, the slope in a force versus temperature plot is represented by the derivative of this term with respect to the temperature:

$$\frac{df^*}{dT} = -\frac{k_B}{x_u} \left[\ln \left(\frac{k_B T}{x_u \tau_D r_f} \right) + 1 \right] \quad (2)$$

Using this formula, we fitted our experimental data (Figure 3) by inserting a potential width of 0.3 nm (see below), a loading rate of ≈ 1 nN/s (r_f in our experiments ranged from 600 to 3000 pN/s) was determined according to Dettmann *et al.* (2000), and a diffusion time of 10^{-10} s was used as suggested by Evans (1998). The potential

width of 0.3 nm was determined by two independent approaches: first, we fitted the decrease of the unfolding force over the entire temperature range for unfolding peaks observed at 148 aa (Figure 3A), 158 aa (Figure 3D), 175 aa (Figure 3D) and 219 aa (Figure 3A). We selected these peaks since it can be assumed that contributions to their unfolding forces by structural transitions of lipids are minimal (see Discussion), and that only kinetic effects contributed to their thermal destabilization. The peaks were fitted by applying equation (2), revealing values of x_u lying within the range from 0.25 to 0.4 nm. Secondly, dynamic force pulling experiments on BR revealed the same potential width of ≈ 0.3 nm detected for all secondary structure elements of BR (H.Janovjak, J.Struckmeier, M.Kessler, H.E.Gaub and D.J.Müller, manuscript in preparation). Therefore, we used 0.3 nm as estimate for all fits.

In most cases, the calculated values are in good agreement with the experimental data, lying within their standard deviations (Figure 3, dotted lines). As expected from above discussions on the temperature-dependent phase transition of the lipids, maximal deviations were observed in the temperature regime from 8 to 32°C. Since the structural transitions of lipids due to removal of transmembrane helices were only maximal after extraction of the first helices (see above), smaller deviations of the experimental data from the calculated values were observed for the structural elements that were directly extracted after the main peak at 88 aa and side peaks at 94 and 105 aa. Taking these explanations into account, it may be concluded that kinetic weakening dominated the thermal destabilization of these potential barriers. However, from the force shift of each fit it may be assumed that additional constant factors contribute to the unfolding of each secondary structure. From equation (1) it can be assumed that this shift may be due to different energetic contributions stabilizing individual helices and polypeptide loops.

A multidimensional unfolding landscape?

In previous studies, we and others have shown that unfolding forces are rate dependent and that additional information on the geometry of the potential barriers may be extracted from the unfolding traces by varying the pulling speed (Rief *et al.*, 1998a; Merkel *et al.*, 1999). From above results, we assume that different velocities may also influence the probability of the BR unfolding pathways. Since all external parameters, such as pulling speed, temperature, electrolyte and pH are freely adjustable in the experiments shown, it is expected that the knowledge of their influence on the structural stability of proteins will provide a wealth of new insights towards understanding factors and parameters that drive molecular interactions in proteins under physiological relevant conditions. It will be challenging to exploit these effects and to determine all the parameters that influence the unfolding pathways together to reveal a multidimensional unfolding landscape of a protein.

Concluding remarks

Every secondary structural element of BR exhibits a certain intrinsic stability, which appears to be sufficient to regard single transmembrane α -helices and polypeptide

loops as stable structures. As a result, the structural elements build up an internal potential barrier against extraction and mechanical unfolding. Mechanical pulling on the cytoplasmic terminus of BR is followed by the extraction and unfolding of its secondary structural elements from purple membrane. These observations strongly support the two-stage model of membrane protein folding. Temperature enhancement of the physiological environment lowers these potential barriers, which is directly reflected in the force peaks of the unfolding spectra. It is concluded that this temperature-dependent phenomena may be attributed to two effects: a thermal transition of purple membrane influencing the lipid-protein interaction, and the thermal destabilization of BR. Most interestingly, each secondary structure element of BR was observed to choose individual unfolding pathways. Their intrinsic probability, to unfold in a separate event or collectively with other structural elements, depends critically on the physiologically relevant temperature of the environment. The collective unfolding process of two transmembrane helices and of their connecting loop became dominant at elevated temperatures, suggesting interactions between helices to dominate the unfolding process.

Materials and methods

Purple membrane preparation

Wild-type purple membrane was extracted from *H.salinarum* as described previously (Oesterhelt and Stoeckenius, 1974) and adsorbed onto freshly cleaved mica in buffer solution (Müller *et al.*, 1997). All buffer solutions were prepared with nanopure water, and the pH was adjusted using an electrode pH-Meter with a built-in temperature sensor ($\Delta\text{pH} < 0.01$, $\Delta T = 0.3^\circ\text{K}$; pH-Meter 766 calimatic, Knick, Berlin, Germany). Chemicals utilized were purchased from Sigma/Merck and were p.a. grade.

Attachment of BR to the AFM tip

In previous studies, two different strategies have been developed in order to attach the protein to the tip. We have shown that the cysteine of the G241C mutant binds with a likelihood of 90% to a gold-coated cantilever (Oesterhelt *et al.*, 2000) when the tip is brought into contact with the cytoplasmic purple membrane surface, even at forces below 200 pN. This procedure allows a highly efficient and defined attachment. However, it requires the AFM tip to be replaced after a few experiments since it is covered with bound proteins. An alternative method, the non-specific attachment in combination with subsequent imaging and force trace classification, was shown to provide equivalent results and allows a much higher throughput (Müller *et al.*, 2002). Since this study is a systematic investigation, we chose the non-specific attachment in combination with AFM imaging as described below.

Single-molecule force-spectroscopy and imaging

The contact mode AFM (Nanoscope E, Digital Instruments, Santa Barbara, CA) used was equipped with a 100 μm piezo scanner. The spring constants k of the 200 μm long Si_3N_4 AFM cantilevers (Digital Instruments) were calibrated in solution using the equipartition theorem (Butt *et al.*, 1995; Florin *et al.*, 1995). Within the uncertainty of this method ($\approx 10\%$) all cantilevers used exhibited the same constant, $k = 0.06$ N/m. All experiments were performed in buffer solution. To perform force-spectroscopy experiments on BR we recorded high-resolution AFM topographs of the cytoplasmic purple membrane surface as described previously (Oesterhelt *et al.*, 2000). To adsorb the C-terminal end of BR to the AFM stylus, both surfaces were kept in contact for about 1 s while applying a force of 0.5–1 nN. Stylus and protein surface were then separated at a velocity of 87 nm/s while recording the force spectrum. In about 15% of all retraction curves we detected one or more adhesive peaks. About 30% of these retraction curves showed a force extension curve exhibiting a length between 60 and 70 nm (see *Data analysis*). After detecting one discontinuous force curve, the same area of

the protein surface was re-imaged. Defects of missing BR monomers allowed unambiguous correlation of the force spectra with a single protein (Oesterhelt *et al.*, 2000).

Temperature adjustment

An electric heating stage (Nanoscope Thermoheater, Digital Instruments) was magnetically mounted between the piezo scanner and support. The actual sample temperature was controlled within an accuracy of 1°C using a calibrated digital thermometer. Measurements at 8°C were performed in a cold room. The pH of the buffer (300 mM KCl, 20 mM Tris pH = 7.8) was adjusted at the temperature at which the experiments were performed.

Data analysis

To analyze the force curves, a clear criterion is required that distinguishes curves of BR molecules attached to the AFM tip with different regions of their polypeptide backbone. One suitable criterion is the overall length of the force curve, which reflects the tip-sample distance at which the last force peak occurs. It is obvious that a molecule attached to the cantilever by one of its loops results in a force curve with smaller overall length than that of a molecule attached by one of its termini. It was previously shown that force-extension curves exhibiting an overall length between 60 and 70 nm result from completely unfolded and extended BR molecules which were attached with their C-terminus to the AFM tip (Oesterhelt *et al.*, 2000; Müller *et al.*, 2002). All force curves exhibiting these overall lengths were selected and aligned at the force peak, which occurred at a tip-to-purple membrane separation of ≈25 nm (Figure 1). The reason that the force curves were aligned at this peak is due to the fact that in principle every amino acid of the C-terminal can bind to the AFM tip and that the point of contact (Figure 1, region around 0 nm) is not necessarily located at the tip apex but can also occur at the side of the tip. Additionally, force peaks located within the contact region below 20 nm show a broad variance, making them unsuitable for alignment. To avoid statistical difficulties, we analyzed only relative positions of the peaks. We used identical procedures and criteria to align each data set.

To analyze the side peaks, however, we superimposed every main peak separately (Figure 2). Every single peak of these superimpositions was fitted using the WLC model using a persistence length of 0.4 nm (Rief *et al.*, 1997) and a monomer length of 0.36 nm. We calculated the number of unfolded aa at each peak using the contour length as obtained from the WLC model. When pulling the polypeptide from the cytoplasmic surface, the anchor of the peptide, for example an extracellular loop, was sometimes located at the opposite extracellular surface. In this case, the membrane thickness (≈4 nm) had to be considered and 11 aa (11 × 0.36 nm ≈ 4 nm) were added to the number of aa determined using the WLC model. This allowed calculation of the entire rupture length of the polypeptide. To compare the polypeptide length derived from the WLC fits with the BR structure, we have chosen the atomic model of Mitsuoka *et al.* (1999).

Acknowledgements

We thank Norbert Dencher, Tim Salditt, Matthias Rief, Martin Stark and Stephen White for stimulating discussions. This work was supported by the Volkswagenstiftung and the Deutsche Forschungsgemeinschaft.

References

Baldwin, J.M. (1993) The probable arrangement of the helices in G protein-coupled receptors. *EMBO J.*, **12**, 1693–1703.
 Bell, G.I. (1978) Models for the specific adhesion of cells to cells. *Science*, **200**, 618–627.
 Belrhali, H., Nollert, P., Royant, A., Menzel, C., Rosenbusch, J.P., Landau, E.M. and Pebay-Peyroula, E. (1999) Protein, lipid and water organization in bacteriorhodopsin crystals: a molecular view of the purple membrane at 1.9 Å resolution. *Structure Fold. Des.*, **7**, 909–917.
 Blume, A. (1983) Apparent molar heat capacities of phospholipids in aqueous dispersion: effects of chain length and head group structure. *Biochemistry*, **22**, 5436–5442.
 Booth, P.J., Templer, R.H., Meijberg, W., Allen, S.J., Curran, A.R. and Lorch, M. (2001) *In vitro* studies of membrane protein folding. *Crit. Rev. Biochem. Mol. Biol.*, **36**, 501–603.
 Brouillette, C.G., Muccio, D.D. and Finney, T.K. (1987) pH dependence of bacteriorhodopsin thermal unfolding. *Biochemistry*, **26**, 7431–7438.

Bustamante, C., Macosko, J.C. and Wuite, G.J. (2000) Grabbing the cat by the tail: manipulating molecules one by one. *Nat. Rev. Mol. Cell. Biol.*, **1**, 130–136.
 Butt, H.-J., Jaschke, M. and Ducker, W. (1995) Measuring surface forces in aqueous solution with the atomic force microscope. *Bioelectrochem. Bioenerg.*, **38**, 191–201.
 Chignell, C.F. and Chignell, D.A. (1975) A spin label study of purple membranes from *Halobacterium halobium*. *Biochem. Biophys. Res. Commun.*, **62**, 136–143.
 Cladera, J., Galisteo, M.L., Sabes, M., Mateo, P.L. and Padros, E. (1992) The role of retinal in the thermal stability of the purple membrane. *Eur. J. Biochem.*, **207**, 581–585.
 Clausen-Schaumann, H., Seitz, M., Krautbauer, R. and Gaub, H.E. (2000) Force spectroscopy with single bio-molecules. *Curr. Opin. Chem. Biol.*, **4**, 524–530.
 Dammer, U., Hegner, M., Anselmetti, D., Wagner, P., Dreier, M., Huber, W. and Güntherodt, H.J. (1996) Specific antigen/antibody interactions measured by force microscopy. *Biophys. J.*, **70**, 2437–2441.
 Dettmann, W., Grandbois, M., Andre, S., Benoit, M., Wehle, A.K., Kaltner, H., Gabius, H.J. and Gaub, H.E. (2000) Differences in zero-force and force-driven kinetics of ligand dissociation from β-galactoside-specific proteins (plant and animal lectins, immunoglobulin G) monitored by plasmon resonance and dynamic single molecule force microscopy. *Arch. Biochem. Biophys.*, **383**, 157–170.
 Evans, E. (1998) Energy landscapes of biomolecular adhesion and receptor anchoring at interfaces explored with dynamic force spectroscopy. *Faraday Discuss.*, **111**, 1–16.
 Fisher, T.E., Oberhauser, A.F., Carrion-Vazquez, M., Marszalek, P.E. and Fernandez, J.M. (1999) The study of protein mechanics with the atomic force microscope. *Trends Biochem. Sci.*, **24**, 379–384.
 Florin, E.L., Rief, M., Lehmann, H., Ludwig, M., Dornmair, C., Moy, V.T. and Gaub, H. (1995) Sensing specific molecular interactions with the atomic force microscope. *Biosens. Bioelectron.*, **10**, 895–901.
 Fritz, J., Katopodis, A.G., Kolbinger, F. and Anselmetti, D. (1998) Force-mediated kinetics of single P-selectin/ligand complexes observed by atomic force microscopy. *Proc. Natl Acad. Sci. USA.*, **95**, 12283–12288.
 Grandbois, M., Beyer, M., Rief, M., Clausen-Schaumann, H. and Gaub, H.E. (1999) How strong is a covalent bond? *Science*, **283**, 1727–1730.
 Haltia, T. and Freire, E. (1995) Forces and factors that contribute to the structural stability of membrane proteins. *BBA-Bioenergetics*, **1228**, 1–27.
 Hanggi, P., Talkner, P. and Borkovec, M. (1990) Reaction rate theory—50 years after Kramers. *Rev. Mod. Phys.*, **62**, 251–341.
 Hasler, L., Heymann, J.B., Engel, A., Kistler, J. and Walz, T. (1998) 2D crystallization of membrane proteins: rationales and examples. *J. Struct. Biol.*, **121**, 162–171.
 Haupts, U., Tittor, J. and Oesterhelt, D. (1999) Closing in on bacteriorhodopsin: progress in understanding the molecule. *Annu. Rev. Biophys. Biomol. Struct.*, **28**, 367–399.
 Helmreich, E.J.M. and Hofmann, K.-P. (1996) Structure and function of proteins in G-protein coupled signal transfer. *Biochim. Biophys. Acta*, **1286**, 285–322.
 Heymann, B. and Grubmüller, H. (2000) Dynamic force spectroscopy of molecular adhesion bonds. *Phys. Rev. Lett.*, **84**, 6126–6129.
 Israelachvili, J. (1991) *Intermolecular & surface forces*. Academic Press Limited, London, UK.
 Jackson, M.B. and Sturtevant, J.M. (1978) Phase transitions of the purple membrane of the *Halobacterium halobium*. *Biochemistry*, **17**, 911–915.
 Kellermayer, M.S., Smith, S.B., Granzier, H.L. and Bustamante, C. (1997) Folding-unfolding transitions in single titin molecules characterized with laser tweezers. *Science*, **276**, 1112–1116.
 Koltover, I., Raedler, J.O., Salditt, T., Rothschild, K.J. and Safinya, C.R. (1999) Phase behavior and interactions of the membrane-protein bacteriorhodopsin. *Phys. Rev. Lett.*, **82**, 3184–3187.
 Kramers, H.A. (1940) Brownian motion in a field of force and the diffusion model of chemical reactions. *Physica (Utrecht)*, **7**, 284–304.
 Kühlbrandt, W. (1992) Two-dimensional crystallization of membrane proteins. *Q. Rev. Biophys.*, **25**, 1–49.
 Lanyi, J.K. (1999) Progress toward an explicit mechanistic model for the light-driven pump, bacteriorhodopsin. *FEBS Lett.*, **464**, 103–107.
 Lee, G.U., Kidwell, D.A. and Colton, R.J. (1994) Sensing discrete streptavidin-biotin interactions with atomic force microscopy. *Langmuir*, **10**, 354–357.

- Luecke, H., Richter, H.-T. and Lanyi, J.K. (1998) Proton transfer pathways in bacteriorhodopsin at 2.3 Å resolution. *Science*, **280**, 1934–1937.
- Luecke, H., Schobert, B., Richter, H.T., Cartailier, J.P. and Lanyi, J.K. (1999) Structure of bacteriorhodopsin at 1.55 Å resolution. *J. Mol. Biol.*, **291**, 899–911.
- Marszalek, P.E., Lu, H., Li, H., Carrion-Vazquez, M., Oberhauser, A.F., Schulten, K. and Fernandez, J.M. (1999) Mechanical unfolding intermediates in titin modules. *Nature*, **402**, 100–103.
- Merkel, R., Nassoy, P., Leung, A., Ritchie, K. and Evans, E. (1999) Energy landscapes of receptor-ligand bonds explored with dynamic force microscopy. *Nature*, **397**, 50–53.
- Mitsuoka, K., Hirai, T., Murata, K., Miyazawa, A., Kidera, A., Kimura, Y. and Fujiyoshi, Y. (1999) The structure of bacteriorhodopsin at 3.0 Å resolution based on electron crystallography: implication of the charge distribution. *J. Mol. Biol.*, **286**, 861–882.
- Moy, V.T., Florin, E.-L. and Gaub, H.E. (1994) Intermolecular forces and energies between ligands and receptors. *Science*, **266**, 257–259.
- Müller, D.J., Amrein, M. and Engel, A. (1997) Adsorption of biological molecules to a solid support for scanning probe microscopy. *J. Struct. Biol.*, **119**, 172–188.
- Müller, D.J., Kessler, M., Oesterhelt, F., Moeller, C., Oesterhelt, D. and Gaub, H. (2002) Stability of bacteriorhodopsin α -helices and loops analyzed by single-molecule force spectroscopy. *Biophys. J.*, **83**, 3578–3588.
- Müller, J., Münster, C. and Salditt, T. (2000) Thermal denaturing of bacteriorhodopsin by X-ray scattering from oriented purple membranes. *Biophys. J.*, **78**, 3208–3217.
- Nishiyama, T., Tabushi, I. and Maeda, A. (1987) Circular dichroism study of bacteriorhodopsin-lipid interaction. *Biochem. Biophys. Res. Commun.*, **144**, 836–840.
- Oberhauser, A.F., Marszalek, P.E., Erickson, H.P. and Fernandez, J.M. (1998) The molecular elasticity of the extracellular matrix protein tenascin. *Nature*, **393**, 181–185.
- Oberhauser, A.F., Marszalek, P.E., Carrion-Vazquez, M. and Fernandez, J.M. (1999) Single protein misfolding events captured by atomic force microscopy. *Nat. Struct. Biol.*, **6**, 1025–1028.
- Oesterhelt, D. (1998) The structure and mechanism of the family of retinal proteins from halophilic archaea. *Curr. Opin. Struct. Biol.*, **8**, 489–500.
- Oesterhelt, D. and Stoekenius, W. (1974) Isolation of the cell membrane of *Halobacterium halobium* and its fraction into red and purple Membrane. *Methods Enzymol.*, **31**, 667–678.
- Oesterhelt, F., Oesterhelt, D., Pfeiffer, M., Engel, A., Gaub, H.E. and Müller, D.J. (2000) Unfolding pathways of individual bacteriorhodopsins. *Science*, **288**, 143–146.
- Popot, J.L., Gerchmann, S.-E. and Engelmann, D.M. (1987) Refolding of bacteriorhodopsin in lipid bilayers: a thermodynamically controlled two-stage process. *J. Mol. Biol.*, **198**, 655–676.
- Popot, J.L. and Engelman, D.M. (2000) Helical membrane protein folding, stability, and evolution. *Annu. Rev. Biochem.*, **69**, 881–922.
- Racker, E. and Hinkle, P.C. (1974) Effect of temperature on the function of a proton pump. *J. Membr. Biol.*, **17**, 181–188.
- Radford, S.E. (2000) Protein folding: progress made and promises ahead. *Trends Biochem. Sci.*, **25**, 611–618.
- Rief, M., Gautel, M., Oesterhelt, F., Fernandez, J.M. and Gaub, H.E. (1997) Reversible unfolding of individual titin immunoglobulin domains by AFM. *Science*, **276**, 1109–1112.
- Rief, M., Fernandez, J.M. and Gaub, H.E. (1998a) Elastically coupled two-level-systems as a model for biopolymer extensibility. *Phys. Rev. Lett.*, **81**, 4764–4767.
- Rief, M., Gautel, M., Schemmel, A. and Gaub, H.E. (1998b) The mechanical stability of immunoglobulin and fibronectin III domains in the muscle protein titin measured by atomic force microscopy. *Biophys. J.*, **75**, 3008–3014.
- Rief, M., Gautel, M. and Gaub, H.E. (2000) Unfolding forces of titin and fibronectin domains directly measured by AFM. *Adv. Exp. Med. Biol.*, **481**, 129–136.
- Shen, Y., Safinya, C.R., Liang, K.S., Ruppert, A.F. and Rothschild, K.J. (1993) Stabilization of the membrane protein bacteriorhodopsin to 140 °C in two-dimensional films. *Nature*, **366**, 48–50.
- Shnyrov, V.L. and Mateo, P.L. (1993) Thermal transitions in the purple membrane from *Halobacterium halobium*. *FEBS Lett.*, **324**, 237–240.
- Subramaniam, S. (1999) The structure of bacteriorhodopsin: an emerging consensus. *Curr. Opin. Struct. Biol.*, **9**, 462–468.
- Taneva, S.G., Caaveiro, J.M., Muga, A. and Goni, F.M. (1995) A pathway for the thermal destabilization of bacteriorhodopsin. *FEBS Lett.*, **367**, 297–300.
- Tanford, C. (1980) *The hydrophobic effect*. John Wiley & Sons, Inc., New York, NY.
- Tristram-Nagle, S., Yang, C.P. and Nagle, J.F. (1986) Thermodynamic studies of purple membrane. *Biochim. Biophys. Acta*, **854**, 58–66.
- White, S.H. and Wimley, W.C. (1999) Membrane protein folding and stability: physical principles. *Annu. Rev. Biophys. Biomol. Struct.*, **28**, 319–365.
- Wilkinson, D.A. and Nagle, J.F. (1982) Specific heats of lipid dispersions in single phase regions. *Biochim. Biophys. Acta*, **688**, 107–115.
- Zhang, B., Xu, G. and Evans, J.S. (1999) A kinetic molecular model of the reversible unfolding and refolding of titin under force extension. *Biophys. J.*, **77**, 1306–1315.

Received March 24, 2003; revised and accepted August 12, 2003

Probing the Energy Landscape of the Membrane Protein Bacteriorhodopsin

Harald Janovjak,¹ Jens Struckmeier,³
Maurice Hubain,¹ Alexej Kedrov,¹
Max Kessler,² and Daniel J. Müller^{1,*}

¹BIOTEC

University of Technology Dresden
01307 Dresden

²Lehrstuhl für Angewandte Physik
Ludwig Maximilians Universität München
80799 München

Germany

³Veeco Metrology

Digital Instruments

Santa Barbara, California 93117

Summary

The folding and stability of transmembrane proteins is a fundamental and unsolved biological problem. Here, single bacteriorhodopsin molecules were mechanically unfolded from native purple membranes using atomic force microscopy and force spectroscopy. The energy landscape of individual transmembrane α helices and polypeptide loops was mapped by monitoring the pulling speed dependence of the unfolding forces and applying Monte Carlo simulations. Single helices formed independently stable units stabilized by a single potential barrier. Mechanical unfolding of the helices was triggered by 3.9–7.7 Å extension, while natural unfolding rates were of the order of 10^{-3} s⁻¹. Besides acting as individually stable units, helices associated pairwise, establishing a collective potential barrier. The unfolding pathways of individual proteins reflect distinct pulling speed-dependent unfolding routes in their energy landscapes. These observations support the two-stage model of membrane protein folding in which α helices insert into the membrane as stable units and then assemble into the functional protein.

Introduction

Biological membranes are essential to all living organisms, as they provide selective permeability barriers and environments for a multitude of functional processes such as signal transduction, molecular transport, cell-to-cell communication, and cell adhesion (Lodish et al., 1999). Most functions of cellular membranes are carried out by integral membrane proteins which are therefore of fundamental biological interest and form major targets for drug development. However, the steadily increasing number of known gene sequences coding for membrane proteins contrasts sharply with our lacking knowledge of their functional three-dimensional structures as well as of their biosynthesis and stability within the lipid bilayer (Booth et al., 2001).

Membrane proteins acquire their unique functions

through the specific folding of their polypeptide in the anisotropic environment of the lipid bilayer (Haltia and Freire, 1995; Popot and Engelman, 2000; White and Wimley, 1999). In a so-called two-stage model, the sequential folding of α -helical transmembrane proteins was described based on experimental results revealed from bacteriorhodopsin (BR) (Popot et al., 1987), which has now been confirmed on human aquaporin-1 and on the sodium-proton antiporter NhaA from *E. coli* (A. Kedrov, submitted; Möller et al., 2003). First, transmembrane helices form independently stable fragments which then assemble into the functional protein. Thus, it is suggested that the helices act comparably to domains in soluble proteins. Together with their connecting loops, the helices then assume a free energy minimum by the characteristic tertiary structure. Force spectroscopy data generated by mechanical unfolding of membrane proteins suggest that pairwise association of transmembrane helices drives them into a conformation of comparable stability to single transmembrane helices (A. Kedrov, submitted; Müller et al., 2002). This experimental finding is in agreement with the model given two decades ago that pairwise association builds a common structural motif in membrane protein folding and secretion (Engelman and Steitz, 1981).

The stability or resistance to unfolding of proteins is usually investigated by thermal or chemical denaturation in ensemble measurements. However, such bulk experimental methods only probe the average behavior of a large number of molecules and thus cannot resolve simultaneously occurring multiple (un)folding pathways and nonaccumulative intermediate folding states. Perceptions of protein (un)folding such as described by multidimensional landscapes or folding funnels can be seen as a result of the complexity of inter- and intramolecular interactions (Radford, 2000). Different (un)folding pathways may be populated in a manner dependent on small alterations of the physiological environment requiring novel investigative approaches (other than ensemble measurements) to observe coexisting minor and major pathways.

Experiments using the atomic force microscope (AFM) (Binnig et al., 1986) and similarly other force probe methods (Leckband and Israelachvili, 2001) provide novel techniques to reveal detailed insights into the molecular interactions determining the (un)folding of proteins. In these experiments, an external force applied to single proteins leads to sequential unfolding of their three-dimensional structure. Using this method in an assay will allow the screening of physiologically relevant parameters such as pH, electrolyte concentration, temperature, and other factors that modulate inter- and intramolecular interactions of the protein. In single-molecule force spectroscopy experiments using the AFM, a microfabricated cantilever detects molecular forces down to a few pN. A single molecule is tethered between the tip of the cantilever and a supporting surface while the tip-surface separation is continuously increased using a piezoelectric actuator. Recording the force against

*Correspondence: mueller@mpi-cbg.de

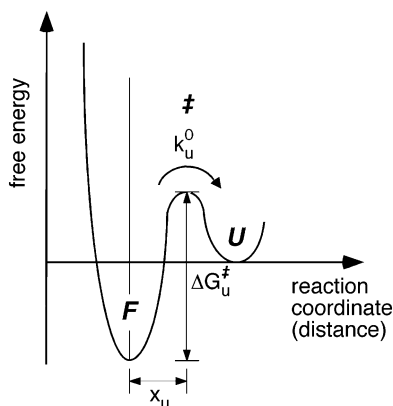


Figure 1. Two-State Model for the Interpretation of Mechanical Unfolding Experiments

A simple two-state potential exhibiting a single sharp potential barrier separating the folded low-energy state (F) from the unfolded state (U) can be applied to describe the mechanical unfolding experiments. Here the unfolding of single secondary structure elements of the membrane protein BR is interpreted using this model. The activation energy for unfolding is given by ΔG_u^\ddagger , while x_u (the width of the potential barrier) is the distance along the reaction coordinate from the folded state to the transition state (\ddagger) and the natural (thermal) transition rate is denoted k_u^0 . DFS experiments allow determining the width of the potential barrier and the unfolding rate by monitoring the unfolding forces as a function of pulling speed.

tip-surface separation yields a force-extension curve characteristic for the particular molecule. In initial experiments, Rief and coworkers applied single-molecule force spectroscopy to the muscle protein titin which consists of repeats of globular immunoglobulin and tennascin domains (Rief et al., 1997). The continuous extension of the protein resulted in the subsequent unfolding of the globular domains while the forces necessary for unfolding of each domain are deduced from the force curve.

It was recently shown that dynamic force spectroscopy (DFS) experiments provide further insights into the energy landscape underlying the mechanical properties of single proteins and receptor ligand pairs. In DFS, single-molecule force spectroscopy AFM is extended to measure unfolding or unbinding forces at various pulling speeds. Monitoring the most probable rupture force as a function of the pulling speed allows resolving the width of potential barriers crossed during the unfolding process (Figure 1). Additionally, the natural transition rates over these barriers can be determined. Using this approach, the binding properties of individual ligand-receptor pairs (Merkel et al., 1999) and the unfolding behavior of globular proteins such as immunoglobulin were previously investigated (Carrion-Vazquez et al., 1999; Merkel et al., 1999; Williams et al., 2003). In case of immunoglobulin 27 (Ig 27) it was shown that a 3.3 Å extension triggers unfolding from an intermediate state (Carrion-Vazquez et al., 1999; Williams et al., 2003). Merkel and coworkers demonstrated that during unbinding of biotin from (strept)avidin several potential barriers are crossed and their positions along the separation distance could be localized (Merkel et al., 1999).

Here we apply DFS to probe the energy landscape of the integral membrane protein BR. To this end, single

proteins were unfolded from native purple membranes of *Halobacterium salinarum* at seven different pulling speeds in the range of 10 nm/s to 5.23 $\mu\text{m/s}$. We have previously shown that the combination of single-molecule AFM imaging and force spectroscopy can be applied to unfold individual membrane proteins and determine the stability of their secondary structure elements (Möller et al., 2003; Müller et al., 2002; Oesterhelt et al., 2000). In contrast to most unfolding experiments on globular proteins, the membrane protein BR unfolds stepwise yielding surprisingly detailed insights into inter- and intramolecular interactions (Janovjak et al., 2003; Müller et al., 2002). In subsequent experiments, unfolding barriers stabilizing individual secondary structure elements of BR (such as transmembrane α helices and polypeptide loops) were localized and the influence of external physiologically relevant parameters on these barriers was characterized (Janovjak et al., 2003; Müller et al., 2002). The DFS experiments performed in this work provided new detailed insights into potential barriers established by secondary structure elements. While single helices were found to be stabilized by a single potential barrier, they also associated pairwise, thereby establishing a different collective potential barrier. Mechanical unfolding of these structures was triggered by extension of a few angstroms, whereas natural unfolding rates were of the order of 10^{-3} s^{-1} .

The light-driven proton pump BR was chosen as model system for this study because it represents one of the most extensively studied membrane proteins. Its structural analysis has revealed the photoactive retinal embedded in seven closely packed transmembrane α helices (Belrhali et al., 1999; Essen et al., 1998; Grigorieff et al., 1996; Luecke et al., 1999; Mitsuoka et al., 1999), a common structural motif among a large class of related G protein coupled receptors (Baldwin, 1993; Helmreich and Hofmann, 1996; Kolbe et al., 2000; Palczewski et al., 2000; Royant et al., 2001). Hydrophilic polypeptide loops link the seven membrane embedded hydrophobic BR helices lettered A through G, to which the C-terminal end is connected. With increasing knowledge of its structural and functional properties, BR has become a paradigm for α -helical membrane proteins in general and for ion transporters in particular (Lanyi, 1999; Subramaniam, 1999).

Results

Each superimposition shown in Figures 2A–2E is composed of ~ 15 force curves, each recorded by unfolding a single BR molecule at the indicated pulling speed. It was previously shown that secondary structure elements of single BR molecules sequentially unfold when an external force is applied to the C terminus of the protein. Extension of the already unfolded elements then results in a characteristic pattern in the force spectrum (Figure 3). Apparently, the pulling speed did not change the unfolding pattern of BR and the individual force peaks remained at their positions (Figures 2A–2E). However, it is evident that the height of the force peaks and thus the average forces required to unfold parts of the protein increased with increasing pulling speed. By correlation to the three-dimensional structure of BR, we

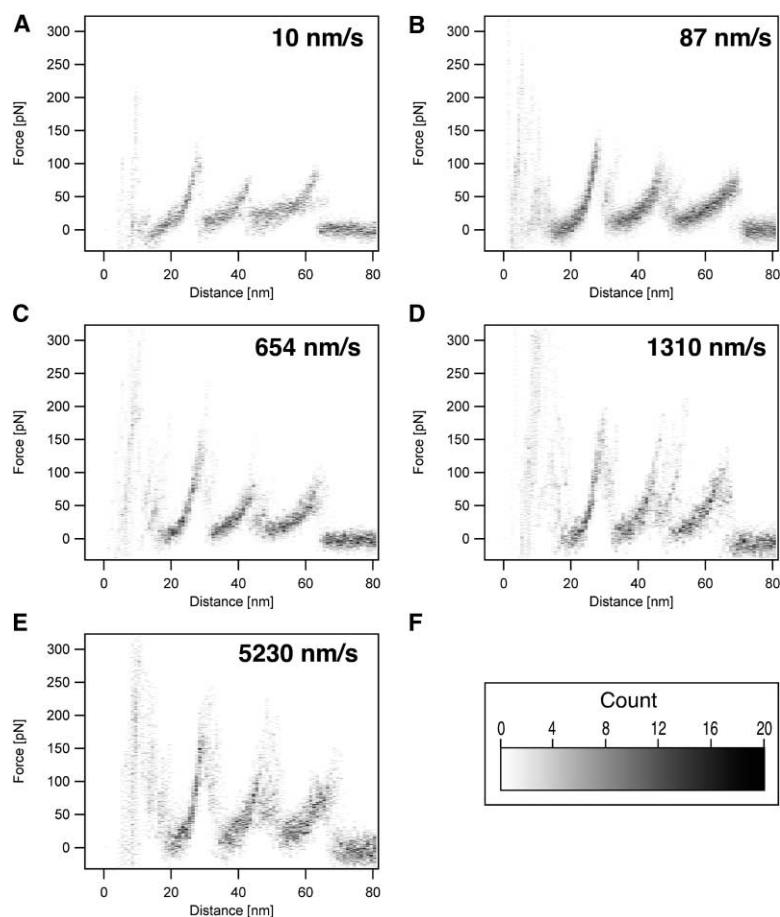


Figure 2. Superimpositions of BR Force Curves Recorded at Different Pulling Velocities

(A)–(E) show superimpositions of around 15 force versus distance traces each recorded on a single BR molecule at the pulling speed indicated (10 nm/s [A], 87 nm/s [B], 654 nm/s [C], 1310 nm/s [D], and 5230 nm/s [E]). As observed from the superimpositions, the unfolding forces (height of the peaks) increase with the pulling speed. The gray shading of the superimpositions was achieved by applying a grid subdividing each force curve into 1 pN by 1 nm big boxes and counting the number of data points in each box (a two-dimensional histogram). The scale in (F) shows that 20 data points will color individual boxes black (normalized to 10 curves with 2048 data points).

recently assigned the peaks in the force spectra to the unfolding of individual secondary structure elements such as transmembrane α helices or polypeptide loops (Müller et al., 2002) (Figure 3).

Figure 4 shows the unfolding forces of secondary structure elements as a function of the logarithm of the pulling velocity, what is referred to as a dynamic force spectrum. The dynamic force spectrum for pairwise unfolding of two transmembrane helices is shown in Figure 4A, while those of single secondary structure elements are given in Figures 4B–4F. For all unfolding events, a single linear regime was observed in the dynamic force spectrum.

Among the different methods to analyze dynamic force spectra data we have chosen Monte Carlo (MC) simulations (Rief et al., 1998) as they take the (changing) length of the flexible polypeptide linker between the cantilever and membrane surface into account. MC simulations allow us to obtain the width (x_u) and the natural unfolding rate (k_u^0) of the potential barrier(s) crossed during an unfolding or unbinding process. This is achieved by systematically varying the two parameters of the MC simulation (x_u and k_u^0) until the simulated forces and the measured forces are in best agreement. The goodness of the simulation was assessed by a chi-square comparison (see Experimental Procedures). The solid and dashed lines in Figure 4 represent the simulated forces as determined by the MC simulation with the minimal chi-square deviation from the measured data. The width

of the potential barrier and the natural unfolding rate used in these simulations are summarized in Table 1. For individual transmembrane helices we observed potential barriers' widths from 3.9 to 7.7 Å and spontaneous unfolding rates from 1.8×10^{-6} to 1.7×10^{-2} molecules per second. Pairwise unfolding of two helices and unfolding of the bc loop was characterized by potential barrier widths and unfolding rates in the same range of magnitude (3.2–6.8 Å for x_u and 3.4×10^{-5} to 1.0×10^{-2} for k_u^0).

The above analysis showed that each individual structural element exhibited a free energy minimum, thereby establishing an internal potential barrier against mechanical unfolding. Although the transmembrane helices were sufficiently stable to unfold individually, they, at the same time, exhibited a distinct probability to unfold pairwise (Müller et al., 2002). Figure 5 shows that these unfolding probabilities were highly dependent on the pulling speed. While the unfolding probability of single transmembrane helices (dashed lines) increased with the pulling speed that of pairwise unfolding (solid lines) decreased.

Discussion

Force Spectroscopy of Individual Membrane Proteins

Single-molecule force spectroscopy experiments on membrane proteins such as BR, human aquaporin-1,

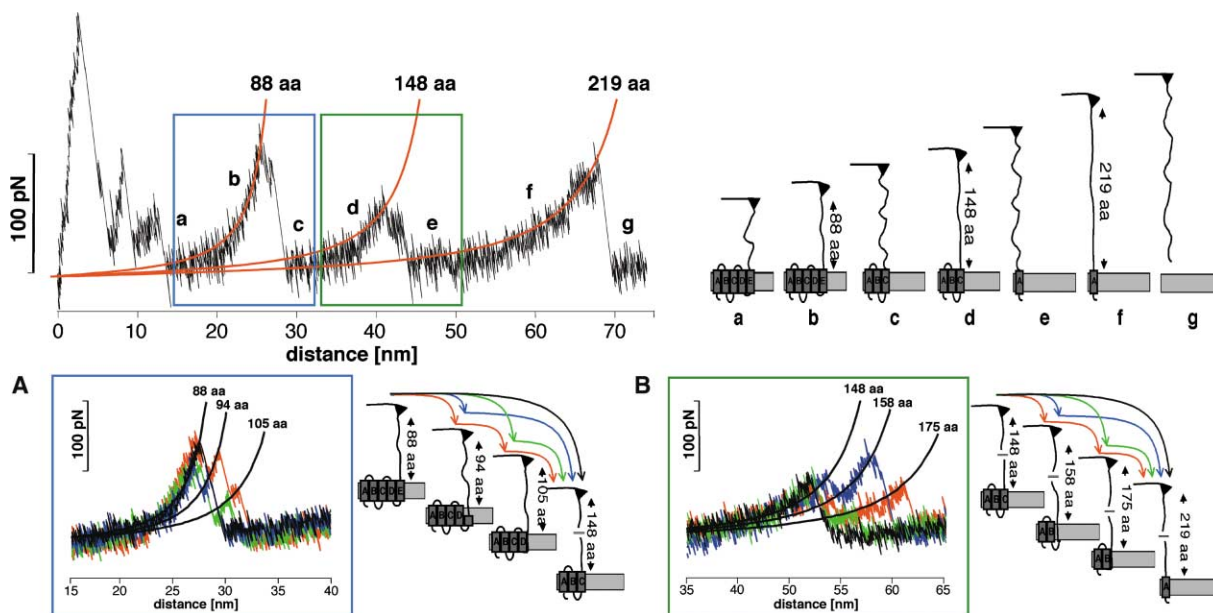


Figure 3. Unfolding Pathways of BR

Top, pairwise unfolding pathway of transmembrane α helices. The experimental curve to the left shows a representative unfolding spectrum of a single BR, while the schematic unfolding pathway is sketched on the right. The worm-like chain model was applied to derive the length of the unfolded elements based on their force-extension pattern (solid lines). These lengths were then used to reconstruct the corresponding unfolding pathway (Müller et al., 2002). The first force peaks detected at tip-sample separations below 15 nm indicate the unfolding of transmembrane α helices F and G. However, nonspecific interactions between the purple membrane surface and AFM tip are frequently observed in this part of the force spectrum and make a detailed analysis of these peaks difficult. After unfolding these elements, 88 aa are tethered between the tip and the surface (a). Separating the tip further from the surface stretches the polypeptide (b), thereby exerting force to helix E and D. At a certain critical load, the mechanical stability of helices E and D is overcome and they unfold together with loop DE. As the number of amino acids linking the tip and the surface is now increased to 148, the cantilever relaxes (c). In a next step, the 148 aa are extended thereby pulling on helix C (d). After unfolding helices B and C and loop BC in a single step, the molecular bridge is lengthened to 219 aa (e). By further separating tip and purple membrane, helix A unfolds (f) and the polypeptide is completely extracted from the membrane (g).

(A and B) Examples showing the unfolding of individual secondary structure elements. (A) Occasionally the first unfolding peak at 88 aa shows two shoulder peaks, which indicate the stepwise unfolding of the helical pair. If both shoulders occur, the peak at 88 aa indicates the unfolding of helix E, that at 94 aa of loop DE, and the peak at 105 aa corresponds to the unfolding of helix D. (B) The shoulder peaks of the second peak indicate the stepwise unfolding of helices C and B and loop BC. The peak at 148 aa indicates the unfolding of helix C, that at 158 aa of the loop BC, and the peak at 175 aa represents unfolding of helix B. The arrows indicate the observed unfolding pathways. In certain pathways (black arrows), a pair of two transmembrane helices and their connecting loop unfolded in a single step. In other unfolding pathways (colored arrows), these structural elements unfolded in several intermediate steps. We focused our analysis on the unfolding of single secondary structure elements, although in small number of events loops also unfolded together with helices.

and the bacterial sodium-proton antiporter NhaA recently yielded surprisingly detailed insights into their inter- and intramolecular interactions (A. Kedrov, submitted; Möller et al., 2003; Müller et al., 2002). To this end, one of the termini of the protein is attached to the tip of the AFM cantilever either by a covalent bond or more commonly by nonspecific attachment. Attachment of multiple sites of the terminus, polypeptide loops connecting the helices or intramembranous parts of the protein is largely excluded by limiting the analysis to force traces that show the length of a fully unfolded molecule (see Experimental Procedures). The protein is then mechanically unfolded using the cantilever as a force transducer applying an external force. Interactions that stabilize individual structural elements such as transmembrane α helices and polypeptide loops were detected in terms of unfolding forces and different unfolding pathways (Müller et al., 2002). In this study, we investigated the speed dependence of the unfolding

forces to probe the energy landscape and the stability of single secondary structure elements.

Unfolding Forces Depend on the Pulling Speed

As first shown in Bell's seminal work and later in a more elaborate description by Evans and Ritchie, the escape over a potential barrier under a constant force ramp occurs within a time range determined by the applied force rate (Bell, 1978; Evans and Ritchie, 1997; Evans, 1999). At zero applied force, the spontaneous unfolding rate k_u^0 (Figure 1) determines the time required to cross the barrier. Fast pulling speeds will result in low lifetimes, while low pulling speeds will render the bonds weak but lifetimes long. The unfolding force is thus governed by the pulling velocity and the width of the potential barrier x_u (the distance from the folded state to the transition state along the separation distance as the reaction coordinate) as well as the natural transition rate k_u^0 (Figure

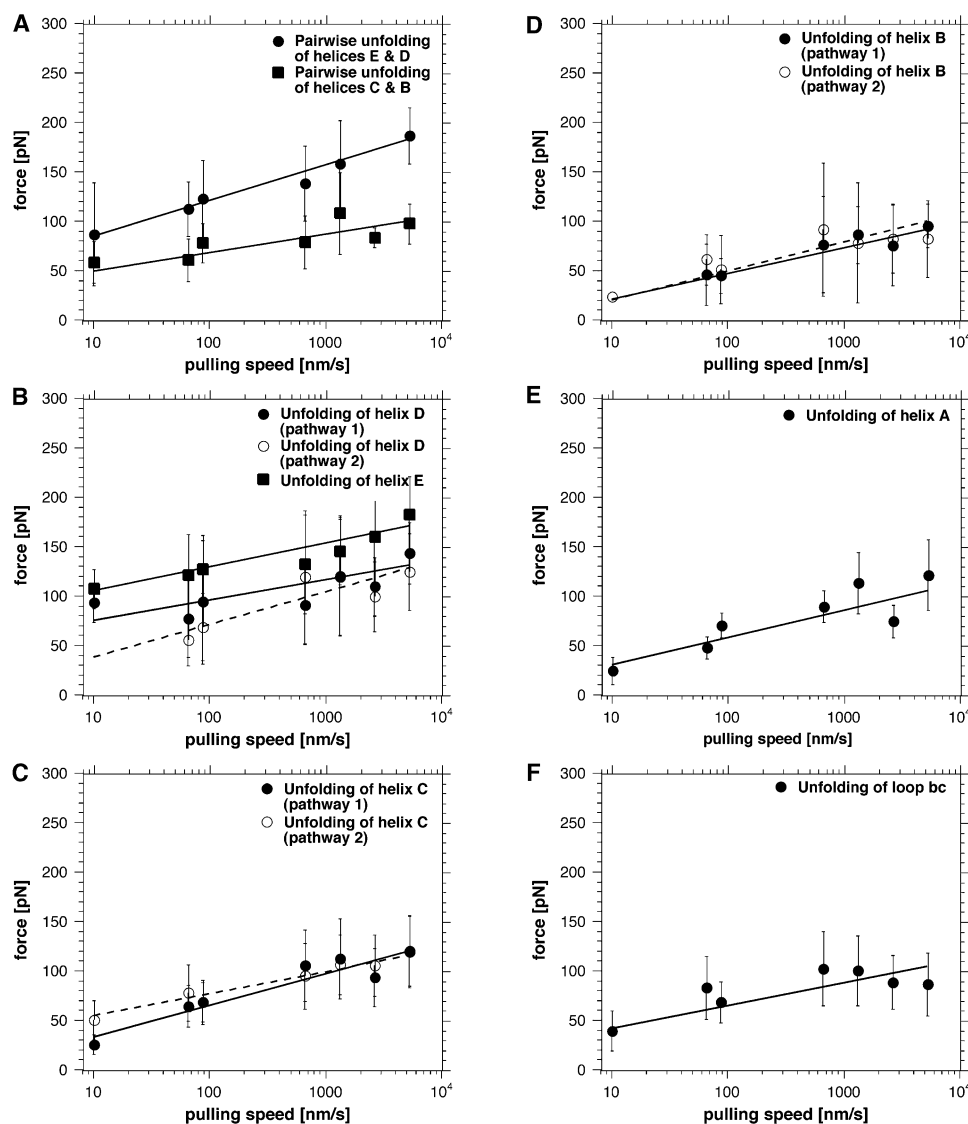


Figure 4. Unfolding Forces as a Function of Pulling Speed

For single and groups of secondary structure elements, the unfolding force increased with the pulling speed. A logarithmic dependence of the force on the pulling speed was clearly resolved. This indicated that a single sharp potential barrier as shown in Figure 1 was to be crossed to unfold the structural elements. Force versus $\ln(\text{speed})$ plots for the pairwise unfolding of helices are shown in (A) and for single secondary structure elements (i.e., transmembrane α helices and polypeptide loops) in (B)–(F). Solid and dashed lines represent Monte Carlo simulations (see Experimental Procedures) used to analyze the experimental data given by filled (in case of solid lines) and open symbols (in case of dashed lines). As unfolding of helices D, C, and B occurred in two different unfolding pathways (1 and 2), two data sets were obtained and analyzed independently. Although in both pathways these helices unfolded individually, other helices unfolded together with extracellular loops, and therefore the events were analyzed separately (Müller et al., 2002).

1) can be explored when pulling at different speeds (Evans and Ritchie, 1997; Evans, 1999).

Secondary Structure Elements of BR Establish Single Potential Barriers

The linear regime in force versus logarithm of the pulling speeds plots (Figure 4) suggests that a single sharp potential barrier such as shown in Figure 1, must be overcome (Evans and Ritchie, 1997; Evans, 1999). Thus, the potential landscape of mechanical unfolding can

be approximated by a two-state model. In this simple model, the low-energy folded state (F) is separated from the unfolded state (U) by the energy barrier located at the transition state (\ddagger). Extension of the folded state by the width of the potential barrier (x_u) triggers the unfolding process, and therefore x_u describes the position of the transition state along the reaction coordinate (separation). To obtain x_u from the data shown in Figure 4, we applied MC simulations (Rief et al., 1998). For individual transmembrane helices we observed x_u rang-

Table 1. Parameters Describing the Potential Barriers that Stabilize Secondary Structure Elements of BR against Mechanical Unfolding

Secondary Structure Element	Width of Potential (x_u [Å])	Natural Unfolding Rate (k_u^0 [s^{-1}])
Pairs of helices (Figure 4A)		
Helices E and D	3.2	1.0×10^{-2}
Helices B and C	8.6	3.4×10^{-5}
Individual helices (Figures 4B–4E)		
Helix E ^a	4.6	1.1×10^{-4}
Helix D ^b	4.0 / 7.7	5.6×10^{-2} / 1.5×10^{-6}
Helix C ^b	4.9 / 3.9	6.0×10^{-3} / 5.6×10^{-2}
Helix B ^b	5.7 / 5.4	1.7×10^{-2} / 3.1×10^{-2}
Helix A	6.8	1.8×10^{-4}
Individual loop (Figure 4F)		
Loop bc	5.8	3×10^{-3}

The widths of the potential barrier and the natural unfolding rate of single and groups of secondary structure elements were determined by monitoring the unfolding force of each element as a function of the pulling speed.

^aIncluding the 3 aa long loop ed.

^bThese elements unfold in two different unfolding pathways. Therefore, two values were obtained for x_u and k_u^0 .

ing from 3.9 to 7.7 Å and for pairwise unfolding of transmembrane helices 3.2 and 8.6 Å (Table 1).

Extraction or Unfolding of Transmembrane Helices?

When extracting a biotinylated C18-lipid from stearyl-oleoyl phosphatidylcholine (SOPC) bilayers, Evans and Ludwig found that two potential barriers had to be crossed at 7 and 12 Å respectively (Evans and Ludwig, 2000). In agreement with the idea that lipid molecules are simply extracted from the membrane without a large degree of conformational change and consistent with the concept of hydrophobic interaction, the outer barrier is of comparable magnitude to half the bilayer membrane and the inner barrier correlates to the position of the unsaturated bond in the oleoyl chain (Evans and Ludwig, 2000). As one would expect, the position of the transition state during unfolding of a transmembrane helix is in apparent contrast to the ones observed during the extraction of lipid molecules from a membrane bilayer. The values observed here are much smaller than half the thickness of the purple membrane (which would correspond to about 30 Å) and thus suggest that breakage of inter- or intramolecular bonds stabilizing the structure starts the unfolding process. This initial step would then be followed by cooperative unfolding or “un-zipping” of the helical structures, in agreement with a

recently suggested model in which transmembrane helices unfold within the membrane rather than being first displaced from the hydrophobic membrane core (Janovjak et al., 2003). Molecular dynamics simulations will provide further insights into the details of the unfolding process including the exact sequence of events associated with the unzipping of individual helices. Complementary information about the interactions that stabilize single BRs can then also be obtained from the study of protein fragments (Hunt et al., 1997; Marti, 1998).

Stability of Individual Secondary Structure Elements

The MC simulations performed allow determination of the natural (zero applied force) transitions rate over the potential barriers. We found spontaneous unfolding rates in the range from 1.5×10^{-6} to $1.7 \times 10^{-2} s^{-1}$ for single transmembrane helices and 3.4×10^{-5} to $1.0 \times 10^{-2} s^{-1}$ for pairs of helices (Table 1). These values are of comparable magnitude to small globular proteins like barnase ($k_u^0 = 2.3 \times 10^{-5} s^{-1}$) (Best et al., 2001) and Ig 27 ($k_u^0 = 1.2 \times 10^{-4} s^{-1}$) (Carrion-Vazquez et al., 1999; Williams et al., 2003). This suggests that individual transmembrane helices which are considered important folding intermediates exhibit sufficient stability to form stable fragments prior to their assembly during the fast folding process (Allen et al., 2001).

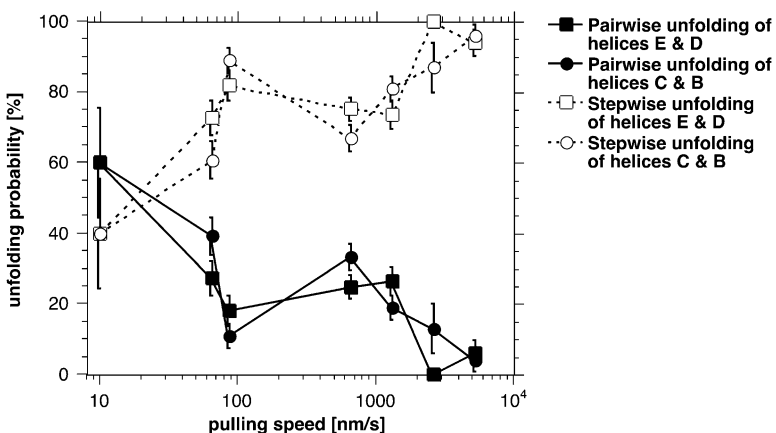


Figure 5. Unfolding Pathways Depend on Pulling Speed

Individual BR molecules exhibited distinct probabilities to follow different unfolding pathways when unfolded by mechanically pulling on the C terminus. Although single helices were sufficiently stable to unfold in individual steps (dashed lines), they exhibited a certain probability to unfold pairwise (solid lines). We found that changing the pulling speed affected these unfolding probabilities. As a result, the probability of unfolding single secondary structure elements increased with the pulling speed. This suggests that in the absence of a pulling force (smallest pulling speeds) two transmembrane helices would preferentially show a pairwise behavior (Figure 6).

Unfolding Pathways of Individual BRs

It was previously shown that individual BR molecules follow well-defined unfolding pathways (Müller et al., 2002). These pathways differ as to whether secondary structure elements unfold individually or as grouped structures as observed for pairwise unfolding of transmembrane helices. Each of these pathways exhibits a distinct probability to be chosen. These probabilities can be altered by varying the physiological environment as well as by structural modifications of the protein (Janovjak et al., 2003; Müller et al., 2002). However, it could not be answered unambiguously whether changes in the probabilities to follow certain unfolding pathways reflected different unfolding trajectories in the potential landscape of the protein rather than different amounts of energy stored in the cantilever (Heymann and Grubmüller, 2000; Janovjak et al., 2003).

Our data clearly shows (Table 1) that the location of the transition state for certain unfolding events was different if they occurred in different unfolding pathways. For example, unfolding of the single helix E occurred at the same position in the force spectrum as pairwise unfolding of helices E and D (as the force is in both cases applied to helix E). However, in case of individual extraction of helix E an extension of 4.6 Å triggered unfolding, while in case of the pairwise unfolding of helices D and E the polypeptide had to be extended only 3.2 Å (Table 1). This indicates that two distinct unfolding routes along two different transition states were taken. This effect was also observed for the pairwise and stepwise unfolding of helices B and C.

Rate Dependency of the Unfolding Pathways

The above observation is in agreement with the DFS data showing that the probabilities of the unfolding pathways depend on the pulling speed (Figure 5). By increasing the pulling speed, unfolding of individual transmembrane helices clearly dominated over pairwise unfolding. This indicates that the applied force tilted the potential barrier in such a way that the unfolding barrier for single transmembrane helices elements was lowered more than that for pairwise unfolding.

Pairwise association of transmembrane helices was suggested to play an important role in membrane protein stability and folding (Engelman and Steitz, 1981). Extrapolating the speed dependence of the pairwise unfolding pathways (Figure 5) to smaller pulling speeds (which at some point corresponds to zero unfolding force) suggests transmembrane helices almost exclusively unfold in a pairwise conformation. This indicates that under native conditions (zero applied force) the unfolding barrier for pairwise unfolding is smaller compared to the barrier for individual unfolding of the corresponding helices. Accordingly, the energy landscape can be approximated qualitatively such as shown in Figure 6. This behavior is also partly reflected in the natural transition rates revealed by the MC simulations (Table 1), where higher transition rates indicate the lower potential barrier. It should be noted however that the unfolding rates determined using MC simulations usually have a corresponding error of one order magnitude and thus cannot solely be used to justify our approximation of the potential landscape (Best et al., 2002).

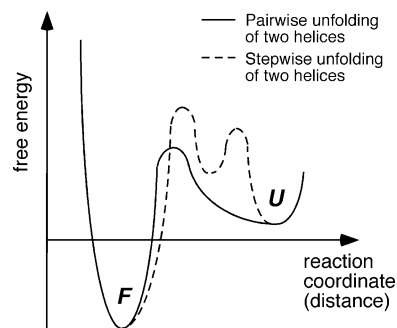


Figure 6. Potential Landscape as Revealed by Dynamic Force Spectroscopy

Two possible unfolding routes exist for pairs of transmembrane helices in BR. From the folded state (*F*), the two helices are either unfolded individually (dashed line) or pairwise (solid line) to the unfolded state (*U*). The shown approximation of the potential landscape at native conditions (zero force) was generated by extrapolating the speed-dependent unfolding probabilities to zero force (Figure 4). Since the experimental data showed that between two possible routes the pairwise unfolding was chosen more frequently, its potential barrier must be lower than for unfolding of individual helices.

Conclusions

According to the currently accepted model, the biogenesis of multispinning membrane proteins occurs in two well-separated steps. First, transmembrane α helices insert into the membrane as independently stable units before they assemble into the functional protein (Popot et al., 1987). Individual helical domains therefore are considered as important folding intermediates. Single-molecule force spectroscopy revealed that single helices form independently stable units and established potential barriers against mechanical unfolding. The experimental results revealed in this work show that individual helices are stabilized by one sharp potential barrier. It was also observed that helices associate pairwise forming a collective potential barrier. Both observations strongly support the two-stage model of membrane protein folding. The stability of single helices lies in the order of 10^3 s, which seems to be sufficient for assembly during the very fast folding process which takes place in milliseconds (Allen et al., 2001). We have shown that mechanical unfolding of single transmembrane helices is triggered by an extension of only ~ 4 Å, which indicates that breakage of intramolecular interactions between or within secondary structure elements represents the starting point of a cooperative unfolding process.

Experimental Procedures

Purple Membrane Preparation

Wild-type purple membrane was extracted from *H. salinarum* as described previously (Oesterhelt and Stoerkenius, 1974) and adsorbed onto freshly cleaved mica from buffer solution (300 mM KCl, 20 mM Tris, pH 7.8) (Müller et al., 1997). All buffer solutions were prepared with nanopure water and p.a. grade chemicals from Sigma/Merck.

Single-Molecule Force Spectroscopy

The AFM optimized for force spectroscopy (Multimode PicoForce, Nanoscope IIIa; Veeco Metrology, Santa Barbara, CA) was equipped with a 50 μ m X-Y-piezo scanner with a closed-loop 20 μ m z axis. The

spring constants of the 100 μm long silicon nitride AFM cantilevers (Olympus OTR4, Veeco Metrology; nominal spring constant ~ 0.08 N/m) were calibrated in solution using thermal fluctuation analysis (H.J. Butt and M. Jaschke, 1995, Nonotechnology, abstract; Florin et al., 1995). To perform force spectroscopy experiments, we recorded AFM topographs of the cytoplasmic purple membrane surface in 150 mM KCl, 10 mM Tris, and pH 7.8 (Müller et al., 1995). The AFM stylus was then approached to the cytoplasmic membrane surface and kept in contact with the proteins for about 1 s while applying a force between 300 and 1000 pN. Stylus and protein surface were then separated at velocities in the range of 10 nm/s to 5.23 $\mu\text{m/s}$. In about 15% of all retraction curves we detected one or more adhesive peaks.

Attachment of BR to the AFM Cantilever

In earlier work we developed two different strategies to attach the protein to the tip. We have shown that a thiol group of the cysteine residue in the G241C mutant binds with a likelihood of $\sim 90\%$ to a gold-coated cantilever when the tip is brought into contact with the cytoplasmic purple membrane surface at forces below 200 pN (Oesterhelt et al., 2000). Although this procedure allows a highly defined attachment, it requires replacement of the AFM cantilever after a few experiments since the tip is covered with bound proteins. An alternative method, nonspecific attachment to a silicon nitride cantilever using higher contact forces was shown to provide equivalent results and allows a much higher throughput (Müller et al., 2002). Since this study is a systematic investigation, we chose the nonspecific attachment as described above.

Force Curve Analysis

A clear criterion is required to distinguish curves of BR molecules attached to the AFM tip with different regions of their polypeptide backbone. One suitable criterion is the overall length of the force curve, which reflects the tip-sample distance at which the last force peak occurs (Oesterhelt et al., 2000). It is evident that a molecule attached to the cantilever by one of its loops results in a force curve of smaller overall length than a molecule attached by one of its termini. We have previously shown that force extension curves exhibiting an overall length between 60 and 70 nm result from completely unfolded and extended BR molecules attached with their C terminus to the AFM tip (Müller et al., 2002; Oesterhelt et al., 2000). This selection of force traces also assures that the protein has been contacted at the free C terminus and not in the intramembraneous part of the protein. All force curves exhibiting these overall lengths were selected and aligned with computer software according to the adhesion peak, which occurred at a tip-to-purple membrane separation of ~ 25 nm (Figure 2). The alignment also compensates for attachment at multiple and/or different sites of the C terminus. To assign events in the force spectra to secondary structure elements, we have used the recently published mechanical unfolding pathways of BR (Müller et al., 2002). As proposed in this study, every peak of the force curves was fitted using the wormlike chain (WLC) model with a persistence length of 4 Å and a monomer length of 3.6 Å (Rief et al., 1997). The number of extended amino acids (aa) at each peak was then calculated using the contour length obtained from the WLC fits. To compare the polypeptide length with the BR structure the atomic model of Mitsuoka et al. (Mitsuoka et al., 1999) was chosen. To derive the unfolding forces and probabilities of the individual elements, every event of each curve was analyzed. We analyzed 10 (10 nm/s), 84 (50 nm/s), 79 (87 nm/s), 165 (654 nm/s), 121 (1310 nm/s), 23 (2620 nm/s), and 51 (5230 nm/s) individual force traces at the indicated pulling speed.

Dynamic Force Spectroscopy and MC simulations

We found that the unfolding forces of single secondary structure elements show a logarithmic dependence on the pulling velocity (Figure 4). This indicates that a single sharp potential barrier (as the one shown in Figure 1) is crossed during the unfolding process. To obtain the width of the potential barrier (x_u) and the natural off-rate (k_u^0) from the DFS data we applied MC simulations (Rief et al., 1998). We performed simulations for pairs of x_u (ranging from 1 to 10 Å with 80 linear increments) and k_u^0 (ranging from 1 to 10^{-5} s $^{-1}$ with 20 logarithmic increments). For each pair of x_u and k_u^0 the goodness

of the simulations was determined by calculating chi-square (χ^2) according to:

$$\chi^2(\chi_u, k_u^0) = \sum_{i=1}^N \left(\frac{f_{\text{exp}}(v_i) - f_{\text{sim}}(v_i; \chi_u, k_u^0)}{\sigma_i} \right)^2, \quad (1)$$

where f_{exp} is the measured forces, f_{sim} the forces determined by MC simulations at the same speed, and σ denotes the standard deviation of the measured forces (Best et al., 2002). The best pair of parameters was found by looking for minimal χ^2 (Best et al., 2002).

Acknowledgments

We would like to thank Matthias Rief, Kate Poole, and Tanuj Sapra for fruitful discussions. The Volkswagenstiftung, European Community, and State of Saxony supported this work.

Received: November 23, 2003

Revised: February 26, 2004

Accepted: March 2, 2004

Published: May 11, 2004

References

- Allen, S.J., Kim, J.M., Khorana, H.G., Lu, H., and Booth, P.J. (2001). Structure and function in bacteriorhodopsin: the effect of the interhelical loops on the protein folding kinetics. *J. Mol. Biol.* **308**, 423–435.
- Baldwin, J.M. (1993). The probable arrangement of the helices in G protein-coupled receptors. *EMBO J.* **12**, 1693–1703.
- Bell, G.I. (1978). Models for the specific adhesion of cells to cells. *Science* **200**, 618–627.
- Belrhali, H., Nollert, P., Royant, A., Menzel, C., Rosenbusch, J.P., Landau, E.M., and Pebay-Peyroula, E. (1999). Protein, lipid and water organization in bacteriorhodopsin crystals: a molecular view of the purple membrane at 1.9 Å resolution. *Struct. Fold. Des.* **7**, 909–917.
- Best, R.B., Li, B., Steward, A., Daggett, V., and Clarke, J. (2001). Can non-mechanical proteins withstand force? Stretching barnase by atomic force microscopy and molecular dynamics simulation. *Biophys. J.* **81**, 2344–2356.
- Best, R.B., Fowler, S.B., Toca-Herrera, J.L., and Clarke, J. (2002). A simple method for probing the mechanical unfolding pathway of proteins in detail. *Proc. Natl. Acad. Sci. USA* **99**, 12143–12148.
- Binnig, G., Quate, C.F., and Gerber, C. (1986). Atomic force microscope. *Phys. Rev. Lett.* **56**, 930–933.
- Booth, P.J., Templer, R.H., Curran, A.R., and Allen, S.J. (2001). Can we identify the forces that drive the folding of integral membrane proteins? *Biochem. Soc. Trans.* **29**, 408–413.
- Carrion-Vazquez, M., Oberhauser, A.F., Fowler, S.B., Marszalek, P.E., Broedel, S.E., Clarke, J., and Fernandez, J.M. (1999). Mechanical and chemical unfolding of a single protein: a comparison. *Proc. Natl. Acad. Sci. USA* **96**, 3694–3699.
- Engelman, D.M., and Steitz, T.A. (1981). The spontaneous insertion of proteins into and across membranes: the helical hairpin hypothesis. *Cell* **23**, 411–422.
- Essen, L., Siegert, R., Lehmann, W.D., and Oesterhelt, D. (1998). Lipid patches in membrane protein oligomers: crystal structure of the bacteriorhodopsin-lipid complex. *Proc. Natl. Acad. Sci. USA* **95**, 11673–11678.
- Evans, E.B. (1999). Looking inside molecular bonds at biological interfaces with dynamic force spectroscopy. *Biophys. Chem.* **82**, 83–97.
- Evans, E., and Ludwig, F. (2000). Dynamic strengths of molecular anchoring and material cohesion in fluid biomembranes. *J. Phys. Condens. Matter* **12**, A315–A320.
- Evans, E., and Ritchie, K. (1997). Dynamic strength of molecular adhesion bonds. *Biophys. J.* **72**, 1541–1555.
- Florin, E.L., Rief, M., Lehmann, H., Ludwig, M., Dornmair, C., Moy, V.T., and Gaub, H.E. (1995). Sensing specific molecular-interactions

- with the atomic force microscope. *Biosens. Bioelectron.* **10**, 895–901.
- Grigorieff, N., Ceska, T.A., Downing, K.H., Baldwin, J.M., and Henderson, R. (1996). Electron-crystallographic refinement of the structure of bacteriorhodopsin. *J. Mol. Biol.* **259**, 393–421.
- Haltia, T., and Freire, E. (1995). Forces and factors that contribute to the structural stability of membrane proteins. *Biochim. Biophys. Acta* **1241**, 295–322.
- Helmreich, E.J., and Hofmann, K.P. (1996). Structure and function of proteins in G-protein-coupled signal transfer. *Biochim. Biophys. Acta* **1286**, 285–322.
- Heymann, B., and Grubmüller, H. (2000). Dynamic force spectroscopy of molecular adhesion bonds. *Phys. Rev. Lett.* **84**, 6126–6129.
- Hunt, J.F., Earnest, T.N., Bousche, O., Kalghatgi, K., Reilly, K., Horvath, C., Rothschild, K.J., and Engelman, D.M. (1997). A biophysical study of integral membrane protein folding. *Biochemistry* **36**, 15156–15176.
- Janovjak, H., Kessler, M., Oesterhelt, D., Gaub, H., and Muller, D.J. (2003). Unfolding pathways of native bacteriorhodopsin depend on temperature. *EMBO J.* **22**, 5220–5229.
- Kolbe, M., Besir, H., Essen, L.O., and Oesterhelt, D. (2000). Structure of the light-driven chloride pump halorhodopsin at 1.8 Å resolution. *Science* **288**, 1390–1396.
- Lanyi, J.K. (1999). Progress toward an explicit mechanistic model for the light-driven pump, bacteriorhodopsin. *FEBS Lett.* **464**, 103–107.
- Leckband, D., and Israelachvili, J. (2001). Intermolecular forces in biology. *Q. Rev. Biophys.* **34**, 105–267.
- Lodish, H., Berk, A., Zipursky, L.S., Matsudaira, P., Baltimore, D., and Darnell, J.E. (1999). *Molecular Cell Biology*, Fourth Edition (New York: W.H. Freeman and Company).
- Luecke, H., Schobert, B., Richter, H.T., Cartailler, J.P., and Lanyi, J.K. (1999). Structure of bacteriorhodopsin at 1.55 Å resolution. *J. Mol. Biol.* **291**, 899–911.
- Marti, T. (1998). Refolding of bacteriorhodopsin from expressed polypeptide fragments. *J. Biol. Chem.* **273**, 9312–9322.
- Merkel, R., Nassoy, P., Leung, A., Ritchie, K., and Evans, E. (1999). Energy landscapes of receptor-ligand bonds explored with dynamic force spectroscopy. *Nature* **397**, 50–53.
- Mitsuoka, K., Hirai, T., Murata, K., Miyazawa, A., Kidera, A., Kimura, Y., and Fujiyoshi, Y. (1999). The structure of bacteriorhodopsin at 3.0 Å resolution based on electron crystallography: implication of the charge distribution. *J. Mol. Biol.* **286**, 861–882.
- Möller, C., Fotiadis, D., Suda, K., Engel, A., Kessler, M., and Muller, D.J. (2003). Determining molecular forces that stabilize human aquaporin-1. *J. Struct. Biol.* **142**, 369–378.
- Müller, D.J., Schabert, F.A., Büldt, G., and Engel, A. (1995). Imaging purple membranes in aqueous solutions at sub-nanometer resolution by atomic force microscopy. *Biophys. J.* **68**, 1681–1686.
- Müller, D.J., Amrein, M., and Engel, A. (1997). Adsorption of biological molecules to a solid support for scanning probe microscopy. *J. Struct. Biol.* **119**, 172–188.
- Müller, D.J., Kessler, M., Oesterhelt, F., Möller, C., Oesterhelt, D., and Gaub, H. (2002). Stability of bacteriorhodopsin alpha-helices and loops analyzed by single-molecule force spectroscopy. *Biophys. J.* **83**, 3578–3588.
- Oesterhelt, D., and Stoekenius, W. (1974). Isolation of the cell membrane of *Halobacterium halobium* and its fractionation into red and purple membrane. *Methods Enzymol.* **31**, 667–678.
- Oesterhelt, F., Oesterhelt, D., Pfeiffer, M., Engel, A., Gaub, H.E., and Müller, D.J. (2000). Unfolding pathways of individual bacteriorhodopsins. *Science* **288**, 143–146.
- Palczewski, K., Kumasaka, T., Hori, T., Behnke, C.A., Motoshima, H., Fox, B.A., Le Trong, I., Teller, D.C., Okada, T., Stenkamp, R.E., et al. (2000). Crystal structure of rhodopsin: A G protein-coupled receptor. *Science* **289**, 739–745.
- Popot, J.L., and Engelman, D.M. (2000). Helical membrane protein folding, stability, and evolution. *Annu. Rev. Biochem.* **69**, 881–922.
- Popot, J.L., Gerchman, S.E., and Engelman, D.M. (1987). Refolding of bacteriorhodopsin in lipid bilayers. A thermodynamically controlled two-stage process. *J. Mol. Biol.* **198**, 655–676.
- Radford, S.E. (2000). Protein folding: progress made and promises ahead. *Trends Biochem. Sci.* **25**, 611–618.
- Rief, M., Gautel, M., Oesterhelt, F., Fernandez, J.M., and Gaub, H.E. (1997). Reversible unfolding of individual titin immunoglobulin domains by AFM. *Science* **276**, 1109–1112.
- Rief, M., Fernandez, J.M., and Gaub, H.E. (1998). Elastically coupled two-level systems as a model for biopolymer extensibility. *Phys. Rev. Lett.* **81**, 4764–4767.
- Royant, A., Nollert, P., Edman, K., Neutze, R., Landau, E.M., Pebay-Peyroula, E., and Navarro, J. (2001). X-ray structure of sensory rhodopsin II at 2.1-Å resolution. *Proc. Natl. Acad. Sci. USA* **98**, 10131–10136.
- Subramaniam, S. (1999). The structure of bacteriorhodopsin: an emerging consensus. *Curr. Opin. Struct. Biol.* **9**, 462–468.
- White, S.H., and Wimley, W.C. (1999). Membrane protein folding and stability: physical principles. *Annu. Rev. Biophys. Biomol. Struct.* **28**, 319–365.
- Williams, P.M., Fowler, S.B., Best, R.B., Toca-Herrera, J.L., Scott, K.A., Steward, A., and Clarke, J. (2003). Hidden complexity in the mechanical properties of titin. *Nature* **422**, 446–449.

Unfolding Barriers in Bacteriorhodopsin Probed from the Cytoplasmic and the Extracellular Side by AFM

Max Kessler¹ and Hermann E. Gaub^{1,*}

¹Center for Nano Science
Physics Section
Ludwig Maximilians University
Munich, 80799
Germany

Summary

Selecting an individual membrane protein and probing its mechanical properties has become possible by AFM-based single-molecule force spectroscopy. In contrast to earlier studies, we extracted and unfolded bacteriorhodopsin monomers from the purple membrane not only from the cytoplasmic side, but also from the extracellular side, and recorded the force extension profiles. This way different pathways through the potential landscape are explored. A map of the 21 most dominant barriers with their positions relative to the amino acid sequences is given at an accuracy of ± 3 aa. Most barriers were found to provide resistance to forced unfolding only when extracted toward one of the sides. However, certain barriers have identical positions to within a few amino acids when probed from either of the sides, which typifies them as structural traps.

Introduction

Single-molecule force spectroscopy has evolved into a powerful tool for unfolding individual proteins with unparalleled precision. In the past, this high-resolution technique has allowed for the measurement of those interactions in proteins that mediate molecular recognition (Fritz et al., 1998; Kienberger et al., 2004; Lee et al., 1994; Moy et al., 1994a, 1994b; Viani et al., 2000), stabilize molecular structures (Fisher et al., 1999; Rief et al., 2000), and drive intermolecular actions (Dammer et al., 1996). Molecular bonds (Grandbois et al., 1999; Merkel, 2001) and polymer elasticity (Bustamante et al., 2000; Clausen-Schaumann et al., 2000; Rief et al., 1998, 1999) were investigated. Mechanical unfolding of fibronectin (Rief et al., 2000), tenascin (Oberhauser et al., 1998), and titin (Kellermayer et al., 1997; Li et al., 2000; Oberhauser et al., 1999; Rief et al., 2000; Smith and Radford, 2000; Williams et al., 2003) has revealed that these modular proteins predominantly unfold domainwise. In some cases, intermediate states have been reported (Marszalek et al., 1999). Schwaiger et al. (2004, 2005) managed to map a fast refolding intermediate state on the F-actin crosslinking protein ddFLN to its molecular structure by mutation of several loops. Recently, Dietz and Rief (2004) reported the existence of two intermediate states in the unfolding path of GFP.

In the notion of the 3N-dimensional energy landscape, unfolding of a protein occurs along a path, which is

biased along a certain direction when an external force is applied. During the course of unfolding, different valleys will be reached by traversing saddle points, whose rising slopes will be detected in our experiments as peaks in the force distance curves. Structures like certain H bonds or kinks in helices, which by their mechanical stability give rise to these slopes, act as barriers against further unfolding and will be referred to as such in the following sections. When soluble proteins are stretched, the force is applied between both ends and is transmitted via the polypeptide chain into the folded entity under investigation. The sequence of the unfolding events is determined by the hierarchy in stability of the structural elements. As a result of the increasing force, the remaining activation barrier for unfolding this particular entity is gradually decreased until, at some point, thermal fluctuations suffice to overcome the barrier and the structure unfolds. Height and widths of the barrier can be derived from rate-dependent measurements, but no absolute information on the position of the barrier can be derived from the data.

In the case of membrane proteins, the folded structure is anchored in the membrane, and, thus, the sequence of unfolding steps follows the amino acid (aa) sequence. This means that the barriers can be localized with high accuracy by measuring the length of the already unfolded segment of the protein. Upon gradual unfolding, a very detailed sequence of barriers can be identified, and their position, their height, and their width can be determined. The additional option of imaging the membrane prior to force spectroscopy allows, in principle, for the selection of a certain protein and, afterwards, the verification of the unfolding event, ensuring that just one protein was extracted. However, the zone behind a barrier is hardly accessible because of the mechanical instability caused by the soft cantilever in combination with the entropic elasticity of the already unfolded protein. Whenever the force gradient of the folding potential becomes steeper than the cantilever potential, the system will hop into the next minimum rather than probing the descendent slope potential. Since the cantilever stiffness needs to be low in order to allow for imaging, this instability cannot be circumvented with instrumentation currently available, if at all. This means that only the rising parts of the potential barriers can be characterized. Nevertheless, this approach was very successfully employed in the past to characterize the stability of a series of membrane proteins (Cisneros et al., 2005; Janovjak et al., 2003, 2004; Kedrov et al., 2004; Kienberger et al., 2005; Moller et al., 2003; Muller et al., 2002; Oesterhelt et al., 2000). Detailed information on the potential landscape, to our knowledge not available with any other technique, was revealed.

Membrane proteins, which, like bacteriorhodopsin, expose one terminus to each side of the membrane (this is the case for all membrane proteins with an even number of helices and for many barrel-type structures) and exhibit a nonalternating orientation within the two-dimensional crystals, have an additional advantage in terms of single-molecule force spectroscopy that is

*Correspondence: gaub@lmu.de

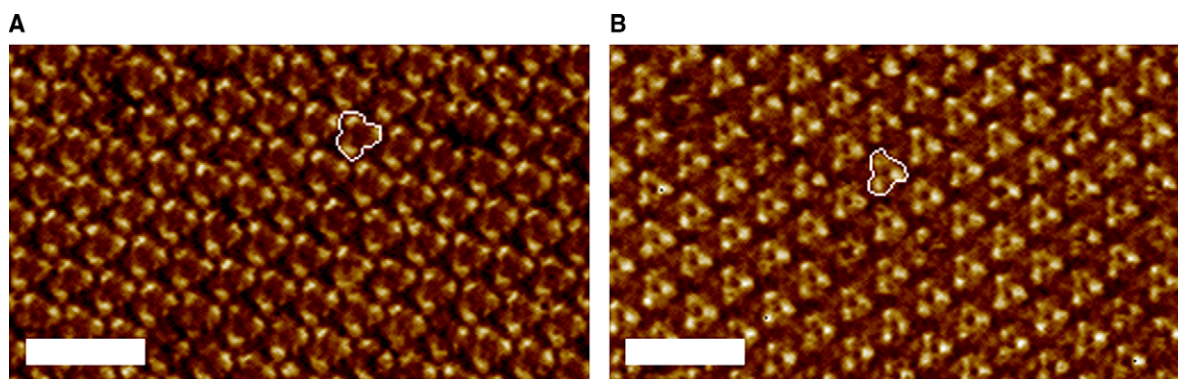


Figure 1. High-Resolution Imaging Reveals Membrane Orientation.

(A and B) AFM images from the (A) cytoplasmic and the (B) extracellular sides of a purple membrane patch on mica recorded in buffer at room temperature. Encircled are the trimers of BR, which form the basis of the hexagonal lattice. Both pictures were recorded at a contact force of ~ 150 pN. The color range from black to white corresponds to a vertical distance of 1.2 nm and 1 nm in (A) and (B), respectively. Scale bars are 15 nm in both pictures.

exploited in this paper: the two membrane orientations can be distinguished by high-resolution imaging. Therefore, the assignment of force curves to the two orientations can be made without any presumptions on the position of unfolding barriers within the molecule. This expands the options that were exploited in recent publications on mechanical unfolding experiments of human aquaporin-1 (Moller et al., 2003) and the sodium-proton antiporter NhaA (Kedrov et al., 2004) and halorhodopsin (Cisneros et al., 2005). Generally, when probed from the “other side,” the unfolding sequence of a membrane protein is reverted and, as a consequence, the different structural elements are approached in reverse order. In addition, new barriers, formerly hidden in the “blind zone,” become accessible. When unfolding BR from both termini, we found several pairs of one C-terminal and one N-terminal force peak each, which can be mapped to the same barrier position within the three-dimensional structure of the molecule. Although, upon unfolding a protein from its different ends, the physical structure that gives rise to a barrier (e.g., a kink in a helix) remains at the same position in three dimensions, it represents different points in the 3N-dimensional space of the energy landscape, since the conformations of the entire protein differ drastically when the different ends are already unfolded. Therefore, the strength of the barrier may be altered depending on the remaining local interactions; thus, both the height and slope of the saddle differ at these two passage points in 3N-dimensional space.

Results and Discussion

In this paper, we present a detailed map of 21 force peaks of bacteriorhodopsin together with a characterization of their magnitude and the position up to which the protein is unfolded in each case. Those peaks that occur at every force curve are referred to as main peaks (MP). The number of occurrence of other peaks, which occur occasionally and are referred to as side peaks, is given in Tables S1 and S2 (see the Supplemental Data available with this article online).

Two-dimensional patches of purple membrane were adsorbed onto freshly cleaved mica under conditions in which they are adsorbed in both orientations in sufficient amounts (Muller et al., 1997, 1999). (In an earlier study, we showed that the positions and distributions of peaks do not change if the substrate is changed to hydrophobic graphite or the experiments are performed on stacks of purple membrane patches. Because it is highly unlikely that a hypothetical adhesive interaction of the loops with mica is the same as with graphite or another purple membrane, we conclude that such effects can be neglected [Muller et al., 2002].) The orientation of each patch on which we performed force spectroscopy measurements was determined by high-resolution imaging. As can be seen in Figure 1, both membrane sides can easily be distinguished. By alternately probing membrane patches of the two orientations in the same sample, we ensured the acquisition of both sets of data under identical experimental conditions. Following the protocol established in earlier studies (Muller et al., 2002; Oesterhelt et al., 2000), we extracted and unfolded individual proteins from the purple membrane patches by placing the AFM cantilever over a patch and allowing it to interact for 0.2–0.5 s at forces between 0.5 and 2 nN. Afterwards, the tip was retracted and the force was recorded as a function of the distance between the tip and membrane surface. Again, as in earlier studies, only those force distance curves with an overall length exceeding 60 nm, which corresponds to the fully unfolded protein, were analyzed. In doing so, it was assured that only those events in which the protein is attached to the tip either close to the N- or the C-terminal end are analyzed. The overall length was the only parameter used for the selection of force curves in the present study, and all curves exceeding an overall length of 60 nm were analyzed.

The force distance traces were superpositioned in Figure 2. As can be seen, they exhibit a richness of detail whereby each peak corresponds to the rim of a local minimum in the energy landscape of the protein. A comparison of both columns shows that the traces exhibit more details at shorter distances. This has two main reasons: first, the longer the already extracted and unfolded

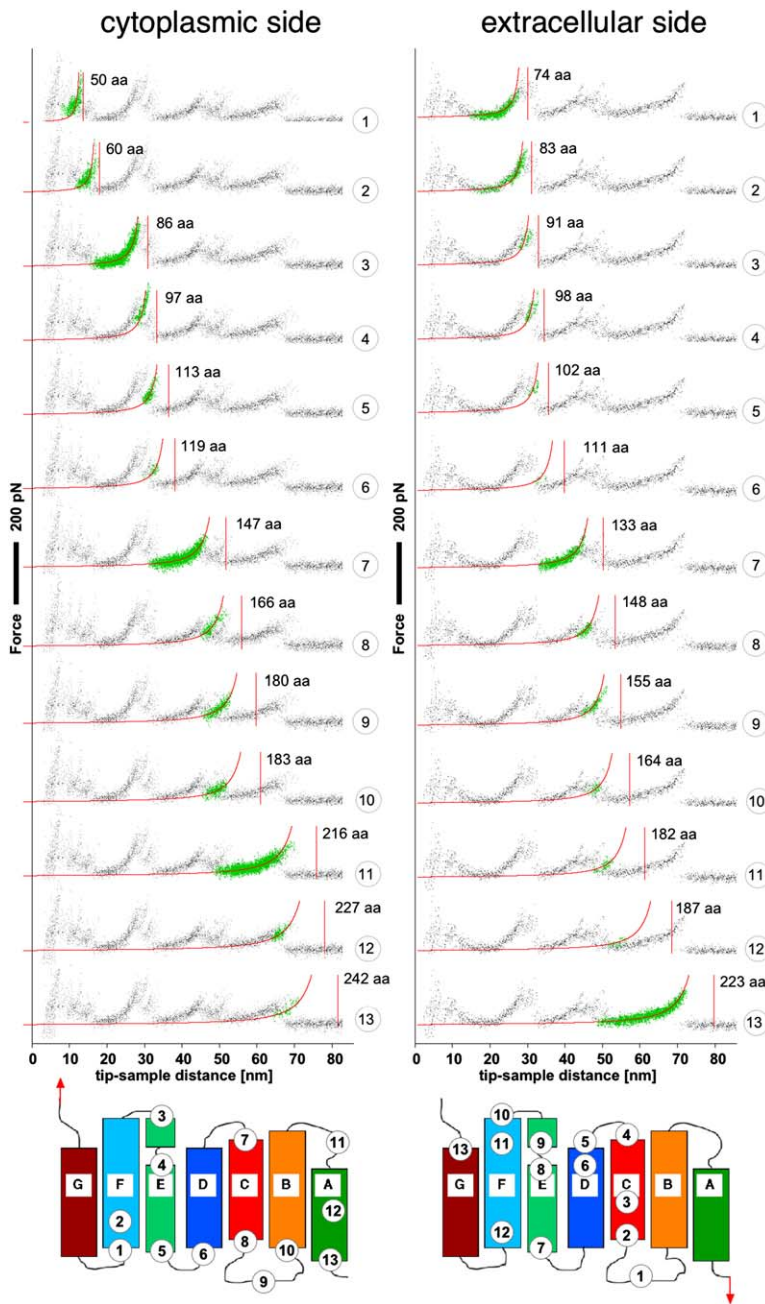


Figure 2. Assignment of Measured Contour Lengths and the Position of the Corresponding Anchoring Points

Top: superposition of force versus distance curves recorded when unfolding from the C terminus (left) and the N terminus (right). The data points corresponding to each of the 13 N-terminal (right) and C-terminal (left) peaks discussed here are highlighted in green in the superposition of all force distance curves, which is shown in gray. The corresponding WLC-fit curves and their asymptotes are shown in red. The contour lengths of the fits are given in lengths of aa (one aa = 0.36 nm) and are plotted next to the fit-curves. In the case of the extracellular curves, this number corresponds to the number of the aa of the BR sequence. For the cytoplasmic curves, the contour length (given in aa) has to be subtracted from the total amount of aa of BR (248) to calculate the barrier position within the model. The superpositions contain 12 and 24 curves in the extracellular and cytoplasmic sides, respectively. Bottom: the position of the barrier corresponding to each peak (as calculated from the WLC-fit) is shown in a schematic representation of the BR secondary structure. Peak positions are indicated by encircled numbers, which correspond to those in the upper part of the figure. The direction of the acting force is indicated by arrows. In most cases, the peaks are located close to the end of helices. Notably, in some cases, the barriers corresponding to an extracellular and a cytoplasmic peak are located at comparable positions within the molecule. The stepwise unfolding of the tertiary structure is illustrated in [Movies S1 and S2](#).

part of the protein is, the softer its spring constant, which means that small corrugations in the potential landscape are hopped over. The other reason is that more and more of the native environment of the protein is lost when the neighboring helices are extracted, as illustrated in [Movies S1 and S2](#) for the cytoplasmic and the extracellular sides, respectively. Here, the complementary approach of analyzing the unfolding process from both sides has proven to be extremely versatile since the sequence of events is reverted when the proteins are extracted from the different sides; thus, the different ends of the protein are seen with complementary resolution. As discussed earlier ([Muller et al., 2002](#); [Oesterhelt et al., 2000](#)), the main peaks observed on the cytoplasmic curves at tip-sample distances of approxi-

mately 25, 45, and 65 nm reflect the extraction of helices E, C, and A, respectively. In comparison, the extracellular curves show fewer details and generally lower peaks in the region close to the surface (tip-sample distance less than 15 nm), where the cytoplasmic spectra are also more complicated due to the influence of the retinal bond ([Muller et al., 2002](#)).

While the first main peak occurs at a comparable tip-sample distance of ~ 25 nm for both sample orientations, the relative distance between the first and second main peaks is significantly smaller for the extracellular curves. We interpret the extracellular peak at ~ 40 nm, as the result of a potential barrier at the extracellular side of HE. However, the most striking result of the analysis of the extracellular data set is that the last main

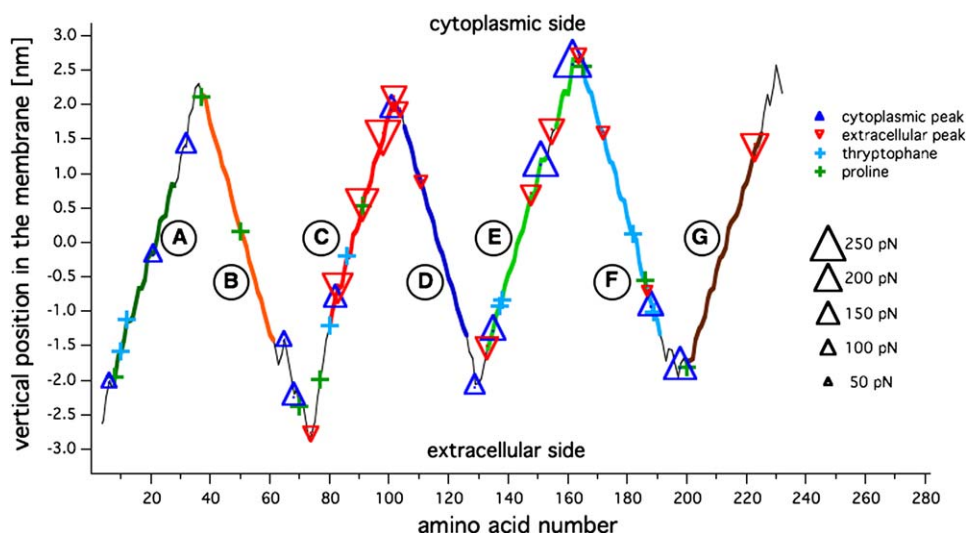


Figure 3. Schematic Representation of Measured Potential Barrier Positions and the BR Secondary Structure

Unfolding barriers identified in Figure 2 mapped in a plot, which displays the vertical separation of each aa from the middle of the membrane (calculated from X-ray data [Essen et al., 1998]) against its sequence number. Those stretches, which are known to be part of the α helices, are highlighted in color. The triangles mark the positions of the barriers approached from the cytoplasmic side (blue triangles pointing upward) and the extracellular side (red triangles pointing downward). The average force needed to overcome the corresponding energy barriers at the given extraction rate ($1.4 \mu\text{m/s}$) is represented by the size of the triangles. Additional information about rupture forces and the frequency of these peaks can be found in Table S1 (cytoplasmic data) and Table S2 (extracellular data). As additionally described in Experimental Procedures, we estimate the accuracy of the given barrier positions to ± 3 aa.

peak, observed at ~ 65 nm, is caused by a barrier at the cytoplasmic side, and not, as we had expected, at the extracellular side of HG. In this context, it is interesting to note that Hunt et al. (1997) discovered that short polypeptide strands corresponding to BR α helices A–E spontaneously form stable transmembrane α helices in reconstituted phospholipid vesicles, while HF does not form any stable secondary structure and HG forms a β sheet structure oriented perpendicular to the membrane plane under these conditions. The authors suggest that folding of HG and HF might require external constraints such as the links between the helices, interactions with the rest of the protein, or the bound retinal. Therefore, once helices E and F have been unfolded, it might be that HG is not able to act as a stable structure on its own. Notably, while the average rupture forces of the cytoplasmic main peaks continually decrease (HE: 262 ± 54 pN, HC: 160 ± 34 pN, HA: 146 ± 47 pN), the force of the last extracellular main peak rises again significantly (HC: 222 ± 65 pN, HE: 151 ± 61 pN, HG: 203 ± 51 pN). It remains to be noted that both membrane orientations may be distinguished on the basis of the mentioned properties of force curves alone. This might be useful for future experiments with functionalized cantilevers, which don't allow for high-resolution scanning.

The position of each barrier was determined by fitting the gradually rising slope of the peak to the elastic response of the already unfolded polypeptide. The Worm-like chain model has been shown in several studies to provide a reliable basis for the fit. The only free parameter of this fit is the length of the already unfolded part of the protein. To allocate the measured peaks to a certain aa, we developed an approach which is new to our knowledge, to incorporate the position of that aa along the perpendicular membrane into our analysis. There-

fore, we assumed two extreme cases: first, a polypeptide that is fully elongated within the membrane, and, second, a polypeptide that is able to freely fluctuate in the membrane void left upon unfolding. For all observed peaks, the differences between both methods lie within the errors of the experiments, which were estimated to be ± 3 aa. It should be noted that this method implies that the vertical positions of the barriers do not shift due to tilting of α helices or similar processes. The height of the peaks depends on the speed at which the protein is extracted. A speed-dependent study of bacteriorhodopsin unfolding was recently published by Janovjak et al. (2004).

All barriers were mapped in the graph displayed in Figure 3. Here, the vertical positions of the aa that were calculated from the X-ray model of Essen et al. (1998) (PDB code: 1BRR) are plotted against their sequence number, and are thus arranged in a zigzag pattern. Highlighted in color are those stretches, which are helical according to the model of Essen et al. (1998). The triangles mark the positions at which anchoring points were found. The size of the triangles code the barrier heights, and the orientation codes whether the barrier was measured from the extracellular or the cytoplasmic side. Several striking results emerge: certain barriers are located in the loop regions—most prominent are one cytoplasmic and two extracellular peaks on the BC loop, which is known to form a β sheet structure. It is possible that this β sheet moves slightly during unfolding, which again increases the errors of the given barrier positions. However, certain barriers were also found in the middle of seemingly homogeneous structural elements like helices without intramolecular hydrogen bonds to neighboring helices (Adamian and Liang, 2002) or helix breakers like proline and tryptophan nearby. A more

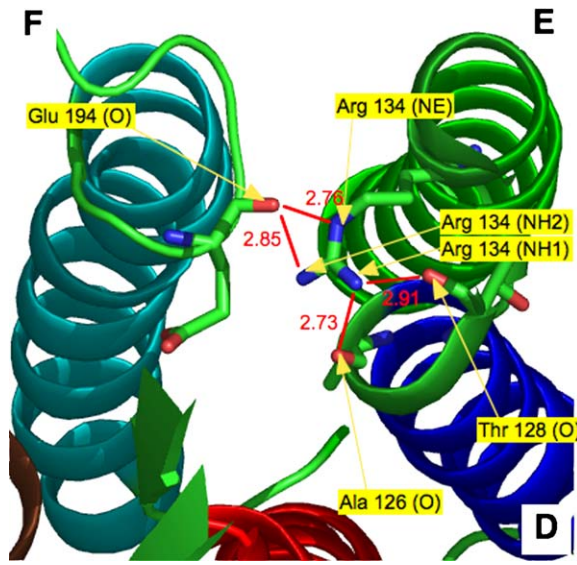


Figure 4. Stabilization of Potential Barriers by Multiple Interhelical Hydrogen Bonds

View of the hydrogen bond network, which possibly plays a role in stabilizing the potential barrier that has been detected at the extracellular end of HE (around aa 134) in both the extracellular and the cytoplasmic force curves (data taken from [Luecke et al., 1999]). The residues participating in the hydrogen bonds are shown as sticks, and the distances between the oxygen and the nitrogen atoms (shown in red and blue, respectively) are given in Å. In N-terminal force curves, the corresponding peak is observed at 133 ± 3 aa at a point at which HD is already unfolded. Therefore, only the hydrogen bonds between Arg134 and the oxygen of Glu194 are left to stabilize this intermediate state. In C-terminal force curves, the peak observed at 135 ± 3 aa is probably caused by the hydrogen bonds between Arg134 and Thr128 or Ala126. So, basically, there are two hydrogen bonds left for stabilizing the remaining part of the tertiary structure in each case. Interestingly, there are two other anchoring points on the extracellular membrane surface that give rise to both a C-terminal and an N-terminal force peak. They are probably stabilized by similar means: the peak observed around 83 ± 3 aa (HC) on N-terminal force curves might result from the H bond between Tyr83 and Trp189, while the corresponding C-terminal peak (observed at 82 ± 3 aa) is stabilized by the H bond between Arg82 and Tyr57. In the same fashion, the peak observed at 187 ± 3 aa (HF) in N-terminal force curves might be caused by the H bond between Tyr185 and Asp212, while the corresponding C-terminal peak at 188 ± 3 aa might be due the H bond between Pro186 and Trp138.

sophisticated molecular modeling will be needed to interpret this finding.

On the cytoplasmic ends of HC and HE, as well as close to the extracellular ends of HC, HE, and HG, we found barriers whose position coincide within two aa when approached from the cytoplasmic and the extracellular sides. Notably, the three barriers on the extracellular side are stabilized by at least one hydrogen bond in each direction [Luecke et al., 1999]. By this means, no matter which half of the molecule was unfolded already, at least one H bond remains to act as a barrier at this particular position, as shown for the barrier on HE in Figure 4.

In spite of the fact that $\sim 90\%$ of the observed peaks can be assigned to structural features like ends of helices, breaks in helices (like the break on HE between aa 153 and 156), residues like proline and tryptophan, or in-

terhelical H bonds within a range of two aa around the measured position, the assignment is still not unambiguous in all cases. For about 10% of all peaks, there is no prominent structural feature within a range of four aa. Generally, we think that single-molecule force spectroscopy experiments as presented in this paper work well in context with other experimental techniques like X-ray crystallography, NMR, and theoretical methods, in order to increase the understanding of protein folding and intramolecular interactions.

Mainly, two points are of importance regarding this topic. First, we believe that single-molecule force spectroscopy on proteins with known tertiary structure and genetically mutated variations complement each other with theoretical methods, e.g., molecular dynamics simulations in terms of elucidating the underlying molecular mechanisms of potential barriers.

In a second step, the improved understanding of the connection between mechanical stability and characteristic features of a protein sequence that we expect from such studies might, in turn, help to improve the accuracy of structure prediction of membrane proteins that have not been crystallized yet.

Experimental Procedures

Abbreviations

Abbreviations used in this paper are as follows: aa, amino acid; WLC, wormlike chain; H, helix (helices are named from A to G, e.g. HC means helix C); BR, bacteriorhodopsin; MP, main peak.

Sample Preparation

Wild-type purple membrane, extracted from *H. salinarum* as described [Oesterhelt and Stoeckenius, 1974], was adsorbed onto freshly cleaved mica, and rinsed with buffer solution [Muller et al., 1997].

Experiment

The multimode AFM (Nanoscope IIIa, Digital Instruments, Santa Barbara, CA) was equipped with a 90 nm J piezo scanner. The spring constants of the 100 μm Si₃N₄ AFM cantilevers (OMCL TR400PS, Olympus, Tokyo, Japan) were calibrated in solution after the experiments by using the equipartition theorem [Butt and Jaschke, 1995; Florin et al., 1995]. Within the uncertainty of this method (10%), all cantilevers used exhibited a spring constant of 90 pN/nm. All experiments were performed in buffer solution (300 mM KCl, 10 mM Tris-HCl [pH 7.8]) at room temperature. The fluid cell was operated without the O-ring. The orientation of each purple membrane patch was determined by high-resolution imaging [Muller et al., 1999] prior to force spectroscopy on this patch. To allow the terminal end of a BR monomer to adsorb onto the cantilever tip, the tip was kept in contact with the protein for 0.2–0.5 s at a force of 0.5–2 nN. This results in unspecific adhesion to the cantilever tip in some cases. Then, the AFM stylus and protein surface were separated at a velocity of 1.4 $\mu\text{m}/\text{s}$ while recording the force spectrum. In less than 1% of all retraction curves, we detected adhesive peaks, which were correlated to the removal of a single BR molecule. When performing measurements on the cytoplasmic side, $\sim 30\%$ of these adhesion curves showed a force extension curve exhibiting a length between 60 and 70 nm and four significant main peaks (see Data Analysis below). In the case of the extracellular surface, only a relatively small percentage ($\sim 7\%$) of the adhesion events showed a characteristic pattern of four main peaks; the total length of these curves is between 60 and 75 nm.

Data Analysis

To analyze the force curves, a clear criterion is required that distinguishes curves of BR molecules attached to the AFM tip with different regions of their polypeptide backbone. One suitable criterion is the overall length of the force curve, which reflects the tip-sample

distance at which the last force peak occurs. It is evident that a molecule attached to the cantilever by one of its loops results in a force curve with smaller overall length than a molecule attached by one of its termini. As we have shown elsewhere (Muller et al., 2002), a cytoplasmic force curve with an overall length of more than ~ 50 nm can only occur if the C terminus of the molecule is attached to the cantilever tip. With similar considerations, one can prove that, if one of the extracellular loops has attached to the cantilever, then extracellular curves also show a length of less than ~ 50 nm. For both membrane sides, we therefore only analyzed force curves significantly longer than 50 nm, thereby avoiding obscurities that arise with the assignment of peaks when two strands are stretched in parallel (which would occur in the case of attachment to a loop). Given that the likelihood of adhesion of one BR molecule to the cantilever is far less than 1%, the probability of simultaneous attachment of more than one monomer seems negligible. We did not observe any evidence for it in any of the experiments.

Superposition and Fitting

The point of contact between the protein and the cantilever tip can occur at different positions of the terminus and also is not necessarily located exactly at the tip apex. Both effects cause relative horizontal shifts from one curve to the other in the raw data. Because for our analysis, only the relative positions of the peaks are of importance, the force curves were aligned at their main peaks. We used identical procedures and criteria to align each data set. To analyze the side peaks, however, we superimposed every main peak separately (not shown).

Since it is not yet known how far the unfolded part of the protein is able to fluctuate within the hydrophobic membrane interior, we assumed two extreme scenarios for describing potential barriers that aren't located on the membrane surface. In the first scenario, the flexibility of the polypeptide is not limited by the surrounding lipids, which results in a contour length, L , that equals that of a WLC-fit to a barrier located on the membrane surface. But, because of the change of the anchoring point, the entire fit-curve exhibits an offset of $-d$, where d is the distance between the barrier and the surface. In the other extreme case, we assume that the intramembrane part of the polypeptide is fully elongated, which results in a WLC-fit with a contour length diminished by the distance between the barrier position and surface (basically, this is a refined version of the method we introduced earlier [Muller et al., 2002]).

Assuming a flexible polymer (first scenario), the corresponding WLC-curve of a known potential barrier exhibits a contour length of $n \cdot 0.36$ nm and an offset of d , where n is the number of aa between the barrier and the cantilever tip and d equals the vertical distance between the barrier and membrane surface, which can be calculated from the X-ray structure of BR. The length of one aa is 0.36 nm. By using the atomic model of Essen et al. (1998), we computed WLC-curves for each aa within a sufficient range around each estimated barrier position and calculated the standard deviation between all of the data points (of all curves) belonging to that peak and each of these WLC-curves to find the barrier position. To simulate the second scenario we fitted each peak of each force curve separately and compared the average values of the obtained contour lengths to the theoretical contour lengths that were calculated by diminishing $n \cdot 0.36$ nm, the length of the unfolded portion of the polypeptide, by d , the vertical separation between the theoretical barrier and the membrane surface as calculated from X-ray data (the WLC-curves have no offset here). Due to fitting each peak of each force curve individually, the determination of contour length is quite accurate; the standard deviation of the contour length of each peak is given in Tables S1 and S2. For all WLC-fits, we used a persistence length of 4 Å.

The error of this method is dominated by the standard deviation of the fitted contour lengths, which is in the order of ~ 2 aa. Another factor that influences the accuracy of the determination of the barrier positions is the "quantization" of the calculated contour lengths, which also depends on the direction in which an α helix is unfolded. If a helix is unfolded top-down (like helices A, C, E, and G if the molecule is unfolded from the C-terminal side), the increase in contour length due to a shift of the barrier position by one aa is partly compensated by the vertical separation of two aa within a helix. This results in an effective step height of ~ 0.58 aa. (The theoretical contour

length, L_N , of N unfolded aa equals $L_N = N - d$, where d is the vertical separation between the barrier position and the membrane surface. Considering the length of one aa, which equals ~ 0.36 nm, and the vertical separation between two aa in an α helix, which equals ~ 0.15 nm, a shift of the barrier position by one aa results in $L_{N+1} = N + 0.36 - (d + 0.15 \text{ nm})$, and this is equal to $L_{N+1} = L_N + 0.21$ nm. Therefore the separation between L_{N+1} and L_N is ~ 0.58 aa.) Helices B, D, and F are unfolded top-down. Here, both effects sum up to an effective step height of ~ 1.41 aa. Therefore, in the latter case, the average error due to this effect is on the order of 0.7 aa in the worst case. Under these considerations, an estimated total error of ± 3 aa seems to be appropriate for nearly all of the detected peaks. The differences between the determined barrier positions when treating the intramembrane part of the unfolded polypeptide as fully flexible or completely elongated lie within the estimated error of ± 3 aa.

Supplemental Data

Supplemental Data including the fitted data of each peak and two movies that illustrate the unfolding process are available at <http://www.structure.org/cgi/content/full/14/3/521/DC1/>.

Acknowledgments

Fruitful discussions with Daniel Müller and Kay Gottschalk as well as assistance in preliminary experiments by Hilde Rinia and Marcus Braun are gratefully acknowledged. Ingo Schwaiger kindly provided help with the calibration of the spring constants of the cantilevers, and Dieter Oesterhelt kindly provided the purple membranes. This work was supported by the Deutsche Forschungsgemeinschaft and the Fonds der Chemie.

Received: September 26, 2005

Revised: November 17, 2005

Accepted: November 17, 2005

Published online: March 14, 2006

References

- Adamian, L., and Liang, J. (2002). Interhelical hydrogen bonds and spatial motifs in membrane proteins: polar clamps and serine zip-pers. *Proteins* 47, 209–218.
- Bustamante, C., Smith, S.B., Liphardt, J., and Smith, D. (2000). Single-molecule studies of DNA mechanics. *Curr. Opin. Struct. Biol.* 10, 279–285.
- Butt, H.-J., and Jaschke, M. (1995). Calculation of thermal noise in atomic force microscopy. *Nanotechnology* 6, 1–7.
- Cisneros, D.A., Oesterhelt, D., and Muller, D.J. (2005). Probing origins of molecular interactions stabilizing the membrane proteins halorhodopsin and bacteriorhodopsin. *Structure (Camb)* 13, 235–242.
- Clausen-Schaumann, H., Seitz, M., Krautbauer, R., and Gaub, H. (2000). Force spectroscopy with single bio-molecules. *Curr. Opin. Chem. Biol.* 4, 524–530.
- Dammer, U., Hegner, M., Anselmetti, D., Wagner, P., Dreier, M., Huber, W., and Güntherodt, H.J. (1996). Specific antigen/antibody interactions measured by force microscopy. *Biophys. J.* 70, 2437–2441.
- Dietz, H., and Rief, M. (2004). Exploring the energy landscape of GFP by single-molecule mechanical experiments. *Proc. Natl. Acad. Sci. USA* 101, 16192–16197.
- Essen, L., Siegert, R., Lehmann, W.D., and Oesterhelt, D. (1998). Lipid patches in membrane protein oligomers: crystal structure of the bacteriorhodopsin-lipid complex. *Proc. Natl. Acad. Sci. USA* 95, 11673–11678.
- Fisher, T.E., Oberhauser, A.F., Carrion-Vazquez, M., Marszalek, P.E., and Fernandez, J.M. (1999). The study of protein mechanics with the atomic force microscope. *Trends Biochem. Sci.* 24, 379–384.
- Florin, E.L., Rief, M., Lehmann, H., Ludwig, M., Dommair, C., Moy, V.T., and Gaub, H.E. (1995). Sensing specific molecular interactions with the atomic force microscope. *Biosensors Bioelectr.* 10, 895–901.

- Fritz, J., Katopodis, A.G., Kolbinger, F., and Anselmetti, D. (1998). Force-mediated kinetics of single P-selectin/ligand complexes observed by atomic force microscopy. *Proc. Natl. Acad. Sci. USA* 95, 12283–12288.
- Grandbois, M., Beyer, M., Rief, M., Clausen-Schaumann, H., and Gaub, H.E. (1999). How strong is a covalent bond? *Science* 283, 1727–1730.
- Hunt, J.F., Rath, P., Rothschild, K.J., and Engelman, D.M. (1997). Spontaneous, pH-dependent membrane insertion of a transbilayer α -helix. *Biochemistry* 36, 15177–15192.
- Janovjak, H., Kessler, M., Oesterhelt, D., Gaub, H., and Muller, D.J. (2003). Unfolding pathways of native bacteriorhodopsin depend on temperature. *EMBO J.* 22, 5220–5229.
- Janovjak, H., Struckmeier, J., Hubain, M., Kedrov, A., Kessler, M., and Muller, D.J. (2004). Probing the energy landscape of the membrane protein bacteriorhodopsin. *Structure (Camb)* 12, 871–879.
- Kedrov, A., Ziegler, C., Janovjak, H., Kuhlbrandt, W., and Muller, D.J. (2004). Controlled unfolding and refolding of a single sodium-proton antiporter using atomic force microscopy. *J. Mol. Biol.* 340, 1143–1152.
- Kellermayer, M., Smith, S.B., Granzier, H.L., and Bustamante, C. (1997). Folding–unfolding transitions in single titin molecules characterised with laser tweezers. *Science* 276, 1112–1115.
- Kienberger, F., Mueller, H., Pastushenko, V., and Hinterdorfer, P. (2004). Following single antibody binding to purple membranes in real time. *EMBO Rep.* 5, 579–583.
- Kienberger, F., Kada, G., Mueller, H., and Hinterdorfer, P. (2005). Single molecule studies of antibody–antigen interaction strength versus intra-molecular antigen stability. *J. Mol. Biol.* 347, 597–606.
- Lee, G.U., Kidwell, D.A., and Colton, R.J. (1994). Sensing discrete streptavidin–biotin interactions with atomic force microscopy. *Langmuir* 10, 354–357.
- Li, H., Oberhauser, A.F., Fowler, S.B., Clarke, J., and Fernandez, J.M. (2000). Atomic force microscopy reveals the mechanical design of a modular protein. *Proc. Natl. Acad. Sci. USA* 97, 6527–6531.
- Luecke, H., Schobert, B., Richter, H.T., Cartailler, J.P., and Lanyi, J.K. (1999). Structure of bacteriorhodopsin at 1.55 Å resolution. *J. Mol. Biol.* 291, 899–911.
- Marszalek, P.E., Lu, H., Li, H., Carrion-Vazquez, M., Oberhauser, A.F., Schulten, K., and Fernandez, J.M. (1999). Mechanical unfolding intermediates in titin modules. *Nature* 402, 100–103.
- Merkel, R. (2001). Force spectroscopy on single passive biomolecules and single biomolecular bonds. *Phys. Rep.* 346, 343–385.
- Moller, C., Fotiadis, D., Suda, K., Engel, A., Kessler, M., and Muller, D.J. (2003). Determining molecular forces that stabilize human aquaporin-1. *J. Struct. Biol.* 142, 369–378.
- Moy, V.T., Florin, E.-L., and Gaub, H.E. (1994a). Intermolecular forces and energies between ligands and receptors. *Science* 266, 257–259.
- Moy, V.T., Florin, E.-L., and Gaub, H.E. (1994b). Adhesive forces between ligand and receptor measured by AFM. *Coll. Surf.* A93, 343–348.
- Muller, D.J., Amrein, M., and Engel, A. (1997). Adsorption of biological molecules to a solid support for scanning probe microscopy. *J. Struct. Biol.* 119, 172–188.
- Muller, D.J., Fotiadis, D., Scheuring, S., Muller, S.A., and Engel, A. (1999). Electrostatically balanced subnanometer imaging of biological specimens by atomic force microscope. *Biophys. J.* 76, 1101–1111.
- Muller, D.J., Kessler, M., Oesterhelt, F., Moller, C., Oesterhelt, D., and Gaub, H. (2002). Stability of bacteriorhodopsin α -helices and loops analyzed by single-molecule force spectroscopy. *Biophys. J.* 83, 3578–3588.
- Oberhauser, A.F., Marszalek, P.E., Erickson, H.P., and Fernandez, J.M. (1998). The molecular elasticity of the extracellular matrix protein tenascin. *Nature* 393, 181–185.
- Oberhauser, A.F., Marszalek, P.E., Carrion-Vazquez, M., and Fernandez, J.M. (1999). Single protein misfolding events captured by atomic force microscopy. *Nat. Struct. Biol.* 6, 1025–1028.
- Oesterhelt, D., and Stoekenius, W. (1974). Isolation of the cell membrane of *Halobacterium halobium* and its fractionation into red and purple membrane. *Methods Enzymol.* 31, 667–678.
- Oesterhelt, F., Oesterhelt, D., Pfeiffer, M., Engel, A., Gaub, H.E., and Muller, D.J. (2000). Unfolding pathways of individual bacteriorhodopsins. *Science* 288, 143–146.
- Rief, M., Fernandez, J.M., and Gaub, H.E. (1998). Elastically coupled two-level-systems as a model for biopolymer extensibility. *Phys. Rev. Lett.* 81, 4764–4767.
- Rief, M., Clausen-Schaumann, H., and Gaub, H. (1999). Sequence-dependent mechanics of single DNA molecules. *Nat. Struct. Biol.* 6, 346–349.
- Rief, M., Gautel, M., and Gaub, H.E. (2000). Unfolding forces of titin and fibronectin domains directly measured by AFM. *Adv. Exp. Med. Biol.* 481, 129–136.
- Schwaiger, I., Kardinal, A., Schleicher, M., Noegel, A.A., and Rief, M. (2004). A mechanical unfolding intermediate in an actin-crosslinking protein. *Nat. Struct. Mol. Biol.* 11, 81–85.
- Schwaiger, I., Schleicher, M., Noegel, A.A., and Rief, M. (2005). The folding pathway of a fast-folding immunoglobulin domain revealed by single-molecule mechanical experiments. *EMBO Rep.* 6, 46–51.
- Smith, D.A., and Radford, S.E. (2000). Protein folding: pulling back the frontiers. *Curr. Biol.* 10, R662–R664.
- Viani, M.B., Pietrasanta, L.I., Thompson, J.B., Chand, A., Gebeshuber, I.C., Kindt, J.H., Richter, M., Hansma, H.G., and Hansma, P.K. (2000). Probing protein–protein interactions in real time. *Nat. Struct. Biol.* 7, 644–647.
- Williams, P.M., Fowler, S.B., Best, R.B., Toca-Herrera, J.L., Scott, K.A., Steward, A., and Clarke, J. (2003). Hidden complexity in the mechanical properties of titin. *Nature* 422, 446–449.

Bacteriorhodopsin Folds into the Membrane against an External Force

Max Kessler¹, Kay E. Gottschalk¹, Harald Janovjak², Daniel J. Müller² and Hermann E. Gaub^{1*}

¹Chair of Applied Physics and Center for NanoScience Ludwig-Maximilians Universität, Amalienstrasse 54 80799 München, Germany

²Biotechnological Center University of Technology Tatzberg 47, 01307 Dresden Germany

Despite their crucial importance for cellular function, little is known about the folding mechanisms of membrane proteins. Recently details of the folding energy landscape were elucidated by atomic force microscope (AFM)-based single molecule force spectroscopy. Upon unfolding and extraction of individual membrane proteins energy barriers in structural elements such as loops and helices were mapped and quantified with the precision of a few amino acids.

Here we report on the next logical step: controlled refolding of single proteins into the membrane. First individual bacteriorhodopsin monomers were partially unfolded and extracted from the purple membrane by pulling at the C-terminal end with an AFM tip. Then by gradually lowering the tip, the protein was allowed to refold into the membrane while the folding force was recorded.

We discovered that upon refolding certain helices are pulled into the membrane against a sizable external force of several tens of piconewton. From the mechanical work, which the helix performs on the AFM cantilever, we derive an upper limit for the Gibbs free folding energy. Subsequent unfolding allowed us to analyze the pattern of unfolding barriers and corroborate that the protein had refolded into the native state.

© 2005 Elsevier Ltd. All rights reserved.

Keywords: bacteriorhodopsin; folding; helical hairpin; membrane insertion; single molecule force spectroscopy

*Corresponding author

Introduction

Membrane proteins make up of about 30% of the proteins encoded by the genomes of organisms of every kingdom and are therefore a very important class of proteins.^{1,2} Though they are responsible for diverse tasks like signal transduction or regulation of the chemical composition of the cell lumen, the basic principles of membrane protein folding still are a subject of intense investigation.^{2–7} To learn more about the physics of membrane protein folding, we probed the folding of a well-studied member of this class, bacteriorhodopsin (BR), with

single molecule atomic force spectroscopy. The knowledge of the structure of BR^{8–14} enables us to relate our results to specific unfolding intermediate states.

In the single molecule force spectroscopy experiments described previously,^{15,16} individual BR-monomers are unfolded by attaching their C-terminal ends to the tip of an AFM cantilever. During retraction of the cantilever, the piezo position and the deflection of the cantilever are monitored. By multiplying the deflection with the spring constant of the cantilever and plotting it against the tip-sample distance a force *versus* distance curve (F–D curve) is obtained. The course of the F–D curve represents conformational changes in the protein during the process of unfolding. Since every possible conformation of the polypeptide strand corresponds to a certain point on the potential landscape of the protein, a F–D curve displays the pathway through that landscape. The numerous characteristic peaks of F–D curves

Abbreviations used: aa, amino acid(s); AFM, atomic force microscope; BR, bacteriorhodopsin; F–D curve, force *versus* distance curve; HA, HB, ..., HG, helix A, B, ..., G, respectively; PM, purple membrane; TM, trans-membrane; WLC, wormlike-chain.

E-mail address of the corresponding author: gaub@lmu.de

correspond to traversed local minima in the potential landscape. While some characteristic peaks occur on every F–D curve, which means that the corresponding minima are passed through by all allowed pathways, other minima are probed only by some trajectories. Force peaks corresponding to the first type of minima we refer to as main peaks, whereas peaks, which are not observed in every curve, we call side peaks.

In contrast to soluble proteins, which also have been investigated by single molecule spectroscopy,^{17–23} the folded part of a membrane protein is anchored within the membrane and the sequence of the unfolding peaks follows the amino acid (aa) sequence of the protein. For each peak the number of already unfolded aa can be determined from the length of the unfolded part of the polypeptide, the so-called contour length, which is obtained by a wormlike-chain (WLC) fit (see Materials and Methods). By subtracting the number of unfolded aa from the total number of aa in BR (248), the transition point between the folded and the unfolded portion of the molecule can be calculated with high spatial accuracy.¹⁶ At the three observed main-peaks (contour lengths 86, 147, and 216 aa) the polypeptide is unfolded up to the cytoplasmic ends of helices E, C and A, respectively†. In the case of the side peaks, the transition point is often located at extracellular ends of the α -helices.^{5,16}

Here, we report on the investigation of refolding events once the protein has been unfolded. If the unfolded part of the protein is highly extended, refolding does not occur, because a relatively high force has to be overcome by the protein. For refolding to occur, a sufficiently large accessible conformational space of the polypeptide strand is required. Here we achieved refolding by moving the cantilever on a zigzag pathway as shown in Figure 1(a). Thereby we partially unfolded a single BR molecule and then relaxed the applied force to allow these parts of the protein to refold. Finally, we unfolded the corresponding part of the polypeptide again, probing the refolded structures. This experimental setup monitors the unfolding forces of identical sequences of the protein under different circumstances. This refinement of an approach previously reported by Kedrov *et al.*⁶ enables us to focus on the folding behavior of individual helical hairpins, single helices, and even parts of single helices. If the refolding step yields the native state, identical main peaks are detected in the initial unfolding trace and the unfolding trace of the refolded structure. Still, the curves may differ regarding their side peaks, because the protein can follow different unfolding pathways in both cases.

† Since the retinal is covalently bound to helix G, it is very likely to be removed from the membrane at the very beginning of a C-terminal F–D curve. This is in accordance with a model proposed by Booth *et al.*,^{42,43} which states that folding of helices F and G into the membrane occurs together with the retinal only after helices A to E form a folding intermediate.

If, on the other hand, non-native folds or folding intermediates are formed, the main peaks of the second unfolding F–D curve are either missing or deviate from those of the first curve, despite of the fact that the identical sequence is sampled in both cases. Thus, comparison between the first and the second unfolding curve can potentially resolve folding intermediates. Indeed, our experiments show that comparison of the initial extraction curves with the curves after partially refolding reveal a complex folding pattern with different folding sub-states.

Results and Discussion

In a total of 40 recorded unfolding/refolding experiments we observed the same characteristic main peaks as in conventional unfolding whenever the segment under focus was unfolded for the first time (Figure 1(b)). Thus, all refolding curves discussed here result from single BR-molecules, which were attached to the tip of the cantilever at their C terminus (also see Materials and Methods).

Native refolding of helices D and E

The piezo actuator trace described in Figure 1 was designed such that refolding of helices D and E can take place during steps (II) and (VI). As expected for successful refolding of these helices, the characteristic unfolding peak of helical hairpin DE was indeed observed at its characteristic contour length of 86 aa during some of the subsequent unfolding curves (Figure 2(a), position 9). The probability of observing this event is influenced by the closest distance reached during the refolding trace (Figure 1(a)). A total of 80% of all detected refolded 86 aa peaks were observed for a closest approach distance of less than 17.5 nm. At this distance, the force, which has to be exerted by the polypeptide in order to decrease the contour length far enough for the formation of the helical hairpin ED, is ~ 12 pN, as calculated by the WLC model using the contour length of 86 aa. Above a closest approach distance of 17.5 nm we observed mainly the folding of individual helices or of parts of helices. These states can be detected upon their unfolding in the subsequent unfolding traces, because they show the same contour lengths as the known side peaks. In three cases after refolding, the 86 aa peak showed a rupture force comparable to the native unfolding force of the ED helices (~ 140 pN; Figure 2(a) and Table 1). In two of them the 86 aa peak was accompanied by characteristic side peaks,¹⁶ which correspond to intermediate states in which the protein is unfolded up to a position within the membrane or at its bottom side (Figure 2(a), position 10). This gives strong evidence that in these cases helices D and E refolded natively into the membrane.

In ten cases, a snap-in force peak exhibiting a contour length of 86 aa was detected while

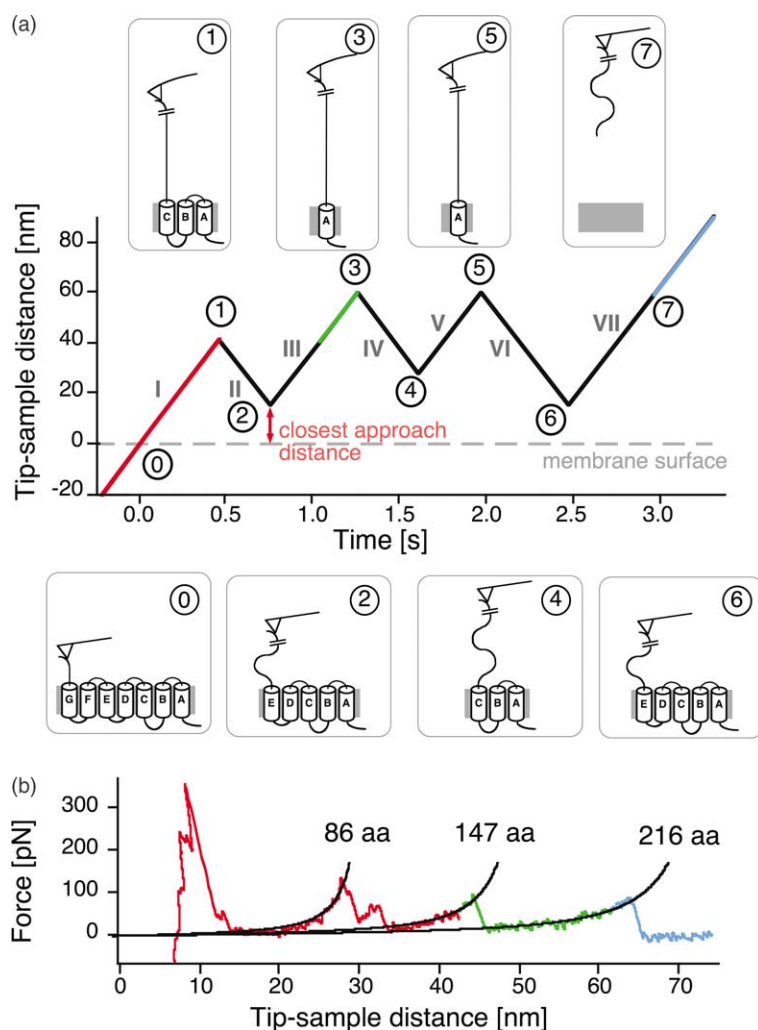


Figure 1. (a) Pathway of the piezo actuator. The cytoplasmic surface of the sample is represented by a dotted line, while the cartoons above the piezo trace represent the folding state of the BR at the upper turning points. During the steps marked by even Roman numbers the tip-sample distance is decreased. The cartoons beneath the graph indicate the maximum possible number of folded helices at each point of time. At the beginning of the experiment the cantilever has to be pushed onto the purple membrane surface to enable the adhesion of the C-terminal end of one BR monomer to the cantilevers tip (not shown in the Figure). Afterwards the cantilever is retracted to position 0, from where on the C terminus is stretched, causing helices G, F, E and D to unfold during the first part of the curve (I). In the next step (II), the tip-sample distance is decreased by 26 nm, and insertion of the amino acids composing helices D and E, which are closest to the membrane surface at that point, can take place. During step (III), the molecule is unfolded up to helix A, before the cantilever is moved towards the surface again by 32 nm in step (IV) allowing helices B and C to refold. After step (V) the molecule remains unfolded up to helix A again. Step (VI) (45 nm) allows helices B, C, D and E to reinsert into the purple

membrane before the entire molecule is unfolded during the last step (VII). The tip-sample distance at those points where the cantilever comes closest to the surface (points 2, 4, and 6) is referred to as “closest approach distance” (see red arrow). (b) Comparison to the results of conventional unfolding experiments. It is evident that the concatenated sections of the F-D trace, during which a certain part of the molecule is unfolded for the first time, should result in similar BR unfolding curves as measured before.^{15,16} These sections are shown in color in (a) and (b) depict the F-D traces corresponding to the identically colored parts in (a). These traces are taken from a refolding experiment and closely resemble a C-terminal BR unfolding curve. The black curves are WLC fits with a contour length of 86, 147 and 216 amino acids (1 aa \approx 0.36 nm) and correspond to states in which the molecule is unfolded up to the cytoplasmic side of helix E, C and A, respectively.^{15,16} The horizontal offset of the F-D curves result from the fact that, in order to measure the contour lengths, all curves were superimposed at the main peaks to compensate for variations in the point of attachment, which varies over the C terminus.

the cantilever was approaching the surface (stage II in Figure 1, snap-in peak in Figure 2(a)). These snap-in peaks indicate that the folding peptide performed considerable mechanical work against the cantilever. This force, which was actively built up by the molecule during cantilever approach, reached up to \sim 50 pN. A similar behavior has been reported by Kedrov *et al.*,⁶ who observed a snap-in peak during the refolding of one or a pair of the α -helices of the sodium antiporter NhaA. The most probable explanation for the observed work is an active, cooperative folding event of secondary structure elements. Here the question arises

whether the snap-in peaks can be interpreted with regard to the free energy of folding. For DNA it has been shown that the area between retract and approach curve can be correlated to the free energy of the folding process.²⁴ Thus, conceptually the peaks observed during the refolding of BR allow us to approximate the free energy of the observed folding event. Analyzing the area between the snap-in curve and a WLC curve exhibiting a contour length of 147 aa (Figure 2(a), inset) showed that the observed snap-ins correspond to a work between 8 and 43 $k_B T$ (here k_B is Boltzmann’s constant and T the absolute temperature). However, the peaks

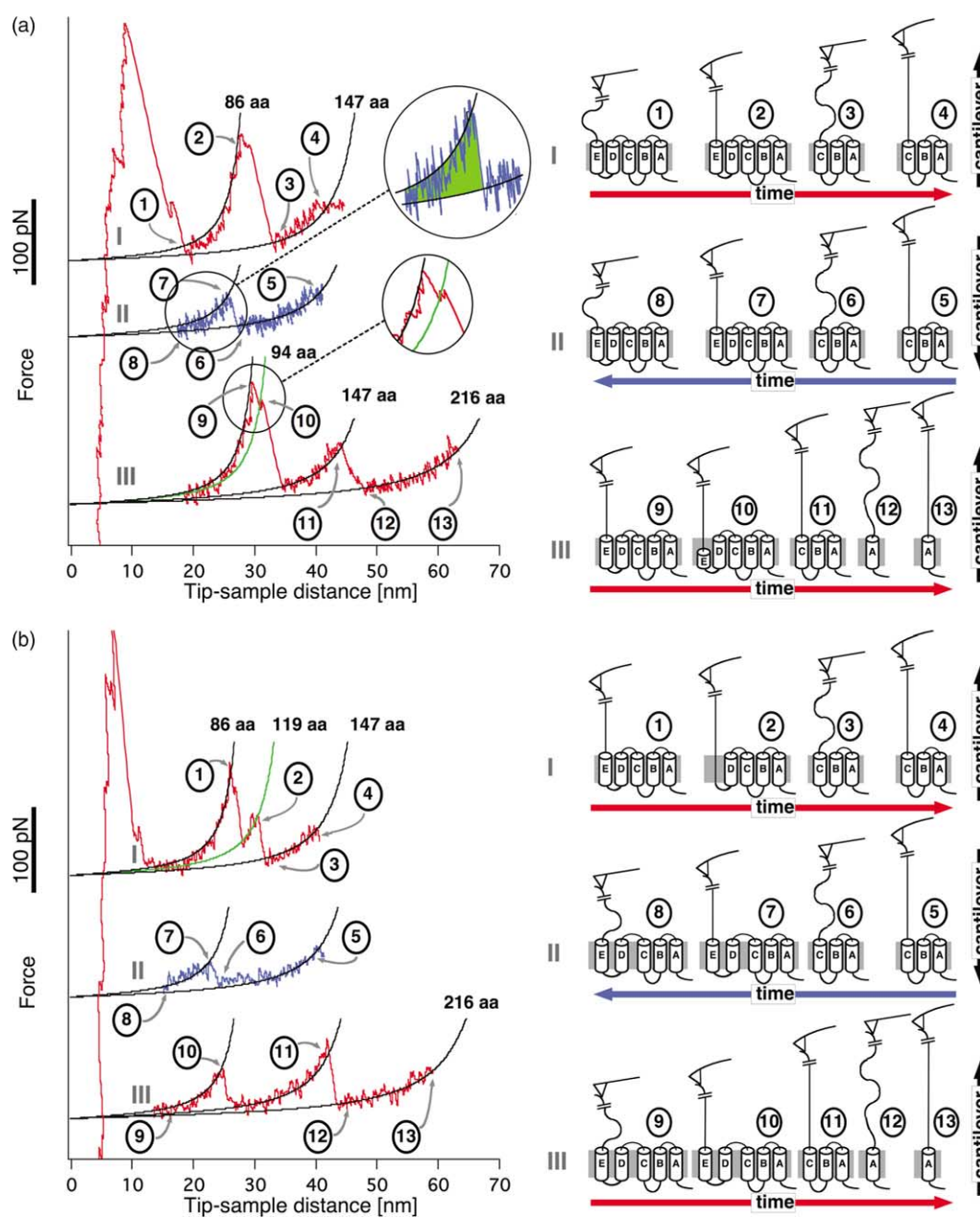
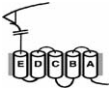
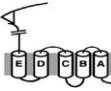








Figure 2. (a) Native pair-wise refolding of helices D and E. F–D curves recorded during the first three steps of the piezo trace shown in (a). The individual steps are indicated by Roman numbers (compare with Figure 1 (a)); the curves are vertically separated for better illustration. Data-points recorded during the increase of the tip–sample distance are shown in red while the blue curve was recorded during refolding. The contour length of each peak was calculated using the WLC model (black curves) and is given in numbers of aa which are only shown next to the first curve of each contour length. The most probable folding status of the polypeptide at the positions marked by encircled numbers is illustrated by the cartoons on the right side of the Figure. Trace I shows the unfolding of the molecule up to the cytoplasmic side of helix C as illustrated by cartoons 1 to 4. The very first peak (before position 1) represents the unfolding of helices G and F. After position 4, the cantilever is moved towards the surface again (trace II), thereby increasing the conformational space of the molecule, which leads to a decrease in force up to position 6. The sudden increase in force exerted onto the cantilever by the molecule on position 7 is caused by a decrease in contour length from 147 to 86 aa due to the refolding of helices D and E. The work performed by the folding polypeptide is given by the area highlighted in green (inset). After the relaxation to a force close to zero (position 8), the cantilever is retracted again (curve III). At position 9 helix E unfolds again, the rupture force being comparable to that of the first unfolding event shown in trace I. The observed side peak at 94 aa (green WLC curve, position 10) corresponds to an intermediate state, in which the BR is unfolded up the hydrocarbon core of helix E.¹⁶ Both facts indicate that helix E has inserted into the membrane native-like. Position 11 marks the unfolding peak of helices C and B. (b) Non-native refolding of helices D and E. Similar to (a), the first trace (I) shows the unfolding of the polypeptide up to the cytoplasmic side of helix C. The only significant difference to trace I is the side peak at 119 aa, at the extracellular side of HD (see references above). Trace II exhibits an 86 aa snap-in peak of comparable force to that in (a). Notably, the rupture force of the refolded structure (trace III, position 10) is significantly lower than that of the corresponding part in (a) and the curve exhibits no side peaks. Both of these facts indicate that the interactions stabilizing the native tertiary structure of BR have not been formed to the full extent yet.

Table 1. Schematic representation of the most prominent refolded peaks observed

Contour length	Model		Position	Number of occurrence (rupture force \pm SD)
	Native	Non-native		
86 aa			Cytoplasmic side of Helix E	Native (left): 3 (129.6 \pm 29.0 pN) Non-native (right): 12 (55.5 \pm 9.2 pN)
119 aa			Extracellular side of Helix D	5 (70.6 \pm 22.2 pN)
125 aa			Helix D, the barrier is inside the membrane	16 (52.2 \pm 26.4 pN)
147 aa			Cytoplasmic side of Helix C	Native (left): 2 (93.3 \pm 3.0 pN) Non-native (right): 7 (33.5 \pm 9.0 pN)
183 aa			Extracellular side of Helix B	7 (55.6 \pm 27.1 pN)
195 aa			Helix B, the barrier is inside the membrane	10 (54.6 \pm 21.0 pN)

The aa that marks the transition point between the unfolded and the folded part of the polypeptide, was obtained by subtracting the fitted contour length (column 1) of each peak from the total amount of aa found in BR. On the right side of column 2, the non-native orientation of helical hairpins DE and BC during the intermediate states is represented in a schematic way by increased inter-helical distances. The unfolding forces of these intermediate states are significantly lower than those of the unfolding states of the correct hairpins. Those states, in which the folded part of the BR shows its native formation, are shown on the left hand side of column 2. Refolded peaks at 97 aa and 113 aa, which represent the unfolding of the upper half of HE and the unfolding of the entire HE respectively, each were observed only once and therefore are not listed herein.

corresponding to the lower values are difficult to resolve because of the noise of the measurement and are therefore not reliable. Assuming that helices D and E folded completely and that the short connecting loop can be neglected, this work has been performed by the formation of a helical hairpin with 51 residues. Thus, a free energy gain of up to $0.84 k_B T/\text{residue}$ can be approximated. For this estimate we assume that the refolding occurs close to equilibrium. One argument in favor of this assumption is that the snap-in is not forced, but happens spontaneously. Therefore, the observed work presumably does not exceed the maximum work, which would be exerted at equilibrium. Kedrov *et al.* showed that snap-in peaks are suppressed if NhaA is relaxed at high velocities.²⁵ Evidently, under these conditions the system is not in equilibrium anymore and spontaneous folding events are not recorded. This indicates that out of equilibrium the observed forces decrease, since the relaxation time is slower than the approach. Therefore, our values might underestimate the folding energy. Nevertheless, our results are in good agreement with free energy estimates of peptides folding at a membrane/water interface. Wieprecht *et al.* measured the enthalpy of helix formation of a

peptide on vesicles as $\Delta H = 1.3 k_B T/\text{residue}$ and the free energy of helix formation as $\Delta G = 0.2 k_B T/\text{residue}$,²⁶ while Ladokhin *et al.* measured a free energy difference of melittin helix formation on the membrane water interface of $\Delta G = 0.69 k_B T/\text{residue}$.²⁷ In these two estimates, the helix does not fold into the membrane, but associates with the vesicle surface. Therefore, the systems are somewhat different from the insertion observed here. Yet, Soekarjo *et al.* estimated the free energy of helix insertion of the M13 coat protein to be in the order of $0.58 k_B T/\text{residue}$,²⁸ Ladokhin & White reported the free energy of helix insertion of an artificially designed transmembrane (TM) peptide to be in the order of $0.17 k_B T/\text{residue}$.²⁹ The latter value is probably a lower limit, since the analyzed peptide was designed to be stable and non-aggregating both in solution and in the membrane. All these values agree well with our observations, strengthening our assumption that the observed refolding was taking place close to thermodynamic equilibrium. Thus, in principle, due to the high spatial resolution of the AFM, the energy of folding can be measured for each independent folding unit, here the helical hairpin D and E, on a single molecule basis. For a more accurate estimate of this folding energy using

non-equilibrium statistical thermodynamic approaches like the Jarzynski theorem³⁰ a larger, better-defined dataset is necessary.

Non-native refolding of helices D and E

In 12 cases the 86 aa peaks recorded after refolding showed a significantly lower rupture force ($55.5(\pm 9.2)$ pN; Figure 2(b), position 10) than in the native state and exhibited no side peaks. The snap-in peaks occasionally observed prior to such “low-force” unfolding peaks are indistinguishable from those of the insertion leading to a native-like unfolding curve. The correct contour length, the observed snap-in peaks and the high reproducibility of the rupture force argue for the correct formation and insertion of the helical hairpin as opposed to some random misfolding event. However, the lower rupture force and the lack of side peaks argue against the native packing of the inserted hairpin. That strengthens the assumption of a folding intermediate state: the secondary structure of the hairpin was correctly folded, but the hairpin did not occupy its final position within the tertiary structure of the protein. This is reflected by a decreased stability compared to the native structure. These results are in good accordance to the two-stage model of TM protein folding.^{31–33} This model states that membrane protein folding is governed by two equilibria: the first equilibrium describes the partitioning of the peptide between membrane and water, while the second one describes the specific association between the lipid-embedded peptides. Thus insertion (first stage) and packing (second stage) of helices constitute the two stages of folding, each of which might have numerous sub-states. The observed snap-in peaks were caused by the spontaneous insertion of the peptide into the bilayer and therefore could represent the first step of the model. Interestingly, our results indicate that helical hairpins can act as basic folding units. This is indicated by the existence of snap-in peaks, which represent the folding of a helical hairpin without observable intermediate states (e.g. see Figure 2(a), position II).

Notably, during step (VII) of the piezo trace (Figure 1(a)) the low-force 86 aa peaks were also observed on curves where no refolding of helices B and C was observed. This was concluded from the absence of a 147 aa peak in part VII of the force curve (data not shown). It indicates that the sampled sub-state is independent of the folding status of helices B and C. Thus, the mechanisms stabilizing this folding intermediate could not be caused by interactions with helices B or C. Apparently, the membrane/protein environment without helices B and C is sufficient to form a template for the cooperative folding and insertion of the helical hairpin DE. While in 15 cases we observed the refolding of the helical hairpin, refolding of only helix D (119 aa; see Table 1) was observed in just five curves.

Refolding of helices B and C

For helices B and C (peak at 147 aa) we gained similar results compared to helices D and E. As illustrated in Figure 3(a) (position 10) and Table 1, two of the observed refolding peaks at 147 aa showed a rupture force of $93.3(\pm 3.0)$ pN, which is comparable to the native rupture force of $88.6(\pm 40.6)$ pN. That suggests that both helices have folded and inserted into the membrane correctly. The remaining seven peaks showed an average force of $33.5(\pm 9.0)$ pN at this contour length and exhibit no side peaks (Figure 3(b)), comparable to the low-force peaks of helix D and E. Again, we assume that both helices have inserted into the membrane but did not form their final orientation and packing. A reason that possibly aggravates the insertion of these two helices might be the rather long hydrophilic BC loop, which has to permeate the hydrophobic interior of the membrane. Furthermore, helix C contains two asparagine residues, which render this helix slightly amphiphilic. Indeed, it has been observed that helix C does not insert spontaneously at high pH due to deprotonation of these asparagine residues.³⁴ Corroborating our assumption that both the BC loop as well as helix C do not fold easily into the membrane is the rather frequent observation of a peak at 183 aa, which is caused by the insertion of only helix B (Table 1).

(Partial) Refolding of single helices

In addition to the peaks described so far we frequently detected peaks exhibiting a contour length around 125 and 195 aa (Table 1 and Figure 4). These peaks were observed very rarely (<12%) when the respective part of the protein was unfolded for the first time. Snap-in peaks of the same contour lengths were also observed in some cases. Both observations indicate that these peaks correspond to folding intermediates.

Notably, both of these peaks were reported previously by Janovjak *et al.*,³⁵ who observed them during unfolding measurements with oscillating cantilevers. As discussed there, the peak at 195 aa corresponds well to the unfolding of the extracellular half of helix B. In helix B, Pro50 may act as a potential conformational trap by inducing a kink in the middle of helix B.³⁶ The force peak at 125 aa corresponds to amino acid $117(\pm 3)$ aa, which is located in the middle of helix D (see Materials and Methods).

Janovjak *et al.* also considered that those peaks might be due to partial refolding of helices B and D. This seems plausible in the framework of their experimental setup and in comparison to our results, because the oscillation of the cantilever with an amplitude of 6 nm to 9 nm results in a large number of small movements towards the surface, even though the average cantilever position is continuously retracted from the sample in their experiments. The magnitude of these small

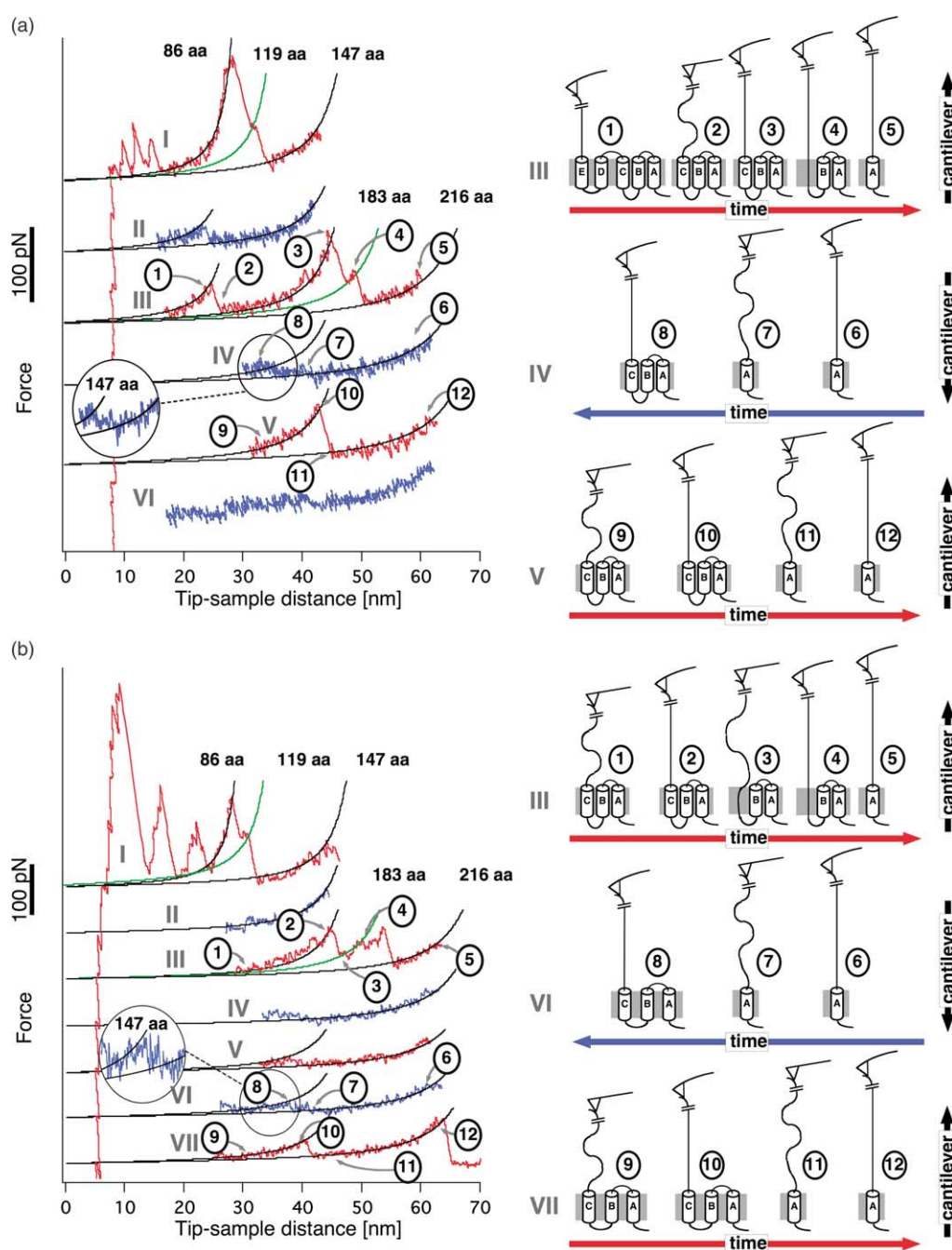


Figure 3. (a) Native pair-wise refolding of helices B and C. Helices B and C are first unfolded in trace III after the unfolding of helices D and E (step 1 to 2, compare with Figure 2(b)). At position 3 the force acting on the cytoplasmic side of helix C becomes sufficiently high to unfold helix C and the BC loop. Thereby the contour length of the unfolded portion of the molecule increases to 183 aa as illustrated in the cartoons on the right hand side. Helix B is unfolded at position 4 leaving only helix A in the membrane, the contour length amounts to 216 aa at this point. During step (IV) the tip-sample distance is decreased again allowing helices B and C to refold. The refolding probably occurs around position 8, where the signal significantly deviates from the 216 aa WLC curve and the 147 aa WLC curve fits the data in a better way (see inset). The detected force, however, barely exceeds the thermal noise of the cantilever, whereas the rupture force of the refolded helices (position 10) is within the force range of native BC peaks. (b) Non-native refolding of helices B and C. As in (a), the first unfolding of helices B and C occurs in step (III), but the two following traces show no evidence of any folding process. A possible reason is, that the minimal tip-sample distance reached during step (IV) was not sufficiently small to allow refolding of the constituents of helices B and C. However, at the next approach towards the surface (step (VI)) there is a region (enlarged in the inset) where the deviation from the 216 aa WLC curve becomes significant and a 147 aa curve might fit the data better. Trace VII exhibits a distinct peak with a contour length of 147 aa at position 10 before helix A is extracted from the membrane at position 12. Since the rupture force of the 147 aa peak is significantly lower than the native rupture force of helices B and C, we interpret this scenario in the same way as in Figure 2(b). Probably both helices have refolded into the membrane using helix A and possibly neighboring BR-monomers as a template, but the inter-helical interactions stabilizing both helices in the native molecule have not entirely developed yet.

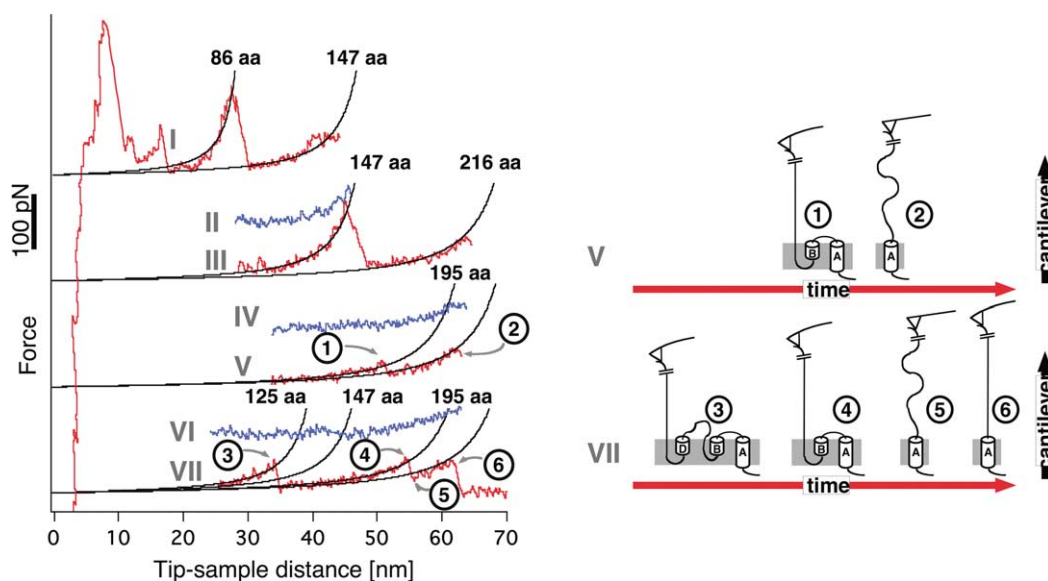


Figure 4. Partial insertion of helices. Here, helices D and E are unfolded during the first step, followed by unfolding of helices B and C during step (III) (illustrated by the WLC curves at 86 and 147 aa; curves are drawn in black). The peak at 195 aa (position 1 and 4) corresponds well to a proline (Pro50), which acts as a potential trap by inducing a kink in the middle of helix B. Similarly, the peak at 125 aa (position 3) corresponds to an anchoring point in the hydrocarbon core of helix D. Both peaks are rarely (<12%) observed on conventional unfolding curves, but were detected more frequently (up to 30%) during the refolding measurements reported here. As illustrated in the cartoons, our current view is that in both cases the first helix of the helical hairpin partly refolds while the rest of the hairpin remains unfolded. From the absence of any peak between the 125 aa and 195 aa (trace VII) we conclude that the polypeptide strand exhibits no stable structure between the hydrocarbon core on helix B and the cytoplasmic side of helix D. Considering the low hydrophobicity of the BC loop and the pH-dependent insertion behavior of helix C, we assume that helix C does not have a high propensity for refolding into the membrane.

movements would be just high enough to enable partial folding of a single helix. Since these peaks are observed with fast oscillating cantilevers, the time required for refolding the corresponding parts of the helices appears to be very short (<0.3 ms). The agreement between our data and the study mentioned above, which used an entirely different experimental approach, is striking and underlines the high precision of state-of-the-art force spectroscopy, being able to resolve and to monitor molecular conformational changes in high speed, high spatial and force resolution. As both peaks are located within the hydrocarbon core on the sequentially first helix of a helical hairpin (B–C or D–E) it appears to be possible that the corresponding states represent very fast folding intermediate states of the insertion of helical hairpins. Partially folded helices thus might be a common intermediate state in membrane protein folding.

Conclusion

This study demonstrates that handling of individual proteins by AFM-related techniques has meanwhile reached a level of precision which allows the control of the conformation of membrane proteins at the level of secondary structure elements. Individual helices or loops may be unfolded and subsequently refolded while the force required to do so is controlled with piconewton accuracy. In our refolding

experiments we found that the contour lengths of structures, which are newly folded after the relaxation of a partial unfolded BR-molecule, closely match the contour lengths of peaks already known from conventional unfolding studies of BR in almost every case. Together with the snap-in peaks, which are frequently observed during the relaxation of the cantilever and which we interpret as folding processes against an external force, this provides strong evidence that our data represent the refolding of individual BR hairpins and helices. We have shown that the partial refolding of BR is possible at least for helices B to E. In some cases, the rupture forces of helices B and C as well as D and E detected after their refolding is comparable to the native rupture force of these helices. Occasional side peaks, a signature of natively folded BR, are observed as well. In other cases, the rupture forces corresponding to the helical pairs BC and DE are significantly lower and the curves lack side peaks. This indicates that the interhelical interactions responsible for those side peaks have not been formed yet. Furthermore, we observe folding intermediates with correctly formed secondary structure which are most probably inserted into the membrane but lack tertiary contacts. They exhibit significantly lower stability compared to the native conformation. That is a very strong experimental evidence for the concept of two-stage folding of membrane proteins. Further, we detected the insertion of helix B or helix D without its partners (C and E, respectively), and even the partial formation of B and

D (see Table 1). According to the results presented here and in an earlier paper,³⁵ the latter states most probably are fast-forming folding intermediates. Thus, we were able to detect a number of folding intermediates with differing complexity. In the complete folding event, these folding intermediates might occur sequentially, or the protein uses different folding pathways. Further studies are necessary to distinguish these possibilities. In particular, it will be informative to test the lifetime of these folding intermediates by varying the waiting time before the cantilever tip is retracted after allowing the protein to fold into an intermediate. It is interesting, that the AFM-induced folding behavior of BR seems to be much more complex than that of the only other membrane protein that was refolded with AFM so far, NhaA,⁶ where snap-in peaks occur at only one contour length. Future experiments on other membrane proteins using even more sophisticated experimental approaches, e.g. force-clamp techniques, seem very promising.

Materials and Methods

Sample preparation

We allowed wild-type purple membranes (PM), extracted from *Halobacterium salinarum* as described,³⁷ to adsorb onto a freshly cleaved mica surface and rinsed it with buffer solution (300 mM KCl, 10 mM Tris-HCl (pH 7.8)).³⁸ The buffer solution was prepared with nanopure water and p.a. grade chemicals from Sigma/Merck.

Refolding experiments

The refolding experiments were performed with a commercial AFM (Multimode PicoForce, Nanoscope IIIa; Veeco Metrology, Santa Barbara, CA) equipped with a piezo actuator with a lateral scan range of 50 μm and a closed-loop vertical range of 20 μm . For calibrating the spring constants of the 100 μm long Si_3N_4 cantilevers (OMCL TR400PS, Olympus, Tokyo, Japan) in solution we used the equipartition theorem.^{39,40} Within the uncertainty of this method ($\sim 10\%$), all cantilevers exhibited a spring constant of 0.08 N/m. All experiments were performed in buffer solution (300 mM KCl, 10 mM Tris-HCl (pH 7.8)) at room temperature. To probe the partial refolding of BR we repeatedly extended and contracted the piezo as depicted in Figure 1. The piezo velocity was adjusted to 90 nm/s. Control experiments at lower velocities between 40 and 50 nm/s showed the same qualitative behavior. During some of the experiments we kept the piezo position constant for up to 1 s at the points of return close to the surface (positions 2, 4, and 6 in Figure 1(a)) to provide the molecule more time for refolding. Nevertheless, it turned out that the secondary structure elements tend to fold on a relatively fast time scale, if they fold at all. The influence of the waiting time on the rearrangement of larger parts of the protein is subject to further investigation.

Data analysis

The attachment of the cantilever tip to one of the loops of a membrane protein results in two polypeptide

strands, which are unfolded simultaneously. To avoid uncertainties with the assignment of peaks arising from such a situation, we restricted our analysis to F-D curves of BR-monomers that are attached to the tip of the cantilever with their C terminus. As discussed elsewhere,¹⁶ we achieved this by selecting F-D curves with an overall length of significantly more than 60 nm.

Since PM patches adsorb in both orientations and the AFM used for the refolding experiments was not capable of producing molecular resolution scans, we used criteria derived from another study (M.K. and H.E.G. unpublished results) where we show that N-terminal F-D curves significantly differ from C-terminal F-D curves in terms of the relative contour lengths of force peaks.

For analyzing the force peaks we used the WLC model, which describes the elastic behavior of an unfolded polypeptide strand. Fitting the increasing slope of a force peak with this model yields the contour length of the unfolded portion of the molecule, L , and therefore the amount of unfolded aa. If unfolding from the C terminus, the position of the aa acting as anchoring point is given by subtracting the amount of unfolded aa from the total amount of aa in BR (248). However, if the anchoring point is not located at the cytoplasmic membrane surface, the distance d between the membrane surface and the anchoring point has to be considered. In this case, the measured contour length L_m does not equal the amount of unfolded aa (L) anymore but is reduced by d . This refinement of an approach we described earlier¹⁶ (where d was set to 11 aa if the anchoring point was assumed at the extracellular surface) is based on the assumption, that the intra-membrane part of the polypeptide, d , is fully elongated and not able to fluctuate, so that it does not contribute to the measured contour length L_m . Since the anchoring point is not known at this stage, we turned things around. Therefore, we made a list containing, n , the number of each aa within the sequence of BR as well as d , which was calculated from the 3D model of BR published by Essen *et al.*,¹¹ and the expected value for L_m † and used that to find the anchoring position, which best corresponds to the fitted values. For the WLC fits we used the interpolation formula by Bustamante *et al.*⁴¹ with a persistence length of 0.4 nm and a monomer length of 0.36 nm.¹⁷

Acknowledgements

We thank Dieter Oesterhelt for fruitful discussions and kindly providing purple membranes. Furthermore we thank Uta Steinbach for critical reading and valuable suggestions concerning the manuscript. This work was supported by the Deutsche Forschungsgemeinschaft. K.E.G. is supported by a Liebig Fellowship of the Fonds der Chemischen Industrie.

† Calculated by $L_m = 248 - n - d$, due to $n = 248 - L$ and $L = L_m + d$ (L denotes the real contour length, all lengths are given in numbers of aa).

References

- Krogh, A., Larsson, B., von Heijne, G. & Sonnhammer, E. L. (2001). Predicting transmembrane protein topology with a hidden Markov model: application to complete genomes. *J. Mol. Biol.* **305**, 567–580.
- Daley, D. O., Rapp, M., Granseth, E., Melen, K., Drew, D. & von Heijne, G. (2005). Global topology analysis of the *Escherichia coli* inner membrane proteome. *Science*, **308**, 1321–1323.
- White, S. H. & Wimley, W. C. (1999). Membrane protein folding and stability: physical principles. *Annu. Rev. Biophys. Biomol. Struct.* **28**, 319–365.
- Booth, P. J., Curran, A. R., Templar, R. H., Lu, H. & Meijberg, W. (2001). Manipulating the folding of membrane proteins: using the bilayer to our advantage. *Biochem. Soc. Symp.* **68**, 27–33.
- Cisneros, D. A., Oesterhelt, D. & Muller, D. J. (2005). Probing origins of molecular interactions stabilizing the membrane proteins halorhodopsin and bacteriorhodopsin. *Structure (Camb)*, **13**, 235–242.
- Kedrov, A., Ziegler, C., Janovjak, H., Kuhlbrandt, W. & Muller, D. J. (2004). Controlled unfolding and refolding of a single sodium-proton antiporter using atomic force microscopy. *J. Mol. Biol.* **340**, 1143–1152.
- Kienberger, F., Kada, G., Mueller, H. & Hinterdorfer, P. (2005). Single molecule studies of antibody–antigen interaction strength versus intra-molecular antigen stability. *J. Mol. Biol.* **347**, 597–606.
- Buldt, G., Heberle, J., Dencher, N. A. & Sass, H. J. (1998). Structure, dynamics, and function of bacteriorhodopsin. *J. Protein Chem.* **17**, 536–538.
- Dencher, N. A., Sass, H. J. & Buldt, G. (2000). Water and bacteriorhodopsin: structure, dynamics, and function. *Biochim. Biophys. Acta*, **1460**, 192–203.
- Belrhali, H., Nollert, P., Royant, A., Menzel, C., Rosenbusch, J. P., Landau, E. M. & Pebay-Peyroula, E. (1999). Protein, lipid and water organization in bacteriorhodopsin crystals: a molecular view of the purple membrane at 1.9 Å resolution. *Struct. Fold. Des.* **7**, 909–917.
- Essen, L., Siebert, R., Lehmann, W. D. & Oesterhelt, D. (1998). Lipid patches in membrane protein oligomers: crystal structure of the bacteriorhodopsin–lipid complex. *Proc. Natl Acad. Sci. USA*, **95**, 11673–11678.
- Grigorieff, N., Ceska, T. A., Downing, K. H., Baldwin, J. M. & Henderson, R. (1996). Electron-crystallographic refinement of the structure of bacteriorhodopsin. *J. Mol. Biol.* **259**, 393–421.
- Luecke, H., Schobert, B., Richter, H. T., Cartailler, J. P. & Lanyi, J. K. (1999). Structure of bacteriorhodopsin at 1.55 Å resolution. *J. Mol. Biol.* **291**, 899–911.
- Mitsuoka, K., Hirai, T., Murata, K., Miyazawa, A., Kidera, A., Kimura, Y. & Fujiyoshi, Y. (1999). The structure of bacteriorhodopsin at 3.0 Å resolution based on electron crystallography: implication of the charge distribution. *J. Mol. Biol.* **286**, 861–882.
- Oesterhelt, F., Oesterhelt, D., Pfeiffer, M., Engel, A., Gaub, H. E. & Muller, D. J. (2000). Unfolding pathways of individual bacteriorhodopsins. *Science*, **288**, 143–146.
- Muller, D. J., Kessler, M., Oesterhelt, F., Moller, C., Oesterhelt, D. & Gaub, H. (2002). Stability of bacteriorhodopsin alpha-helices and loops analyzed by single-molecule force spectroscopy. *Biophys. J.* **83**, 3578–3588.
- Rief, M., Gautel, M., Oesterhelt, F., Fernandez, J. M. & Gaub, H. E. (1997). Reversible unfolding of individual titin immunoglobulin domains by AFM. *Science*, **276**, 1109–1112.
- Carrion-Vazquez, M., Oberhauser, A. F., Fowler, S. B., Marszalek, P. E., Broedel, S. E., Clarke, J. & Fernandez, J. M. (1999). Mechanical and chemical unfolding of a single protein: a comparison. *Proc. Natl Acad. Sci. USA*, **96**, 3694–3699.
- Rief, M., Gautel, M. & Gaub, H. E. (2000). Unfolding forces of titin and fibronectin domains directly measured by AFM. *Advan Exp. Med. Biol.* **481**, 129–136.
- Li, H., Oberhauser, A. F., Fowler, S. B., Clarke, J. & Fernandez, J. M. (2000). Atomic force microscopy reveals the mechanical design of a modular protein. *Proc. Natl Acad. Sci. USA*, **97**, 6527–6531.
- Gergely, C., Voegel, J., Schaaf, P., Senger, B., Maaloum, M., Horber, J. K. & Hemmerle, J. (2000). Unbinding process of adsorbed proteins under external stress studied by atomic force microscopy spectroscopy. *Proc. Natl Acad. Sci. USA*, **97**, 10802–10807.
- Altmann, S. M., Grunberg, R. G., Lenne, P. F., Ylanne, J., Raae, A., Herbert, K. *et al.* (2002). Pathways and intermediates in forced unfolding of spectrin repeats. *Structure (Camb)*, **10**, 1085–1096.
- Schwaiger, I., Kardinal, A., Schleicher, M., Noegel, A. A. & Rief, M. (2004). A mechanical unfolding intermediate in an actin-crosslinking protein. *Nature Struct. Mol. Biol.* **11**, 81–85.
- Clausen-Schaumann, H., Rief, M., Tolksdorf, C. & Gaub, H. E. (2000). Mechanical stability of single DNA molecules. *Biophys. J.* **78**, 1997–2007.
- Kedrov, A., Janovjak, H., Ziegler, C., Kuhlbrandt, W. & Muller, D. J. (2006). Observing folding pathways and kinetics of a single sodium-proton antiporter from *Escherichia coli*. *J. Mol. Biol.* **355**, 2–8.
- Wieprecht, T., Beyermann, M. & Seelig, J. (2002). Thermodynamics of the coil-alpha-helix transition of amphipathic peptides in a membrane environment: the role of vesicle curvature. *Biophys. Chem.* **96**, 191–201.
- Ladokhin, A. S. & White, S. H. (1999). Folding of amphipathic alpha-helices on membranes: energetics of helix formation by melittin. *J. Mol. Biol.* **285**, 1363–1369.
- Soekarjo, M., Eisenhawer, M., Kuhn, A. & Vogel, H. (1996). Thermodynamics of the membrane insertion process of the M13 procoat protein, a lipid bilayer traversing protein containing a leader sequence. *Biochemistry*, **35**, 1232–1241.
- Ladokhin, A. S. & White, S. H. (2004). Interfacial folding and membrane insertion of a designed helical peptide. *Biochemistry*, **43**, 5782–5791.
- Hummer, G. & Szabo, A. (2001). Free energy reconstruction from non-equilibrium single-molecule pulling experiments. *Proc. Natl Acad. Sci. USA*, **98**, 3658–3661.
- Engelman, D. M., Chen, Y., Chin, C. N., Curran, A. R., Dixon, A. M., Dupuy, A. D. *et al.* (2003). Membrane protein folding: beyond the two stage model. *FEBS Letters*, **555**, 122–125.
- Popot, J. L. & Engelman, D. M. (1990). Membrane protein folding and oligomerization: the two-stage model. *Biochemistry*, **29**, 4031–4037.
- Popot, J. L. & Engelman, D. M. (2000). Helical membrane protein folding, stability, and evolution. *Annu. Rev. Biochem.* **69**, 881–922.
- Hunt, J. F., Rath, P., Rothschild, K. J. & Engelman, D. M. (1997). Spontaneous, pH-dependent membrane insertion of a transbilayer alpha-helix. *Biochemistry*, **36**, 15177–15192.

35. Janovjak, H., Muller, D. J. & Humphris, A. D. (2005). Molecular force modulation spectroscopy revealing the dynamic response of single bacteriorhodopsins. *Biophys. J.* **88**, 1423–1431.
36. Faham, S., Yang, D., Bare, E., Yohannan, S., Whitelegge, J. P. & Bowie, J. U. (2004). Side-chain contributions to membrane protein structure and stability. *J. Mol. Biol.* **335**, 297–305.
37. Oesterhelt, D. & Stoekenius, W. (1974). Isolation of the cell membrane of *Halobacterium halobium* and its fractionation into red and purple membrane. *Methods Enzymol.* **31**, 667–678.
38. Muller, D. J., Amrein, M. & Engel, A. (1997). Adsorption of biological molecules to a solid support for scanning probe microscopy. *J. Struct. Biol.* **119**, 172–188.
39. Butt, H.-J. & Jaschke, M. (1995). Calculation of thermal noise in atomic force microscopy. *Nanotechnology*, **6**, 1–7.
40. Florin, E. L., Rief, M., Lehmann, H., Ludwig, M., Dornmair, C., Moy, V. T. & Gaub, H. E. (1995). Sensing specific molecular interactions with the atomic force microscope. *Biosens. Bioelectr.* **10**, 895–901.
41. Bustamante, C., Marko, J. F., Siggia, E. D. & Smith, S. (1994). Entropic elasticity of lambda-phage DNA. *Science*, **265**, 1599–1600.
42. Booth, P. J. & Curran, A. R. (1999). Membrane protein folding. *Curr. Opin. Struct. Biol.* **9**, 115–121.
43. Booth, P. J. (2000). Unravelling the folding of bacteriorhodopsin. *Biochim. Biophys. Acta*, **1460**, 4–14.

Edited by G. von Heijne

(Received 12 October 2005; received in revised form 15 December 2005; accepted 17 December 2005)
Available online 6 January 2006

Lebenslauf

Name: Max Raimund Keßler
Geburtsdatum: 23. Mai 1974
Geburtsort: München

Ausbildung

1980 - 1984: Grundschule in München
1984 - 1993: Pestalozzi-Gymnasium, München
1993 - 2000: Studium der Physik an der Ludwig-Maximilians-Universität München
1996: Vordiplom
1999 - 2000: Diplomarbeit am Lehrstuhl für angewandte Physik der Ludwig-Maximilians-Universität München zum Thema:
„Untersuchung von Struktur und Aktivität von Proteinkomplexen“
2000 - 2005: Promotion am Lehrstuhl für angewandte Physik der Ludwig-Maximilians-Universität München zum Thema:
„Kraftspektroskopie an einzelnen Membranproteinen“

Danksagung

An dieser Stelle möchte ich mich bei all denjenigen bedanken, die zum Entstehen der vorliegenden Arbeit beigetragen haben.

- Bei Hermann Gaub bedanke ich mich dafür, daß er mir ermöglichte, meine Promotion an seinem Lehrstuhl durchzuführen, und daß er meine Arbeit stets mit großer Geduld und Interesse verfolgt hat. Vielen Dank für zahllose Diskussionen und die Freiheit, eigene Ideen verwirklichen zu können.
- Daniel Müller und seiner Gruppe danke ich für die Gastfreundschaft in Basel und Dresden und die Gelegenheit, im Austausch gegen mitgebrachte Weißwürste an den dortigen Kraftmikroskopen einen Teil der Messungen durchführen zu können. Insbesondere möchte ich mich auch bei Clemens Möller für die Einführung in das hochauflösende Abbilden mit dem AFM und bei Harald Janovjak für die langjährige gute Zusammenarbeit an Bakteriorhodopsin und für zahlreiche fruchtbare Diskussionen bedanken.
- Dieter Oesterhelt danke ich für sein stetes Interesse an meiner Arbeit, hilfreiche Diskussionen sowie die großzügige Bereitstellung zahlreicher Proben, die von seiner Gruppe dankenswerter Weise in konstant exzellenter Qualität zur Verfügung gestellt wurden.
- Hilde Rinia und Marcus Braun danke ich für ihre Mithilfe an den Projekten in München und dafür, daß sie trotz zahlreicher technischer Schwierigkeiten nicht ihr Interesse daran verloren haben.
- Für zahlreiche Tips und Diskussionen und ihre stets gute Laune möchte ich mich insbesondere auch bei Rupert Krautbauer und Ingo Schwaiger bedanken. Ihr wart für mich stets eine Quelle der Motivation.
- Bei Kay Gottschalk bedanke ich mich für seine Hilfe bei der Interpretation der Daten zur Rückfaltung von BR in der Endphase des Projektes.
- Für das Korrekturlesen dieser Arbeit möchte ich mich neben Gregor Neuert und Kay Gottschalk vor allem bei Uta Steinbach bedanken, die nie den Glauben an meine Arbeit verloren hat, und der es gelang, mich in den vergangenen drei Jahren immer wieder zu motivieren.
- Allen weiteren hier nicht namentlich aufgeführten Mitgliedern des Lehrstuhls sowie Matthias Rief und seiner Gruppe danke ich für zahllose kleinere und größere Gefallen, die freundliche Atmosphäre und dafür, daß meine Zeit hier nicht nur wissenschaftlich sehr interessant und produktiv war, sondern auch viel Spaß gemacht hat.
- Zuletzt möchte ich mich auch noch bei meiner Familie für die Unterstützung bedanken.

Erklärung

Hiermit versichere ich, die vorliegende Arbeit selbstständig ausgeführt und keine weiteren Hilfsmittel als die im Text und im Literaturverzeichnis aufgeführten verwendet zu haben.

Max Keßler, München, den 28. November 2005